

NOVEL NANOCARRIERS FOR INVASIVE GLIOMA

A Dissertation
Presented to
The Academic Faculty

By

Jennifer M Munson

In Partial Fulfillment
of the Requirements for the Degree
Doctor of Philosophy in the
School of Chemical and Biomolecular Engineering

Georgia Institute of Technology
August 2011

NOVEL NANOCARRIERS FOR INVASIVE GLIOMA

Approved by:

Dr. Ravi V Bellamkonda, Advisor
School of Biomedical Engineering
Georgia Institute of Technology

Dr. Jack L Arbiser
Department of Dermatology
Emory University

Dr. Thomas A Barker
School of Biomedical Engineering
Georgia Institute of Technology

Dr. Daniel J Brat
Department of Pathology & Laboratory
Medicine
Emory University

Dr. Hang Lu
School of Chemical and Biomolecular
Engineering
Georgia Institute of Technology

Dr. Lakeshia Taite
School of Chemical and Biomolecular
Engineering
Georgia Institute of Technology

Date Approved: June 3, 2011

ACKNOWLEDGEMENTS

This dissertation would not have been possible without a multitude of people who have supported, taught, and questioned me throughout my PhD.

I would like to thank my committee members for reading my thesis and for advising me throughout my graduate career. Jack Arbiser, thank you for opening your lab and your amazing biochemistry abilities to me; I would not have a thesis without you. Tom Barker, thank you for being an honest and open advisor about everything from acting to Switzerland. Hang Lu, thank you for convincing me to come to Georgia Tech when I was still a lowly intern at Genentech, it was definitely the right choice for me and I'm glad you knew that. Dan Brat, thank you for answering all of my questions about histology and for looking at my slides with me; I never thought I'd know so much about glioma. Lakeshia Taite, thank you for taking a chance and opening your classroom to me for a semester and for listening to all my ramblings, I really appreciate it.

And, of course, Ravi, thank you for challenging me from the start (by telling me to finish my PhD in 3 years) and for continuing to challenge me. You really allowed me to grow on my own without many limitations and I appreciate that flexibility and freedom. You are an amazing advisor and life coach and I appreciate your support and confidence in me (and the occasional candid advice).

I would like to thank several laboratories. First, I want to thank the Neurological Biomaterials and Cancer Therapeutics Laboratory, present, past, and future, for teaching and advising me. More than that though, for being comrades in the battle of graduate school with late nights and early mornings full of experiments or last minute presentations. I especially want to thank a few people: Balakrishna Pai and Lohitash Karumbaiah for their wealth of biological knowledge and willingness to step in when I'm overwhelmed; Michael Tanenbaum and Shannon Barker for support and

encouragement.; Benjamin Roller and Clare Gollnick for being great friends and confidants throughout my graduate career and hopefully beyond. And last, Kathleen McNeeley, I could not have been a success without her amazing advisement and critical questioning. I enjoyed spending my journey with all of these people and am excited to be associated with them forever.

I'd like to thank the Arbiser Lab at Emory for giving me such an amazing molecule around which to build my thesis and for bearing with me through the arduous process of developing my knowledge about it. I especially want to thank Michael Bonner and Levi Fried. They were immensely helpful and made it so pleasant to visit my Emory family.

The last lab I'd like to acknowledge is my lab family across the pond in Switzerland, the Laboratory for Lymphatic and Cancer Bioengineering. In particular Melody Swartz and Adrian Shieh for mentoring me and making me feel incredibly welcome in a very different place. My year in Switzerland was incredibly important in my motivation and development as a researcher and they were integral to that experience.

I'd like to also acknowledge all of the people who have helped me along the way whether through advising, collaborating, listening, or teaching: Johannes Leisen, Hui-Kuo Shu, Jeffrey Olson, Byron Ford, and Constantinos Hadjipanayis. Also, I'd like to thank Chris Ruffin for administrative support and navigating me through the difficulties in my course of study. Last, I'd like to thank my professors back at Tulane, particularly WT Godbey, who inspired me to become a researcher.

I also want to thank Laura O'Farrell, Kimberly Benjamin, and the entire PRL staff for their extensive care with my studies. Special shout out to Odell and Andrea for being so awesome and making my work a success with their careful attention and friendly attitude.

And of course, I need to acknowledge my undergraduate lab family (in no particular order): Shalini Nemani for keeping me on my toes with endless questions.

Eleanor De Hitta for being my Swiss buddy and always an amazing person and cryosectioner; Rania Khan for her natural curiosity, care for detail, and willingness to laugh at my jokes; Mona Ahmad for turning everything to gold and always doing so with a smile (mostly giggling though); Sydney Rowson for her maturity and inspiring excitement about research and life; Safkat Alkindi for his attention to detail and ability to do amazing things with minimal direction. In all, I would not have been successful without these students and they made my life richer by having known them.

I'd like to thank my funding sources, Nora Redman Foundation for early project support, the Coulter Foundation, and Ian's Kids Foundation for later project support. I'd also like to thank the National Science Foundation for the graduate research fellowship support at home and le Confederación Suisse and Fulbright Foundation for support while abroad.

On a personal note, I'd like to thank my friends Ashley, Carla, and Lindsey for being my support system whenever I need them for fourteen years. Alex, for being awesome all the time, allowing me to vent and get me ice cream at the same time, for helping me both in lab and out, even when I'm 5000 miles away. I'd like to thank my future family, the Calderwoods for support and understanding. I'd like to thank my family and particularly my parents, Chris and Joan Munson, who have always supported me in whatever I do. They allowed me to always be who I want to be and encouraged me to follow my dreams and I love them for that. They're my biggest fans. Last, I want to thank my fiancé Charles, who has been on this journey with me. For taking me to check on my animals, picking me up late after a long day of work, and understanding me through the tough times. It's not easy to have two graduate students in one relationship but he makes it easy, fun, amazing, and worthwhile.

TABLE OF CONTENTS

	Page
ACKNOWLEDGEMENTS	iii
LIST OF TABLES	ix
LIST OF FIGURES	x
LIST OF SYMBOLS AND ABBREVIATIONS	xiii
SUMMARY	xvi
<u>CHAPTER</u>	
1 CHAPTER 1: INTRODUCTION	1
1.1 Brain cancers: types and treatments	1
1.2 Invasion of glioblastoma	14
1.3 Mechanisms of brain tumor invasion	24
1.4 Molecules that stop invasion	31
1.5 Nanocarriers for drug delivery in cancer	34
1.6 Summary	39
2 CHAPTER 2: COMPOUND SCREEN	40
2.1 Summary	40

2.2	Introduction	40
2.3	Methods	42
2.4	Results	45
2.5	Discussion	48
3	ENCAPSULATION AND TESTING OF IMIPRAMINE BLUE	51
3.1	Summary	51
3.2	Introduction	51
3.3	Methods	53
3.4	Results	60
3.5	Discussion	76
4	CO-LOADING OF IMIPRAMINE BLUE AND DOXORUBICIN	81
4.1	Summary	81
4.2	Introduction	81
4.3	Methods	83
4.4	Results	87
4.5	Discussion	94

5	CANDIDATE MECHANISM OF ACTION OF IMPRAMINE BLUE	97
5.1	Summary	97
5.2	Introduction	97
5.3	Methods	100
5.4	Results	102
5.5	Discussion	108
6	DISCUSSION	112
6.1	Discussion of Overall Thesis	112
6.2	Future Directions	120
	APPENDIX A: MICROARRAY DATA FOR IB-AFFECTED GENES	129
	APPENDIX B: EFFECT OF IB ON ANGIOGENESIS	131
	APPENDIX C: COMBINATORIAL TREATMENT WITH TEMOZOLOMIDE	144
	APPENDIX D: IB-DXR NANOCARRIERS AGAINST U87MGEGFRVIII	150
	APPENDIX E: EFFECTS OF INTERSTITIAL FLOW ON GLIOMA INVASION	152
	REFERENCES	180
	VITA	209

LIST OF TABLES

Table 1.1: Categories of tumor models.....	11
Table 1.2: Animal models of glioma	15
Table 1.3: Common invasion and migration assays used in cancer research	23
Table 1.4: Molecules showing or predicted to have anti-invasive activity in glioma.	33
Table 1.5: Types of nanocarriers used for cancer drug delivery.....	36
Table 1.6: FDA-Approved liposomal formulations of drugs and their indications.....	37
Table 4.1 Characterization of liposomes	108
Table B.1: Timeline of treatment and imaging	138
Table B.2: Endothelial Transfer Coefficients (K^{PS}).....	141

LIST OF FIGURES

Figure 1.1: Current treatment paradigm for glioblastoma	4
Figure 1.2: Enhanced Permeability and Retention Effect.....	38
Figure 2.1: Honokiol derivatives	44
Figure 2.2: Triphenylmethane dyes	45
Figure 2.3: Cytotoxicity in RT2 glioma at high doses.....	46
Figure 2.4: Cytotoxicity in RT2 glioma at low doses.....	46
Figure 2.5: Invasion inhibition of RT2 glioma.	47
Figure 2.6: Cytotoxic effect against primary rat astrocytes	48
Figure 3.1: Strategy of treatment with IB	53
Figure 3.2: Synthesis of Imipramine Blue	61
Figure 3.3: Dose dependent cytotoxicity of glioblastoma RT2 and Astrocytes	62
Figure 3.4: Imipramine Blue inhibits invasion in glioma cell lines.....	63
Figure 3.5: Structural components of RT2 glioma	64
Figure 3.6: Encapsulation of IB in liposomes activity and characterization.. ..	65
Figure 3.7: Encapsulation of IB in liposomes testing <i>in vivo</i>	66
Figure 3.8: IB yields no observable toxicity towards non-target organs	67
Figure 3.9: <i>In vivo</i> delivery of nano-IB yields a decreased in invasion.....	69
Figure 3.10: A candidate mechanism of action was determined <i>in vivo</i>	71
Figure 3.11: Effects on cell spreading seen <i>in vitro</i>	72
Figure 3.12: Delivery of IB before Doxorubicin (DXR) yields increased survival.....	74

Figure 3.13: T ₂ - and T ₁ -weighted MRI of DXR alone treated tumor.	76
Figure 4.1: Co-loading of IB and DXR in liposomes	87
Figure 4.2: There is no enhancement of cytotoxicity with dual liposomes <i>in vitro</i>	89
Figure 4.3: IB-DXR increases survival over DXR alone treatment in RT2 glioma.....	90
Figure 4.4: Pre and post treatment MRI for all groups.	91
Figure 4.5: Tumor growth curves for all groups.....	92
Figure 4.6: IB-DXR treated tumor in MRI and histology	93
Figure 5.1: Inhibition of invasion in other models of invasive cancer.	102
Figure 5.2: Cell spreading in presence of IB	103
Figure 5.3: IB does not inhibit actin directly	104
Figure 5.3: IB inhibits H ₂ O ₂ generation by Nox4.....	105
Figure 5.5: IB binds to Nox4	106
Figure 5.6: IB localizes to the nucleus of RT2 cells.	107
Figure 5.7: Proposed mechanism of action of IB with known downstream effects	111
Figure B.1: MMP Activity in IB treated glioma.....	139
Figure B.2: Treated HUVEC invasion decreased but was not significant.....	140
Figure B.3: T ₁ MR Brain Image Color maps.....	141
Figure B.4: Effects of Imipramine Blue on Blood Vessels of Rat Glioma (RT2).....	142
Figure C.1: Viability with Temozolomide and IB treatment.....	148
Figure D.1: Kaplan-Meier Survival Plots of mice bearing U87MG EGFRVIII.....	150
Figure E.1: Flow pathways, CXCL12 gradients, and tumor invasion in the brain.....	161
Figure E.2 Glioma invasion is increased by interstitial flow in a 3D culture model.....	163
Figure E.3 Flow response correlates with chemotaxis and invasion in cell lines.....	164

Figure E.4: Flow-enhanced invasion is CXCR4 dependent165

Figure E.5 Blocking or activating CXCR4 inhibits flow-enhanced invasion.....166

Figure E.6 CXCL12 and CXCR4 expression levels are unchanged under flow.166

Figure E.7: Cell migration favors the flow direction.....169

Figure E.8: Cells tend to migrate in the direction of flow when analyzed.170

Figure E.9: Flow-directed cell migration is consistent with autologous chemotaxis.171

Figure E.10 CXCL12 binds to the hyaluronan/collagen matrix.173

Figure E.11: Hypothesized mechanism of how fluid flow affects glioma invasion.177

LIST OF SYMBOLS AND ABBREVIATIONS

μm	micron
μM	micromolar
ABP	Actin-binding protein
ATP	Adenosine triphosphate
BCNU	Bis-chloronitrosourea (Carmustine)
BME	Basement membrane extract
Cp	Concentration of gadolinium in plasma
CT	Computerized Tomography
Ct	Concentration of gadolinium in tumor
Ct	Concentration of gadolinium in tumor
CXCL12	Chemokine (C-X-C motif) ligand 12 (aka Stromal-cell derived factor 1)
DAPI	4',6-Diamidino-2-phenylindole
DMEM	Dulbecco's Modified Eagle's Medium
DNA	Deoxyribonucleic Acid
DPPC	1,2-dipalmitoyl- <i>sn</i> -glycero-3-phosphocholine
DSPC	Distearoyl (<i>sn</i> -glycero) phosphotidylcholine
DXR	Doxorubicin
ECM	Extracellular Matrix
EGCG	Epigallocatechin gallate
EGFR	Epidermal Growth Factor Receptor
EPR	Enhanced permeability retention
FAK	Focal Adhesion Kinase
FITC	Fluorescein isothiocyanate

FOV	Field of view
GBM	Glioblastoma
Gd	Gadolinium DTPA
GEM	Genetically Engineered Mouse/Mice
GFP	Green fluorescent protein
GTP	Guanine Triphosphate
HD	Honokiol Derivative
HIF-1α	Hypoxia inducible factor 1 alpha
IACUC	Institutional Animal Care and Use Committee
IB	Imipramine Blue
IC₅₀	Inhibitory Concentration 50%
KPS	Endothelial transfer coefficient
lacZ	β -galactosidase-encoding operon
M199	Medium 199
MGMT	Methyl-O6-Guanine-Methyltransferase
MMP	Matrix metalloproteinase
MRI	Magnetic resonance imaging
Nano-IB	Liposomally encapsulated Imipramine Blue
NFκB	Nuclear factor kappa B
nm	nanometer
nM	nanomolar
Nox	NADPH Oxidase
OCT	Optimal cutting temperature compound
PBS	Phosphate buffered saline
PDGF	Platelet-derived growth factor
PEG	Polyethylene glycol

RECA-1	Rat endothelial cell antibody 1
RES	Reticuloendothelial system
ROS	Reactive Oxygen Species
RNA	Ribonucleic Acid
RSV	Rous Sarcoma Virus
RTK	Receptor Tyrosine Kinase
Src	Sarcoma kinase
TE	Echo time
TMZ	Temozolomide
TPM	Triphenylmethane
TR	Repetition time
UPAR	Urokinase-type Plasminogen Activator Receptor
VEGF	Vascular Endothelial Growth Factor

SUMMARY

Gliomas present a significant clinical burden. In 2008, there were 22,000 new cases of brain and nervous system cancers in adults. The five-year survival rate is markedly poor with only 35% of diagnosed patients surviving. Nearly 20% of the tumors were glioblastoma exhibiting an invasive phenotype that has even poorer prognosis. This results in malignant glioma being the second leading cause of cancer death in middle aged adults. Primary malignant brain tumors are also the second leading cause of cancer death in adolescents. Surgical resection has poor outcomes, and chemotherapy and local therapy do not significantly affect survival. There is an urgent need to develop alternative, more effective therapy for glioma and enhance current treatments for better prognosis.

The primary reason for poor outcomes for glioma after therapy is their invasive nature which, when combined with the need to minimize amount of normal tissue damaged to preserve neural function, almost always leads to incomplete resection. While the standard chemotherapy with temozolomide has enhanced clinical options, this is a cytotoxic agent whose ability to be effective is hampered by invasive tumor fronts being surrounded by normal brain tissue, complicating dosing, delivery and effectiveness.

Therefore it would be useful if there were effective 'anti-invasive' agents that limit the migration of tumor away from the primary site. This ability would enhance the outcomes of surgical resection, and make chemotherapy and radiation more likely to succeed due to the proximity of tumor regions without risking damage to normal brain. Unfortunately, while there are several candidate cytotoxic agents such as temozolomide, BCNU, and doxorubicin, currently there are no effective anti-invasive agents for glioma in the clinic. If an effective anti-invasive agent were identified, we hypothesize that a combinatorial therapy, with an anti-invasive agent that limits the aggressive invasion of

glioma and an effective cytotoxic agent delivered preferentially to tumors would significantly increase the success of treatment.

To test this hypothesis, we proposed to identify an anti-invasive, but not cytotoxic agent by using *in vitro* screening methods. Further, we encapsulated this compound in order to passively target brain tumor to test the efficacy of the compound *in vivo*. Lastly, we determined if use of an anti-invasive agent will enhance the efficacy of current chemotherapeutic compounds *in vivo*.

In all, this thesis encompasses work surrounding the invasion of glioma. Through determination of a compound that will halt invasion in a glioblastoma model without causing cytotoxicity (Chapter 2) we identified a compound, Imipramine Blue. Then, using liposomes and *in vitro* and *in vivo* invasion quantification methods we show that this compound halts invasion and can assist the efficacy of doxorubicin to enhance survival (Chapter 3). In Chapter 4, we co-encapsulated IB and doxorubicin in a single nanoparticle and showed again, enhanced survival but with a disadvantage in survival time. Last, in Chapter 5, we performed a series of experiments, and, along with information from collaborators, determined a plausible mechanism of action of Imipramine Blue through binding of NADPH Oxidase 4. This thesis offers a new method of treatment and validation of the hypothesis that halting invasion can, in fact, enhance common anti-tumor therapy.

CHAPTER 1

INTRODUCTION

1.1 Brain cancers: types and treatments

Brain tumors only affect a small proportion of the adult population, however, the most malignant form, glioblastoma, has such poor prognosis that they are a significant clinical problem. The incidence of brain tumors is about 14 in every 100,000 people in the United States [1]. This is a relatively low proportion when compared to more common cancers, such as breast (124 out of 100,000 women) [2] and prostate (166 per 100,000 men) [3]. However, the success of treatment of these latter cancers is much better than that seen with brain tumors. The 5-year survival rate after brain tumor diagnosis is around 35%, as compared to an average 5-year survival rate in breast cancer of 89% and prostate of nearly 100%. This progress is due to several reasons: 1. There is more funding given yearly to development of new treatments and changes to current clinical treatments and therefore 2. There is more research going into how these cancers grow and develop. 3. Many of these non-central nervous system tumors share commonalities of treatment that are not shared by brain tumors [4, 5].

Brain tumors are different from other cancers treatment and progression-wise due to the environment in which these tumors grow, how they interact with the host environment, and the types of cells from which they develop [6]. For these reasons, brain tumors present a unique and difficult challenge for cancer researchers and neurologists alike. This has led to failure of treatments commonly used with other cancers when brain tumor treatment is attempted. Hence, it is difficult to advance treatment and survival in this regard. In the following introduction, I will discuss the types of brain tumors and the specific difficulties involved in treatment of the most malignant of these: glioblastoma (GBM). Next, I will highlight the attributes of glioblastoma with an in depth look at cancer cell invasion with a focus on clinical implications of invasion and methodology

for studying this phenomenon. Next, I will discuss particular mechanisms involved in glioma cell invasion and migration with a focus on those relevant to the dissertation work. From this, I will move onto a discussion of the types of compounds currently available as anti-invasive agents preclinically and clinically. Last, I will describe nanocarriers and how they can and are used to assist in delivery of compounds for cancer. In all, we will see that development of agents for brain tumors specifically to halt invasion is a necessary entity and a possible paradigm shift in the battle against this deadly disease.

1.1.1 Types of primary brain tumors

Brain tumors most often develop from glial cells in the brain and hence, are termed “gliomas”. More specifically, the majority of brain tumors in adults originate from astrocytes, leading to the subtype term astrocytoma. There are differing grades of tumors but, unlike non-central nervous system tumors, brain tumors are not staged because they do not metastasize outside of the brain. Grade I and II brain tumors tend to be easier to treat while Grade III and IV are more deadly. Grade I (pilocytic astrocytoma), Grade II (astrocytoma), Grade III (anaplastic astrocytoma) and grade IV (glioblastoma) tumors are defined by the degree of abnormality of the nuclei and involvement of anatomical features [7, 8]. Glioblastoma, the most common form of primary brain tumor, is the most deadly because it exhibits all of these features resulting in extremely rare survival after diagnosis.

1.1.2 Anatomy of GBM

The anatomy of glioblastoma has been well-studied and contains many particular attributes that account for the ineffective treatment of the disease. In 1938 Hans Scherer identified key features that were apparent in glioblastoma, which were henceforth named Scherer’s structures, and include: 1) perivascular invasion, 2) perineuronal satellitosis, 3) subpial spread, and 4) white matter tract invasion [9]. These structures are optimized by

the glioma for diffuse spread of disease. The reasons for this pattern of formation have been partially attributed to protein preference, chemokine gradients, fluid flow patterns, and cell-cell interactions through a variety of studies [10-15]. However, there has yet to be a compound that can combat this type of tumor development. More recently, a more microscopic view of glioblastoma development has revealed particular sub structures in the tumor bulk known as pseudopalisading necrosis [16]. This distinguishing feature results from the growth of small groups of cells resulting in hypoxia (low oxygen levels) and cell death at the center, followed by migration away from this site. This is later followed by induction of growth factors and angiogenesis as the tumor cells survive, selecting for the most invasive and malignant cancer cells [17]. These regions can be seen throughout the tumor bulk as well as in the invading fronts.

1.1.3 Treatment of Glioblastoma

Current treatment of glioblastoma (GBM) is difficult and results in high recurrence rates. Upon display of symptoms of a brain tumor (seizure, chronic headache, loss of consciousness, loss of motor/sensory function) a patient will undergo MRI for detection of the tumor. This is followed by a host of treatments to remove the bulk of the tumor if possible [18]. Patients are then monitored for recurrence. This is standard protocol for treatment of glioma regardless of grade [19]. This line of treatment can often lead to decreased quality of life. Last, if tumor recurs, there are last line treatments given after which there is no ability to treat further. The treatment of glioma is varied depending on grade, but this discussion will focus on the treatment of the most aggressive form: glioblastoma (GBM).

1.1.3.1 Clinical treatments

Clinically there have been many changes in the treatment approaches to GBM, but there have not been any major advances in the survival of these patients [19-21]. The common treatment after detection has several components including: 1. Surgical

resection of tumor from the primary site, 2. Lining of the primary site with carmustine wafers designed to kill cells in the close proximity 3. Metronomic oral temozolomide chemotherapy and 4. Radiotherapy to the brain. As mentioned previously, in the case of recurrence, this treatment is coupled with anti-angiogenic therapy to prolong patient life (Figure 1.1).

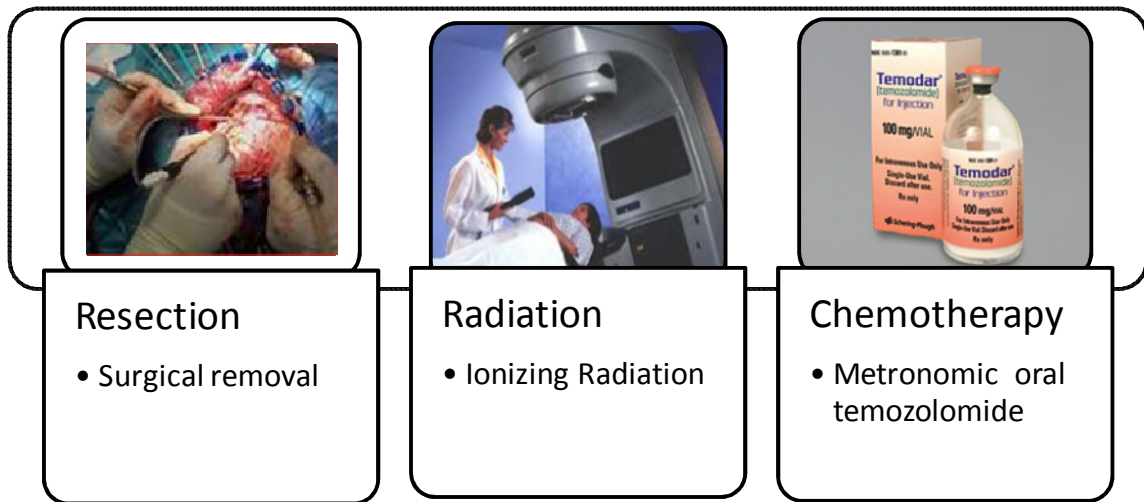


Figure 1.1: Current treatment paradigm for glioblastoma including resection, radiation and chemotherapy with temozolomide, a DNA alkylating agent. After this treatment fails, anti-angiogenics are given to halt glioma growth and eventually lead to recurrence.

Surgical Resection is the removal of the tumor from the primary site by a skilled neurosurgeon. The general procedure involves craniotomy followed by suction of tumor from the site. Though there are experimental imaging agents, such as optically visible fluorescent dyes coupled with intravital magnetic resonance imaging of the brain for guidance and assessment of accuracy and completion, this is not an exact science [19, 22-24]. The skill of the neurosurgeon is vital to success and speaking with neurosurgeons they describe that the “feel” of the tissue is the defining factor [personal

communications]. Once the tumor is removed, surgeons often remove extra tissue between 2-10 mm of the border in an attempt to remove any extraneous cancer cells [25].

Local chemotherapy is applied in the resection site after removal of the bulk in the form of Poly (lactic-co-glycolic acid)-BCNU wafers that slowly degrade and release the chemotherapeutic BCNU (Carmustine®) into the resection site [26]. This technology has been reported to yield a slight increase in survival times, as opposed to leaving the tumor site empty, however, it still does not allow adequate decrease in recurrence. Use of this BCNU wafer has become less commonplace due to both cost-benefit analysis and preference of use by surgeons [27, 28]. Since development in the 1990's, many alternative therapies have been developed pre-clinically to fill the site of resection, but thus far there is not a better option for local chemotherapy [29]. However, stereotactic radiosurgery (SRS) is being used clinically with some success in reducing regrowth of tumor and is a viable replacement after bulk resection [25, 30].

Systemic Chemotherapy in the form of orally delivered temozolomide (TMZ) is given metronomically to patients post-surgery (as well as to those bearing non-surgically accessible tumors). Findings in the New England Journal of Medicine in 2005 showed that coupling of this treatment with current resection and radiotherapy yields a significant increase in survival time compared to resection alone [31]. Other chemotherapeutics have been tried but are unsuccessful in the clinic. Most promising of which, in animal studies, is liposomal Doxorubicin (Doxil ®, Caelyx®), however, clinical studies using free Doxorubicin have tainted use of this product in brain tumor patients due to toxicity [32]. Temozolomide (TMZ) is a DNA-alkylating agent which acts to induce apoptosis in cancer cells through randomly quieting genes in an epigenetic manner. Though effective overall, many patients are resistant to TMZ due to upregulation or overactivity of the gene methyl-guanine-methyl-transferase (MGMT), which acts to undo the methylation performed by TMZ thus reducing its effect [33]. Patients are often screened for overactivity of this gene after resection to determine use of this drug [34]. Another

problem with TMZ is the side effects from the oral delivery [35], however, this effect has been reduced due to the metronomic on/off scheduling of the treatment. TMZ has benefits reported in pre-clinical research, showing inhibition of invasion of glioma cells, though there are contradictory reports citing TMZ as a cause of far-distant metastases in the brain [36, 37]. These discrepancies are likely due to the response of different tumor models and patients to the compound and resistances therein.

Radiotherapy involves the use of gamma-irradiation in order to induce cell death through DNA damage. This therapy is used in over 50% of all cancer patients at some point during treatment and has been in use in cancer for almost a century [38]. In brain tumors, this treatment works by sending gamma rays through to the site of the tumor to directly damage DNA, but in longer-lasting effects, create free radicals which can go on to cause further damage [39, 40]. Radiation therapy involves not just radiation of the tumor, as would be desirable, but irradiation of an area which can include both tumor tissue and healthy brain tissue. This treatment can, therefore, be difficult on a patient with neurological detriments reported after treatment [41]. Radiation can result in death of large amounts of the tumor, however, recent discoveries suggest that radiation may actually be causing side effects which can aid in recurrence. For example, research in rats has shown that irradiating the mammary fat pad prior to injection of non-malignant pancreatic cancer cells causes them to have a more malignant phenotype leading to invasion [42]. Additionally, glioma cells exposed to radiation *in vitro* show increased invasion post treatment, indicating enhanced malignancy of disease [43]. Further, radiation leads to many side effects associated with cancer malignancy and disease progression, including the creation of free radical species, degradation of the extracellular matrix, inflammation and immune cell recruitment, and increased blood flow to the area [40, 44, 45].

Anti-angiogenic therapy has traveled a bumpy road in the past ten years since its advent. Most therapeutics were designed as monoclonal antibodies against Vascular

Endothelial Growth Factor (VEGF), this drug acts by scavenging VEGF and preventing the tumor from promoting angiogenesis through endothelial cell recruitment and tube formation [46]. The most common agent, bevacizumab (Avastin ®), was first successful in colorectal cancer yielding phenomenal results which led to clinical trials in many other cancers [47, 48]. However, a growing body of evidence suggests that for many cancers, including those of the brain, bevacizumab is actually detrimental to the ability to “cure” the disease [49]. This has been attributed to later effects occurring from loss of vasculature. Therefore, there has been a move towards normalization of tumor vasculature in place of complete removal to prevent these effects [50]. Thus, in brain tumor treatment, use of these compounds is only used after other treatments have failed repeatedly to prolong life.

1.1.3.2 Experimental treatments

Many experimental treatments involve combinations of many existing FDA-approved drugs for both brain cancer and other forms of cancer [51-54]. To date, none of these combinations has been stronger at halting the progression of disease better than the currently implemented therapy. In the clinical trial setting, there has been a push for novel cancer prevention agents (EGCG, antioxidants, curcumin), novel anti-invasive agents (Marimastat®), and novel inhibitors of specifically active proteins (EGFR, Src, PDGF) [55-58]. Cancer preventive agents range in activity, including simple antioxidants which act to scavenge free radicals from areas of potential tumor initiation, more advanced compounds which may have antioxidant activity, and compounds that work downstream of antioxidant induced changes (e.g. NFκB activation) [59]. These compounds are difficult to move to market because they are “preventive” in nature and thus, if not included in dietary needs, could be difficult to both study clinically and maintain patient compliance.

1.1.4 Physiology of GBM

Hanahan and Weinberg defined the hallmarks of cancer ten years ago and recently offered a revised version to account for the ever growing list of implicated biological changes that contribute to progression of disease [60, 61]. Like all cancers, brain cancer cells are defined by the many malignant characteristics inherent to the disease, including an unedited proliferative capacity, a resistance to inhibitory and apoptotic signaling mechanisms, and a self-sufficiency in growth factors. Furthermore, there are attributes that involve the interaction of the cells with their environment including inflammation, angiogenesis, and invasion. Outside of the hallmarks of cancer typically applied to the disease there are other commonly recurring themes in glioblastoma such as hypoxia, extracellular matrix properties (e.g. stiffness), and stromal cell interactions which can progress the disease [61, 62]. Further, these properties all affect the development and implementation of therapeutics.

1.1.4.1 Cell growth and death

The ability of tumor cells to proliferate unendingly is a vital step in their growth and malignancy. Further, cancer cells have the ability to evade apoptosis through ignoring death signals (e.g. TRAIL ligand binding, caspase activation), but also through self-sufficiency of growth signals (e.g. EGF, PDGF, VEGF) [63]. These changes are the primary targets of many anti-tumor agents. Taxanes inhibit cell division. Anthracyclines, alkylating agents, and radiation induce DNA damage leading to apoptosis. Growth receptor inhibitors inhibit self-sustaining growth and can lead to apoptosis. Death receptor inducers directly trigger apoptotic signaling [64]. While the other classes are universally used, the receptor targeted molecules are highly specialized and often, the efficacy of these compounds can be pre-screened based on inherent tumor mutations during biopsy [65].

1.1.4.2 Inflammatory microenvironment

Recently, the hallmarks of cancer were amended to include inflammation and interactions with the host immune system as part of the disease progression [66]. In cancer, the immune microenvironment plays an important role in the ability of the disease to persist and invade. In systemic cancers, this is vital for metastasis and proliferation. It is proposed that the cancer actually acts to train T-cells in the immune system creating an immunoprivileged microenvironment in which the cancer can persist. In the brain, an already immunoprivileged organ, this is particularly striking as immune cells infiltrate and assist in development of disease [67]. There has been evidence of T-cell infiltration into glioma from systemic circulation as well as macrophage and dendritic cell homing [68]. Further, the inflammatory microenvironment of the brain is highly activated during glioma progression. Reactive astrocytes and microglia can be found throughout the tumor bulk. These reactive glial cells have been implicated in enhancing secretion of many chemokines and growth factors that lead to a more invasive tumor phenotype. Astrocytes are involved in crosstalk with tumor cells that, through an uPAR mediated mechanism, causes increased secretion of matrix metalloproteinases [69]. Microglia are known to secrete CXCL12 and EGF, which can cause increased tumor cell proliferation, angiogenesis, invasion and reduced apoptosis [70, 71]. In all of these cases, the glial cells are initiating inflammatory responses to the tumor and thereby can increase its malignancy. This response causes difficulties when translating *in vitro* or preclinical study results to *in vivo* or human neoplasms.

1.1.4.3 Sustained angiogenesis

Angiogenesis is a hallmark of the most malignant forms of brain cancer and is nicely reviewed in [72]. As a tumor develops the individual cells begin to proliferate at a high rate, until eventually, there is not enough nutrient supply to sustain the cells. At this point, the cells either die via necrosis, leading to the trademark necrotic cores of solid

tumors and the pseudopalisading necrosis of glioblastoma, or they begin to recruit blood supply [72]. This can either happen through co-option of nearby blood vessels or through neo-angiogenesis by tumor cells [73]. The angiogenesis resulting from endothelial cell recruitment through growth factors such as VEGF or angiopoetin results in sustained angiogenesis. These factors are highly expressed in glioblastoma [74]. This process is similar to that seen during wound healing and development, and thus, is highly disorganized and leads to the altered vasculogenic state of tumor as compared to healthy tissue. This disorganization is advantageous for targeting and will be discussed further in the nanocarrier delivery section. There have been many therapeutics aimed at inhibiting angiogenesis and thereby starving the tumor of nutrients [75]. However, more recently, the idea of ablating the vasculature has met high criticism because of the ensuing tissue invasion and increased malignancy of tumors once this treatment has occurred [49, 76]. Further, once the vasculature has been removed, systemic delivery to the tumor is lost as the primary conduits are gone. Therefore, there has been a recent push from the tumor angiogenesis community to move more towards a model of vasculature normalization and away from eradication [50]. In this way, it is proposed that delivery of chemotherapeutic agents can be more steadily delivered and the tumor almost maintained in a quiescent state, as opposed to enhancing the invasive potential.

1.1.4.4 Tissue invasion

Complementary to angiogenesis is invasion of cancer cells into healthy tissue. Without invasion, it would be difficult for cancer cells to recruit and allow formation of blood vessels [77]. In glioblastoma, the histopathological feature of pseudopalisading necrosis is a result of a multistep process whereby cancer cells proliferate, necrose, invade, and then secrete blood vessel recruitment factors [16]. Invasion will be discussed in greater detail in section 1.2.

1.1.5 Animal models of glioblastoma

There is no consensus on the appropriate model for glioblastoma in the literature [78-81]. However, there are certain attributes and factors that must be taken into account when deciding on the appropriate model. The choice depends largely on the application and outcome measures desired. The models fall into several categories. There are implantable, or injected models, and inducible, or external stimulus driven models; xenograft, human tumor in an immunocompromised animal, or syngeneic, where species are the same for tumor and host; and orthotopic, within the brain, and flank models which are location dependent. These categories are not mutually exclusive and the cost and benefits along with examples of each are listed in **Table 1.1**.

Table 1.1: Categories of tumor models. Taken from a survey of the literature [78-82].

Model	Benefits	Drawbacks	Examples
Xenograft	Human model, derived from patient GBM	Immunocompromised animal, can vary on implant success	U87MG, LN229
Syngeneic	Intact immune system, efficient gliomagenesis, invasive	Rodent derivation,	C6, 9L, RT2, GL261
Implantable	Consistent growth and location, efficient gliomagenesis	Quick growing, don't resemble normal tumor development	Any model above
Inducible	Better mimic normal tumor development	Wait time can be long and varied, inconsistent location, rely on a single mutation	H-Ras, v-Src transgenic; PDGFR-B transfected
Naturally occurring	Mimic tumor development, consistent with human GBM features	Only occurs in dogs and non-human primates, logistically difficult	Canine GBM in Boxers
Orthotopic	Tumor grows in its normal environment	Tumor size is limited, imaging in the head is difficult	Any implantable or inducible model
Flank	Imaging is simple, tumor can grow to human-size	Does not mimic the natural environment-loose GBM structure	Any implantable model

1.1.5.1 Selection of a model of glioblastoma

The difficulty in selecting a model is to determine how closely they resemble the human form of glioblastoma and how closely they mimic the genetic make-up of human glioblastoma. Further, it is important to know what attribute of glioblastoma you are interested in testing be it invasion, angiogenesis, or proliferation. Several of the most common models are highlighted in **Table 1.2** with their derivations. The most widely used model of GBM for testing is U87MG. This is a human derived cell line from a female patient in 1966 [83]. This cell line is popular for its invasive phenotype *in vitro* however, upon cortical implantation in nude mice, it is not very invasive. Further, as with all xenograft, human models of glioma, the immune system must be compromised in the animal and this can affect outcomes of experiments. Rodent models of glioma are generally created through induction of tumor by chemical means (BCNU) or viral infection (RSV) followed by maintenance in culture [78]. These models have the appropriate immune response to cancer which can aid in its development, and they are also more robust *in vivo* due to minimization of tumor rejection by the host. Further, many of these models show invasive phenotypes to varying degrees including RT2, GL261, and C6. Newer models of glioblastoma involve development of genetically engineered mice (GEM), in which an oncogene can be turned on and a tumor will begin to develop [79, 81]. These models more closely resemble the development and progression of glioma in humans (unlike the implantation models which grow very quickly), but they can be unpredictable in establishment and location, making treatment difficult.

Table 1.2: Animal models of glioma taken from a survey of the literature [78-81, 84, 85].

Model name	Origin	Similarities to Human GBM	Used to test
9L	Rat, carcinogen induced cell line	Immune response, angiogenesis	Chemotherapy, radiation, vaccine
C6	Rat, virus induced cell line	Immune response, angiogenesis, invasion	Chemotherapy, resection, radiation, gene therapy, immune therapy
RT2	Rat, virus induced cell line	Immune response, angiogenesis, Scherer's structures	Chemotherapy, radiation, gene therapy
GL26	Mouse, MCA induced cell line	Immune response, angiogenesis	Chemotherapy, radiation, immune therapy, vaccine
CNS1	Rat, NMU induced cell line	Immune response, angiogenesis	Chemotherapy, radiation, immune therapy
U87MG	Human, patient derived cell line	Genome, angiogenesis	Chemotherapy, resection, radiation, gene therapy, vaccine
U251	Human, patient derived cell line	Genome, angiogenesis	Chemotherapy
Primary Neurosphere	Human, primary cells from patient	Invasive (with Scherer's structures), heterogeneous cell population, primary cells, angiogenesis	Chemotherapy, stem cell specific therapy
Genetically Engineered Mouse Model	Mouse, mutation specific induction	Invasion, development of disease, progression of disease, variability in groups	Chemotherapy, protein specific therapy

1.1.5.2 Tumor visualization methods

The ability to visualize the tumor once growing in an animal model is of high importance because it can dictate the type of information and measures used in a single study. This can weigh heavily on model selection depending on the scope of the research. There are two main categories of techniques that include *in vivo* live imaging and *ex vivo* postmortem imaging that can be used for analysis. The former is a newer category that can include a large range of techniques and use of different imaging agents nicely reviewed in [86]. The latter is more straightforward and involves mostly histological analyses or specific tumor cell identification methodology.

Live Imaging has the ability to give you more within subject information throughout an experiment. With decreasing cost of methods and increasing abundance of molecular imaging agents available these techniques are becoming more commonplace. *Optical Imaging* through near infrared or bioluminescent imaging allows low resolution detection of molecules and tumor cells [86]. This is particularly useful in biodistribution studies to detect clearance and general organ distribution over time of new therapeutics [87, 88]. Further, this technique can be used for tracking of tumor growth and has been used with U87MG and 9L models of glioblastoma *in vivo* in survival studies, yielding more information as to the growth kinetics and response to treatment [89, 90]. This technique has been used to detect MMP levels, EGFR expression and cell death via Annexin V staining in separate experiments resulting in increased information after treatment and in development of tumor models [91-93]. *Computed Tomography (CT)* and the higher resolution microCT are often used to determine the angiogenic state of the tumor as it grows and in response to treatment [94]. In particular, with angiogenesis research, this technique has been important in understanding the leakiness of vasculature live when formerly this was a postmortem analysis.

Postmortem analysis primarily involves removal of the brain containing tumor and subsequent immunohistological methods for tumor definition. This can be followed or supplemented with a variety of staining techniques for particular proteins or advanced image analysis methods for determination of tumor morphology and characteristics. [95] offers a good review of many of these techniques and they will be discussed for invasion in particular in section 1.2.

1.2 Invasion of glioblastoma

As aforementioned, glioblastoma invasion is a significant attribute of the disease. There are particular patterns in the brain by which GBM cells invade which have already been highlighted. Further, the invasion of glioblastoma is intricately linked with other

attributes of its malignancy including angiogenesis. In this section we will look in depth at how invasion is determined clinically and explored experimentally.

1.2.1 Invasion in a clinical context

Brain tumor invasion is the single most important attribute for failure of therapy in the clinic. The first documentation of invasion in glioblastoma patients dates back to the 1800's, however, only recently, has a significant effort been put forth to try and observe the invasive front of tumors [9]. With MRI scans, it has been possible to determine the course of treatment based on contralateral involvement and extent of invasion. Through recent use of diffusion tensor imaging, the degree of invasion can be more distinctly seen, as determined by the anisotropy of proton relaxation rates [96]. This is preliminarily being used to better assess the borders for radiation treatment [97]. In most cases though, tumors are resected as usual and the degree of invasive potential is determined by the degree of differentiation of the cells histologically [7]. Where invasion comes into play more is in the response to treatment in the clinic and recurrence as multi focal tumors arise.

1.2.1.1 Failure of first-line treatment

The first line of treatment involves surgical resection, followed by rounds of radiation therapy and chemotherapy with temozolomide [98]. This treatment fails in the majority of cases, and this is largely due to the invasive characteristics of the glioblastoma. Resection is limited by surgical experience and availability of equipment such as MRI for intraoperative monitoring of tumor removal [24]. Though many intraoperative imaging agents are in preclinical stages to enhance tumor borders and aid in tumor removal, most surgeons still rely on the feel of the tissue and MRI to determine tumor edges [99]. This technique still results in the inability to remove the entire tumor due to the invasion of cells into the healthy brain. Similarly, due to the invasion of cells, radiotherapy will miss many of the tumor cells in the brain in order to prevent damage to

healthy tissue. Chemotherapy is delivered systemically and enters the tumor via the blood vessels and thus is limited by diffusion through the tumor [100, 101]. This means that often chemotherapeutics cannot reach invading cells and thus do not kill them.

1.2.1.2 Induction of invasion by treatment

It has been purported that all of the methods of treatment of glioma can lead to invasion of tumor cells into healthy tissue in some animal or human case. These changes have been proven to various degrees but it is difficult to determine what is attributable to the treatment versus progression of the tumor after longer survival in the patient. The most direct links with invasion and treatment are between radiation therapy and anti-angiogenic therapy [43, 49]. In other cases, resection has been shown to increase malignancy of tumors through a stem cell proliferation effect termed repopulation [102]. Chemotherapy causes a large range of alterations in malignancy of cancer cells [20]. However, the degree to which this process is accelerated as opposed to tumors that are untreated is unknown due to survival effects.

Radiation is closely linked with increasing tumor invasion in several different types of tumors *in vitro* and *in vivo* including glioma, breast cancer, and prostate cancer [103]. This effect is highly pronounced and appears to have to do with both low radiation levels to the tumor cells themselves and through effects on the surrounding tumor stroma that can lead to increased invasion. Using human breast carcinoma cells, it was seen that irradiating the injection area before injecting the tumor cells enhanced the invasion and metastasis of the cells upon implantation [104]. Further, it has been shown that irradiation causes activation of fibroblasts in the tumor area which enhances the invasive potential of prostate cancer cells through cell-cell interactions [42]. In glioma, *in vitro* studies have indicated increased invasion when low-dose radiation is applied in culture in both U87MG and C6 tumor model [43, 105-107]. Last, radiation therapy in glioblastoma is rarely contained to just the tumor due to the ill-defined borders and desire to reach all

invasive cells. This can lead to priming of the stroma and area around the tumor yielding increased invasion [42]. Radiation also acts to activate astrocytes and microglia which could also enhance the invasive potential of the tumor [105].

Anti-angiogenic treatment as previously alluded to, yields enhanced invasion in many tumor types. Each year, new evidence correlating anti-angiogenic therapy with enhanced tumor invasion surfaces, bringing the usefulness of treatments such as sunitinib and bevacizumab into question [108]. Though there have been effects in many different cancer types, in glioma this effect is particularly pronounced. Used as a last line of treatment in glioblastoma because it extends life by a few months, the invasiveness of the tumor into the brain is apparent postmortem. It is thought that the invasion is enhanced due to the removal of blood supply, yielding increased hypoxia in the regions of high proliferation [46]. This effect results in a lot of cell death and necrosis, but also causes switching on of many pro-invasive factors that will yield increased migration away from the tumor site [46, 77]. This change can also be seen after treatment with chemotherapeutics that affect blood vessels, but it's not as enhanced as with the anti-angiogenics [109, 110].

With chemotherapeutics, it has been observed that treatment of brain tumors can lead to far-distant metastases in humans and animal models. This can be due to the increase in invasion accorded to the reduced blood supply; however, it is often attributed to the clonal selection that can result from treatment [111, 112]. It is known that glioma stem cells, a subpopulation of highly proliferative and invasive tumor cells, show resistance to apoptosis induced by etoposide, camptothecin, cisplatin, temozolomide, doxorubicin, vincristine, and methotrexate at doses that are toxic to comparable non-stem cell populations [113]. This is also highlighted by the tenacity of cancer stem cells to establish tumors. It is known that through implantation of a single cancer stem cell, a tumor will establish and grow to normal proportions, hence highlighting the particularly dangerous nature of leaving these cells behind after treatment [114]. Further, these cells

are commonly localized to the invasive front of tumors and along blood and lymphatic vessels of solid tumors during their development indicating an association with these tumor elements [115]. The ability of chemotherapy to actually induce invasion is thought to be largely through this selection mechanism of the most deadly of the cancer cells. Therefore, though the effect is slightly delayed as compared to the anti-angiogenic treatment, the results are the same in the long run.

The last area of treatment and its effects on invasion is more controversial. The surgical removal of brain tumors is necessary due to the immense pressure increases within the brain and the ensuing symptoms. It is known that in the most invasive brain tumors, resection does not remove the entire tumor, which is why this treatment is coupled with radiation and chemotherapy. However, the degree to which resection actually aids in the invasive and proliferative potential of the tumor cells left behind is speculative. Models have been developed explaining the recurrence of tumors in the resection site post surgery indicating an increased propensity to proliferate and resist cytotoxicity of this population [98, 116]. However, this effect could be due to the fact that the tumor cells left behind are often the invasive cancer stem cells which have tumor generating potential. One observation that does occur only after resection is the presence of metastasized tumors outside of the central nervous system [30]. Several case studies have been documented with patients showing metastasis in the cervical lymph nodes, the draining lymph nodes from the brain vasculature, and in other regions of the body [117-119]. It is highly unusual for brain tumor cells to be found metastasized outside of the brain and the reasons for this are largely not understood. In recent studies it is thought to be due to the large blood brain barrier disruption that occurs during surgery as the tumor is dissected away leaving hemorrhaging blood vessels where tumor cells can enter. This is a largely unstudied area though, as it is a rare occurrence and therefore there are few to no hypotheses. Regardless, the invasion of glioma cells is closely connected with the success and future outcomes of treatments.

1.2.2 Methods for measuring invasion *in vivo*

Methods for measuring invasion *in vivo* are only recently moving into the clinical setting. The development of advanced MRI methods such as diffusion tensor imaging is the primary method that can be used to visualize invasive fronts in tumors. This is now being used clinically to reassess the tumor margins for subsequent radiotherapy to prevent unnecessary damage and invasive side effects. Other than this methodology, invasion is only really observed after or during treatment using MRI for after recurrence. The development of methods for assessing this attribute of tumors is only now gaining focus in the clinic in a pre-treatment sense.

In animal models, measuring invasion is becoming a more common part of survival studies and drug response monitoring. The use of diffusion tensor imaging is a possible technique, though size limitations in rats makes this type of imaging difficult as the induction of gradients through the brain are necessary [96, 120]. More common is the use of stably transfected cell lines to monitor invasion live and postmortem for assessment of tumor invasion and treatment response [84, 121, 122].

Postmortem analysis involves the use of marked cell lines for antibody detection and simple distinction from the surrounding brain by reporter genes such as green fluorescent protein or lacZ for β -gal activation and pigment change. Though cancer cells can be distinguished from surrounding brain, these methods make imaging analysis for tumor size and structure simpler and assist the untrained eye in examining the tumor. Similar stable transfections have been successful for **in vivo analysis** of tumor cell invasion, though many imaging modalities are still limited by resolution and signal detection. Use of MRI detectable nanocarriers such as ferromagnetic dendrimers and iron oxide nanocarriers is possible for tracking of cells in the brain though the signal quickly declines as the cells proliferate thus diluting the cytosolic agent[123]. To counteract this problem, cells have been stably transfected to overexpress ferritin light and heavy chain which will act to sequester iron in the cytosol and create an endogenous T_2 enhancement

on MRI. This technique has been successful with C6 glioblastoma [123, 124]. Other methods for determination of glioma invasion *in vivo* are limited by the resolution of the imaging modalities including bioluminescent imaging via endogenous luciferase reporters [125].

Other methods exist to try to understand the invasive molecular profile of the tumor *in vivo* in experimental animal techniques. This can be an indirect measure of invasion and has been successful in detecting the changes in matrix metalloproteinase expression, chemokine secretion, and common markers of invasive and malignant phenotype such as EGFR and uPAR [123, 126]. This result can be achieved through stable transfection resulting in switching on of a fluorescent or bioluminescent marker but can also be delivered systemically. For instance, MMP-cleavable fluorescent probes have been developed that will only give off signal if there is specific MMP activity in the tumor [126, 127]. In this way, it is possible to determine how an experimental compound can affect the phenotype of the tumor without actually seeing the micromorphology of the tumor. However, there is the limitation of having to know a particular function of a tested compound or treatment and how the target molecule affects both the reporter and the tumor phenotype. This validation generally involves postmortem analysis in addition to the *in vivo* live imaging. Further, at this time, these methods are highly experimental and can become very expensive when compared to more traditional histological techniques.

1.2.3 Methods to determine invasion *in vitro*

Since invasion can be difficult to determine *in vivo* in a reproducible, high throughput way, many assays have been developed to examine this phenomenon *in vitro*. In this way compounds can be screened as anti-invasive agents and cell morphology can be examined in a more controlled environment. The evolution of these types of assays has moved from 2-dimensional migration assays based on wound healing to 3-

dimensional invasion assays consisting of tissue culture insert assays. More recently, use of organotypic brain slices has become popular as the movement of cells along structures in the brain can be observed and mimics white matter tract invasion *in vivo*.

Early models for cell migration include the wound healing scratch assay and the agarose spot assay. Scratch assays are popular for fibroblast migration due to the ability to mimic a wound through a monolayer of cells. In this way, the distance of closing of the wound can be examined over time and inhibitors of such migration can be assessed [128]. This assay has fallen out of popularity in the cancer literature primarily due to the inherent differences in how cancer cells invade and how healthy cell types migrate. The spot assay and agarose spot assay is still in use with some modifications. The general principle is that cells are plate in a spot (either in 2D or within an agarose gel) and the radiation outward of cells as they migrate into the gel is measured. Many studies are using this technique with tumor spheroids to assess invasion though agarose is being substituted with naturally occurring extracellular matrix proteins such as collagen and laminin to better mimic the degradation necessary for cell movement [129]. Currently, primary glioblastoma cells are embedded in matrices and can be both assessed for invasion and stained for various markers to determine degree of malignancy for screening of drug resistance, mutations, and transformation [130].

The Boyden Chamber Assay is the most popular of the invasion assays with over 1200 hits in PubMed as of 2011. This assay involves the use of a tissue culture insert with a permeable membrane that will allow cells to pass through. Cells migrate through the pores and into the lower chamber where they can be quantified through imaging or collection and counting. This assay is very powerful for its adaptability and thus has been used with a variety of ECM protein coatings, many different chemokines, with combinations of cells, and in 2D and 3D gels [131, 132]. Modifications of this chamber have also been used for assessment of permeability of endothelial cells layers, interstitial flow examination for lymphatic homing, and live imaging of cell invasion

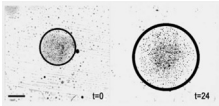
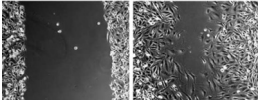

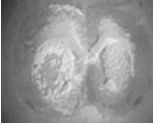
[133, 134]. Further, the commercial availability of a variety of sizes, coatings, and quantification methods has made these assays the most popular choice of cell invasion and migration experimentalists.

Organotypic brain slices are sections of rodent brains that can be maintained in a tissue culture environment for testing of compounds against a more structurally relevant tumor invasion mode [135]. These systems offer the benefit of a more clinically relevant ECM and cell type microenvironment for the cancer cells to interact with and migrate along. They have successfully been used with certain MMP inhibitors to assess degree of inhibition of invasion [136]. Further, they are often used to determine the changes afforded to glioma cells through siRNA mediated inhibition of particular genes. They offer the advantage of *in vivo* systems of being able to view in real time the progression of disease in a more approachable clinical manner without the limitations of imaging and drug delivery [137]. Further, a single animal can be used for screening of multiple compounds or constructs thus minimizing need for large animal numbers. These systems do have drawbacks though. For one, they can be difficult to work with and must be equilibrated in culture for 6-8 weeks after initial explants. Because of this, many of the cell types will die and the actual slice, though beginning as thick as 800 μ m, will flatten to an almost 2-dimensional substrate. Therefore, many of the conclusions that can be drawn from these systems are not directly relatable to the *in vivo* environment however they do offer a nice alternative for particular applications. All of these invasion assays are summarized in **Table 1.3**.

Newer invasion assays have been largely modifications of these pre-existing assays and mostly focus on increasing throughput or enhancing *in vivo* translatability. Examples include use of microarray type 3D printing arrays for testing of compounds on clinically relevant ECM substrates, use of perfusion chambers for the organotypic brain slices to enhance cell-cell interaction capabilities, and development of live cell migration acquisition systems that monitor cell movement across a plate tracking velocities and

persistence [128, 138]. Further, microfluidics chambers for migration studies are highly desirable due to the ability to create and maintain specific chemokine gradients and integration of the aforementioned attributes such as three dimensionality, high throughput screening and clinical relevance [139-142].

Table 1.3: Common invasion and migration assays used in cancer research. Adapted from [128, 131, 132]

Assay	Benefits	Drawbacks	Example
Agarose spot assay	Imageable, 3D, adaptable to other matrices	Non degradable by cells, imaging involved, low throughput	
Scratch assay	Imageable	No assessment of invasion, imaging involved, low throughput	
Boyden Chamber assay	High throughput, adaptable to a variety of factors	Special equipment required,	
Organotypic brain slice	Resembles <i>in vivo</i> environment, aesthetic	Requires animals, difficult procedures, low throughput	

1.3 Mechanisms of brain tumor invasion

1.3.1 Cellular aspects of invasion

Invasion is a hallmark of brain tumor progression and is the result of a coordinated effort of many intracellular events. A cell is stimulated to invade through many extracellular and intracellular cues resulting from itself, surrounding cells, and the microenvironment. The stimulation of migration is attributed to chemokine gradients and signaling, structural cues such as matrix stiffness and fiber alignment, and cell-cell signaling from the surrounding environment [15, 143]. These characteristics of invasion stimulation are more difficult to control as they involve alteration of the tumor microenvironment. Therefore, much of anti-invasive therapy development has focused on individual cells. For a cell to invade, it needs to be able to alter its connections with the microenvironment through changes in adhesions and matrix composition, and then alter its cytoskeleton to adequately propel forward [144].

1.3.1.1 Adhesion

Cells maintain adhesion to both the extracellular matrix (ECM) and other cells through receptor binding. Adhesion is necessary for most cells' survival and upon detachment they will undergo anoikis. However, cancer cells are able to detach from matrices and cell layers without any effects on viability. A cell maintains binding through interaction of focal adhesions which link the actin cytoskeleton to the cell membrane. These adhesions further interact with a host of different regulatory molecules including integrins, Src, and focal adhesion kinase (FAK) to maintain binding and regulate cell changes [12, 138, 145]. These complexes can contain many different components and therefore, their disassembly and assembly is of vital importance to the dynamics of cell movement and is regulated upstream by Rho-GTPase signaling, and Src kinase through interactions with FAK. In addition, FAK can recruit cytoskeletal proteins and activate RhoGTPases creating a more activated structure and integrating the adhesion process

with cellular cytoskeleton assembly [146]. Src kinase also acts to activate and assemble many of these complex proteins to through homology binding and integration. In cancer, both FAK and Src have been extensively studied. It is known that FAK is highly overexpressed in almost every type of cancer including brain and the degree to which FAK is overexpressed correlates with degree of malignancy in breast, colon, and brain cancer [147]. Src activity is also correlated with degree of malignancy in a host of cancers and has further effects than just those on focal adhesions including cytoskeletal assembly, inflammatory response, and MMP secretion and thus is a highly desirable target for many novel therapeutics [56, 148].

1.3.1.2 Matrix degradation

In order to move through the matrix, cancer cells often need to manipulate the host environment. This can often be avoided by changing route which leads to formation of many of the typical glioma invasion structures mentioned earlier based on cell preferences. However, more often, cancer cells prefer to degrade and alter the environment in which they are growing through degradation of the matrix around them [149]. The most common culprits in matrix alterations are the matrix metalloproteinases (MMPs) which are a class of zinc dependent proteases that degrade a variety of membrane proteins including collagen and gelatin [150]. These proteins are highly upregulated in all cancers, and in brain tumors, MMP-2 and MMP-9, the two gelatinases are overexpressed most universally in tumors [151-153]. These enzymes can also be induced by a variety of intracellular and extracellular signaling mechanisms and cell-cell interactions with normal glial cells [69]. Other matrix degradatory enzymes such as hyaluronidases (degrades hyaluronan) and cathepsin B (degrades laminin) are overexpressed by glioma [154, 155]. Further, glioma cells express and secrete a host of ECM constituents to rebuild the matrix for enhanced motility. A full review of the

interaction of glioma cells with the ECM and its components can be found in [15, 145, 151, 156].

1.3.1.3 Cytoskeleton rearrangement

Along with adhesion assembly and disassembly is the rearrangement of the cytoskeleton. For the cell to protrude forward there must be a large degree of actin polymerization and depolymerization leading to movement of the cell body. Further, the use of myosin to contract the cell as it moves is vital to movement. Last, microtubules and intermediate filaments act to maintain the cell structure internally and hold the organelles in place [157]. Therefore, compounds, such as Cytochalasin D or Paclitaxel that disrupt any of these components can have a large effect on both cell viability and motility. However, many of these compounds are not specific to cancer cells and thus can have toxic side effects on any motile cells.

1.3.2 Actin and invasion

Actin is an essential component of cell morphology and motility and as such, is one of the most well-studied molecules in cells. The role of actin in cancer is largely as a facilitator of cell motility and therefore, therapies that inhibit its ability to structurally change can also inhibit invasion.

1.3.2.1 Types of actin structures involved in cell migration

For a cell to migrate, alteration of the actin cytoskeleton is vital. There are many different structures that a cell can adopt to move through the ECM and invade including filopodia (one dimension), lamellipodia (two dimensions), and in cancers, three dimensional structures called invadopodia [158]. This is a highly specialized structure in cancer cells that is most commonly seen in invading cells. These 3D structures have three primary functions: intracellular signaling, actin reorganization, and membrane trafficking [159]. These functions assist in the ability to protrude into the extracellular space by alteration in focal adhesions, actin filaments, and secretion of matrix proteases.

The development of these structures is regulated by primarily by RhoGTPases and Src kinase, however other intracellular signaling proteins such as PI3K and NFκB can initiate formation and secretion of the proteases [160]. In some cell types, a more specialized actin structure will form called a podosome. The podosome has the same functionality as the invadopodia but is characterized by a ring of focal adhesions surrounding a core of actin filaments [159]. These structures are seen most commonly in healthy cells that have been transformed with constitutively active Src kinase and transformation with Src kinase is the only requirement for development of podosome structures [148].

1.3.2.2 Regulation of actin polymerization and depolymerization

Actin polymerization is one of the oldest studied fields in biochemistry and cell biology. Actin consists of monomer units (G-actin) which are activated with ATP. These monomers assemble into long filaments of actin (F-actin) which will make up the higher order actin structures seen in podosomes, invadopodia, and stress fibers. Actin polymerization and depolymerization is essential to the dynamic motility of cells. Actin provides the fibers along which myosin can contract the cell to propel movement forward and also yield pathways along which intracellular molecules can be transported. There are a host of factors that regulate the process of actin polymerization including actin binding proteins (ABP), the rho GTPases, and other signaling proteins.

Actin binding proteins include a large range of molecules from adhesion complexes, to kinases, to polymerization facilitators. There are many great reviews of actin binding proteins including [161] which covers the various types in general, and [162] which gives more detail about their specific function in cancer progression. In brief, molecules that tend to promote or speed the ability of actin to polymerize and depolymerize are upregulated in cancer and those that cause stability of the filaments are downregulated. This is complicated by proteins that have roles in both functions, such as the profilin proteins, which bind G-actin monomers and can sequester them inhibiting

polymerization or activate them and enhance polymerization [163]. However, this rule holds true for most of the more black and white proteins such as the gelsolins which severs actin filaments (downregulated) and Arp2/3 which is responsible for nucleation of actin filaments (upregulated) [160, 164].

1.3.2.3 Upstream regulators of actin structures

The Rho GTPases are the most well-studied of the upstream regulators of actin polymerization and cell motility. There are three types of Rho GTPases: Rho, Rac, and Cdc42 which are implicated in formation of F-actin is which act by activating polymerization of the actin filaments in a process termed “treadmilling.” [158] In turn, the cell becomes more motile with the ability to push forward with lamellipodia and filopodia to yield bulk migration through ECM. Other proteins, such as scinderin and profilin act as actin regulators by cutting filaments and capping polymerizing ends. Since cells may need to alter their cytoskeletal arrangement at any moment, a baseline level of free actin (G-actin) is pooled in the cytoplasm [165]. Upon activation by the Rho GTPases, these monomers polymerize to form the filamentous F-actin. The ratio of G-actin to F-actin in the cytoplasm regulates the amount of mRNA available to be translated to these proteins [166]. Like the actin protein, actin mRNA is kept in stores in the cytoplasm for translation upon a drop in G-actin in the cell. When G-actin levels are too high, these mRNA stores are degraded leading to a consistent reserve of actin mRNA in the cell. Further, this yields a concise feedback loop where actin controls its own translation. If a drug had the ability to affect any part of this feedback loop by inhibiting actin polymerization the amount of actin mRNA would also decrease leading to an inability of the cell to adequately mobilize [167].

1.3.3 NADPH Oxidases in cell migration

NADPH Oxidases (Nox) are a class of proteins that are responsible for the generation of reactive oxygen species (ROS). When cells are in distress, ROS are produced to enable

a host of downstream signaling effects which lead to rallying of the cells survival system causing migration, angiogenesis, and resistance to apoptosis. This activation is often caused by extracellular events such as inflammatory responses or injury, however cancer cells use this system to their advantage to enable survival. Hence, this system, though not as mainstream as other cancer signaling systems and receptors, is important to the progression of disease [168].

1.3.3.1 Types of NADPH Oxidases

There are six Nox proteins: Nox1, Nox2, Nox3, Nox4, Nox5, and Duox1/Duox2 that function to produce ROS in all cells. Activity of the Noxes is regulated by both expression level changes, and activation by extracellular signals such as PDGF, TGF- β , or angiotensin, as well as intracellular proteins via complex formation and phosphorylation. Nox1-3 are activated by cytosolic subunit regulation including p22_{phox}, p47 and p67 among other variable proteins [169]. Nox4 activation is not fully understood, and Nox5 and the Duox's are regulated by calcium ion concentrations. All Nox family members yield superoxide O₂⁻ and H₂O₂ which can lead to downstream signaling events [168]. Though all family members function in this same way, they are differentiated by the intracellular localization leading to compartmentalization of the ROS that they produce [170]. The ROS react with proteins nearby to alter their function and based on which membrane the Nox proteins are located in they will react with different proteins. Regardless, all Nox proteins are necessary for normal physiological function. Therefore dysregulation or mutation in the Nox proteins leads to a variety of diseases including immune disorders, Alzheimer's, hypertension, atherosclerosis and cancer [171, 172]. The specific function of Nox family members in disease is nicely reviewed in [173, 174].

1.3.3.2. Subcellular localization of Nox Family Proteins

Nox proteins are always associated with membranes but may be located on any membrane throughout the cell. This includes the endoplasmic reticulum where they help to regulate protein translation, the nucleus, where regulation of transcription events can occur, the mitochondria, for metabolism, the cell membrane, for intracellular signaling, and on small endosomes for secretion of proteins. Each Nox protein has been localized to each place for a variety of functionalities. A detailed description of the locations and functions of each protein can be found in [170]. Further, the various Nox proteins have different splice variants. Nox4, for instance, has five known splice variants: two of which localize to the endoplasmic reticulum (4A, 4B), two that localize to the nucleus (4D, 4E) and one that remains in the cytoplasm (4C), likely interacting with endosomes[175].

1.3.3.3. Nox family proteins in cancer

Downstream targets of the Nox family proteins include many common players in cancer progression. This is due to the activation of these proteins by the reactive oxygen species. Similar alterations occur during inflammation and this is one key in the growing evidence that chronic inflammation can result in development of cancer. ROS resulting from all Nox proteins and their ability to enable cancer progression and invasion is nicely reviewed in [176]. In short, ROS lead to a variety of downstream signaling effects involving protein kinase C (PKC), protein tyrosine phosphatases (PTPs), and mitogen-activated protein kinase (MAPK) that can enable a host of phenotypic changes in cells leading to malignant transformation. Further, through activation of NFkB and other proteins, transcriptional level alterations result and cause longer-lasting effects in cells [177]. In all, ROS can lead to induction of every aspect of cell invasion outlined above. Looking at one particular Nox protein, Nox4, which has been shown to increased expression and activity in gliomas, all of these changes are apparent. In fact, it was seen that Nox4 is the most overexpressed of the Nox family proteins in these types of tumors

and that this expression correlates with tumor grade [178]. Further, Nox4 knockdown results in decreased chemoresistance and proliferation yielding a less malignant tumor. Similarly, in studies with cancer cells and Src-transformed 3T3 fibroblasts, Nox4 was found to be essential for the formation of invadopodia and MMP secretion at these sites [179]. Thus, it is apparent that Nox proteins are important to the invasive phenotype and malignancy of cancer in general, and that Nox4 may specifically be an important protein in glioma.

1.4 Molecules that stop invasion

1.4.1 The clinical landscape

There has been an explosion in potential anti-invasive compounds in the past 5 years and many of them are summarized in **Table 1.4**. These compounds are repurposed chemotherapeutics, targeted therapeutics, or chemopreventive agents. For instance, the use of EGCG (green tea) in conjunction with temozolomide against the U87MG model of glioblastoma has shown promise in extending survival in mice [180]. EGCG has been shown to reduce reactive oxygen species and has been heralded as a chemopreventive agent for some time along with acai and lycopene[58]. However, most experimental and more traditional anti-invasives have focused on the ability of compounds to inhibit matrix metalloproteinases (MMPs) and thus limiting invasive progress of cancer cells[55]. One such compound, Marimastat ®, an MMP-2 inhibitor, was developed and showed promise, however in clinical trials, was unsuccessful in enhancing outcomes after treatment in glioblastoma [181, 182]. Since then, MMP inhibitors are still popularly pursued, though growing evidence suggests that assumptions as to the subtypes involved in glioblastoma progression and invasion must be altered [183, 184].

More recently, there has been a shift in the development of novel drugs to that of more personalized therapy. In these cases, specific receptors and signaling molecules are

targeted for inhibition in order to kill cancer cells. Treatment can be modified to the individual cancer type and patient which is advantageous in reducing side effects. They work often by relying on receptor addiction of the cancer cells meaning if the receptor becomes useless through blocking, the cancer cell will almost go through withdrawal and can die [185, 186]. However, this is not known to occur with all potential targets and it is always possible that pathways will be rerouted to compensate. This type of treatment often has a side effect of halting invasion of cancer cells though more commonly treatment leads to cell death. A recent review highlights many of these compounds and their potential anti-invasive effects based on the target molecule for which they were developed [187]. However, the exact anti-invasive effects are unknown for most of these compounds based on lack of in depth studies of invasion opting instead for survival and tumor growth measures.

Most of the targets of this type of therapy are receptor tyrosine kinases (RTKs) which, upon activation by a ligand, will change conformation and phosphorylate intracellular signaling proteins leading to downstream events [188]. In cancer, these receptors are often mutated to be constitutively active and thus require no growth factors to function. A cancer cell can actually become “addicted” to this activation and so by turning it off, the cell will die. This phenomenon and the genes that are privy to it are reviewed in [186]. Inhibitors of RTKs are most often antibodies due to the high specificity. The more notable RTK inhibitors are Herceptin® (against EGFR), Avastin® (against VEGF), and Tarceva® (against PDGFR). These are all used clinically for different types of cancers and have been thought to have possible anti-invasive effects due to their signaling pathways involving targets for invasion [187]. However, there is insufficient evidence to tie their effects to halting glioma invasion and as aforementioned, *in vivo*, Avastin causes glioma invasion[189]. EGFR inhibition is particularly exciting due to the overexpression or mutation of EGFR in >60% of glioblastomas and alteration of glioblastoma to express EGFRvIII causes a more invasive phenotype of cells *in vitro*

[190]. However, these compounds are expensive and difficult to work with. Further, their actual role in invasion prevention is yet to be seen due to the far-reaching effects of the involved pathways.

Inhibitors of downstream proteins such as Src-kinase have shown promise in inhibiting tumor growth and progression [56]. Based on the ability of Src to increase all attributes of an invasive phenotype including cytoskeletal remodeling, MMP secretion, and adhesion disassembly, it was tested for anti-invasive activity. This treatment inhibited invasion in brain, prostate and breast cancers while also inhibiting growth, angiogenesis and proliferation.

Table 1.4: Molecules showing or predicted to have anti-invasive activity in glioma

Inhibitor	Binds	Inhibits	Status
Erlotinib/gefitinib/lapatinib	EGFR	growth, invasion	Phase II/III
Dasatinib/imatinib/tandutinib	PDGFR	growth, invasion, angiogenesis	Phase II
AZD4547	FGFR	growth, invasion	Phase I
XL184	Met	growth, angiogenesis, metastasis	Phase I
WP-1034/LLL12	JAK-STAT	growth, invasion, angiogenesis	Phase I/II
Perifosine	AKT	growth, invasion	Phase I/II
BEZ235/XL765	PI3K	growth, invasion, proliferation	Phase I
Sunitinib	Tyr Kin	Growth, angiogenesis, invasion	Phase I
TLN-4601	Ras	Growth, invasion, proliferation	Phase I
Sorafenib	Raf	Growth, invasion, proliferation	Phase II
WX-671	uPA	Invasion, proliferation	Phase II
PD169316	MAPK	Growth, invasion, proliferation	Preclinical
AP120009	TGF- β	Growth, invasion, proliferation	Preclinical
Everolimus/rapamycin	mTOR	Growth, invasion proliferation	Phase I/II
Dasatinib	Src	Growth invasion proliferation	Phase I
Marimastat	MMP-2	invasion	Phase II
AMD3100	CXCR4	Growth	Phase II
Geldanamycin	Hsp90	Survival, growth, migration	Preclinical
EGCG	ROS	Growth, invasion, angiogenesis	Preclinical

1.4.2 Experimental methods

Other treatments to halt invasion involve genetic interventions using DNA, siRNA, and microRNA delivery via a host of transfection methods [191, 192]. These therapies are all in animal phases at the moment, largely due to the invasive nature of the interventions and the difficulties in the past twenty years with gene therapy in clinical trials. The advantage to these interventions is the ability to directly target specific genes necessary for glioma invasion without need for design of a novel drug and determination of a particular target. However, like all compounds, there are delivery issues associated with these treatments as well as possible unforeseen side effects.

1.5 Nanocarriers for drug delivery in cancer

Upon design of novel compounds and in development of the therapeutics, there is often difficulty in modulating delivery. There is a desire to target the tumor without causing adverse side effects to the rest of the body. Often, drugs will fail from *in vitro* to *in vivo* translation due to poor pharmacokinetics and pharmacodynamics that lead to poor outcomes of anti-tumor effect. Lastly, once the drugs arrive at the site, there may be difficulties in cell uptake and monitoring effect at the site. To overcome these obstacles, nano-sized carriers have been developed to aid in providing reliable and tunable delivery and activity profiles regardless of the compound being delivered.

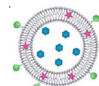
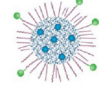
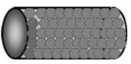
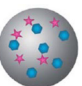

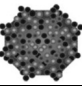
Nanocarrier is a term generally applied to submicron sized particles in cancer, are primarily used as drug delivery vehicles. They have a close history with chemotherapeutics as many of the early developed nanocarriers were for encapsulation of these types of drugs [193, 194]. This is mainly due to the great advantages afforded by encapsulating chemotherapeutics. Namely, reduction in cytotoxicity is afforded through use of nanocarriers through the ability of these to selectively accumulate at tumor sites with reduced toxicity to non-target organs [195, 196]. Second is the ability to modify these types of particles with targeting agents to enhance accumulation at organ sites

further [197]. Lastly, there is the advantage of delivering multiple compounds or agents into a single particle to overcome drug resistance, improve the efficacy of delivery and drug activity. However, though these are advantages to nanocarriers in general, each type of particle comes with specific advantages and limitations and thus selection of a type to use specifically for cancer requires balancing on these factors.

1.5.1 Types of nanocarriers

There are many types of nanocarriers that have been successfully synthesized and used in cancer models [198, 199]. Some of the more popular nanocarriers are highlighted in **Table 1.5**. These variants fall into a few classes of nanocarriers based on the material and method by which they are synthesized which alters the pharmacodynamics and pharmacokinetics *in vivo*. For instance, polymeric nanocarriers are useful because of the well-characterized and tunable degradation rates and thus drug release profiles. Liposomal nanocarriers offer advantages of dual encapsulation based on hydrophobicity of drugs and use of naturally occurring materials reducing immune response. Other compounds, such as dendrimers, which are based on conjugation of drugs as opposed to encapsulation are useful for delivery of both drugs and genetic material.

Table 1.5: Types of nanocarriers used for cancer drug delivery

Nanoparticle	Components	Examples	Image
Liposome	Lipid bilayer with aqueous core	Doxorubicin in aqueous phase	
Micelle	Amphiphilic with hydrophobic core	Paclitaxel	
Carbon Nanotubes	Cylindrical carbon allotrope	Amphotericin B	
Polymer nanoparticles	Solid particle made by emulsion	Vincristine in PLGA	
Dendrimers	Branched macromolecule	5FU combined with microRNA	
Viral-based nanoparticles	Virus capsid with inorganic contents	Doxorubicin	

Further, the FDA approval status for many of these nanocarriers is important in moving molecular delivery systems to clinic. Beginning with a more novel drug delivery vehicle, such as carbon nanotubes, with less information about toxicology, will delay translation of a new anti-cancer therapy. In this regard, liposomes are a useful nanocarrier as there exist many FDA approved formulations already clinically used for various applications including cancer (**Table 1.6**).

Table 1.6: FDA-Approved liposomal formulations of drugs and their indications.

Drug	Clinical Use
Doxorubicin (Doxil [®])	Kaposi's sarcoma
Daunorubicin (Daunoxome [®])	Kaposi's sarcoma
Amphotericin B (Ambisome [®])	Antifungal
Amikasin (MiKasome [®])	Antibiotic
Cytarabine (Depocyte [®])	AML

1.5.2 Use of nanocarriers in cancer

As malignant brain tumors develop, they begin to create new blood vessels through a process called angiogenesis. Cancer angiogenesis is similar to angiogenesis seen during development except that it is less controlled and precise [72]. These blood vessels have many marked features including blind ends, erratic size and connections, and most significantly, large gaps in the endothelial lining. This last feature is important because it signifies that larger molecules can enter the tumor effectively bypassing the blood brain barrier (**Figure 1.2**). In fact, tumor vasculature can have intercellular gaps as large as 2 μm which is large enough for passive accumulation of 100-200nm particles into the tumor interstitium [200].

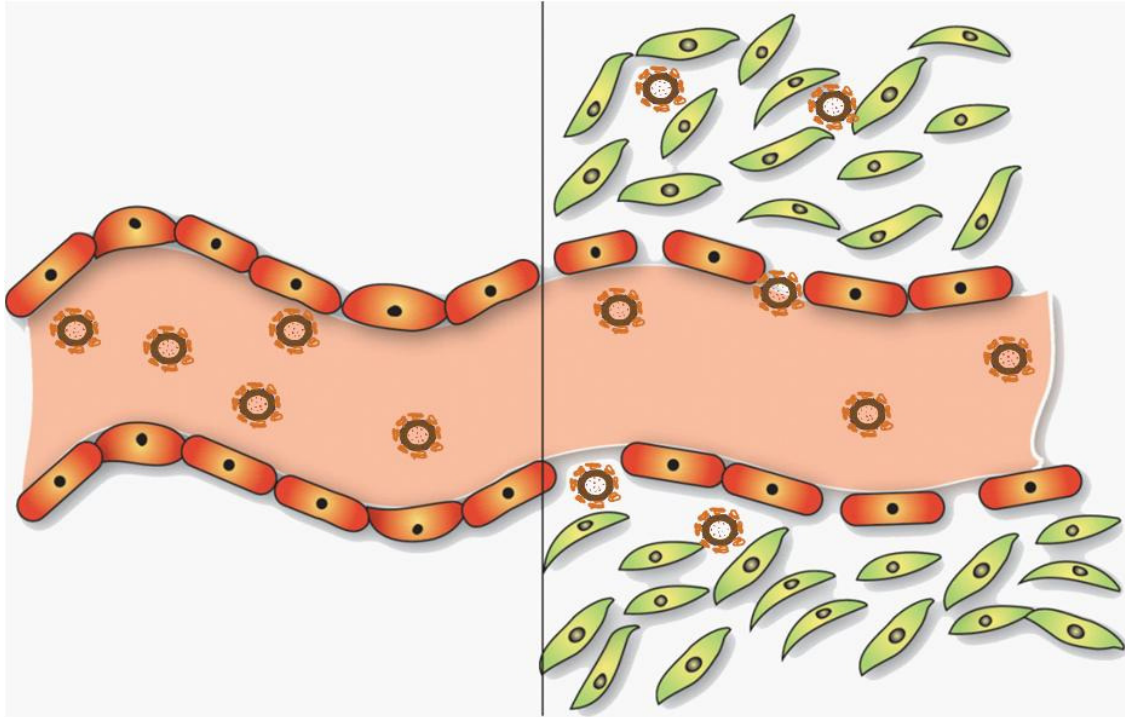


Figure 1.2: Enhanced Permeability and Retention Effect. Gaps in neovasculature allow liposomal accumulation in the tumor but not in healthy organs. Once there, decreased drainage from the tumor retains the particles there after extravasation reducing clearance.

Liposomes are 50-200nm nanocarriers that are composed of phospholipids and cholesterol in order to make a semi-fluid lipid bilayer that mimics the cell bilayer. These nanocarriers have been used to successfully deliver many drugs including lipophilic compounds [201]. In fact, liposomes are particularly useful for lipophilic drug derivatives due to the ability to trap the compounds within the bilayer. This leads to decreased leakiness through the membrane and enhanced loading capabilities. Though liposomes are often drawn as a single lipid bilayer, they are in fact several bilayer stacked together which can yield enhanced entrapment.

The size of liposomes allows for passive accumulation in tumors while avoiding other major organs such as heart and lung and possible side effects [202]. When a solid tumor reaches a size of 2mm diffusion from surrounding blood vessels becomes limited

leading to areas of hypoxia and nutrient deficiency [16]. This impetus leads to development of vasculature within the tumor via recruitment of endothelial cells and secretion of angiogenic factors [203]. These blood vessels are poorly defined as are vessels during development, however, rearrangement and trimming never occurs. This leads to disorganized vessels with large gaps in the endothelial lining. These gaps may be as large as 800nm which is appropriate for extravasation of liposomes into the tumor interstitium where they can act on tumor cells [200]. Further, once there, they remain in the tumor for some time owing to the poor drainage out of the tumor due to heightened blood pooling and pressure build-up. This effect is known as enhanced permeability and retention (EPR) and is a phenomenon that is advantageous when using nanocarriers [204]. Further, PEGylated liposomes have altered clearance routes from small molecule drugs resulting in prolonged circulation times allowing adequate time to accumulate through multiple passes through the vasculature [205]. Therefore, this type of nanocarrier offers benefits of long-circulation and slow clearance along with tumor targeting to deliver compounds in order to halt invasion.

1.6 Summary

Overall, brain tumors present a difficult clinical problem due to their invasive nature. In the same vein, invasion is a highly complex and well-regulated process utilized by cancer cells to survive and grow. There is a need for novel anti-invasive compounds, ways in which to analyze their ability to halt invasion *in vivo*, and a simple way to deliver the novel compound without extensive testing. Therefore, in the dissertation that follows, we have selected a novel compound and used liposomal nanoparticles to deliver it *in vivo*. Further, the compound was studied for anti-invasive activity and paired with common chemotherapy (Doxorubicin) to enhance survival in an animal model of GBM.

CHAPTER 2

COMPOUND SCREEN

Work done in conjunction with: Michael Y Bonner, Levi K Fried, Jack L Arbiser who synthesized the novel compounds.

2.1 Summary

Glioma is a significant clinical problem with treatments both failing and causing invasion of cells. There are currently no compounds that have shown reproducible clinical success at halting glioblastoma invasion in humans. Current therapeutics take aim at growth factors and matrix metalloproteinases but there are none that only inhibit the invasion of the cells, without effects on the environment or viability of the tumor. Such a compound could be integrated with current treatment and result in increased survival in patients. In this study, two classes of novel compounds, honokiol derivatives (HDs) and triphenylmethane dyes (TPMs) are examined with a rat invasive astrocytoma cell line, RT2. Cytotoxicity is assessed at a range of concentrations, followed by invasion inhibition below cytotoxic doses to determine lead compounds. Last, the compounds are tested at anti-invasive doses in healthy astrocytes to assess cancer specificity. This analysis leads to a single compound, Imipramine Blue, which shows invasion inhibition below cytotoxic doses and does not lead to astrocyte toxicity. This compound is interesting for further study in glioma therapy.

2.2 Introduction

Glioblastoma is the deadliest and most common primary brain cancer. Though many compounds are used against glioblastoma, many of these are nonspecific and the primary desired effect is cytotoxicity. This strategy has not changed much in the past decades, with treatment moving from resection alone, to resection coupled with anti-tumor treatments such as radiation therapy and chemotherapy with temozolomide [206].

This treatment regimen has only modestly increased the survival time in patients. The primary reason for failure of these treatments is the invasive nature of the disease [6]. Hence, we propose to find a novel compound that will halt glioma invasion specifically at non-cytotoxic doses. In this way, we hope to find a new molecule that can be integrated with other anti-tumor therapies to yield a new paradigm in treatment.

Honokiol is a compound derived from the magnolia tree and is an ancient herbal remedy. It has been shown to inhibit growth and progression of multiple types of cancer including melanoma, prostate and colon cancers [207-210]. Through these studies it was also determined that honokiol works via modulation of NFkB activity though the direct target is still unknown. NFkB is highly overactive in cancers with constitutive activation in 75% of cancers [211, 212]. This is particularly dangerous because NFkB acts as a transcription factor, regulating the machinery responsible for invasion and metastasis of cancer cells including actin regulatory elements, cell adhesion proteins such as integrins and focal adhesion kinases, and secretion of matrix metalloproteinases [213]. The upregulation of these factors all contributes to the migration of cancer cells. In particular, these attributes are necessary for the invasion of glioblastoma into the surrounding brain. Hence, the class of honokiol derivatives is tested for their possible anti-invasive activity.

Triphenylmethanes (TPM) are a class of compounds modeled after triphenyliodide (TPI) and thought to have NADPH Oxidase (Nox) antagonistic activity [214]. They were explored in the early 1990's as chemopreventive agents though not pursued extensively [215]. The Nox family of proteins is generally active in cancers leading to enhanced presence of reactive oxygen species in the tumor cells and stroma. This leads to activation of a host of intracellular pathways including Src kinase, p38/MAPK, and NFkB which can lead to downstream cytoskeletal rearrangement as well as directly activating matrix metalloproteinases (MMPs) [213, 216]. Triphenylmethane compounds such as TPI have previously been seen to inhibit invadopodia formation, inflammatory response, and cancer cell migration *in vitro* [179]. Therefore, this class of

compounds was of interest for development of novel therapeutics against glioma invasion.

We show here data from a screen of novel compounds from the triphenylmethane and honokiol classes of drugs. These are all novel compounds save for honokiol, and all show anti-tumor activity to some extent. The compounds were synthesized through simple methods to yield derivatives of the original two compounds and thus are divided into Triphenylmethanes (TPMs) and honokiol derivatives (HDs). We test the compounds against the rat astrocytoma invasive cell line RT2 and against healthy primary rat astrocytes for toxicity and invasion screening [84]. It was determined through this screen that the best anti-invasive agent at non-cytotoxic doses to astrocytes or RT2 is Imipramine Blue, a novel triphenylmethane compound.

2.3 Methods

2.3.1 Compounds

Compounds were synthesized according to previous publications and assessed by NMR to confirm the structure (data not shown). All compounds were extracted in the final step using ethanol and then dried for use in experiments. Stock solutions in 100% ethanol (Triphenylmethanes) or DMSO (honokiol derivatives) were made to minimize exposure of cells to the carriers (100x solutions).

2.3.2 Cell Culture

RT2 glioma cells were a generous gift from Helen Fillmore (Virginia Commonwealth University). The cell line was maintained in Dulbecco's Modified Eagle's Medium (Mediatech) supplemented with 10% Fetal Bovine Serum, 1% Penicillin/Streptomycin, 1% Non-Essential Amino Acids (Gibco), and 1% L-glutamine. Astrocytes were harvested from P0 rat pups as described in [217]. Cells were maintained

in DMEM/F12 media supplemented with 10% FBS and 1% P/S. Astrocytes used were passage 3.

2.3.3 Cytotoxicity testing against RT2 glioma

Cells were seeded in 96 well plates at a density of 100,000 cells/ml in serum containing media. After overnight attachment, media was exchanged with serum free media containing the compounds at varying doses (0.5, 5, 25 μ M) or the carrier alone. Cells were continuously incubated with the compounds and readings were taken using the Dojindo cell counting kit 8 (CCK8) at 0h, 24h, 48h, and 72h. Experiments were repeated two times with triplicate samples. Absorbance readings from the kit were normalized to the control samples (carrier only) and reported as normalized viability.

2.3.4 Cytotoxicity testing against astrocytes

Cells were seeded in 24 well plates at a density of 100,000 cells/ml in serum containing media. After overnight attachment, media was exchanged with serum free media containing the compounds at the cytotoxic dose seen in RT2 to determine specificity or the carrier alone. Cells were continuously incubated with the compounds and readings were taken using the Dojindo cell counting kit 8 (CCK8) at 0h, 24h, 48h, and 72h. Experiments were repeated 2 times with triplicate samples. Absorbance readings from the kit were normalized to the control samples (carrier only) and reported as normalized viability.

2.3.5 Invasion assays against RT2 glioma

For invasion assays, chambers were coated with basement membrane extract (BME, 0.5 mg/ml) and cells were starved with serum free medium overnight. Cells were plated at 1E6 cells/ml in top of the Millipore insert. After 2 hours, serum containing medium was placed in bottom well, drug was added to the top well, and cells were allowed to invade for 48 hours. Wells were washed with PBS, incubated with Cell Dissociation Solution (Trevigen) and Calcein AM then assessed at 485/590 and

normalized to control well which had either ethanol for the TPMs or DMSO for the HDs (normalized RT2 invasion).

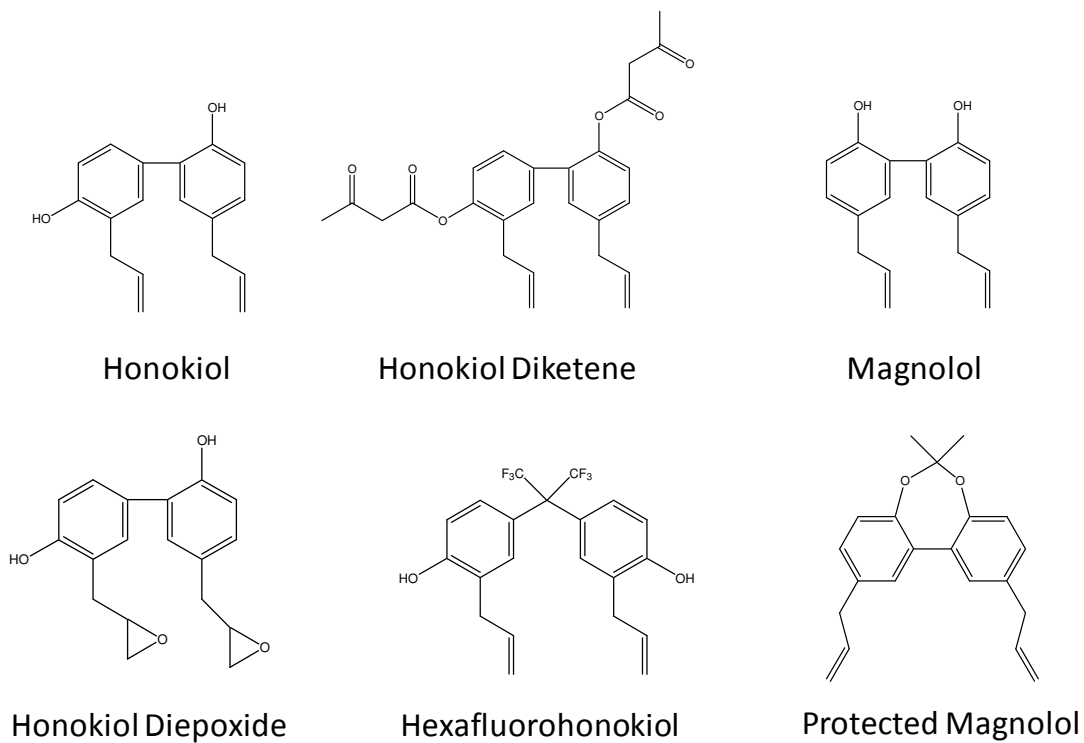


Figure 2.1: Honokiol derivatives These compounds represent several of the honokiol-based compounds used in cytotoxicity studies.

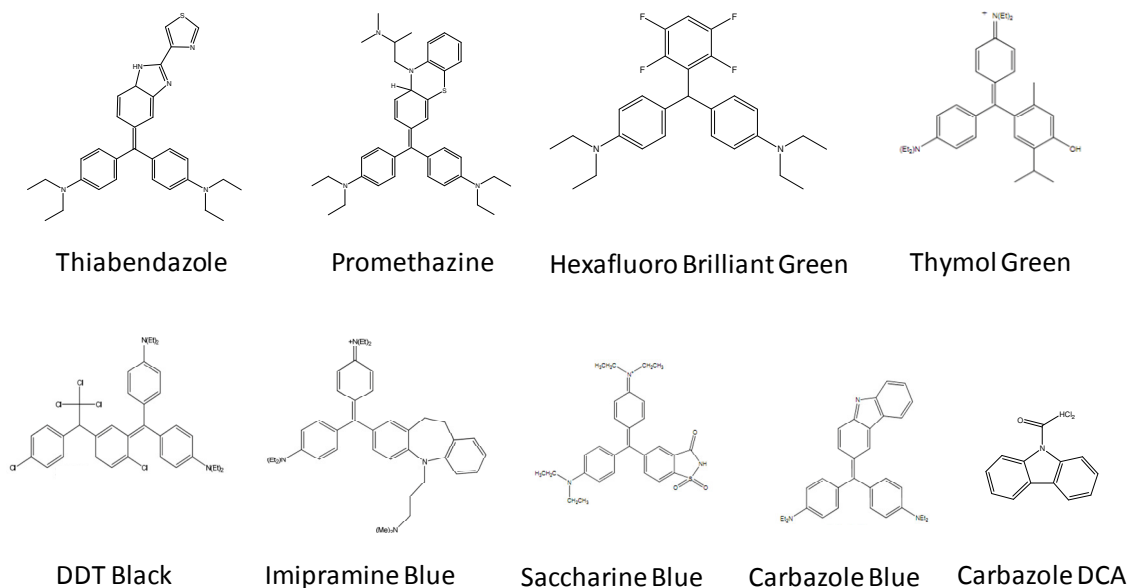


Figure 2.2: Triphenylmethane dyes Representative compounds of the triphenylmethane dye class. All compounds have the signature diphenyl structure attached to a central molecule. Most notable was Imipramine Blue which showed strong anti-invasive potential.

2.4 Results

2.4.1 Honokiol derivatives and Triphenylmethanes have low cytotoxicity

Through testing of the compounds shown in **Figure 2.1** and **2.2** at several doses, we determined the dose at which each compound was cytotoxic against the RT2 tumor cells. Figure 2 shows the cytotoxicity at the dose at cytotoxic (**Figure 2.3**) and below cytotoxic (**Figure 2.4**) doses against the cells for each class of compounds. Many of the compounds showed significant anti tumor activity against RT2 glioma and thus would be good candidates for novel anti-tumor compounds. However, we were interested in the anti-invasive characteristics of the compounds and thus used this assay to determine this dosing.

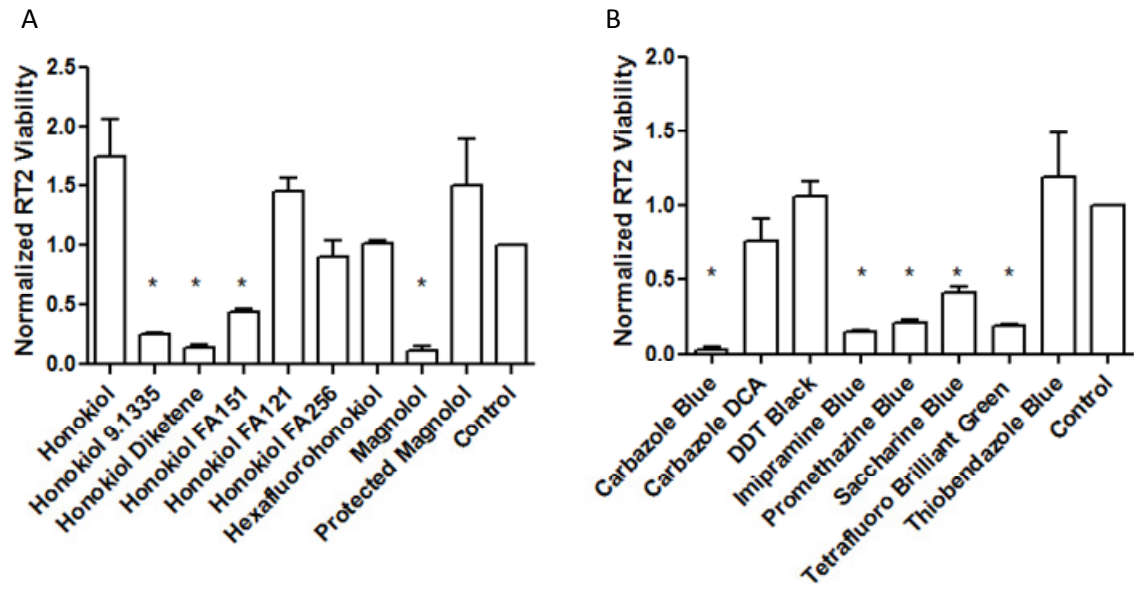


Figure 2.3: Cytotoxicity in RT2 glioma at high doses. (A) Honokiol derivatives and (B) Triphenylmethanes dyes. Some compounds showed no cytotoxicity at any dose (up to 25 μ M), but others were cytotoxic at doses of 5 μ M. Viability readings at 48 h were compared to initial readings before drug application. * $p < 0.05$ in t-tests as compared to control.

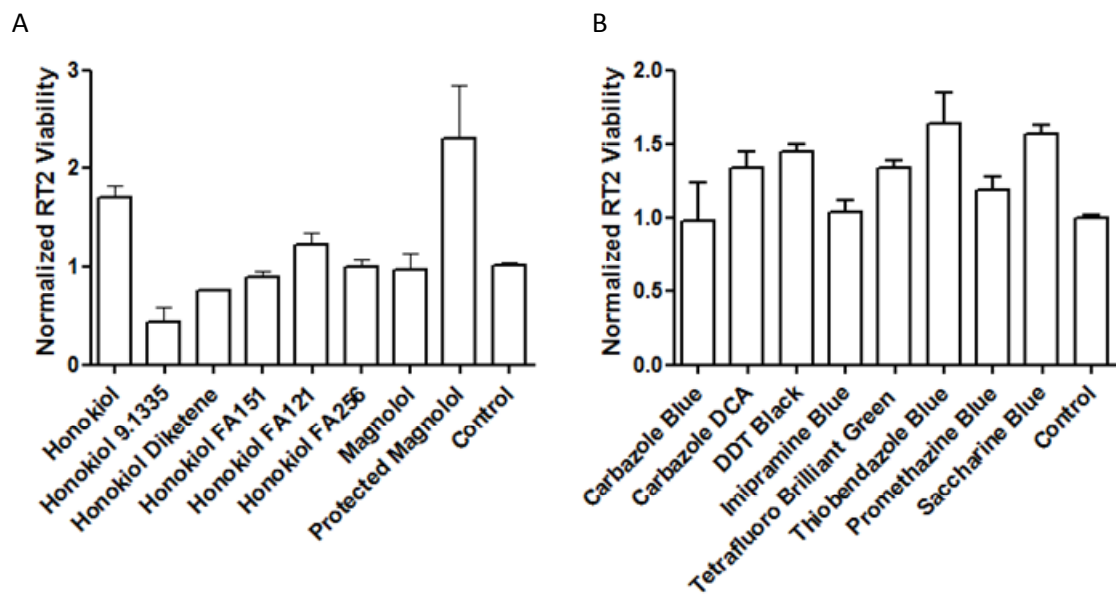


Figure 2.4: Cytotoxicity in RT2 glioma low doses. (A) Honokiol derivatives and (B) Triphenylmethane dyes. Viability readings 48 h were compared to initial readings before drug application. There were no significant differences from control. The dose range was between 0.5 and 5 μ M for non-cytotoxic effects. These doses were used for testing of invasion inhibition to control for confounding effects.

2.4.2 Several compounds showed anti-invasive activity against RT2 glioma

Using the dose below cytotoxic dose to prevent confounding cell death effects, we explored the anti-invasive potential of these compounds (**Figure 2.5**). Through this assay, there were several significant results for compounds including that seen with honokiol, carbazole blue, and Imipramine Blue. These compounds inhibited invasion to below 50% at 5 μ M dose for 48 hours.

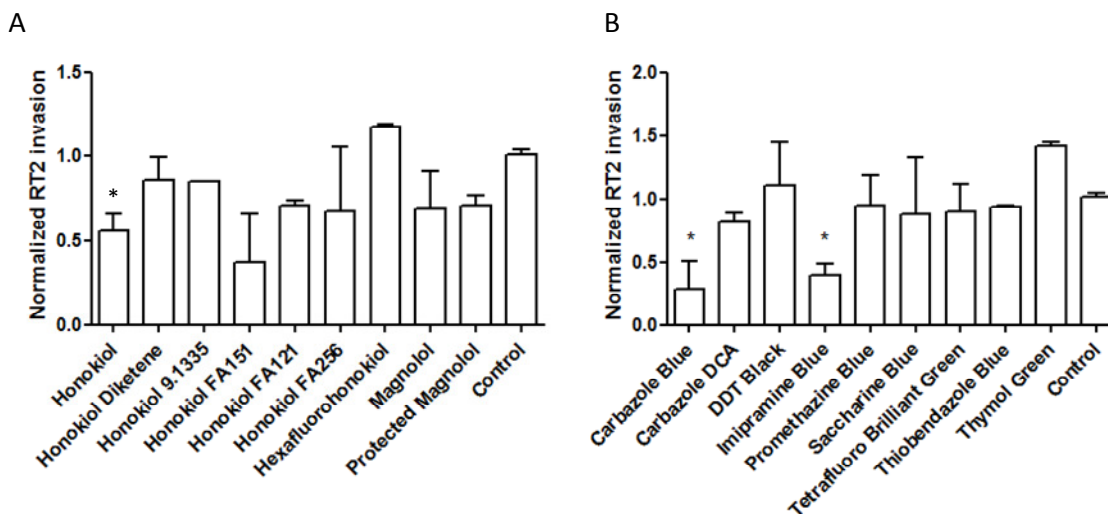


Figure 2.5: Invasion inhibition of RT2 glioma. A) Honokiol derivatives and B) Triphenylmethane dyes in Boyden chamber assay with basement membrane extract coating after 48 h. Only three compounds showed anti-invasive effect that was significant in these screenings. * $p < 0.05$ with t-test as compared to control.

2.4.3 Several compounds were toxic to astrocytes

Astrocytes were selected as a control cell type for the RT2 astrocytoma to determine if there would be any side effects *in vivo*. The cells were incubated with the anti-invasive concentration of the compounds for cytotoxicity measurements. It was found that all compounds but carbazole blue and Honokiol FB56 were benign towards the astrocytes after 72 hours (**Figure 2.6**). Imipramine Blue (IB) and honokiol were both

non-cytotoxic and thus still represent good candidate molecules for use against glioblastoma.

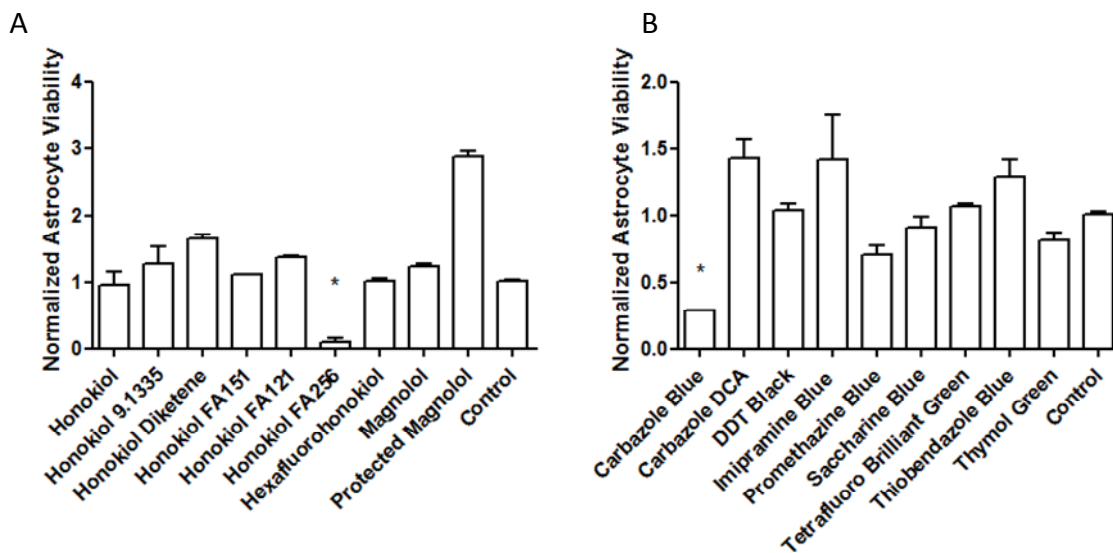


Figure 2.6: Cytotoxic effect against primary rat astrocytes. (A) Honokiol derivatives and (B) Triphenylmethane dyes. Astrocytes were exposed to the compounds for 72 h with measurements taken every 24 h. Viability was compared to initial readings of wells and normalized to the untreated control wells. This assay showed cytotoxic activity with two compounds, one of which, Carbazole blue, was a lead anti-invasive compound. * $p < 0.05$.

2.5 Discussion

The ability of glioblastoma to invade is the primary cause of recurrence and therapeutic failure. Many chemotherapeutics that are used are cytotoxic and as such, they have been correlated with increasing cell invasion and selection of the most malignant cancer cells through chemoresistance [112]. Thus, a new method of treatment with novel compounds is necessary in the treatment of glioma for a real change in survival time. Here we propose the use of two new classes of compounds in glioblastoma including triphenylmethanes and honokiol derivatives. Through inhibition of not previously inhibited pathways including NF κ B and Nox, we show that there is anti-tumor effect in many of these compounds at tens of micromolar doses.

This anti-tumor effect is interesting because as compared to other chemotherapeutics, these compounds are nearly as effective at killing cancer cells [51, 113, 218]. The added benefit of these compounds is that they have the potential to stop invasion via different pathways than previously examined. The RT2 glioma line is a highly invasive and aggressive model of glioma that generally will cause death in inoculated animals within two weeks [84, 219]. Therefore, showing enhancement of death in this line is an indication for further investigation of these cytotoxic compounds. Further, since it seems that the majority of these compounds are benign towards astrocytes at these concentrations these compounds could further be helpful due to the specificity towards astrocytoma. Also, coupled with previously published results showing *in vivo* anti-tumor effect of honokiol and *in vitro* results with DPI showing reduction of invasion of multiple tumor types, we believe that these compounds could have further effect on other cancers [210].

Though the cytotoxic selectivity is exciting, the purpose of the compound screen was to determine a candidate molecule for anti-invasive therapy. The rationale for the selection of the classes of compounds was to find novel possible mechanisms of action. Most anti-invasive compounds focus on inhibition of growth receptors which can have alternate anti-tumor effects, and MMP inhibitors, which have very specific action on the microenvironmental manipulation by the cells, but not the cells themselves [55, 187]. Therefore, these new compounds have the possibility of completely novel activity on cancer cells that could have far reaching effects on the disease.

The final desired outcome is to determine a compound that will show an inhibition of invasion that is not attributable to cell death and that this compound will not kill astrocytes, the healthy counterpart to the astrocytoma. The anti-invasive potential of drugs has been tested with other compounds, however, there is often the confounding effect of cytotoxicity that is rarely controlled [55, 220-222]. In this study we determined first the concentration at which these compounds were cytotoxic and then followed up

with the invasion assay at the lower dose. Last we narrowed down to our final compound for future study by checking the specificity of the compound for cancer cells. The next steps in the investigation are to determine if this compound, Imipramine Blue, in fact inhibits invasion *in vivo* and to further understand its mechanism. The final goal is to integrate this drug with cytotoxic compounds to affect change in the treatment paradigm of glioblastoma and hopefully alter the survival rates.

From another perspective, we introduce a range of compounds that will be effective against glioblastoma in differing ways. Further, preliminary data incorporating combinations of the two classes of compounds shows enhanced cytotoxicity against the glioma that's greater than the additive effect of just the single compounds (data not shown). This data indicates that the two compounds likely activate different pathways, as implied by the compounds from which they are designed, and that this effect is multiplicative. This is a powerful set of compounds to work with if, though NFkB is downstream of both signaling pathways, they in fact activate pathways that are synergistic in the effect. Further work must be done to explore this attribute and to determine the mechanisms by which these compounds inhibit invasion and increase apoptosis so that better combinations can be designed.

In all, we show methodical identification of a novel anti-invasive compound Imipramine Blue, against an aggressive glioma model. Additionally, through examination of these compounds, which have overlapping yet different courses of action, we have revealed several with anti-tumor activity and anti-invasive activity. These compounds are worth further examination and understanding for use against malignant glioma.

CHAPTER 3

ENCAPSULATION AND TESTING IMIPRAMINE BLUE

3.1 Summary

The invasive nature of glioblastoma (GBM) represents a significant challenge to the standard of care and contributes to poor clinical outcomes. This is exacerbated by last line therapies such as Avastin which result in increased invasion of glioblastoma. Here we tested the hypothesis that an effective anti-invasive agent that ‘contains’ glioblastoma will enhance the efficacy of chemotherapy. We report a new anti-invasive agent, Imipramine Blue (IB), which effectively inhibits invasion of highly migratory tumor cells *in vitro* and *in vivo*. Liposomally encapsulated IB (nano-IB) significantly inhibits invasion of GBM in an aggressively invasive RT2 rodent tumor model. We demonstrate that IB inhibits invasion through upstream dysregulation of actin polymerization. Nano-IB therapy followed by liposomally encapsulated Doxorubicin (nano-DXR), resulted in complete survival and remission in a syngeneic, invasive rat glioblastoma model RT2.

3.2 Introduction

Though only accounting for 2% of new cancer cases, brain tumors are a large clinical problem with poor prognosis after treatment and relatively minor change in survival times over the past 50 years [1]. This is mainly due to the minimal treatment response of the most common of primary brain tumors, glioblastoma which has a five-year survival rate of 33% [223]. Current treatments aim to debulk the tumor using surgical resection, radiotherapy, and chemotherapy with temozolomide upon onset of symptoms and detection of tumor via MRI [224]. While non central nervous system cancers can result in metastasis to other regions of the body, brain tumors often do not metastasize outside of the brain, instead they invade and spread within the host

microenvironment [225]. Thus the invasive nature of glioma is a significant contributor to poor clinical outcomes.

The ability to invade host brain tissue is a defining characteristic of glioblastoma compared to other more benign brain tumors. Surgical resection often results in recurrence within 2 cm of the surgical removal [98]. Radiation of the microenvironment alone before implantation of cancer cells has seen enhanced invasion and malignancy of cancers [44]. Therefore, stopping invasion can potentially have significant implications for the efficacy of chemotherapy and radiation therapy. Current experimental anti-invasive drugs such as EGCG, geldanamycin, and UPAR inhibitors are plagued by poor pharmacokinetics and tumor accumulation *in vivo*, high IC₅₀s, unpredictable pharmacobiology leading to adverse side effects, cytotoxic activity at “anti-invasive” doses, and indeed are used as anti-tumor agents and not as anti-invasive agents [51, 191, 220, 222, 226, 227]. Marimastat, an MMP inhibitor currently in Phase II trials, shows promise yet does not offer a cure of the disease in early animal models nor in human studies [55, 181, 228]. Current anti-invasive agents focus on inhibition of matrix metalloproteinases or are cytotoxic compounds (paclitaxel, temozolomide) given at lower doses [51, 229].

Here we describe a novel therapeutic, Imipramine Blue that is truly anti-invasive against glioma in nanomolar concentrations. We have also developed a long-circulating nanoscale liposomal delivery vehicle (nano-IB). PEGylated liposomal nanocarriers (Stealth) offer advantages for drug delivery that include FDA-approved status for several anti-cancer compounds such as cytarabine and Doxorubicin and well-studied pharmacokinetics and biodistribution for prevention and prediction of adverse side effects [230]. Further, due to the enhanced permeability and retention of solid tumors afforded by the neovascularization process, liposomal nanocarriers under 200nm in size will accumulate at the tumor [231, 232]. Therefore, use of such particles in conjunction with the development of a new compound allows prediction and understanding of circulation

times, organ accumulation, tumor dosing, and cell delivery without involved pharmacological studies [230, 233-235].

In this study we report that a combination therapy strategy of first inhibiting invasion in an aggressive syngeneic rodent model of glioma using nano-IB, followed by cytotoxic nano-DXR chemotherapy significantly enhances the efficacy of chemotherapy compared to chemotherapy alone resulting in complete remission of tumor. This strategy is summarized in **Figure 3.1**.

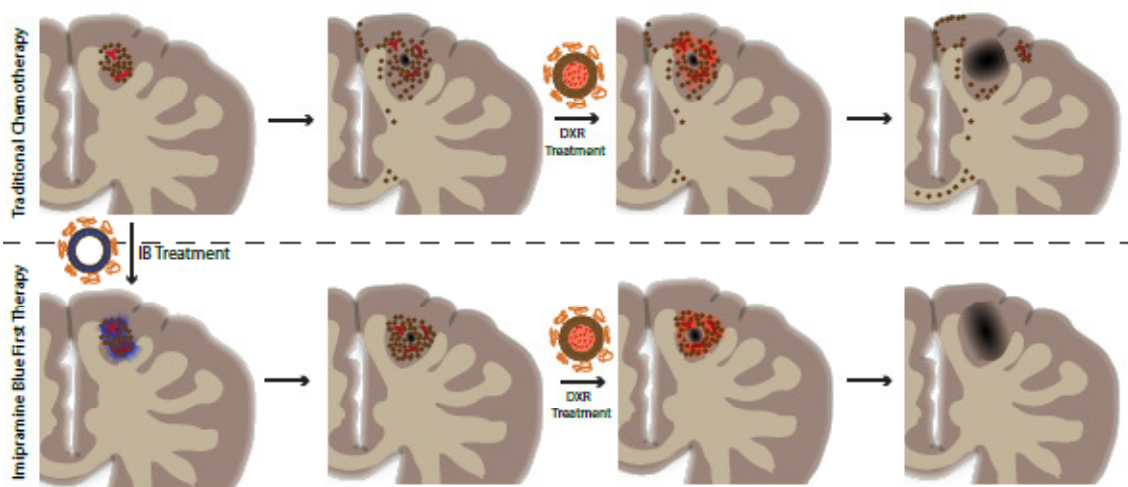


Figure 3.1: Strategy of treatment with IB Traditional chemotherapy with nano-DXR (top row) treats an invasive tumor with chemotherapy and leaves behind residual cells which can create new tumors. By adding nano-IB (bottom row), we can contain the tumor and prime it for treatment with chemotherapy thus removing the tumor completely.

3.3 Methods

3.3.1 Synthesis of Imipramine Blue Dye

Imipramine Blue Dye was synthesized according to [236]. Briefly, 1.0 g Imipramine was added to 1.02 g of 4-4'-diethylaminobenzophenone in a clean, dry flask under an argon atmosphere under constant stirring at room temperature. Phosphorus

oxychloride (0.50 mL) was then added to the flask dropwise, upon completion of addition the solution was heated at 107°C for four hours. The solution changed colors from a brown-black to a metallic blue. After 4 hours, the reaction was quenched with water and the solvent was removed via rotary evaporation at 35° C. The resulting black plaque-like solid was extracted in chloroform. The chloroform fractions were pooled and evaporated on a rotary evaporator resulting in a metallic blue oil. Chromatographic separation over on Alumina with 100:1 Ethyl-Acetate:Hexane to remove excess 4-4'-diethylaminobenzophenone and afterwards 50:50 chloroform:methanol gave Imipramine blue dye in 95% yield as a metallic blue solid. MS: (M+) 588.34.

3.3.2 Cell culture and in vitro assays

RT2 and RT2 glioma cell lines were a generous gift from Helen Fillmore (Virginia Commonwealth University), U87MG and C6 were purchased from ATCC, and 9L was a generous donation from the Neurosurgery Tissue Bank at UCSF. All cell lines were maintained in DMEM (Mediatech, VWR) supplemented with 10% Fetal Bovine Serum, 1% Penicillin/Streptomycin, 1% Non-Essential Amino Acids, and 1% L-glutamine (Gibco) and RT2 were maintained in the same medium with 1 mg/ml G418 (Gemini Biosciences) added for selection. For invasion assays, chambers were coated with basement membrane extract (BME, 0.5 mg/ml; Trevigen) and cells were starved with serum free medium 24 hours prior to assay. Cells were plated at 1E6 cells/ml in top of an 8- μ m pore size tissue culture insert insert (Millipore). After 2 hours, serum containing medium was placed in bottom well, drug was added to the top well, and cells were allowed to invade for 48 hours. Wells were washed with PBS, fixe with 4% Paraformaldehyde, stained with DAPI, imaged and quantified. For cytotoxicity assays, RT2 glioma or astrocytes were plated at 200,000 cells/ml in a 24 well plate and for proliferation assays, RT2 glioma were plated at 25,000 cells/ml in a 24 well plate. CCK8 (Dojindo) was used to count cells at 24 and 48h (RT2) and 72 and 96h (astrocytes). For

combination cytotoxicity studies, cells were plated at 200,000 cells/ml in a 24 well plate and allowed to attach overnight. IB was added at a dose of 5 μ M for 3 hours, removed, and DXR was added at varying doses. Counts were taken using CCK8 over 72 hours and normalized to control conditions. For liposomal studies, the same procedures were followed but liposomal formulations were used in the same concentrations and timelines as above and compared to control liposomes (saline-containing).

3.3.3 Encapsulation of Imipramine Blue

Nano-IB were made according to with modifications. Briefly, 10mol% cholesterol (Sigma), 85mol% Distearoyl-phosphatidyl-choline (DSPC, Avanti), 5mol% poly(ethylene glycol 2000)-distearoyl-phosphatidyl-ethanolamine and 0.01mol% distearoyl-phosphatidyl-ethanolamine-rhodamine and 2mg/ml Imipramine Blue (IB) were dissolved in 100% ethanol at 70°C. The solution was hydrated with 1x Phosphate Buffered Saline to a final concentration of 40mM lipids. The solution was extruded through a 0.8 μ m filter 3 times, a 0.4 μ m filter 5 times, and a 0.2 μ m filter 10 times to a final size of 160nm as assessed by Dynamic Light Scattering. The solution was run through a Sepharose column (Sigma) to remove unbound compound. This solution was diafiltrated to a final drug concentration of 7 mg/ml in 140mM lipids as assessed by absorbance at 610nm(drug content) and fluorescence at 485/610(lipid content).

3.3.4 Doxorubicin nanocarrier fabrication

Doxorubicin was loaded into the liposomal nanocarriers using an ammonium sulfate gradient as previously described[237]. Briefly, liposomal nanocarriers (60mol% DSPC, 35mol% cholesterol, 5mol% DSPE-mPEG) were made by hydration with ammonium sulfate followed by dialysis against PBS. These were mixed with Doxorubicin in saline (2 mg ml⁻¹) at a ratio of 0.04 mg Doxorubicin to 1 mg of lipid and heated to 60°C for 1h. The liposomal nanocarriers were then immediately cooled on ice and subsequently diafiltrated to remove any remaining Doxorubicin and concentrate the

nanocarriers down to the same lipid molarity as the nano-IB. The formulations were sterilized by passing through a 0.2 µm filter. Final Doxorubicin content was assessed by lysing the liposomal nanocarriers with 5% Triton X-100 at 60°C and measuring the UV absorbance at 480nm.

3.3.5 Pharmacokinetic Studies

Animals were anesthetized via isoflurane inhalation. The tail was cleaned with isopropanol and a 24 gauge catheter was inserted into the tail vein. Free IB was prepared according to [238]. Briefly, drug was solubilized in a 50/50 Cremophor EL (Sigma)/Ethanol solution and then diluted with 0.9% saline to a final concentration of 5 mg/ml. Either free IB or Lip-IB was delivered via the catheter after which the catheter was removed and bleeding inhibited. At given time points after injection, an orbital blood draw was performed and blood collected in heparinized gel tubes. The tubes were spun at 15,000xg for 10 minutes at 4°C. Plasma was collected and directly read at 610nm (free-IB) or lysed with 1% Triton solution and read.

3.3.6 Tumor inoculation

Animals were anesthetized via isoflurane inhalation and mounted on a stereotaxic frame. The head was shaved and cleaned and a 3cm incision was made through the skin to expose the skull. A 2mm burr hole was created in the skull using a Dremel hand tool mounted on the frame 2mm lateral and 2mm anterior to lambda. A Hamilton syringe was used to inject 10µl of cell solution over five minutes after which the syringe was slowly removed and the burr hole closed with bone wax. The wound site was closed using sutures (Ethicon), the wound cleaned, and buprenorphine administered intramuscularly. Animals were monitored daily after inoculation.

3.3.7 Comparison and toxicity studies

Animals were inoculated with tumor as described. On Day 4 following inoculation, nano-IB, liposomal Doxorubicin, or saline was administered via tail vein

injection. When animals displayed signs of morbidity they were sacrificed via intracardial perfusion with saline followed by 4% paraformaldehyde in PBS. Brains were postfixed for 1 hour in 4% paraformaldehyde and then transferred to a 30% sucrose in PBS solution for 72 hours. Brains were removed from sucrose, rinsed with PBS, embedded in OCT and frozen at -80°C. Brains were sectioned using a Leica Cryostat at 16µm. Other organs were dissected and paraffin embedded for H&E processing.

3.3.8 Immunohistochemistry and Image Analysis

Sections were stained with anti-neurofilament 160 antibody(Sigma) followed by secondary Alexa 594 (Invitrogen), anti-GFP antibody (Invitrogen) to enhance the GFP signal, and DAPI (Invitrogen). Whole brain slices were imaged using widefield microscopy with Neurolucida tiling functionality. Images for margin quantification were imaged using a Zeiss LSM 510 confocal microscope. Image J was used for tumor density calculations. Invasion beyond borders was assessed on on 3 sections through each tumor at 4 locations beyond the border. Border definition was determined by 2 parties on separate occasions (based on red-green spatial definition) and cells beyond border counted (confirmed with both green fluorescence and nuclear staining with DAPI).

3.3.9 Microarray analysis

Rats were perfused 11 days after inoculation (n=3 per group, treated and untreated as above) using DEPC-treated PBS and brains were removed and frozen at -80°C. Tumors were dissected out and RNA harvested using the Qiagen RNEasy kit (Milipore). Total RNA was quantified using an Agilent Bioanalyzer and converted to cDNA using Superscript Choice System (Invitrogen). The microarray and data analysis was performed as described (Ford paper) using the Affymetrix Rat 230 2.0 gene array. Each sample in the treated tumors was compared to untreated tumor controls using the Affymetrix GeneChip software. A gene was considered differentially expressed when the standard deviation of the signal increase or decrease was significantly smaller than the absolute

change in average difference with a calculated confidence level of a gene greater than 95%. Data were then imported into Genespring software to generate heatmaps and into Ingenuity Pathway Analysis to determine interactions of groups of genes with greater than 2-fold changes.

3.3.10 Quantitative rt-PCR

RNA from tumors *in vivo* was harvested as above and samples were pooled together to yield greater concentrations. RNA was quantified using a Nanodrop spectrophotometer and cDNA was made using Superscript Choice System (Invitrogen). Quantitative rt-PCR was run using SYBR green reagents and the StepOne Plus Analyzer (Applied Biosystems). The following primer pairs were used for each gene (IDT): α -actin (acta1; forward: 5'-GGC AAG CCA GCT TTC ACC-3', reverse: 5'-CCT CAG GAC GAC AAT CGA CC-3'); profilin-1 (pfn1; forward: 5'-GGA AGA CCT TCG TTA GCA TTA CG 3', antisense: 5' CGT CTT GCA GCA GTG AGT CC 3'); calgranulin (S100A8; sense: 5' GCA ATT AAC TTC GAA GAG TTC C 3', antisense: 5' CGA CTT TAT TCT GTA GAC ATA TCC 3'); RhoGDI α (arhgdia, sense: 5' CTA CAT GGT CGG GAG CTA TGG 3', antisense: 5' GTT GTA ACT GCC CCG AGC AA 3'); scinderin (scin, sense: 5' TTC TCC TAC CGC CTG CAC TT 3', antisense: 5'-CGC CCA AAT AGT CGT CCA TCT-3'), .

3.3.11 Western Blotting

Protein lysates were harvested from treated and untreated tumors (n=3 per group) and pooled. Total protein was measured using BCA assay (BioRad). Equivalent total protein amounts (20 μ g protein) were run on a NuSep gel followed by incubation with primary antibodies: rabbit anti-profilin 1 (Abcam), goat anti-S100A8 (Santa Cruz Biotechnology), rabbit anti-arhgdia (Santa Cruz Biotechnology), rabbit anti-acta1 (Abcam), and rabbit anti-scinderin (Abcam). Secondary incubation was performed with HRP-tagged anti-goat (Santa Cruz Biotechnology) or HRP-tagged anti rabbit

(Invitrogen). Gels were stripped and incubated with rabbit anti-GAPDH (AbCam) for normalization of signal. Integrated density measurements were performed with ImageJ.

3.3.11 Survival studies

Tumors were implanted as described for comparison studies into 10-12 week old Fisher 344 male rats. At 4 days after implantation, rats received either IB liposomes (IB) or saline liposomes (Control) via tail vein injection under isoflurane anesthesia. On day 7, MRI was performed as described followed by tail vein injection of either Doxorubicin liposomes (DXR), or IB liposomes (IB). Animals were monitored daily and MRI was performed at intervals to monitor tumor progression. Animals displaying signs of morbidity including hunched posture, abnormal vocalization, weight loss, poor hygiene, or decreased movement in accordance with Georgia Tech IACUC guidelines. Animals were sacrificed by CO₂ inhalation upon display of any of these symptoms and the brain removed to confirm tumor presence and perform histology.

3.3.12 Magnetic Resonance Imaging

Animals were anesthetized by 1-2% Isoflurane and placed in a 7T MRI (Bruker Instruments, Billerica, MA) equipped with a 30mm head coil. A T₂-weighted image was taken through the head using the following parameters: 2.0 s repetition time(TR), 48 ms echo time(TE), FOV=40mm x 40mm with a 256 x 256 matrix, slice thickness=1 mm, number of slices= 20, 2 averages per phase encode step requiring a total acquisition time of about 6 minutes per rat. MRI was performed before treatment began to confirm tumor presence and at intervals throughout the survival study to monitor the progression of the tumor and response to treatment. Rats not showing evidence of tumor were removed from the study. For T₁-weighted MRI, animals were treated with either Gd-loaded nano-IB (for accumulation, 3 mg/kg IB) or free Gd-DTPA (Omniscan) for end of survival study tumor leak (final concentration of Gd was 0.15 mmol/kg). T₁ images were taken according to the following parameters: 2.0 s repetition time(TR), 48 ms echo time (TE), FOV=40mm

x 40mm with a 256 x 256 matrix, slice thickness=1 mm, number of slices= 20, 2 averages per phase encode step requiring a total acquisition time of about 6 minutes per rat.

3.3.12 Statistical Analysis

For *in vitro* assays, a one-way ANOVA was performed followed by Tukey post-test for individual pairs comparisons. For *in vivo* pharmacokinetic studies, points were fitted with a single phase exponential decay curve and compared using nonlinear 3-point regression. For the survival study, we used Mantel-Cox analysis to compare survival curves. In all studies, *p<0.05, **p<0.01, and ***p<0.001. Test statistics are reported as: test statistic (degrees of freedom) = value, p< # to give effect sizes.

3.4 Results

3.4.1 Structure of Imipramine Blue (IB)

Imipramine Blue (IB, **Figure 3.2A**) was synthesized via a single-step process to yield a final diphenyl compound with MW=588 g/mol (**Figure 3.2B**). This compound is crystallized to a dark blue/brown powder that yields a deep blue colored solution when dissolved at neutral pH. The structure of IB was confirmed by NMR Spectroscopy (**Figure 3.2C**). IB absorbs light at 610 nm as determined through absorbance spectrophotometry (**Figure 3.2D**). This property was used throughout experimentation to assess the concentration of IB loaded in nanocarriers.

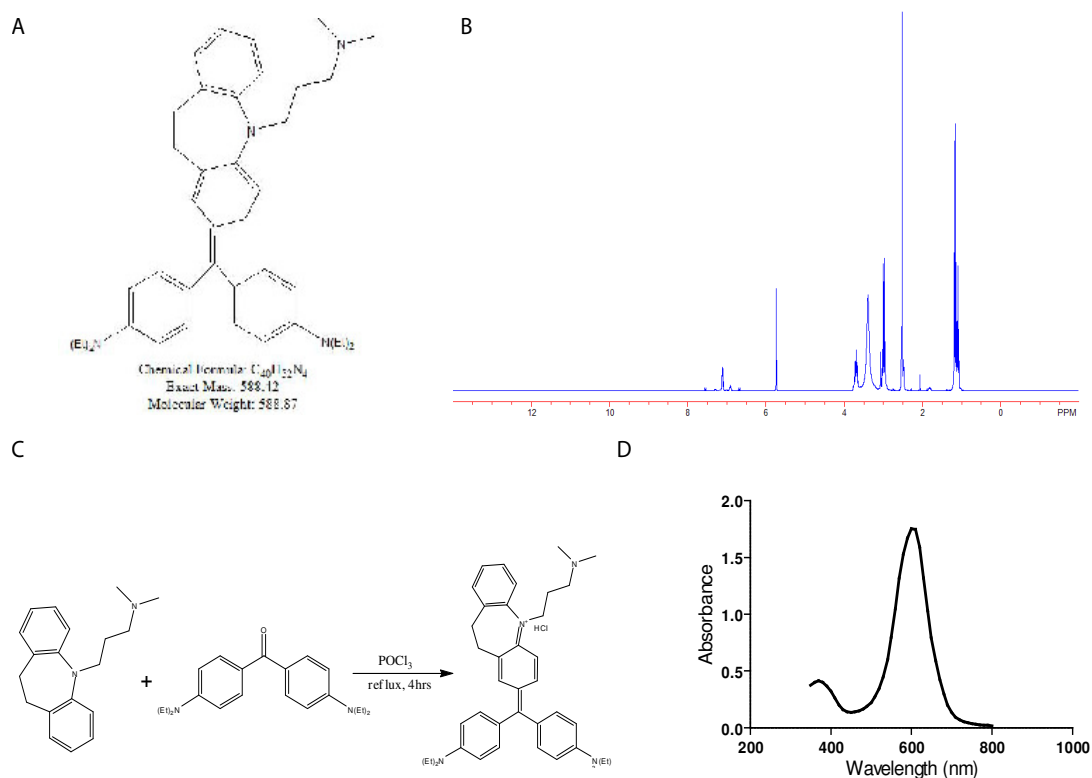


Figure 3.2: Synthesis of Imipramine Blue. A) Structure of Imipramine Blue, a small hydrophobic diphenyl compound weighing 306 g/mol. B) NMR of synthesized Imipramine Blue. C) Single step synthesis method of Imipramine Blue and D) Absorbance spectrum of Imipramine Blue used for assessment of concentration showing a peak at 610nm.

3.4.2 Imipramine Blue (IB) inhibits invasion of multiple glioma lines in vitro

Cells were seeded on basement membrane extract in porous tissue culture inserts were exposed to IB in increasing doses from 0.01-10 μ M and normalized to controls to determine extent of invasion through the matrix. Doses remained below cytotoxic levels of IB as determined in independent experiments (**Figure 3.3**).

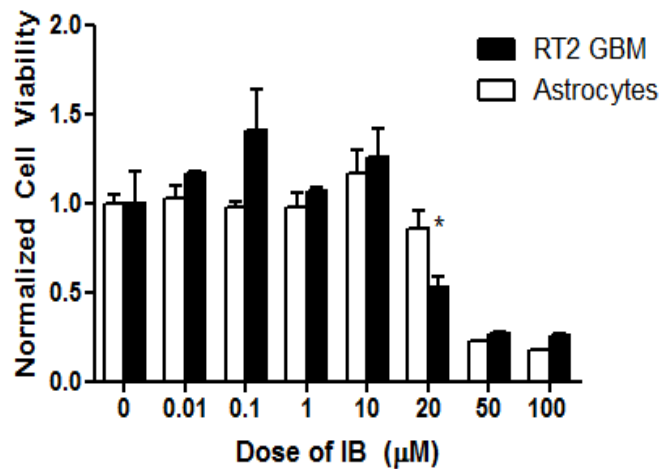


Figure 3.3: Dose dependent cytotoxicity of glioblastoma RT2 and Astrocytes. IB is cytotoxic to RT2 GBM around 20µM though begins to be toxic to astrocytes at 50µM. Regardless, these cytotoxic doses are well above the EC₅₀ of IB for halting invasion.

IB was effective in inhibiting invasion of multiple glioblastoma cell lines at low concentrations (shown here at 5µM, **Figure 3.4A**). Further the ability of IB to inhibit invasion is dose dependent revealing an IC₅₀ in the RT2 glioblastoma model of 10 nM (**Figure 3.4B**). Cells were seen to reduce spreading in 2D using live imaging. This inhibition of invasion was specific to tumor lines, with astrocyte migration remaining unaffected at concentrations that were inhibitory to glioma lines (**Figure 3.4C**).

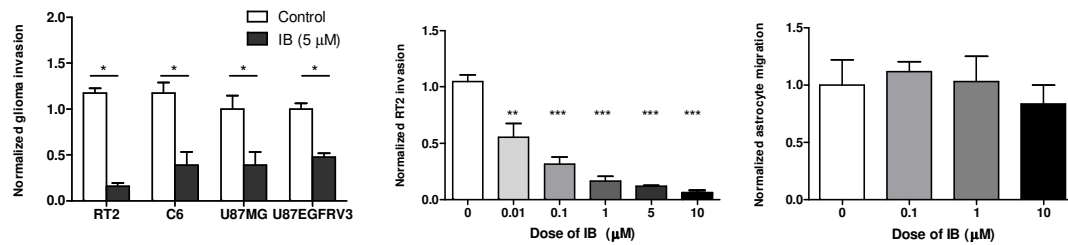


Figure 3.4: Imipramine Blue inhibits invasion in glioma cell lines A) IB inhibits invasion in multiple models of glioblastoma through basement membrane extract at doses below cytotoxic levels (5μM) B) In RT2 rat astrocytoma, IB inhibits invasion in a dose-dependent manner below cytotoxic levels showing an IC50 of 10nM C) Astrocyte migration is not affected by IB in Boyden chamber assay.

In this study, the RT2 glioblastoma model was employed for several reasons: 1) the RT2 model shows many attributes inherent to human glioblastoma that are not consistently observed in xenograft models such as white matter tract and perivascular invasion, pseudopalisading necrosis, extensive vascularization, and subpial spread (**Figure 3.5**) it has consistent time to death after implantation and 3) use of a syngeneic model allows observation of normal host responses to tumor development [239, 240]. Therefore, though IB was effective in inhibiting invasion of several glioma model lines in vitro, *in vivo* studies with an eGFP-RT2 (RT2) glioma intracranial xenograft model were used to fully investigate IB's effects on invasion *in situ* [84].

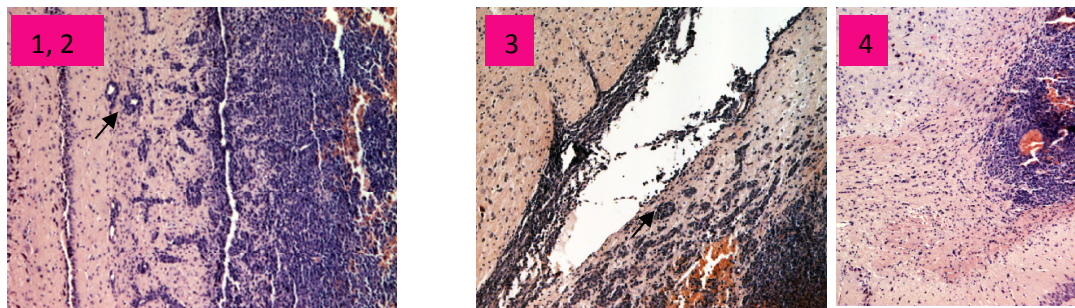


Figure 3.5: Structural components of RT2 glioma RT2 exhibits perivascular invasion (1), white matter tract involvement (4), subpial spread (3), and perineuronal satellitosis (2). Further, this model shows evidence of pseudopalisading necrosis a hallmark of glioblastoma in humans (arrows).

3.4.3 Design and Fabrication of liposomal Imipramine Blue (nano-IB)

To determine the pharmacokinetics of IB alone, it was injected intravenously in Fisher rats using a formulation of cremophor and ethanol that allowed solubilization in saline[238]. This injection (3 mg/kg IB) yielded a poor circulation half-life of 11 minutes in adult male rats without tumor (**Figure 3.7A**, inset). Poor pharmacokinetics were likely due to the highly hydrophobic nature of IB at physiological pH resulting in quick absorption into the intravascular space after tail vein injection. To circumvent this shortcoming, we encapsulated IB in ~160nm PEGylated liposomes which showed comparable anti-invasive activity *in vitro* (**Figure 3.6**) [233].

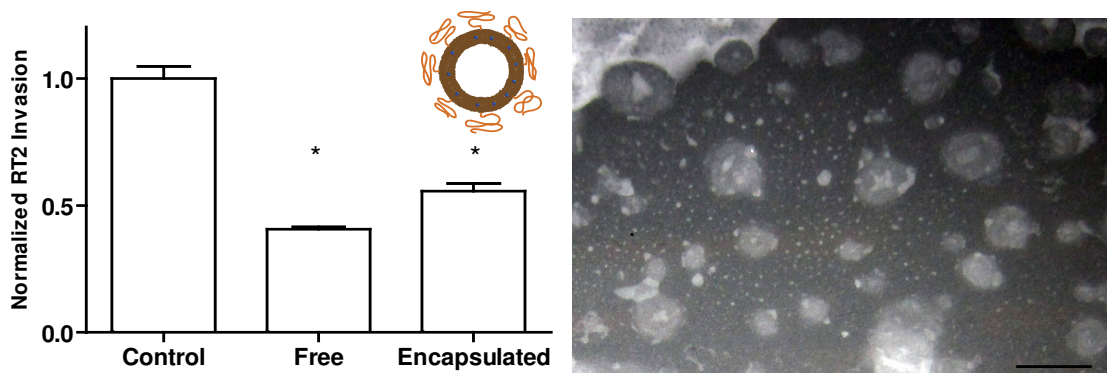


Figure 3.6: Encapsulation of IB in liposomes activity and characterization Using boyden chamber invasion assay at the EC_{50} as determined previously, IB liposomes were seen to inhibit invasion with mild decrease in potency (left). IB liposomes were imaged using Transmission Electron Microscopy and confirmed to be around 160 nm (right, scale bar is 200nm).

IB could consistently be loaded into liposomes with a molar drug:lipid ratio of 0.07. This low encapsulation relative to efficiency of loading compounds such as doxorubicin is due to the hydrophobic nature of IB yielding integration into the lipid bilayer as opposed to the hydrophilic core within the liposomes. Stability analysis revealed that structure of these liposomes was not compromised through IB loading as assessed by both release kinetics of IB incubated with serum at physiological temperatures and through loading and release of doxorubicin. This was further confirmed in subsequent pharmacokinetic studies (**Figure 3.7A**).

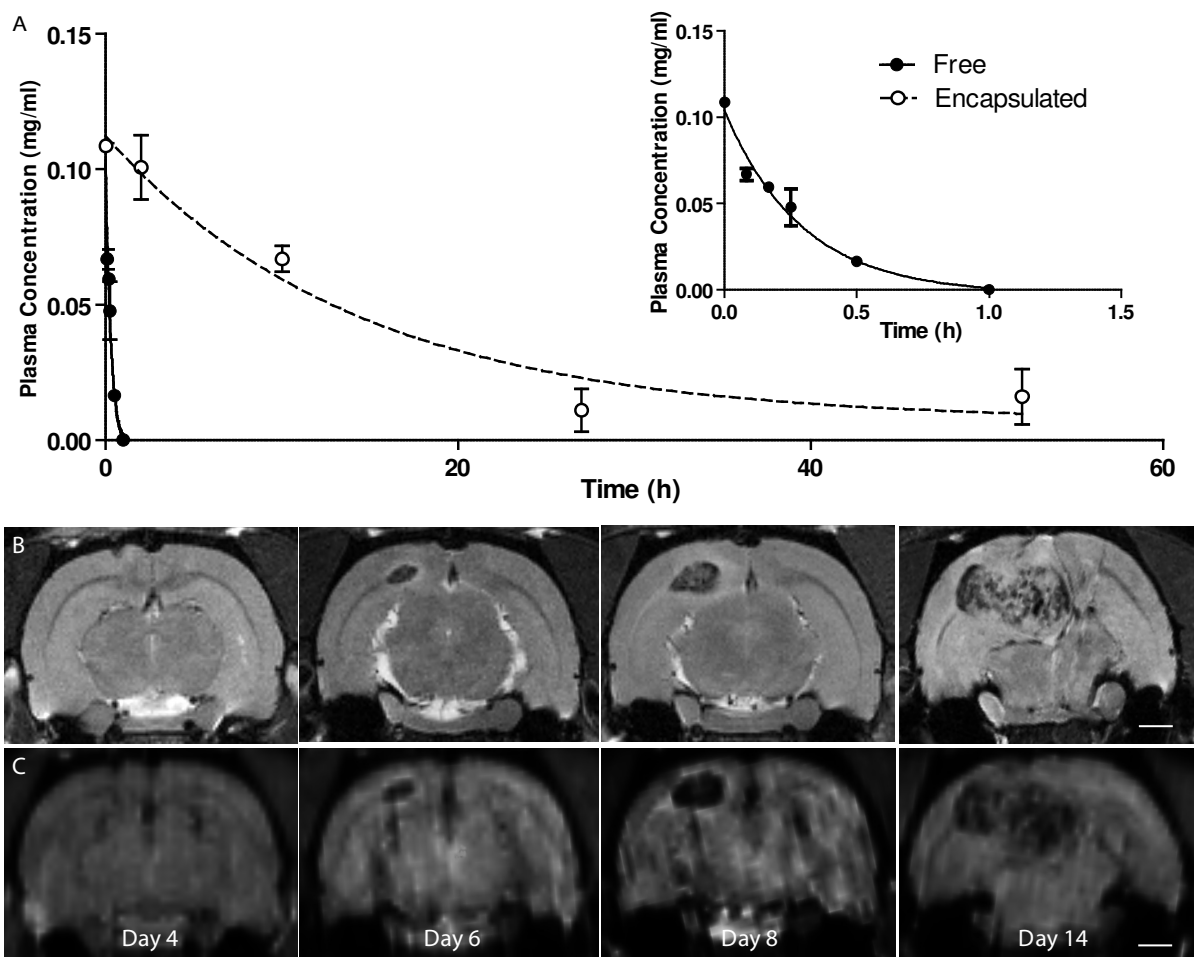


Figure 3.7: Encapsulation of IB in liposomes testing *in vivo* A) *In vivo* IB shows poor circulation time (inset: $t_{1/2}=11$ minutes) and encapsulation prolongs circulation time ($t_{1/2}=18$ hours). B) T₂-weighted images at largest tumor slice in live rats showing brain morphology. C) Omniscan-loaded IB liposomes in tumor site imaged with T₁-weighting on day 4 (precontrast image shown) and after 2, 4, and 10 days. Nano-IB accumulated in tumors after 2 days and showed distribution through brain after 4 days hours. Signal was gone 10 days after injection indicating degradation of nano-IB and dissipation of the gadolinium.

Injection of nano-IB into adult male rats yielded a significant increase in the circulation time of the drug increasing half-life to 18 hours (3 mg/kg IB) (**Figure 3.7A**). It is well-established that many solid tumors exhibit an enhanced permeability and retention (EPR) effect which allows nanoscale particles such as liposomes and micelles to passively accumulate at the tumor in proportion to circulation time due to compromised

tumor vasculature [231, 241]. For the RT2 tumor model, this effect was confirmed both by injection of rhodamine-labeled liposomes with postmortem microscopy and through injection of Gadolinium-DTPA (Omniscan) loaded nano-IB followed by subsequent MRI for T₁ enhancement (**Figure 3.7C** with companion T₂-weighted images in **3.7B**). This revealed that the nano-IB accumulates in RT2 tumors and that the nanocarriers remained at the tumor site for up to 4 days after injection. The signal dissipates and fades over time indicating nano-IB degradation and gadolinium clearance from the site. Using histological techniques, organs in animals receiving the nano-IB were collected and assessed through H&E staining for any signs of toxicity (**Figure 3.8**), particularly in the liver and spleen where it is known that liposomes will accumulate. There was no difference between the untreated and treated animals' organs.

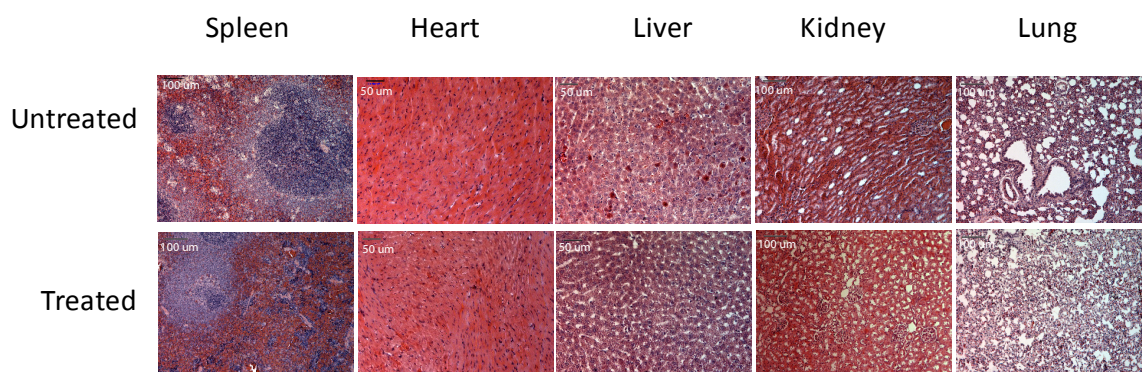


Figure 3.8: IB yields no observable toxicity towards non-target organs as compared to untreated animals. Rats bearing tumors were delivered either nano-IB or saline liposomes and organs harvested after two treatments. There were no observable differences in vital organs.

3.4.4 Nano-IB inhibits invasion in the RT2 model

Nano-IB, (IB concentration of 3 mg/kg) was intravenously injected on day 4 and day 7, post inoculation of animals with RT2 cells. One sub-set of animals were sacrificed 11 days after inoculation for tumor analysis. The nano-IB treated tumors were compacted with fewer regions of necrosis as compared to control tumors (**Figure 3.9A**).

Quantification of tumor density (DAPI stained nuclei/area of coronal section) increased significantly upon treatment (**Figure 3.9D**, right, $t(8)=5.59$, $p < 0.001$). Tumor margins were selected for analysis to account for differences in tumor shape due to invasion of the cells away from the injection site. The margin was defined to be the point at which there was >50% staining for either neurofilament (healthy brain-red) or GFP expressing RT2 (green) as shown in **Figure 3.9C**. Cells crossing this boundary were counted at different locations throughout each tumor ($n=4$ animals per group). There was a significant decrease in the number of cells crossing the margin regardless of how far they migrated (**Figure 8D**, left, $t(6)= 5.36$, $p < 0.01$). Consequently, the data demonstrated that increasing density of tumor inversely correlates with decreased invasion beyond the margin. Similarly, examining the margins using H&E (**Figure 3.9B**), there was a stark difference between the treated and the untreated tumors confirming the fluorescent images and analysis. In a sub-set of animals that were not euthanized on day 11 and allowed to live until they met the criteria for euthanization, nano-IB therapy led to a small (12.5%), yet significant increase in survival ($t(7)=2.35$, $p < 0.05$). No significant increase in survival was seen with single administration on either day 4 or 7 after tumor inoculation (data not shown).

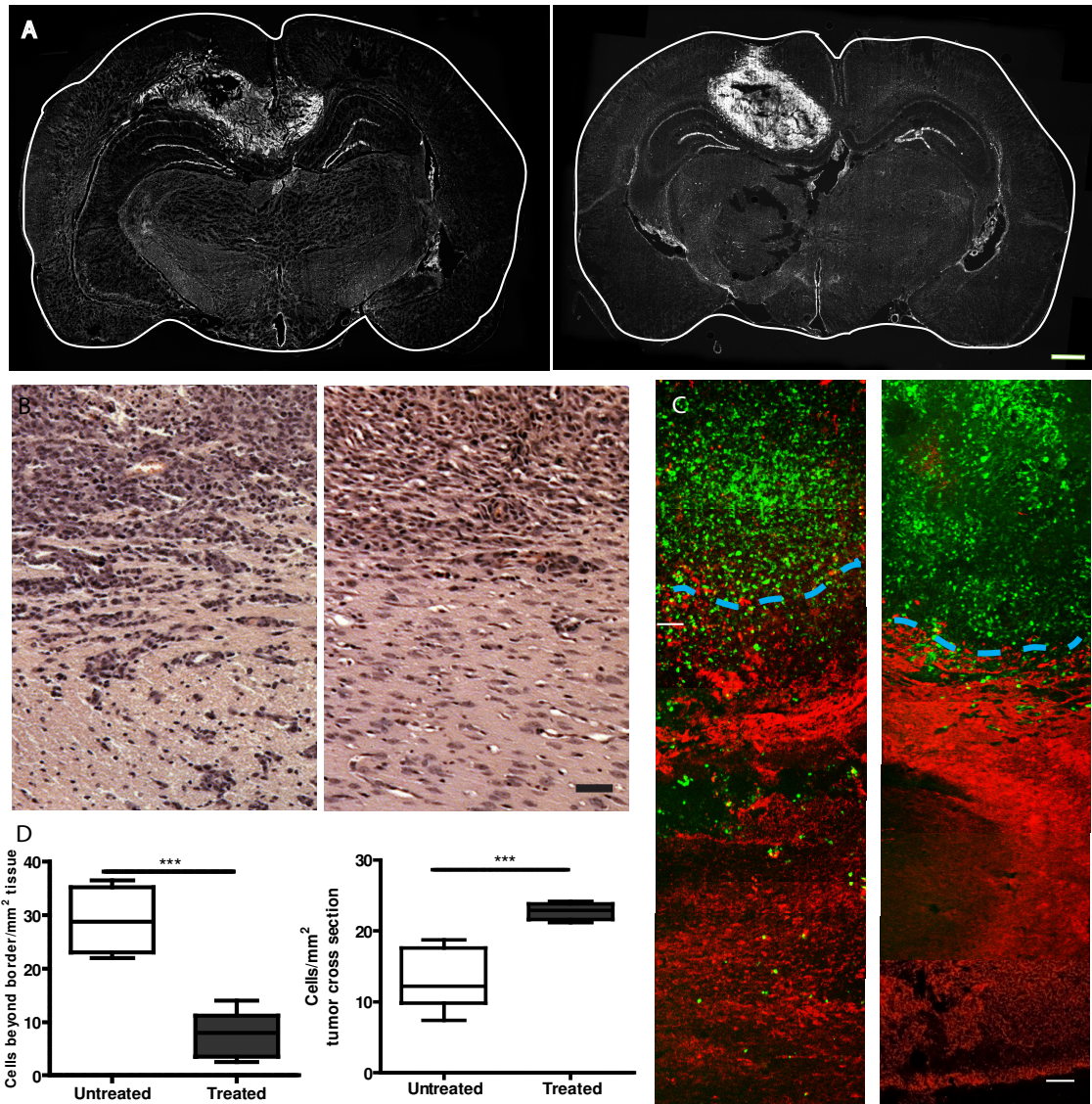


Figure 3.9: *In vivo* delivery of nano-IB yields a decreased in invasion A) Untreated (left) and treated (right) RT2 tumors in coronal slice with tumor stained with DAPI (white) showing a more condensed tumor (representative images from n=5 per group, scale bar=1mm). B) Examination of tumor borders indicates a decrease in invasion shown by H&E staining, left:untreated, and right:treated, scale bar=50 μ m. C) Staining tumor cells for GFP expression (green) and surrounding healthy brain stained with neurofilament (red), quantification of invasion beyond the border (blue dotted line) by counting cells per area of tissue (scale bar =100 μ m). D) left: Quantification of tumor cells beyond borders shows a significant decrease in migrated cells ($t(6)= 5.36, p<0.01$). Right: this inversely correlates with quantification of tumor density ($t(8)=5.59, p< 0.001$) in coronal slices.

3.4.5 IB inhibits invasion through regulation of actin polymerization

After nano-IB was delivered to tumors on day 4 and 7, *in situ* tumor samples were harvested for microarray analysis and western blotting (independent samples). A Rat 230 2.0 affymetrix microarray revealed that the nano-IB treated tumors (n=3) had approximately 70 genes changing as compared to control untreated tumors (n=3) (Appendix 1). Further, this data was compared to healthy, non-tumor regions of brain (Appendix 1) from control animals (n=3) in the same area of the cortex to understand how these changes relate to underlying mutations in the tumor.

Using Ingenuity Pathway Analysis, we determined the relationship between the changes in expression represented in the mRNA microarray and which upstream proteins may be involved in the changes in invasion *in vitro* and *in vivo* (**Figure 3.10A**). Interestingly, one subset of genes involved in actin polymerization and depolymerization: profilin-1 (-2.342), scinderin (+2.891), α -actin (-2.379), calgranulin (-2.101), and rhoGDP dissociation inhibitor alpha (+3.205) were greatly modulated in nano-IB treated tumors. Using rtPCR on pooled mRNA samples from 3 animals, these changes were confirmed quantitatively (**Figure 3.10B**). Further, using Western blotting on pooled protein samples from 3 animals, again most of these changes were confirmed to carry through to protein expression with the exception of the minimal decrease in profilin-1 (**Figure 3.10C and D**). This suggests that alters the invasion of tumors by affecting actin, consistent with *in vitro* effects observed on IB-treated RT2 cells (**Figure 3.11**).

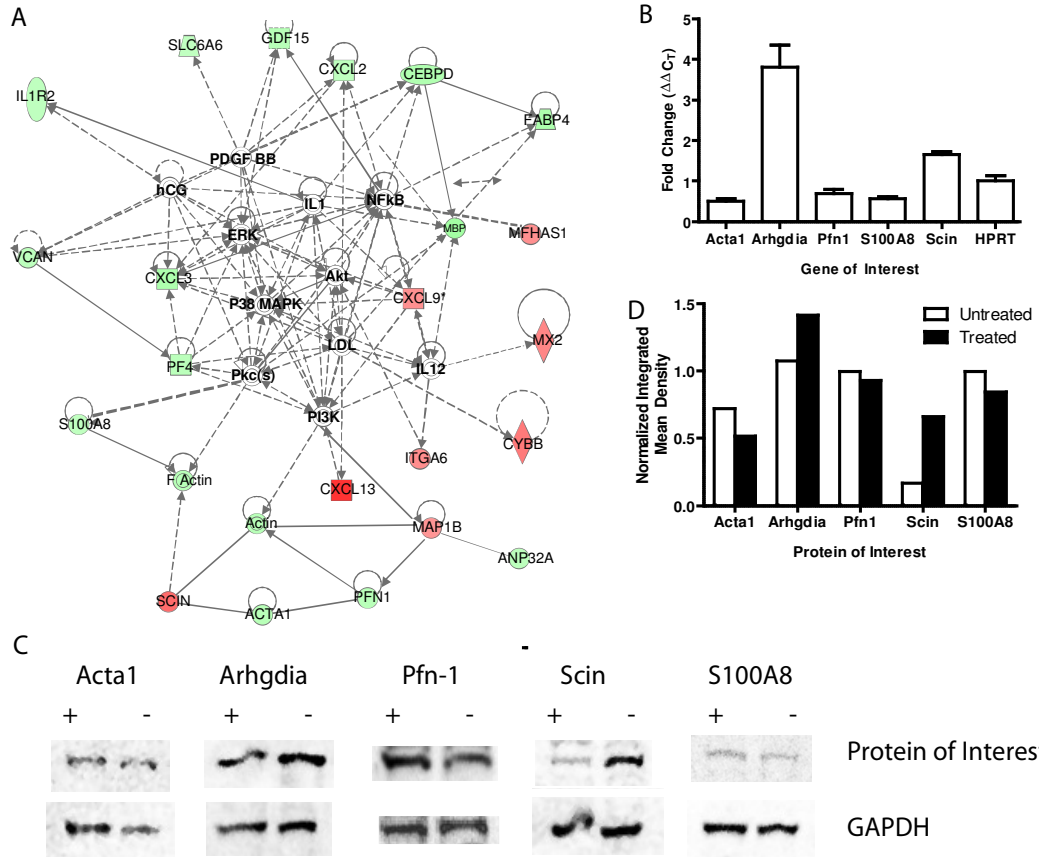


Figure 3.10: A candidate mechanism of action was determined *in vivo* using microarray analysis A) Inegenuity Pathway Analysis on microarray results shows actin regulatory elements and possible upstream protein regulators were shown to be altered in a manner that would decrease invasion of tumor cells. B) Results from microarray were confirmed using rtPCR. C) Analysis of pooled protein samples run on Western blot. D) Western blot gels for each protein.

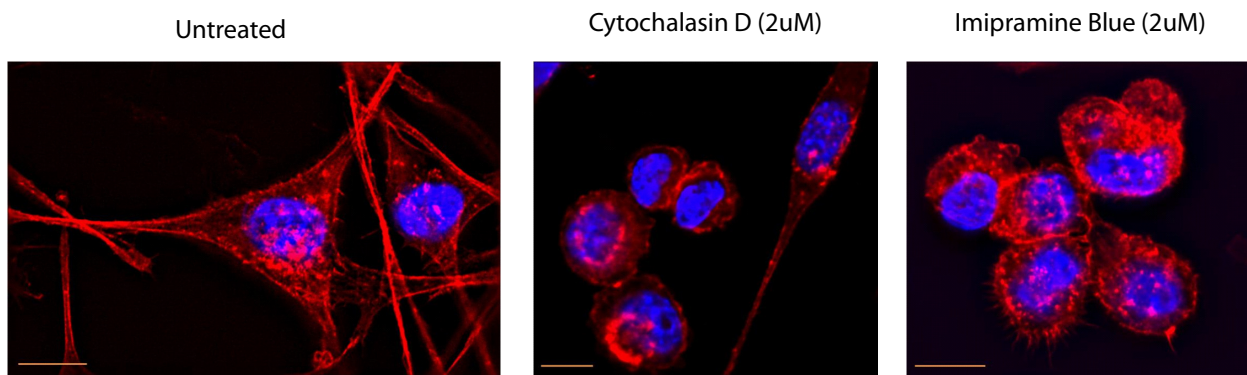


Figure 3.11: Effects on cell spreading seen *in vitro*. RT2 cells were incubated with ethanol, cytochalasin D, or Imipramine Blue for 24 hours then fixed and stained. Red=F-actin (phalloidin), blue=nucleus (DAPI). Scale bar = 10 μ m.

3.4.6 Combination therapy with Doxorubicin causes remission of aggressive glioma

To determine the effect of nano-IB in enhancing survival, we investigated a combination therapy regimen with the chemotherapeutic, Doxorubicin. Doxorubicin was chosen because it has been implicated in enhancing invasion of tumors through its anti-angiogenic effects [110]. Further, it is has been delivered in liposomal formulations minimizing toxicity and yielding similar delivery characteristics to our nano-IB with beneficial effects in brain tumors [32]. Last, to test the hypothesis of anti-invasive treatment aiding in chemotherapy and not some synergy of the two molecules, we performed IPA based on microarray data and known Doxorubicin interactions to show no possible synergy. RT2 cells were treated *in vitro* with DXR and IB (both free and liposomal forms) to determine if there was a synergistic effect (**Figure 3.12A**). Treatment was performed at a range of concentrations (50nM-200 μ M DXR) and shown here for the IC₅₀ of DXR in RT2 glioma [300nM \pm 23.71 (-IB) $R^2=0.97$, 220nM \pm 71.03 (+IB) $R^2=0.71$, n.s.]. These data indicate no synergy in mechanism *in vitro* for enhancing cell death.

Four groups were used in this study: control (saline liposomes), IB (nano-IB), DXR (nano-DXR), and IB + DXR (nano-IB, 3 mg/kg on day 4 followed by nano-DXR, 7

mg/kg, on day 7). All groups received two injections of liposomes on days 4 and 7 to account for any potential lipid load effects [242]. Though previous data indicated a slight increase in survival of RT2 inoculated animals with two injections of IB, there was no increase seen with a single injection. For the conditions of this study, the survival time for this aggressive RT2 line ranged from 13 and 24 days on average over many trials (data not shown). MRI was taken at day 7 (**Figure 3.12C**) to confirm tumor presence before treatment. Animals were excluded if a tumor was not identified via MRI. Lipid load was the same for all groups (55 $\mu\text{mol/kg}$) to account for differences in circulation time and accumulation at tumor attributed to decreased reticuloendothelial (RES) clearance[242].

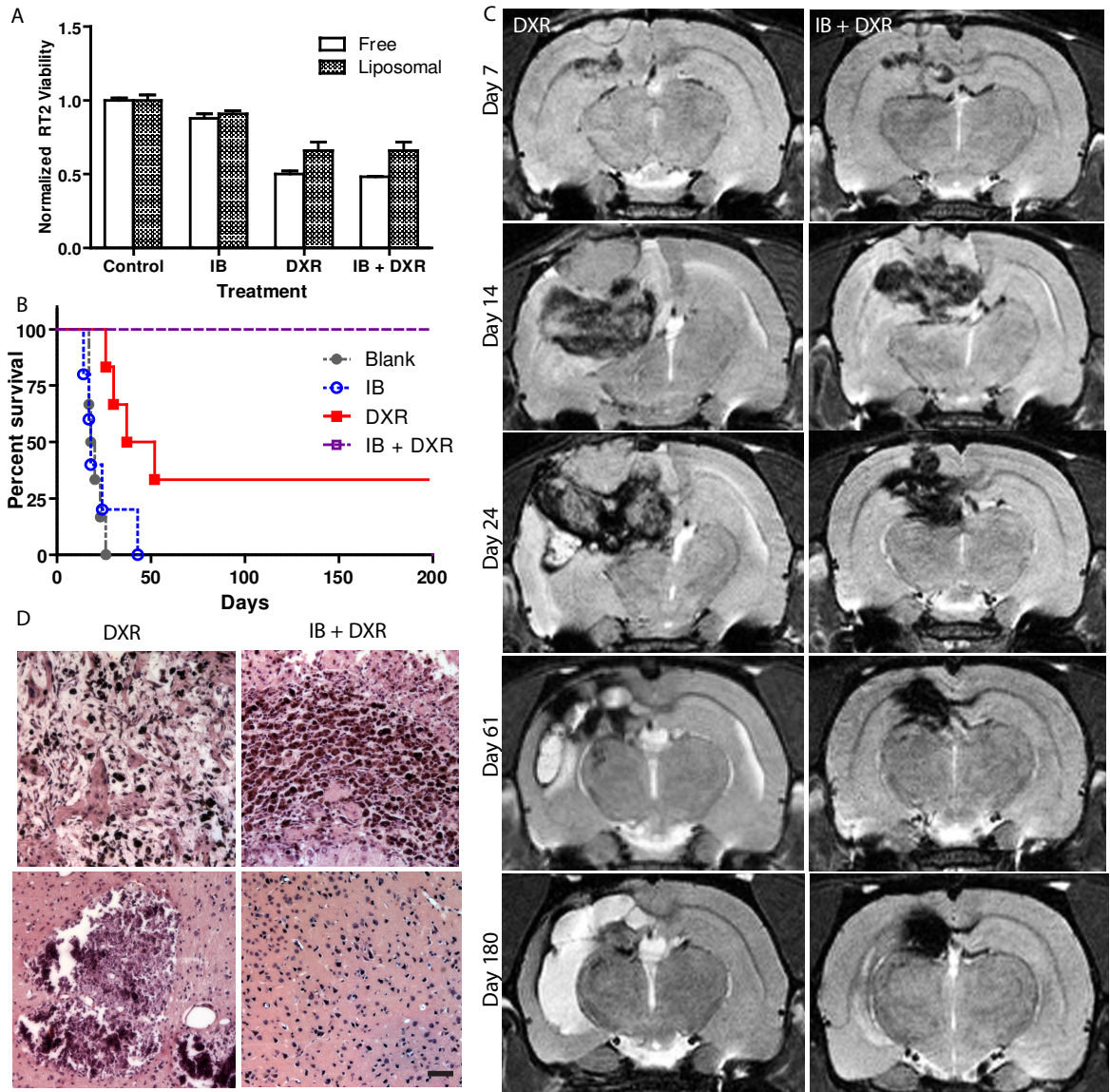


Figure 3.12: Figure 6: Delivery of IB before Doxorubicin (DXR) yields increased survival after a single treatment A) Treatment of RT2 glioma with IB ($5\mu\text{M}$) and Doxorubicin ($0.5\mu\text{M}$) *in vitro* shows no enhancement of cytotoxicity using both free formulations and liposomal formulations. B) Survival study *in vivo* shows increased survival when animals were treated with nano-IB before DXR ($p < 0.05$). C) MRI of animals from the combination group confirms disappearance of tumor over time in co-treated tumor (right) as compared to recurrence in DXR alone treated tumor (left). D) End of study H&E histology shows hemosiderin in tumor site (top) and DXR treated animals show abnormal tissue throughout brain (bottom)

Remarkably, there was 100 percent survival in the sequentially treated group that received nano-IB followed by nano-DXR for a period of 200 days or greater (**Figure 3.12B**). The nano-DXR treated group without nano-IB combination therapy had a small subset showing survival (as of end of study) and with the majority of the groups resulted in death (as assessed by display of signs of morbidity and confirmed by tumor presence) early in the study. There is a significant increase in the median survival time between the DXR group alone and the IB-DXR group from 44.5 days for DXR to >200 days for IB-DXR therapy (**Figure 3.12B**). The survival data indicate that there is dramatic disappearance effect when nano-IB was prior to treatment with nano-DXR. This was confirmed further by premortem MRI (**Figure 3.12C**) and postmortem histology (**Figure 3.12D**) of surviving animals in both groups. The DXR group at six months showed evidence of tumor presence on MRI (left) with large-scale inflammation indicated in T₂-weighted images by excess fluid in the brain, and a necrotic core surrounded by differentially dense tissue (as compared to normal brain tissue). These attributes were similarly seen in earlier timepoint DXR group animals preceding display of signs of morbidity. In contrast, in IB-DXR animals, there was a black mass seen on the T₂-weighted MRI (right) which appeared at day 60 and maintained size and shape until the end of the study. Further, when animals were injected with free Omniscan (Gadolinium-DTPA) and imaged, there was no contrast enhancement seen in the IB-DXR group though there was cortical enhancement in the remaining animals from the DXR group indicating revascularization and disruption of the blood brain barrier (**Figure 3.13**). Lastly, histological analysis of tissue postmortem indicated presence of hemosiderin positive staining indicative of reactive oxygen related stress at the original tumor site and evidence of abnormal tissue in DXR animals but not in IB-DXR animals (**Figure 3.12D**) as assessed by H&E.

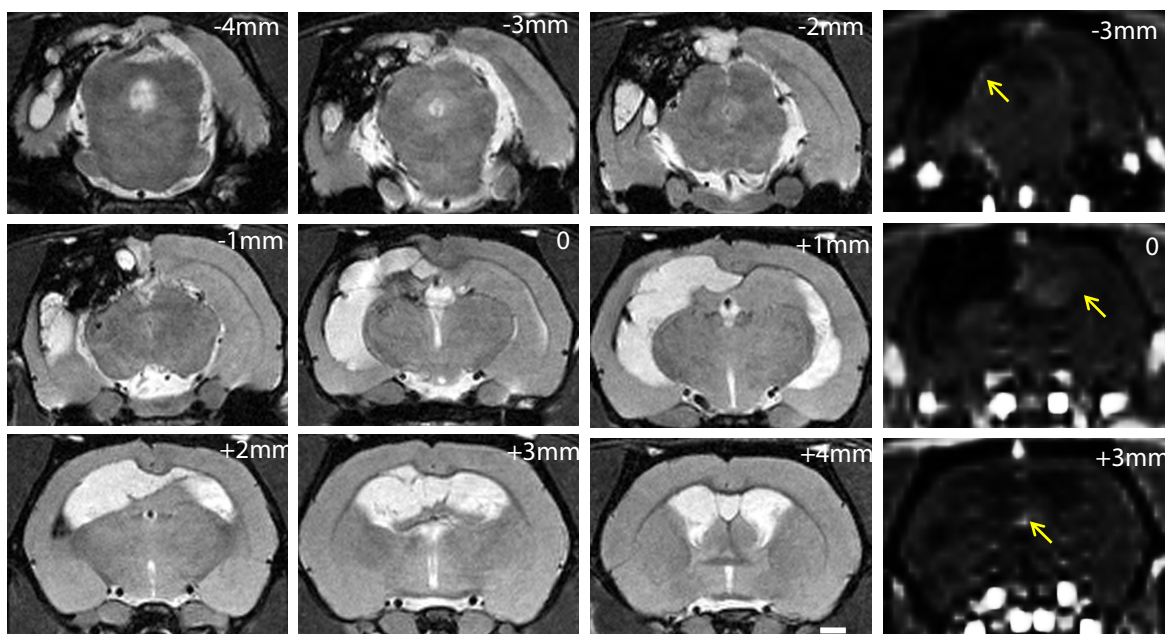


Figure 3.13: T₂- and T₁-weighted MRI of DXR alone treated tumor. DXR treated tumor at end of study showing coronal sections through the brain away from the site of implantation (center square) in 1mm increments. MRI showed incidence of tumor-type structures through the brain. Further, injection of Omniscan showed contrast enhancement on T₁-weighted images (far right, yellow arrows indicate regions of enhancement).

3.5 Discussion

The ability to inhibit glioblastoma (GBM) invasion represents a significant clinical breakthrough. Many drugs have been heralded as being anti-invasive such as chemotherapeutics in low doses and other specially designed molecules [51, 243-245]. However, these drugs fail clinically or to date, there is no way to determine if, in fact, these drugs work as anti-invasive agents. Thus a compound that specifically inhibits glioma invasion, should lead to better outcomes when administered in combination with currently available cytotoxic compounds (such as Doxorubicin) and can have serious, beneficial implications for the management of glioma.

Imipramine Blue (IB) inhibits invasion of many glioma cell lines *in vitro*, and of the RT2 glioma *in vivo*. Through quantitative analysis we show that invasion beyond the tumor border was significantly inhibited upon treatment with nano-IB. Correlatively, IB treatment increased tumor density which is advantageous to all current treatments of GBM. Resection of a more contained tumor (similar to lower grade tumors) has a higher success rate and limiting the area of irradiation prevents adverse side effects and activation of the surrounding brain [98, 106, 229] Further, Imipramine Blue, acts via a novel mechanism of action as compared to previously tested anti-invasive compounds [222, 243, 246, 247].

Regulation of depolymerization of F-actin is one of the mechanisms by which the RT2 tumors are spatially ‘contained’ *in vivo*, however, our analysis indicates that Imipramine Blue causes transcription level alterations as opposed to commonly seen direct interactions with F-actin. Many of the genes that are implicated in the IB mode of action are commonly mutated in cancers leading to decreased cell stability and heightened motility [144]. Altered expression of actin-related genes in general has been seen in many cancers including glioma [248]. Acta1 (↓), scinderin (↑), calgranulin (↓), and profilin-1(↓) are implicated downstream of the RhoGTPases possibly indicating inhibition by RhoGDP Dissociation Inhibitor α (↑) in signaling [158, 249, 250]. Decreased rhoGDI α expression has been correlated with increased malignancy in brain tumors [251]. Overexpression of calgranulin (S100A8), calcium-binding transcription factor, correlates with malignancy of lung adenocarcinoma, colorectal cancer and cervical cancer [252-254]. Scinderin, a gelsolin homologue known to sever and cap actin filaments, is used in general cell motility [164]. Gelsolin has been shown to be downregulated in 60-90% of cancers, though scinderin is largely understudied in cancers [255]. In our analysis, scinderin was the most highly upregulated both at the transcriptional and the protein level indicating a probable role in decreasing the invasiveness of RT2 *in vivo*. Further, since these proteins tend to be preferentially

mutated in cancers, there is a selective effect for tumor tissues that is not translated to other cell types such as astrocytes. However, since analysis was performed many days after exposure of cells to nano-IB (7 days of treatment), it is possible that these transcriptional level alterations may be a result of earlier cellular events. In the same vein, the lasting effect of treatment in the survival study may indicate that these expression level changes are more important than initial alterations in cell functionality.

Ingenuity Pathway Analysis revealed that many proteins upstream may be regulating this cycle of large structure actin changes including the major players in cancer progression and metastasis (NFkB, PI3K, PKC)[216, 256]. Many of the other molecules implicated through microarray could have further anti-tumor activity *in vivo* that may not be seen *in vitro* such as extracellular matrix (ECM) secretion (versican), integrin-binding (ITGA6), and chemokine secretion for immune recruitment or training (CCL2, CCL9, CXCL13)[256, 257]. The ECM and the cell's interaction with it is a major player in tumor progression showing increased motility with lower integrin binding and ECM secretion being vital for invasion [15, 145]. Further, chemokines are highly involved in both immune system interaction and migration of tumor cells away from the primary site[258]. These added changes in phenotype may contribute to the decreased malignancy of these tumors and response to chemotherapy *in vivo*, however, the decreased motility is the primary effect of the compound.

Though nano-IB alone increased survival modestly in rats bearing the RT2 glioma, its ability to enhance the efficacy of clinically approved chemotherapeutics such as DXR potentially represents a significant advance. DXR is an excellent cytotoxic agent for the treatment of RT2 glioma with an IC50 well below that of comparable cytotoxic agents such as paclitaxel and temozolomide. Further, in its liposomal formulation it has been clearly demonstrated to be efficacious in minimization of tumor burden and recurrence after treatment [32]. Lastly, recent reports indicate that liposomal DXR's mechanism of action is potentially like anti-angiogenic drugs in killing the

endothelium and thereby cutting off tumor blood supply[110]. In the RT2 model, we have observed that animals given nano-DXR will often survive longer but the tumors at the time of death are much more diffuse with metastasis throughout the brain. Hence, the use of a drug that could in fact inhibit the cells from invading even with treated with therapies that might enhance invasion presents a stringent test for the evaluation of nano-IB's anti-invasion efficacy.

One hundred percent of animals given sequential treatment of nano-IB with nano-DXR (n=5) survived with no observable tumor mass seen by contrast-enhanced MRI and histology as compared to nano-DXR animals. The ability of this combination of drugs to yield complete survival and tumor disappearance after only a single treatment is striking. Other studies have shown comparable survival with metronomic or multiple treatments but not in a single round of treatment [180]. The use of Doxorubicin has been avoided largely due to toxicity however and cost-benefit to the patient, liposomal encapsulation avoids such an effect and coupling with nano-IB enhances the efficacy and survival such that the cost-benefit ratio shifts[259].

The tissue remaining after treatment with both drugs resembles hemosiderin-laden macrophages which are likely the result of the tissue dying with resulting blood-brain barrier sealing at the original tumor site. This morphology has been seen post resection in tumors both on MRI and histologically [260]. Further, the histology reveals diffuse spread of DXR-treated tumor which was also visible on T₂-weighted MRI through the cortex. The combination of these two treatments is highly beneficial to the treatment of glioblastoma in only a single treatment. It is possible of course that there are, other possible secondary effects of the drug that can lead to enhancement *in vivo* though none was seen *in vitro*. It has been observed that MMP inhibitors have anti-angiogenic effects along with anti-invasive effects which could be occurring with IB as well [221]. This alteration could lead to enhanced delivery to tumor after pre-treatment and enhance the effect. Further, immune system involvement in cancer can dictate the response of

tumor cells to chemotherapy and could be at play here[261]. Regardless, 100% disappearance of a highly invasive glioma model is potentially very significant.

CHAPTER 4

CO-LOADING OF LIPOSOMES WITH IMIPRAMINE BLUE AND DOXORUBICIN

4.1 Summary

Glioblastoma (GBM) is a difficult disease to treat because of its invasive nature. Further, many chemotherapeutics that work against other cancers fail against glioblastoma because of the specific response of cells to invade the brain. There has been success with liposomal formulations of many chemotherapeutics with GBM, the most striking of which is doxorubicin. Further, due to the ability of DXR to efficiently and remotely load into liposomes, this formulation is advantageous for co-delivery with a high hydrophobic drug which will partition to the lipid bilayer of the nanocarrier. Using this approach, we have developed a co-loaded Imipramine Blue- Doxorubicin liposomal nanocarrier for intravenous delivery to highly invasive glioma. Imipramine Blue (IB) is a potent anti-invasive compound that has shown promise in halting invasion and improving chemotherapy against glioblastoma *in vivo*. Here we show that the co-encapsulated IB-DXR liposome enhances survival from a median time of 44.5 days in DXR alone animals to >180 days for IB-DXR in an aggressive rodent model of glioblastoma yielding survival in many animals through a single treatment. Hence, we propose that this formulation would be an efficient means of treating glioblastoma to enhance chemotherapeutic efficacy and attenuate the invasive response after treatment which minimizing patient discomfort.

4.2 Introduction

The ability of glioblastoma to invade in the brain is a primary cause of recurrence and failure of common anti-tumor therapies such as chemotherapy, radiation, and

resection [22, 98, 256]. Recently, a novel compound, Imipramine Blue was shown to inhibit invasion in the malignant glioblastoma model RT2 in rats with complete survival. In this paper, separate nanocarriers were used to deliver IB and doxorubicin. However, clinically, patients would prefer to have a single injection which could yield remission of their tumor. Using nanocarriers for combinatorial therapies is becoming a common application of the nanotechnology and is thought to be a possible way to ease both systemic burden of circulating nanocarriers and minimize patient visits [262].

Imipramine Blue is a compound that halts invasion via a novel mechanism. Further, IB yields increased survival when combined with DXR. DXR kills cancer cells via DNA damage and subsequent apoptosis induction. Many cancers that have active MDR pumps can resist the ability of DXR to kill them [263]. However, it is unclear if IB is affecting this mechanism but instead is only yielding a synergistic effect *in vivo*. The mechanism by which survival is enhanced is purported to be due to the ability of IB to halt invasion. DXR has been shown to actually induce invasion of glioblastoma *in vivo* in rodent models [110, 264]. It is thought that this increase in invasion is due to the anti-angiogenic effect that Doxorubicin has upon delivery. Doxorubicin has been discounted in glioblastoma treatment in patients due to the toxicity that ensues from delivery and poor accumulation at the tumor site though liposomal doxorubicin has shown promise [32, 265].

Nanocarriers can be used to deliver chemotherapeutics in a passively targeted manner to solid tumors such as glioblastoma [235]. Liposomal nanocarriers consist of a phospholipid bilayer with an aqueous core. They can selectively accumulate in the tumor through the enhanced permeability and retention effect which takes advantage of the leaky vasculature of the brain tumor which will allow selective accumulation of the 150nm particles [204]. Use of this formulation for doxorubicin has been successful against colorectal cancer yielding accumulation at the tumor site, tumor death, and

reduced toxicity to the patient [32, 266]. Therefore, liposomal nanocarriers have gained popularity in the clinic for several different drugs after gaining FDA approval [267].

Co-delivery is a popular option for treatment of cancers because of the enhanced delivery and minimized stress to patients. The benefit of co-delivery of compounds is several fold. First, the tumor will receive both drugs without altering the pharmacokinetics of either compound. Second, possible drug interactions that can lead to toxicity if delivered separately are minimized. Third, the discomfort to the patient due to repeated injections is reduced. Many drugs have been co-delivered including doxorubicin and versepamil, and doxorubicin and vincristine leading to promising effects in animal models of cancer [268, 269].

In this study, we develop a stable dual encapsulated IB-DXR liposomal nanocarrier that synthesized through passive encapsulation of IB followed by remote loading of DXR. Further, we conduct survival studies showing that the IB-DXR nanocarrier enhances survival in the glioblastoma model RT2 in rats yielding remission of tumors. Lastly, using MRI analysis we show the progression of the tumor in response to treatment and track its size, following with histology to examine further the effect of combination of these two compounds *in vivo*.

4.3 Methods

4.3.1 Synthesis of Liposomes

Coencapsulated IB-DXR liposomes were synthesized by remote loading of DXR into 40 mM Stealth liposomes with passively loaded IB. IB liposomes were made as previously described with the following modifications: the solution was hydrated with 400 mM ammonium sulfate in place of the phosphate-buffered saline. The solution was dialyzed overnight in 1x PBS to yield the pH gradient for remote loading. DXR (in saline (2 mg mL⁻¹) was added to the solution at a ratio of 0.05 mg DXR per 1 mg lipid and heated to 60°C for 1h. Liposomes were passed through a Sepharose (GE Healthcare)

column and co-loaded liposomes were collected and concentrated via diafiltration to a final IB. IB liposomes, DXR liposomes, and control (lipid only) liposomes were formulated using the same methods with final drug:lipid concentrations within 10% of co-loaded.

4.3.2 Nanocarrier characterization

Nanocarrier size was assessed using Dynamic Light Scattering. Final IB content was assessed by absorbance at 610nm, and final lipid content was assessed by fluorescence detection (485 ex/610 em). For DXR content, liposomal nanocarriers were lysed with 5% Triton X-100 at 60°C before measuring absorbance (480nm) and fluorescence. Leak studies were conducted as previously described[270]. The thermal stability of the coencapsulated Doxorubicin was monitored in vitro. Coencapsulated liposomes were added to 25% v/v PBS and 50% v/v FBS and placed in 37°C water bath. At 24-hour increments, a sample of this mixture was taken and the amount of entrapped Doxorubicin was measured using fluorescence spectroscopy. The amount of encapsulated DXR was reported as a percentage of the initial amount encapsulated.

4.3.3 Cytotoxicity assays

RT2 glioma cell lines were maintained as described. For cytotoxicity assays, cells were plated at 100,000 cells/ml in 24-well plate and allowed to attach overnight. Wells were then treated with media solutions containing either coencapsulated liposomes, DXR liposomes, IB liposomes, or blank liposomes for 2 hours. The concentration of DXR was controlled at 5uM in each well. The concentration of IB in the wells with IB liposomes was equal to the concentration of IB in the wells with coencapsulated liposomes. Drug media was removed and fresh media was added after the two hours. Cells were then incubated with CCK8 (Dojindo) for 1 hour, media was removed and read at 490 absorbance. CCK8 assay was performed again at 72 hr after drug treatment and all readings were normalized to control conditions.

4.3.4 Survival studies

Animals were anesthetized via isoflurane inhalation and mounted on a stereotaxic frame. The head was shaved and cleaned and a 3cm incision was made through the skin to expose the skull. A 2mm burr hole was created in the skull using a Dremel hand tool mounted on the frame 2mm lateral and 2mm anterior to lambda. A Hamilton syringe was used to inject 10 μ l of cell solution over five minutes after which the syringe was slowly removed and the burr hole closed with bone wax. The wound site was closed using sutures (Ethicon), the wound cleaned, and flunixin meglumine administered intramuscularly. Animals were monitored daily after inoculation.

Seven days after implantation, MRI was performed as described followed by tail vein injection of either Doxorubicin liposomes (DXR), IB liposomes (IB), IB-DXR liposomes (IB-DXR), or saline liposomes (Control), at doses of 3 mg/kg IB and 7 mg/kg DXR. Animals were monitored daily and MRI was performed at intervals to monitor tumor progression. Animals displaying signs of morbidity including hunched posture, abnormal vocalization, weight loss, poor hygiene, or decreased movement in accordance with Georgia Tech IACUC guidelines. Animals were sacrificed by CO₂ inhalation upon display of any of these symptoms and the brain removed to confirm tumor presence.

4.3.5 Magnetic Resonance Imaging

Animals were anesthetized by 1-2% Isoflurane and placed in a 7T MRI (Bruker Instruments, Billerica, MA) equipped with a 30mm head coil. A T₂-weighted image was taken through the head using the following parameters: 2.0 s repetition time(TR), 48 ms echo time(TE), FOV=40mm x 40mm with a 256 x 256 matrix, slice thickness=1 mm, number of slices= 20, 2 averages per phase encode step requiring a total acquisition time of about 6 minutes per rat. MRI was performed before treatment began to confirm tumor presence and at intervals throughout the survival study to monitor the progression of the tumor and response to treatment. Rats not showing evidence of tumor were removed from

the study. For T₁-weighted MRI, animals were treated with either Gd-loaded nano-IB (for accumulation, 3 mg/kg IB) or free Gd-DTPA (Omniscan) for end of survival study tumor leak (final concentration of Gd was 0.15 mmol/kg). T₁ images were taken according to the following parameters: 2.0 s repetition time(TR), 48 ms echo time (TE), FOV=40mm x 40mm with a 256 x 256 matrix, slice thickness=1 mm, number of slices= 20, 2 averages per phase encode step requiring a total acquisition time of about 6 minutes per rat.

4.3.6 Histology

Sections were paraffin embedded and hemotoxylin and eosin stained for postmortem analysis.

4.3.7 Image analysis

MRI files were converted to image stacks and the tumor outlined by sight by a blinded student. The area was calculated using ImagePro analysis software and converted to volume based on the interslice thickness (1mm) and summed. When possible, volume was calculated in sagittal slices and compared to ensure there were no artifactual quantification difficulties in the coronal sections. In order to calculate the volumetric growth of tumors, images obtained from MRI were analyzed using the Image-Pro Plus software (Media Cybernetics, Inc., Bethesda, MD). The area where tumor was present was calculated in pixels for each slice of the sequenced images (20 slices). This area was then converted to mm² using a conversion factor of 72.8 pixels/mm². The tumor area from each slice was multiplied by the slice thickness (1mm) to obtain the volume. The tumor volume of the individual slices was then summed up get the total volume of tumor. The results of all the measurements were compiled in excel and analyzed.

4.3.8 Statistical Analysis

For multi-comparison studies, one-way ANOVA was performed with Bonferroni post t-test for pair-wise comparisons. For survival studies, Mantel-Cox analysis was performed between groups to compare curves. * $p < 0.05$, ** $p < 0.01$, *** $p < 0.001$.

4.4 Results

4.4.1 IB and DXR can be co-loaded into stable liposomes

Through the use of both passive and remote loading, we have been able to encapsulate both compounds into single liposomes (**Figure 4.1**). Use of the Imipramine Blue liposome formulation (requiring lower concentrations of cholesterol to enable lipid bilayer loading), DXR is remotely loaded with similar efficiency to literature reported values [233, 265, 271].

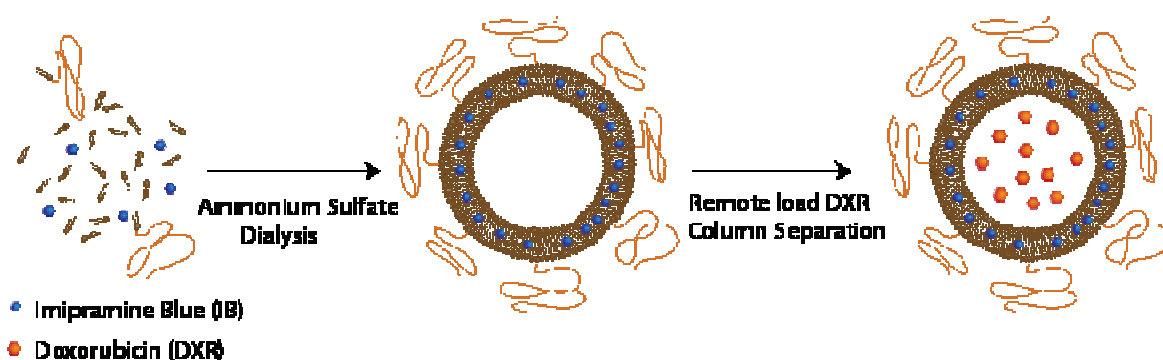


Figure 4.1: Co-loading of IB and DXR in liposomes IB is passively loaded into liposomes and a pH gradient is formed after dialysis. Doxorubicin is then actively loaded via this gradient. Separation by column and subsequent concentration yields the final co-loaded product.

However, it is necessary to load less DXR per lipid so that once liposomes are concentrated to the final IB dose, the same DXR dose is maintained. Further, through plasma stability studies, it was shown that there was only 20% leak of DXR from IB-DXR liposomes which was not significantly different from that seen with the DXR formulation (stealth) (**Table 4.1**). Hence, we are confident in the ability of our nanocarrier to enable delivery to glioma safely through passive targeting.

Table 4.1 Characterization of liposomes Data indicates the size, drug:lipid ratios, and stability (represented by %leak) of the different formulations of liposomes.

Formulation	Average Size (nm)	Leak after 48h	DXR:Lipid Molar Ratio
IB	160 nm	n/a	n/a
DXR	150 nm	16.461%	0.09
IB-DXR	161 nm	16.934%	0.09

4.4.2 IB-DXR nanocarriers show no synergistic cytotoxic effect in vitro

In vitro experiments using both RT2 and U87MG glioma cell lines, the synergistic effects of IB and DXR were examined as a co-encapsulated formulation (**Figure 4.2**). Previous publication has shown that there should be no synergy with the dual encapsulated formulation and that is what our results confirm. Further comparison to separately delivered IB and DXR liposomes versus the co-loaded liposomes at the same total drug concentrations of each yields no increased or decreased cytotoxic effect beyond that of DXR liposomes alone. Therefore, we conclude that there is no advantage of the

IB-DXR co-loaded formulation to the individual cells above that seen with DXR liposomes alone.

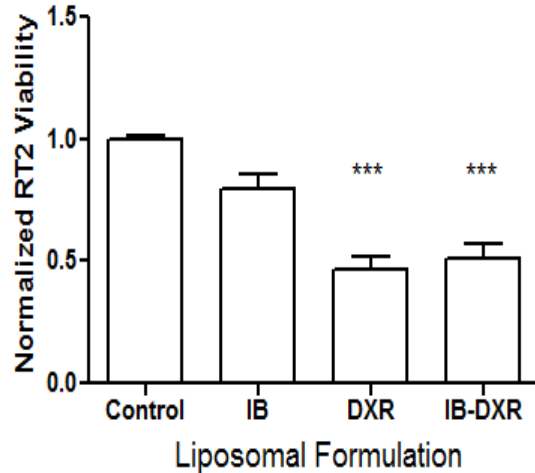


Figure 4.2: There is no enhancement of cytotoxicity with dual liposomes A) Cytotoxicity of RT2 glioma exposed to IB-DXR liposomes versus IB + DXR liposomes showed no change in viability B) Similarly, U87MG did not show enhanced cytotoxicity. *** $p < 0.001$ as compared to control by t-test.

4.4.3 IB-DXR co-loaded liposomes enhance survival over DXR alone in vivo

Through a single injection of the co-loaded liposomes 7 days after tumor inoculation, we saw an enhancement in survival times with a median survival time increase from 44.5 days in DXR alone animals to >200 days in the co-loaded IB-DXR administered animals (**Figure 4.3**). The change in survival curves was not significant, however, when analyzed via Mantel-Cox statistical test ($X^2(1)=1.580$, $p > 0.05$). However, the complete survivors at the end of the study as compared to the DXR alone treated group was greater and we are confident in saying there is a benefit to the delivery of IB-

DXR coloaded as compared to the DXR alone and this is furthered by the postmortem analysis of the animals treated with the co-loaded formulation.

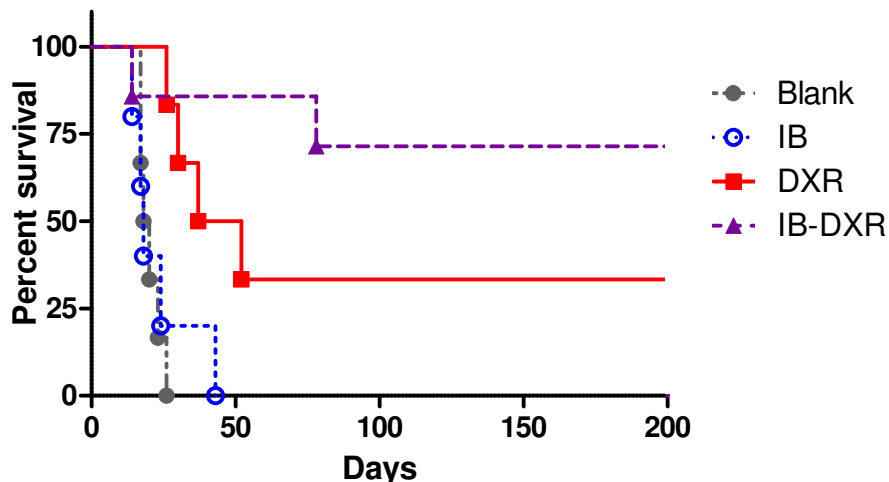


Figure 4.3: IB-DXR increases survival over DXR alone treatment Survival data from 6 month survival study in rats inoculated with RT2 glioma indicating increased survival percentage with the dual-loaded liposome. Animals were treated one time at seven days post tumor inoculation and monitored with MRI. Animals were sacrificed upon display of criteria for euthanasia.

4.4.4 IB-DXR animals have no evidence of tumor

Through MR imaging we were able to track the progression of the tumor growth and response to treatment live (**Figure 4.4**). The control groups with no tumor remission (control and IB treated animals) showed tumor growth without any real remission leading to subsequent death of most animals before day 24 when the third MRI was taken. These animals had strong evidence of fluid influx into tumor represented by white areas (F) and large ventricles in the brain. Further, there was a morphological change in the surrounding brain indicating pressure from the tumor mass. DXR and IB-DXR animals had continued tumor growth after treatment on day 7 and then subsequent necrotic areas (N) as the cancer died due to lack of nutrients or due to treatment.

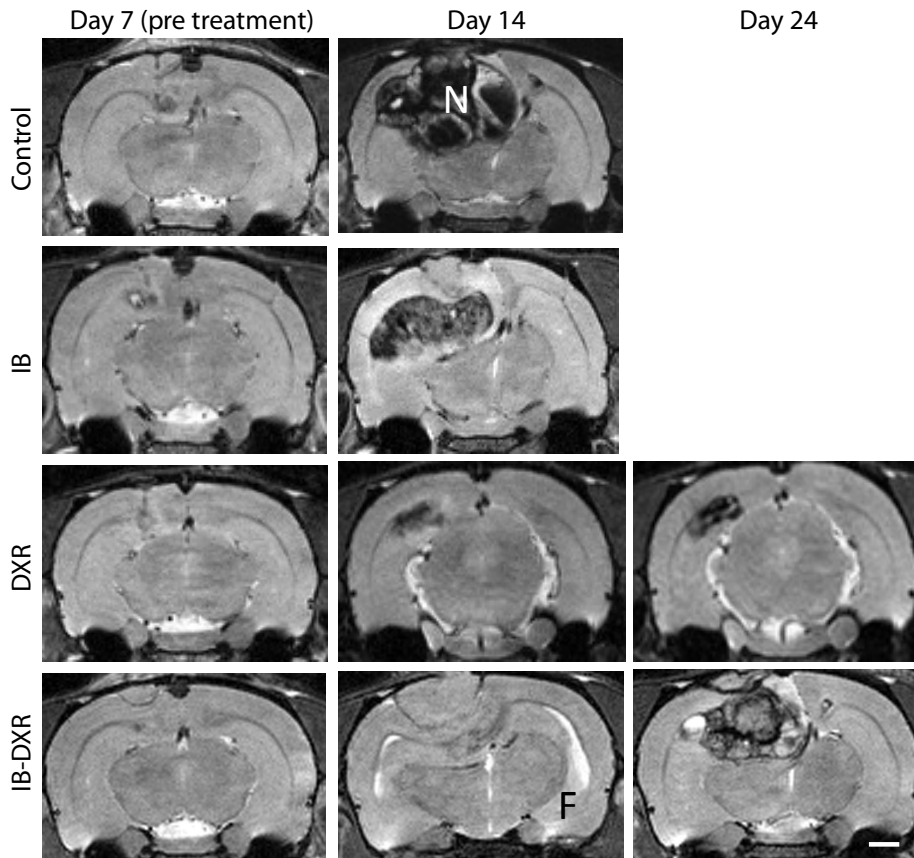


Figure 4.4: Pre and post treatment MRI for all groups. IB and control animals were euthanized before day 24. DXR and IB-DXR animals showed necrosis (N) by day 24 which was 17 days after treatment. Further, through T₂ images, excess fluid in the brain could be seen (F) which was likely due to increased influx into the tumor from leaky blood vessels.

The last interesting result was the recurrence of indicators of inflammation in the DXR animal that was not present in the IB-DXR animals as the area of necrosis seemed to maintain after treatment in complete survivor animals. This result was similarly seen in the previous publication with the co-treated animals in this tumor model. Growth curves indicating the MR image “footprint” of the tumor throughout the study show this growth-reduction-leveling of the growth characteristics in the IB-DXR animals and the subsequent uptick in tumor enhancement in the DXR alone animals (**Figure 4.5**).

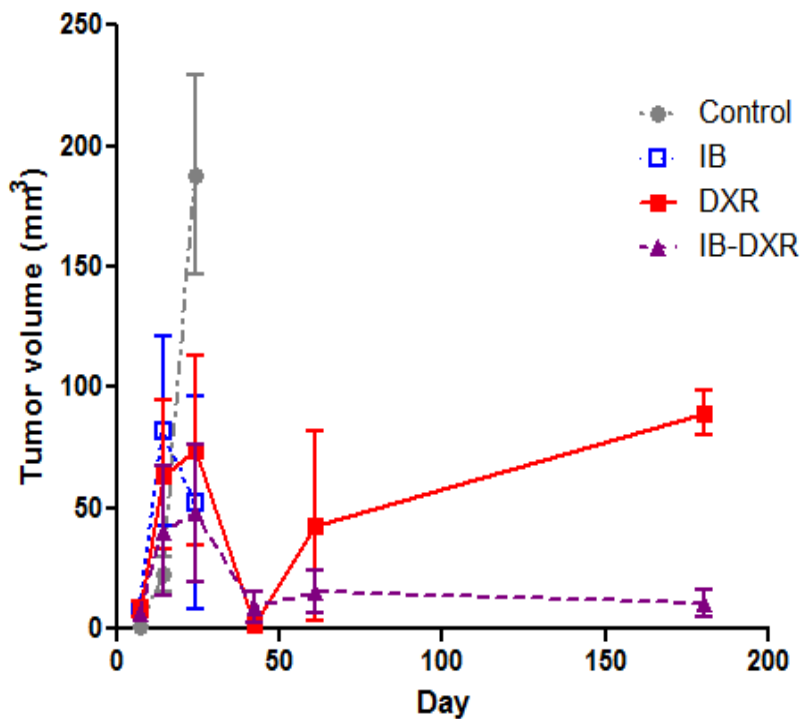


Figure 4.5: Tumor growth curves for all groups shows regrowth of DXR tumors (n=2 at end of study) vs maintenance of tumor size in IB-DXR treated tumors (n=4 at end of study). Other tumors showed exponential growth as is expected in control tumors. Statistical significance could not be calculated due to the low animal numbers at end of study timepoints.

4.4.5 No tumor is present through histological analysis

The ability of IB and DXR together to enhance tumor reduction is further validated in the post mortem histological analysis of the brains of the treated animals (**Figure 4.6**). MRI reveals a black mass that occurs starting at day 42 and persists until the end of the study at 180 days. Upon examination this tissue was brownish in color and when stained using H&E continues to appear brown with no apparent cells present. Further, there was no evidence of tumor tissue throughout the brain indicating eradication of the tumor from the primary site of inoculation. Similarly, there did not appear to be

any accumulation of blood from hemorrhage in the IB-DXR tumor indicating blood brain barrier closing as compared to other groups where there was a large amount of hemorrhage evidence at the time of death. This correlates with the presence or absence of higher levels of fluid on T₂ weighted MRI. Hence, the MRI and survival data suggest that there is an absence of tumor regrowth throughout the brain.

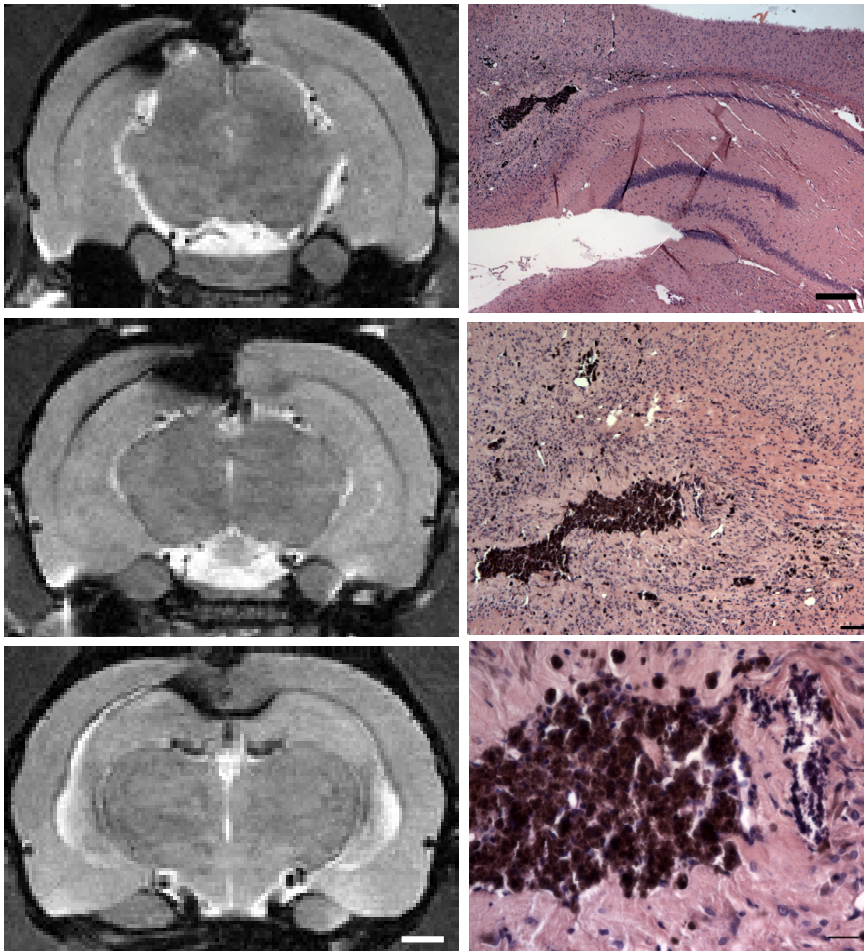


Figure 4.6: IB-DXR treated tumor in MRI (left, scale bar =1mm) and in post study H&E (right, scale bar = 50µm) on day 180 reveals lack of tumor recurrence but presence of hemosiderin-laden macrophages.

4.5 Discussion

The ability to halt glioma invasion has many implications in the treatment of the disease. Development of such drugs is highly desirable because of the secondary effects of many of the common treatments of the disease including chemotherapy and radiation therapy which may induce invasion. Further to minimize patient visits and possibly create a consistent or metronomic therapy, a singly encapsulated nanocarrier is desirable in reducing toxicity, maximizing delivery, and minimizing patient visits for infusions. Here we have shown the development and application of a co-loaded IB-DXR liposomal nanocarrier for the treatment of glioblastoma. Further we have demonstrated that use of this treatment on a highly aggressive model of GBM enhances efficacy above those levels seen with DXR liposomes alone thereby validating the possibility of this combination to enhance survival.

The development of the co-loaded nanocarrier is not a novel technology, however, this represents the first attempt at treating with an anti-invasive and a chemotherapeutic in the same liposome. Previous studies with liposomes include delivery of verapamil, a P-glycoprotein inhibitor, with Doxorubicin to overcome the multi-drug resistance often seen with the chemotherapeutic [268]. This treatment has shown success in overcoming MDR *in vitro* but *in vivo* results are yet to be seen. In another study, DXR and vincristine, an inhibitor of mitosis, were loaded into liposomes together and has shown success in reducing growth of mammary carcinoma and Kaposi's sarcoma [269]. In these formulations, the drugs were remote loaded either by the same mechanism (pH gradients) or through a combination of mechanisms (pH for DXR and transition metal gradient for vincristine). In our study, the use of passive encapsulation of IB followed by remote loading of Doxorubicin was the simplest method by which to enhance encapsulation. However, remote loading of IB, once optimized, could offer equally

efficient loading of both and possibly enhanced release profiles *in vivo* leading to better survival rates.

It should be noted though, that the release kinetics at the liposomal level are not the only reason for differences in efficacy over sequential or subsequent treatments. In the mouse mammary model with vincristine and Doxorubicin, it was seen that the tumors were more responsive to sequential and alternating treatments of the two drugs as opposed to the co-loaded formulation though they were equally toxic *in vitro* [269]. The authors attribute this to changes in pharmacokinetics leading to greater tumor accumulation of injected liposomes. This could be due to the liposomal sequential injections. It has been seen with stealth Doxil liposomes that repeated injections can lead to changes in side effects and biodistribution profiles of the drug even as close as one month apart [265]. Therefore, it could be that alterations in liposomal sequential dosing showing enhanced efficacy over simultaneous dosing should be interpreted loosely due to the potential of the liposomal deliveries to alter subsequent injections. Further, use of combinatorial dosing can be advantageous in this regard because there is avoidance of any unforeseen toxic side effects. In the study examining multiple injections of Doxil, it was seen that unwanted side effects in the form of skin lesions were minimized by spacing out injections to one per month [265]. This could mean that the development of co-loaded nanocarriers offers the best way to deliver more compounds with fewer side effects from delivery alterations. Further, with the promising enhancement of survival times seen in this study, we are confident in promoting use of such a compound in other models of glioma as well as non central nervous system cancers.

Enhancement of survival times can also be attributed to the nature of the interactions of the two drugs *in vivo*. Though no synergy was seen in *in vitro* experiments with IB and DXR liposomes, a host of *in vivo* factors could affect the interactions of these drugs. In previous work with this novel compound it has been shown to be involved in pathways which can lead to a host of microenvironmental changes including immune

response and matrix alterations. Therefore, there could be a secondary effect stemming from IB beyond the anti-invasive attribute that is contributing to enhancement of doxorubicin. In fact, DXR has been shown to induce immune response and stifle inherent immune responses to cancer in breast carcinoma [261]. It also is known to cause upregulation and enhanced secretion of several matrix metalloproteinases (MMPs) in breast cancer and tumor endothelial cells. IB is implicated in pathways reversing these aspects of malignancy [112]. Therefore, the increased response in the presence of both compounds *in vivo* could be explained by these phenomena which cannot be observed readily *in vitro*.

In all, we have shown the development of a novel co-encapsulated therapeutic combination incorporating a novel anti-invasive with a chemotherapeutic. This combination was previously seen to yield long-term survival in the RT2 glioblastoma in rats. Here we see promising survival times with similar tumor remission phenotypes at the end of study, however, there was not long-term survival in all subjects. The ease of using such a nanocarrier along with the development of a simple protocol for co-encapsulation of a novel hydrophobic compound with a potent chemotherapeutic offer an advantage to the cancer field. We can examine the interaction of two drugs *in vivo* and observe there is synergy unobserved by the *in vitro* testing without concern for alterations in delivery profiles of subsequent injections. Further, with the development of a host of novel anti-invasive and chemopreventive agents that are hydrophobic, we can use this protocol to examine interactions of these compounds with chemotherapeutics that are well-defined in liposomal loading such as doxorubicin.

CHAPTER 5

CANDIDATE MECHANISM OF ACTION OF IMPRAMINE BLUE

5.1 Summary

Imipramine Blue has been shown to inhibit invasion of glioma *in vitro* and *in vivo*. It is known that it works through inhibition of actin polymerization through regulatory proteins, however, the exact mechanism is not understood. Further, it was shown that use of this compound in conjunction with chemotherapy (doxorubicin) enhances tumor remission in rat glioblastoma. It would be useful to understand the mechanism of action of IB and thereby better predict and understand its use in cancer. The compound is a triphenylmethane which should have activity similar to that seen with diphenyliodide, a pan-Nox inhibitor. Through a series of studies, we explore the various inhibitory activities of IB *in vitro* beginning with actin polymerization inhibition through timecourse examination and binding assays. Then we show that IB inhibits Src-kinase related activation of invadopodia formation. Then, we show that IB inhibits both activation of NF κ B and Nox4 through functional studies. Last, using a magnetic bead precipitation assay, we show that IB directly binds Nox4 in glioma cells. Therefore, we can say that IB has Nox4 antagonistic activity and complete the model for how IB halts glioma invasion *in vitro* and *in vivo*. Though more studies should follow, this is a base from which to further examine the effects of this interesting compound in cancer.

5.2 Introduction

Cancer invasion and metastasis is a difficult problem to solve for today's therapies. Primary means of treatment of cancer focus on removing the tumor and not the metastasis. However, this method does not work for many types of cancer where metastasis is either an ongoing process when treatment occurs, or therapy that works to

remove the tumor actually enhances invasion. Long thought that cancer cells acquire the ability to invade over time, there is increasing evidence that many tumors are inherently invasive from onset [272]. Therapies such as anti-angiogenics and radiation have both shown increased migration of cancer cells *in vitro* and *in vivo* leading to recurrence and further malignancy of disease [43, 77]. Therefore, compounds that stop invasion are highly desirable as novel therapeutics against cancer.

Imipramine Blue is a novel compound recently shown to inhibit invasion of glioblastoma. This compound was found through a screen of novel triphenylmethane derivatives against malignant glioma. Further, when coupled with more traditional chemotherapy, IB enhanced the ability of Doxorubicin to the point of complete remission. There is a benefit to pre-treating the tumor with IB yielding a sort of priming effect on the tumor. However, the mechanism by which this drug works is still not fully understood.

Through microarray analysis, Imipramine Blue was shown to inhibit actin polymerization through upstream regulators. The effect on the cells was briefly explored through cell morphological observation which showed an inhibition of actin stress fiber formation. The data from microarray coupled with the cell morphology implicates actin polymerization as the key as opposed to loss of focal adhesions for inhibition of cell spreading. There are multiple upstream pathways that can lead to loss of actin stress fibers and cell spreading, however, and thus they should be explored to determine the mechanism by which IB is acting on cancer cells [160].

There are several candidate mechanisms by which actin polymerization can be regulated and several effectors were seen via IPA. These mechanisms include PI3K, PKC, NFkB, MAPK, and the RhoGTPases. PI3K is known to be mutated in a significant number of cancers with overactivity resulting in downstream migration, proliferation, survival, and growth signaling changes [273, 274]. MAPK is dysregulated in many cancers with downstream effects on proliferation via and migration via alterations in

cytoskeletal and adhesion regulation [275]. NF κ B is implicated in every form of malignancy in cancer and can enhance cell motility through adhesion disassembly and assembly, cytoskeletal rearrangement, matrix metalloproteinase secretion and transcriptional level changes of multiple effectors of cell movement [212, 213]. The RhoGTPases are regulated in concert with all of these pathways and lead to the development of actin rich invadopodia [250]. The initial alterations in all of these upstream proteins can be linked to a variety of membrane linked receptors and transmembrane proteins.

NADPH Oxidases are a class of molecules responsible for creating reactive oxygen species (ROS) which include H₂O₂ and O \cdot . These molecules are responsible for inducing a variety of signaling effects including activation of inflammatory, migratory, and angiogenic pathways [176]. There are several different Nox molecules that localize in the membranes of the cell. Nox1-3 and 5 are activated by Rac and Nox4 can be activated independent of Rac [169]. These proteins make different ROS under cell stress conditions which will activate NF κ B through cleavage of the IKK linker of the dimeric protein [276]. This will lead to transcriptional events and protein activation throughout the cell resulting in enhanced migration of the cell. Nox4 is different from the other Nox proteins in that it will activate independently of Rac binding. Further, Nox4 has several different splice variants that are thought to have slightly different functionality in the cell and are known to localize to either the endoplasmic reticulum or the nucleus. Lastly, Nox4 has recently been shown to be mutated in cancers which leads to development of many of the malignant phenotypes seen [178, 277]. This has been one link used in the inflammation to cancer hypothesis.

In this manuscript, we show in multiple invasive cancer models that Imipramine Blue inhibits invasion. Further, that this invasion is indeed due to regulation of actin polymerization and not to direct binding to actin and that this alteration affects invadopodia associated actin structures. Through exploratory signaling studies, we then

show that IB has the ability to inhibit Nox4. Finally, we show, through a modified immunoprecipitation study, that IB actually binds to Nox4 where we believe it exerts its inhibitory effect. This series of studies indicates a first line effort to examine a mechanism of action in a more global way.

5.3 Methods

5.3.1 Invasion assays

Invasion assays were performed according to ref in basement membrane extract (Trevigen) coated tissue culture insert inserts (Millipore). Briefly, 200,000 cells were seeded on top of BME in serum free medium and allowed to migrate towards serum containing media for 16 hours. Tissue culture inserts were fixed, stained with DAPI, and 5 fields counted per tissue culture insert (3 tissue culture inserts per condition). Percent invasion of starting cell numbers was normalized to untreated controls for each cell type.

5.3.2 Actin polymerization and depolymerization assays

The effect of Imipramine Blue on actin polymerization and depolymerization was tested using the Actin Polymerization Biochem Kit (Cytoskeleton, Inc.) using the protocol provided with the kit. Cytochalasin-D (Invitrogen), a known inhibitor of actin polymerization was used as a negative control in the actin polymerization assay; phalloidin (Invitrogen), which inhibits actin depolymerization, was used as a negative control during the actin depolymerization assay.

5.3.3 In vitro immunocytochemistry

Cells were seeded in three 96 well glass-bottom plates (200 μ l/well) at 50,000 cells/ml and incubated at 37°C in a 5% CO₂ atmosphere. The cells were then treated with Imipramine Blue (5 mg/ml) for 0 hours, 15 minutes, 30 minutes, 1 hour, 2 hours, 3 hours, 6 hours, and 24 hours. After treatment, Imipramine Blue was removed and cells were washed with 1X PBS. Cells were then fixed using 4% paraformaldehyde and stained using the following primary antibodies: α -actin (1:100), scinderin (1:5 ug/ml), NF κ B

(1:100) , nox4 (1:100) (AbCam), profilin (1:100), rho-gdi (1:50) (Santa Cruz Biotechnology, Inc.), and acetylated microtubulin (1:200) (Invitrogen). After 24 hours, cells were stained with the following secondary antibodies: AlexaFluor 488 goat anti-rabbit, and AlexaFluor 488 goat anti-mouse (Invitrogen). The cells were then stained with 1X DAPI and phalloidin (1:200) obtained from Invitrogen. Cells were imaged using a Zeiss LSM 510 NLO with META MPE.

5.3.4 Nuclear Localization

Desipramine Blue (DB) was conjugated to amine reactive FITC (Invitrogen) using the protocol provided. Conjugated DB was then encapsulated in liposomes in preparation for delivery. RT2 cells were seeded at 100,000 cells/ml in four 8 chamber slides. Each slide underwent a different drug treatment (liposomal conjugated DB, free conjugated DB, free IB, untreated). Cells were then fixed with 4% paraformaldehyde at the following timepoints: 5 minutes, 15 minutes, 1 hour, 2 hours, 4 hours, 24 hours, and 48 hours. Cells were stained with rhodamine phalloidin (Invitrogen) and DAPI before imaging.

5.3.5 Nox4 Inhibition Studies

HVA assays were performed using Nox4 over-expressing Cos cells as described (1) after treatment with 0, 5, or 10 μ M IB for 1 h.

5.3.6 Magnetic Bead Binding Assay

Dynabeads (DynaL Biotech, Inc.) were conjugated to DB using the protocol provided. Control beads were also made by activating according to the protocol and withholding DB. Protein extracted from RT2 cells was treated with both the conjugated and unconjugated beads. The sorted protein from the conjugated beads, the supernatant from the conjugated beads, the protein from the unconjugated beads, the supernatant from the unconjugated beads, and the unsorted protein were all tested using a Western Blot.

The blot was stained with Nox4 primary antibody (AbCam) and stained with AlexaFluor488 goat-anti rabbit secondary antibody (Invitrogen).

5.4 Results

5.4.1 IB halts invasion in multiple cancer models

Through tissue culture insert invasion assays, it was seen that IB could halt invasion of multiple models of malignant cancer at 5 μ M concentration (**Figure 5.1**). Cell lines had a varying degree of invasive potential ranging from 5% -20% untreated cell invasion. All cell lines responded similarly to the use of IB against them. This indicates IB's ability to halt invasion of multiple cancer types beyond just the previously seen application to glioblastoma.

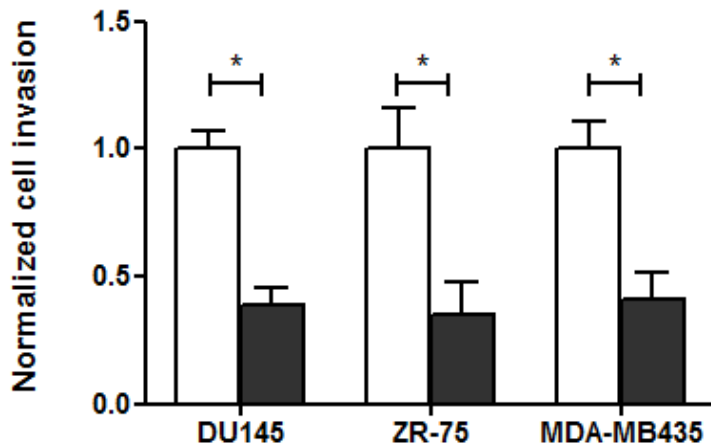


Figure 5.1: Inhibition of invasion in other models of invasive cancer DU145, prostate cancer, ZR-75 breast cancer, and MDAMB435 breast cancer all show below 50% invasion when treated with 5 μ M IB *in vitro*. *p<0.05

5.4.2 IB alters actin structural formation without direct binding to actin

Through cell spreading observation it was apparent that cancer cells would become more rounded when exposed to IB (**Figure 5.2A**). This was further quantified using ImageJ showing a consistent increase in rounded cells over time and indicating increased rounding at 3 hours after treatment and maintaining to 24 hours (**Figure 5.2B**). This effect was only seen in RT2 and U87 glioma cell lines and not with the primary cultured astrocytes indicating the cancer selective effect of IB.

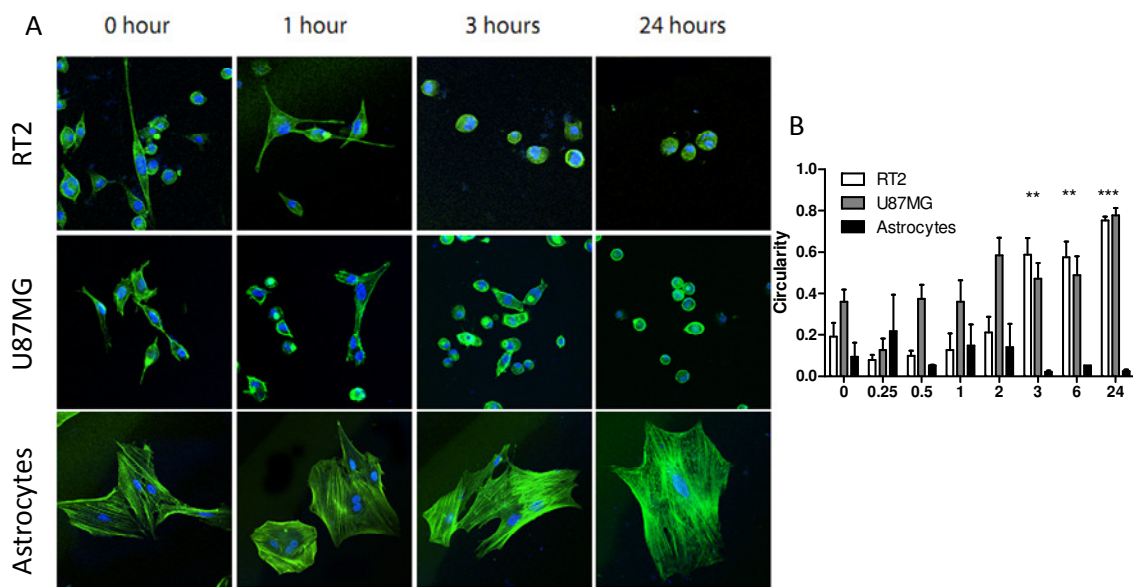


Figure 5.2: Cell spreading in presence of IB. (A) Glioblastoma cells (RT2 and U87) show rounding of cells after 3 hours of incubation with 5 μ M IB. Astrocytes maintained spread morphology even after 24 hours incubation. Green: F-actin (rhodamine phalloidin), Blue: Nuclei (DAPI). Scale bar = 20 μ m. (B) Assessment of circularity of cells through ImageJ indicating enhanced rounding of glioblastoma cells after 3 hours continuing to 24 hours with no change in astrocytes. Significance is based on comparison to initial morphology before any treatment occurred (**p<0.01, ***p<0.001).

We were interested to see if IB would bind actin directly and thus exert its effects through this mechanism. Though it was hypothesized that IB would not bind actin directly based on comparison to Cytochalasin D and Phalloidin compounds which do, assurance of this mechanism was important in future studies. Through use of *in vitro* actin polymerization and depolymerization studies we determined that IB does not inhibit the ability of actin to polymerize or depolymerize as compared to the aforementioned inhibitors at the same doses (**Figure 5.3**). This data confirms further the previous timecourse of IB action as direct actin interacting molecules tend to inhibit cell motility within minutes after application as opposed to hours.

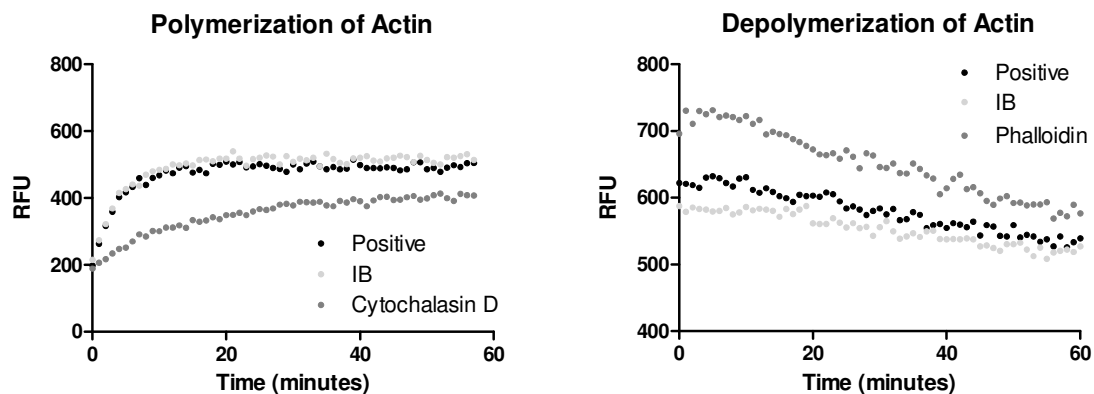


Figure 5.3: IB does not inhibit actin directly Results of *in vitro* polymerization (left) or depolymerization (right) assays indicate no interaction of IB with these processes. Pyrene actin monomers (polymerization) or filaments (depolymerization) were incubated with ATP and drug. Pyrene-actin releases a fluorescent signal as it polymerizes yielding the increase or decrease in signal upon filament formation or removal. Cytochalasin D is an inhibitor of actin polymerization and shows this activity (left) at 1 μ M ($p < 0.05$) as compared to IB at 1 μ M which had no change from control. Phalloidin binds F-actin and prevents depolymerization (right) at 1 μ M yielding a slower decrease in signal as compared to control ($p < 0.05$). IB does not have this effect on F-actin. Curves were compared by nonlinear fit analysis.

5.4.3 IB inhibits and binds Nox4

In conjunction with collaborators, we saw that IB inhibits production of ROS in Nox4 over-expressing cells (**Figure 5.4**). Therefore, we decided to determine if IB binds Nox4 directly. We used protein from the rat cell line RT2 along with a derivative of Imipramine Blue, Desipramine Blue (DB). This compound shows the same inhibition of invasion as IB with similar effects on actin structure formation, though it is less potent with a higher IC_{50} . The advantage to this compound is the ability to conjugate via amide bond formation due to lack of an ethyl group on the nitrogen of the Imipramine side group. Magnetic beads conjugated to this compound were incubated with protein at $37^{\circ}C$ and then pulled down after which they were washed with detergent for removal of protein. This pull down was repeated several times for concentration of the protein for blotting with Nox4 antibody. Further, samples were incubated with IB first, followed by the beads to inhibit conjugation, as well as initial protein sample was taken for comparison. Further, cells were incubated with the conjugated beads to show functionality of the molecule through morphological analysis and revealed the ability of the conjugate to inhibit stress fiber formation and cell spreading after 3 hours (**Figure 5.5**).

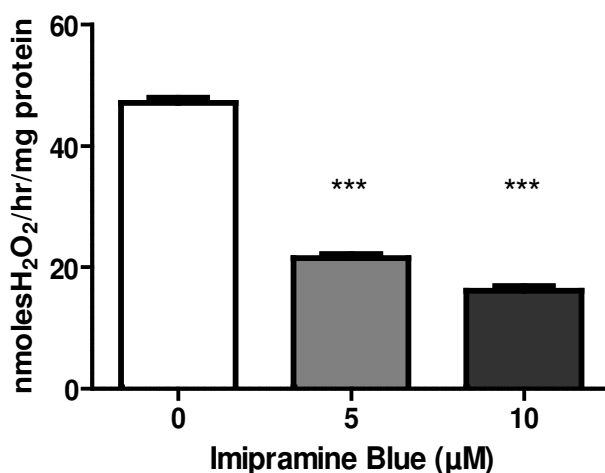


Figure 5.4: IB inhibits H_2O_2 generation by Nox4 Nox4 over-expressing Cos cells were delivered IB for one hour in increasing doses and ROS generation was determined by HVA assay. Inhibition was significant over several trials ($***p < 0.001$). (Data courtesy Knaus, UCD)

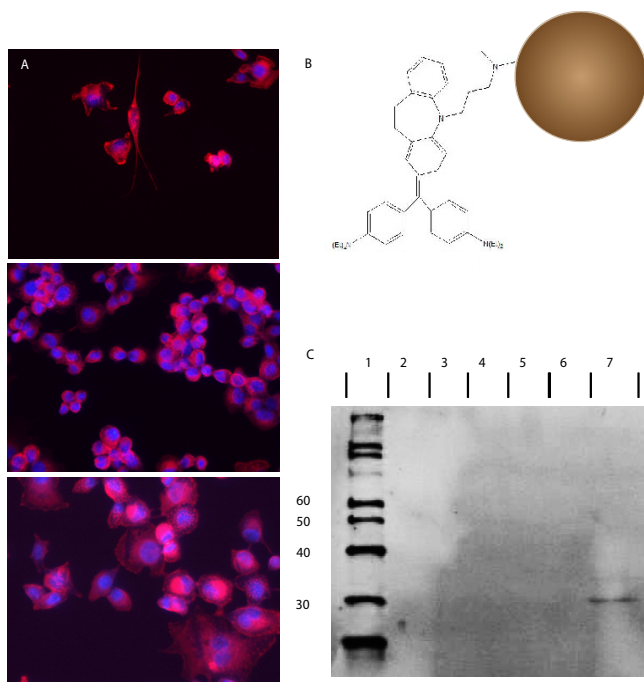


Figure 5.5: IB binds to Nox4. A) Functional capabilities of the DB-particle showing rounding of the cells that are exposed to DB-beads (lower image) showing similar characteristics to DB alone treated cells (middle image). Untreated cells (top image) show minimal rounding. B) Schematic of the DB-magnetic bead conjugate showing binding site of beads. C) Western blot indicating Nox4 presence of pulled down protein with wells as follows: 1-ladder, 2-empty, 3-beads alone after wash, 4-protein from unconjugated beads, 5-protein before incubation with beads, 6-supernatant from pulled down protein, and 7-protein pulled down by beads. Only lane 7 stained positively for Nox4 at a 30kDa band indicative of Nox4 splice variant 4D.

Results indicate a single band (lane 7) from the bead pulldown group around 30kDa with no hybridization elsewhere. The most common band for Nox4 occurs around 65kDa but there are several splice variants of this protein including one at 30kDa with full Nox4 functionality. This variant lacks the transmembrane domain of Nox4, but still is able to produce H_2O_2 effectively. We did not see hybridization in the beads alone after wash (3), incubated protein with non-conjugated beads(4), non-incubated protein (5), or the supernatant from the pulled down protein (6). We expected to see a band in lanes 4 and 5 due to protein in the sample, however, we believe that the concentration of the

protein by using the beads allowed more total Nox4 to be concentrated and thus a stronger band to appear.

5.4.4 IB localizes to the nucleus of RT2 glioma

We were further interested in determining where the drug localizes in the cell. Nox4 is primarily a cell membrane protein but can localize to many other locations within the cell including the endoplasmic reticulum, the cytoplasm, and the nucleus [170]. Using the same conjugation strategy as with the beads, we conjugated DB to a FITC tag and incubated cells with this construct. Cells were also incubated with IB alone, carrier alone, or FITC alone (not shown). After 24 h, cells were stained for actin and the nucleus. In all cells that showed a rounded phenotype, we observed bright FITC localization in the nucleus overlapping with DAPI (**Figure 5.6**). This indicates that the drug localizes to the nucleus after 24 hours.

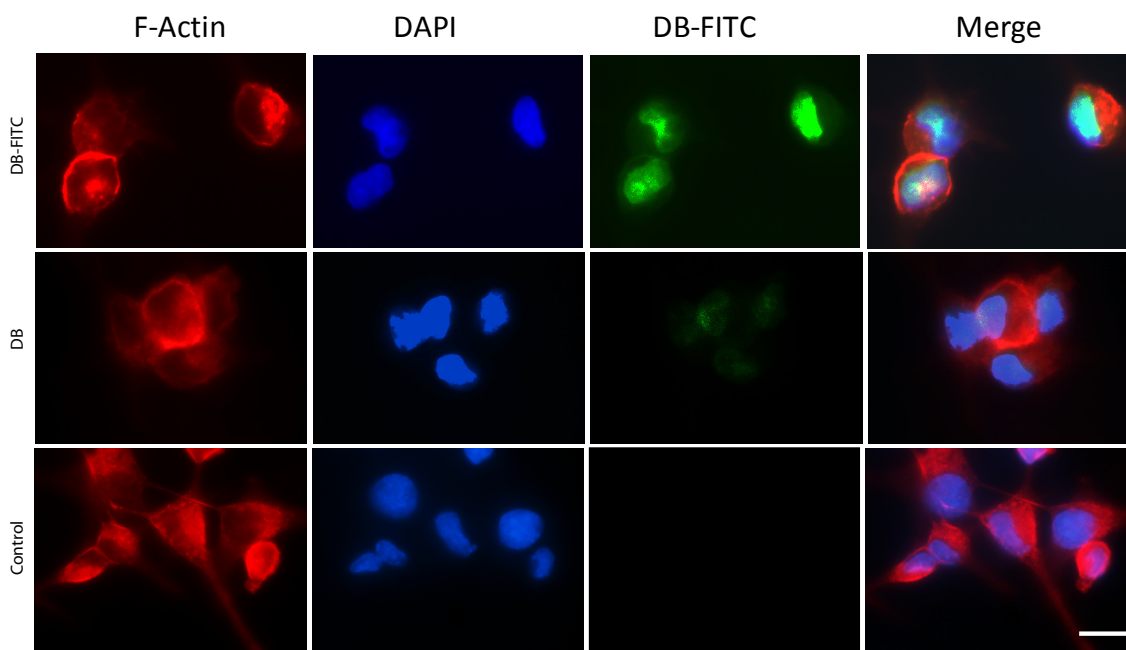


Figure 5.6: IB localizes to the nucleus of RT2 cells. Using FITC-conjugated DB (green, top), we tracked the drug to the nuclei (blue, DAPI) of tumor cells after 24 hours. Cells were counterstained for F-actin (red, rhodamine phalloidin) to determine if cell morphology changed as expected and compared to non-conjugated DB (middle) and untreated cells (bottom).

5.5 Discussion

The use of a novel compound to halt invasion of cancer is a highly desirable pharmaceutical. Imipramine Blue is a potent inhibitor of cancer cell invasion, however, until now, it was unknown through which mechanism this drug was working. It was previously shown that IB potently inhibits actin polymerization through regulation of actin binding proteins such as scinderin and profilin-1, as well as regulatory proteins such as calgranulin and RhoGDI α . However, these changes needed to be effected by upstream signaling proteins.

Through literature searches and the predicted mechanism of IB based on the design of this compound, we set out to determine its specific interactions and how it is changing migration. To begin, the universality of IB's effects were determined in multiple cell types in other cancers. This proved that the inhibition of invasion is nearly universal amongst cancers. This indicates that there is an underlying mechanism for invasion that is inactivated in many cancer types and shows the benefit to using IB in a clinical setting. Further, this proves that the effect of IB is not just glioma specific which is important as there are many differences in glioma development as compared to other non-central nervous system cancers [283]. Further results indicated that IB inhibits cell spreading specifically in cancer cells and not their healthy counterparts yielding rounding of RT2 and U87MG glioma but not astrocytes. It was observed that this change takes about 3 hours confirming previous live imaging analyses of glioma cells treated at the same doses. This result indicates that there is an upstream mechanism involved in the inhibition of invasion which was further confirmed through the actin depolymerization and polymerization studies showing no direct effect on the monomer or polymer actin.

Src-kinase, a key player in invadopodia formation in cancer, has been seen to be inhibited with IB (Diaz, B. & S. Courtneidge, unpublished data). Src-kinase in this regard is known to activate Tks5 leading to activation of Nox4 and ROS generation causing a

host of intracellular changes including invadopodia formation [148]. Src kinase is also known to be involved in just about every other aspect of cancer progression and malignancy so inhibition of this protein in one regard may lead to further reaching effects on cancer [56]. Recently, it has been seen that during inflammation, Src is regulated by the polymerization of actin [284]. It was shown that inhibition of actin polymerization by cytochalasin D inhibited Src activation. Therefore, we thought that the inhibition of Src may be a secondary effect of the inhibition of actin polymerization though further study is necessary to determine the exact events occurring upon treatment.

Using activation assays via TNF- α induction of NF κ B, it has been shown that IB inactivates NF κ B localization to the nucleus and its ability to act as a transcriptional factor (Aggarwal, B., unpublished). NF κ B can also be involved in cytoplasmic protein regulation leading to an ever increasing cascade of signaling mechanisms [216]. Inactivation of this protein is known to inhibit RhoGTPase mediated actin polymerization, nucleation of new actin filaments, and pooling of G-actin [160]. Further, NF κ B is activated by presence of reactive oxygen species. Again though, NF κ B has been shown to inactivate based on the actin dynamic state of the cell, though in cancer, its normal function is highly disrupted due to mutation. This can lead to constitutive activation of the protein but is often mediated by upstream cleavage proteins and transcription factors. Therefore, we proposed that Nox4 is the mediator of this activation of NF κ B as well as the Src kinase mediated mechanism.

It remains to be seen if IB generally decreases the ROS in cancer cells and if this is particularly pronounced in those cancer cells with overactive Nox4 versus other Nox proteins. The ability of IB to bind Nox4 was determined through the magnetic bead assays where IB bound Nox4 enough to yield a significant band of concentrated protein on the Western blot. Further, the ability of IB in culture with the beads to block this binding showed the affinity of the IB alone and the validity of the assay. Future studies

will examine more closely the binding kinetics of this pair, though as an initial effort these results are significant.

The particular splice variant shown to bind from the RT2 cells was interesting. However, this splice variant (4D) may be solely due to the cell line and not the particular specificity of the drug. We believe this to be the case because of the universality of the drug in many cancer types shown here and in previous work and the known non-universality of the particular splice variants[175]. The 4D splice variant lacks the transmembrane domain but is capable of producing ROS. This specificity can begin to give us clues as to the particular inhibitory site of IB and aid in development and description of nanocarrier delivered IB that has been previously used. The 4D splice variant is also known to localize to the nucleus of cells and so using FITC-conjugated IB we see the trafficking of the compound to the nucleus and the resulting effect on actin stress fibers and cell spreading after 3 hours of incubation. These signs, along with the previous results of the effect on invadopodia and polymerization lead to a conclusive model for the inhibition of Nox4 by IB with the resulting downstream effects (**Figure 5.7**).

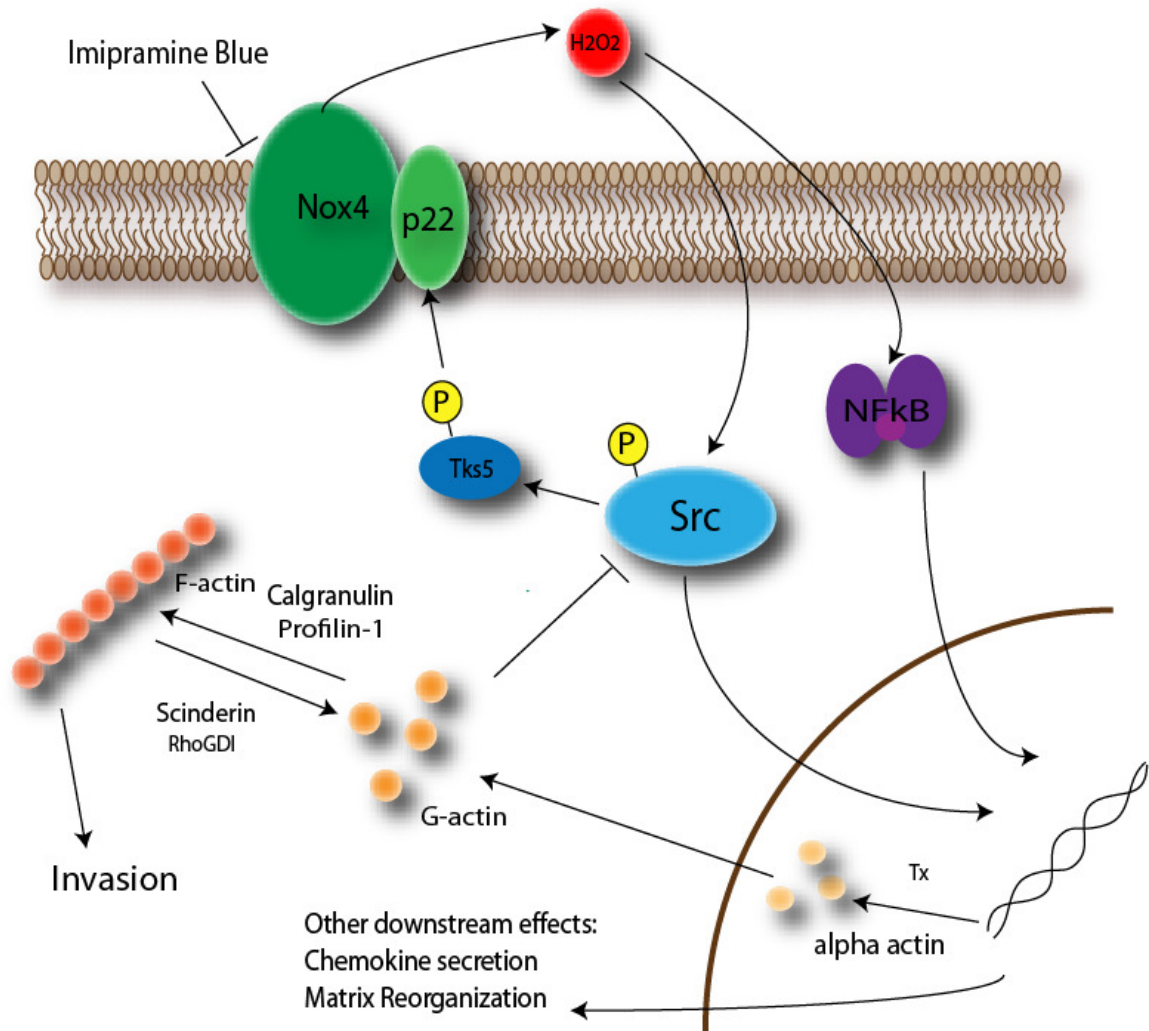


Figure 5.7: Proposed mechanism of action of IB with known downstream effects. IB binds Nox4 and exerts inhibitory activity which leads to decreased ROS (in the form of H₂O₂ or radicals). This leads to downstream inhibition of NFκB and possible changes in actin polymerization and transcription of indicated proteins from previous microarray data which lead to invasion inhibition. Further, actin depolymerization can inhibit Src kinase activation and subsequent activation of Tks5 which leads to podosome formation and Nox4 activity. Therefore, the invasion inhibition is a circular process that leads to enhancement of invasion inhibition. Further, the pathways have other overlapping pathways involving other proteins, but these are the most straightforward interactions involving all known molecules.

CHAPTER 6

DISCUSSION

6.1 Discussion of Overall Thesis

The work of this dissertation represents several first steps in the fight against brain tumor invasion in many regards: 1. A multi-compound screen for a drug that will stop invasion while controlling for other attributes of drug action against cancer, 2. An in depth look at one particular compound, Imipramine Blue, *in vitro* and *in vivo* to determine its effects on cancer, 3. Methodology for incorporating an anti-invasive drug with a chemotherapeutic for remission of glioblastoma, and 4. Discovery that this compound works by a mechanism not extensively pursued in cancer cell invasion.

High-throughput drug screening is a common method for identifying new compounds against a variety of diseases [287]. Use of array technology is an ever-growing area of biomaterials and processing research. Similarly, the generation of these compounds is more and more being moved to *in silico* to assist in the design and development of target specific compounds [288]. Along with this is the modeling of signaling pathways and downstream effects of blocking or activating of the various protein targets. However, these methods all rely on experimental methods to determine the protein definition and role in the large number of pathways in cancer. Also, cancer is a disease in which many of these targets may be mutated for constitutive or variant activity as compared to normal variants and thus represent a difficult modeling challenge [289]. Further, since pathways in cells are not fully elucidated, predicted effects on cells are unclear and movement of such compounds to an *in vivo* setting can represent an even larger challenge where cancer cells are no longer isolated but interacting with a host of different cell types. Efforts to model these changes *in silico* and *in vitro* are becoming more available but the only real way to determine the activity of a drug still is to test *in*

vivo and eventually through clinical studies. That being said, use of drug screening is an effective way to identify an agent for specific purposes.

In the first part of this dissertation, a small drug screen of two select classes of molecules was conducted. These molecules were chosen for a parent molecule's success against tumor invasion coupled with a proposed novel mechanism in hopes of creating a new push forward in the anti-invasive molecule search. Most anti-invasive compounds previously developed focused on inhibition of the matrix metalloproteinases (MMPs). These molecules are upregulated in cancer and are often necessary for invasion, however, they are not the primary role player in the ability of cancer cells to move [290]. In clinical trials, it has been seen that these have moderate effects when coupled with other treatments though still not much more than a few months increase in survival in glioblastoma patients [182]. Cancer cells often need to degrade the ECM to move, however, it's not always necessary. Because of the undifferentiated state of most cancer cells and their amoeboid-like migration, they can instead move through pores in the ECM as opposed to making their own [291]. They also do not need to maintain adhesive contacts with the surrounding ECM and thus can continuously move nonlinearly through the matrix and into the healthy brain [292]. Self-sufficiency in growth signals and chemokines can also assist in this enhanced migration [293]. Therefore, the new push in anti-invasive agents is the growth factor inhibitors such as EGFR, PDGFR, and FGFR antagonists as well as the tyrosine kinase class of inhibitors. These molecules, however, have multiple effects on cancer cells including reduced growth, proliferation, invasion, and angiogenesis [293]. These compounds are also highly specific, which is beneficial to tumor screening methods for overexpression of the particular receptor of interest, however, means they are not universally able to work for every type of cancer in every patient. Further, most of these compounds are monoclonal antibodies which are still very expensive and difficult to manufacture [294].

Therefore, we focused on small molecule compounds with novel mechanisms of action (aside from growth factor receptor and MMP inhibition). Through the screening of compounds using a multi-tiered approach incorporating cytotoxicity and invasion assays in multiple cell types, we identified one compound, Imipramine Blue (IB) that inhibits invasion at low doses and showing cancer-specific cytotoxicity only at higher doses. Most studies of anti-invasive compounds only focus on the decrease in percent invasion without studying the confounding effect of cytotoxicity and thereby can draw inappropriate conclusions. By understanding the concentration at which IB begins to kill cancer cells ($IC_{50}=20\mu M$) and the one at which it will inhibit invasion ($IC_{50}=20nM$) we can understand better the effects of using a specific anti-invasive compound *in vivo*. This is important, because we know that when delivered *in vivo* the compound will have a widely varied effect as opposed to *in vitro* due to the distribution of the drug within the tumor and the possible per cell dose of drug. For instance, compounds such as Doxorubicin and temozolomide are subject to multi-drug resistance (MDR) and this can be selected for over time in populations of cells within the tumor [112]. Due to the heterogeneous nature of their delivery, the low concentration effects of these compounds can lead to induction of MDR or selection of subpopulations of cells which will make it more difficult for repeat treatments to help [101]. Studies incorporate multiple forms of chemotherapies to try to overcome this, but the delivery will always be limited and thus cell populations will be propagated in a heterogeneous way. This is similarly true in radiotherapy where it is known that low-level doses of radiation enhance tumor invasion while high doses will kill tumor cells [43]. Through use of a drug with low-level anti-invasive characteristics can, hopefully, halt invasion of the cells when it's not killing them and thus create an anti-tumor effect without this selection mechanism.

In the third chapter of this dissertation, the drug, Imipramine Blue was closely examined for this anti-invasive effect. Through multiple testing mechanisms including *in vitro* and *in vivo* invasion quantification, it was shown that IB will halt invasion of

glioblastoma. This translation is missing from a lot of studies of novel anti-invasive compounds [136, 222, 226, 295, 296]. Due to problems with delivery issues of potent *in vitro* anti-invasives, translation into *in vivo* studies is difficult. Further, once these studies are conducted, the invasive potential of the drugs takes a sideline to the simpler measures of growth and survival of tumors [191, 244, 245, 247, 297, 298]. Thus, if no change is seen in these attributes, the drug is often sidelined, but if growth is inhibited, this becomes the primary focus of treatment.

With this compound, IB, only a moderate increase in survival was seen (~12% increase) with small effects on tumor size. However, since the initial goal was anti-invasive we were able to detect a much more impressive attribute of activity *in vivo* through quantification of tumor density and border invasion. Thus, though the drug alone was not a potent anti-tumor agent, through careful selection we were able to find a potent-anti-invasive agent at a deliverable dose *in vivo*. In this way we could test the overall hypothesis that using an anti-invasive, but not cytotoxic agent with a potent form of clinically available anti-tumor therapy will result in enhanced efficacy of that therapy leading to increased survival

In chapter three and four, the incorporation of IB with Doxorubicin (DXR) was closely examined using two approaches: sequential nanocarrier delivery and simultaneous co-encapsulated nanocarrier delivery. Both of these strategies resulted in enhanced survival as compared to the chemotherapeutic alone. Though these experiments are presented separately for publication purposes, they were done simultaneously, so the only difference between the studies is the order of delivery. It is interesting that there appears to be a benefit to priming the tumor before treatment with the chemotherapeutic. Further, the lack of synergy *in vitro* with both sequential and simultaneous delivery of compounds indicates that this is an *in vivo* specific enhancement of tumor death. This result indicates that there is a mechanism *in vivo* that is not observable *in vitro* whereby IB is enhancing efficacy of the Doxorubicin. There are many reasons that this could be

occurring including drug delivery, interactions with the tumor microenvironment or alterations of interactions with the host on a systemic level.

It has been seen that multiple injections of liposomal nanocarriers can alter the course of circulation time and clearance from the bloodstream [299]. This has primarily been observed with toxic drugs such as Doxorubicin which, upon uptake by the reticuloendothelial system (RES) damage the primary mediators of clearance, macrophages. This effect is used to determine the saturation levels of lipid in the bloodstream indicating the point at which the RES system can no longer clear liposomes from circulation [300]. This can lead to enhanced circulation times with multiple injections of liposomes and altered toxicity levels. Thus, it is known that multiple injections of Doxorubicin nanocarriers lead to enhanced delivery after first injection. However, for blank liposomes or non-toxic compounds, the saturation level cannot be determined as there is not an observable effect on RES [301]. It remains to be known if IB is actually affecting macrophage function, though it is not expected due to the already seen cancer specificity. Use of saline liposomal nanocarriers for control groups not receiving sequential delivery controlled for any lipid-only based effect.

Another possible reason for enhanced efficacy with sequential treatments by delivery mechanisms is that IB is altering the angiogenic state of the tumor and thereby enhancing the EPR effect for the subsequent nanocarriers [241]. It is common for anti-invasive therapeutics to have effects on angiogenesis and blood vessel structure and function [221, 227, 302]. This could be due to a variety of factors including endothelial cell recruitment through tumor cell signaling, migration of tumor associated endothelial cells, tube formation of endothelial cells, altered cell-cell junctions in blood vessels leading to altered leakiness, or changes in the pressure differential across the blood vessel wall allowing more leak into tumor [272]. In supplementary studies (Appendix B), the alteration in delivery of nanocarriers to tumors was preliminarily examined using advanced MRI imaging techniques with gadolinium-loaded nanocarriers. These studies

were complemented with *in vitro* observation of vascular endothelial cell invasion and matrix degradation. These early results indicate a possible enhancement in liposomal delivery *in vivo* though results are not significant. This validates *in vitro* studies indicating no significant change in endothelial cell invasion with treatment or alterations in the ability of cancer cells to degrade a Collagen IV matrix indicative of changes in vascular cell lining in brain tumors. However, further studies are necessary to statistically prove the lack of effect due to need for increased power. Therefore, it is still possible that there is an alteration in the delivery to the tumor, though the exact reason and extent of this is still unknown.

Therefore, in Chapter 5, we completed work begun in Chapter 3 regarding the determination of the mechanism of action of IB. In this way, we could determine other reasons for synergy between the two compounds as well as predict side effects and combinatorial effects for future integration and clinical studies. In Chapter 3, using microarray analysis to initially determine all molecular changes involved *in vivo*, a host of responses were observed including changes in cytoskeletal regulation, chemokine secretion, matrix degradation and secretion, and adhesion changes. Microarray can be a very useful tool but can also create complicated data sets and difficult interpretations that must be validated. Therefore, we chose to focus on the cytoskeletal components of the microarray since these are most readily linked to invasion of cancer cells without further complications of alternate proteins and pathways as can be seen with adhesions and matrix degradation components [216]. Therefore these cellular changes were quantified on the transcriptional level and confirmed on the protein level to validate these alterations and indicating that the effect on scinderin and rhoGDI α were most pronounced.

Moving *in vitro* in Chapter 5, these elements were more closely examined and various hypotheses were tested to determine the target of IB. We showed that IB halts spreading of glioma cells without affecting astrocytes after 3 hours of drug exposure. Through subsequent indirect studies it was shown that IB inhibits binds to and inhibits

reactive oxygen species production by NADPH Oxidase 4 (Nox4). This leads to inhibition of NF κ B activation and transcriptional control of cytoskeletal dynamics. This in turn can lead to inhibition of Src by decreased actin polymerization and downstream inhibition of Tks5-dependent Nox4 activation and invadopodia formation. Thus, by inhibiting one part of this cycle, there can be a multiplicative change in the ability of the cell to invade through multiple modalities. This is an interesting overall hypothesis but intricate cell signaling and receptor binding studies must be conducted to confirm these changes and their effects in multiple cancer cell types.

However, knowledge of this mechanism opens doors of possibility for the understanding of drug interactions and *in vivo* translation. It is known that ROS induce changes in blood pressure and inflammatory response [174, 303]. These are attributes that are not readily studied *in vitro* and could be effectuating the change seen upon co-treatment *in vivo*. Further immune cell recruitment and matrix reorganization *in vivo* have been shown to have far reaching effects on many cancer therapeutics. Chemotherapy can induce changes in immune cell recruitment by cancer cells to the benefit of the tumor and can also directly affect cells to reduce immune response [304]. Changes in the chemokine environment as indicated by the *in vivo* microarray analysis could play a distinct role in the higher benefit of chemotherapy with IB in both sequential and co-delivery. Further, alterations of the ECM can affect the ability of chemotherapy to work. It is known that through matrix binding in several cancer types including lung and breast, cancer cells can be more resistant to chemotherapy induced apoptosis [305]. Thereby, through alterations in matrix degradation and secretion *in vivo*, IB may be reinstating the ability of Doxorubicin to kill certain subpopulations of cancer cells that were previously resistant. These are just two of the more well-studied ways that IB may be enhancing efficacy *in vivo* over *in vitro* experiments. However, the tumor microenvironment is volatile and complex and therefore the full extent of IB's effects on it would take much more experimentation [62].

That being said, we believe that the primary mechanism by which IB decreases incidence of tumor recurrence is through the inhibition of invasion of cancer cells. Though the extraordinary effect seen with DXR could be due to a number of downstream and upstream mechanistic effects, the inability of the cancer cells to move away from the tumor bulk is undeniable and useful for application in all treatments currently used on glioblastoma. The state of the field at the moment is relatively static. There are many clinical trials ongoing for new therapeutics but each outcome shows only a minor uptick in the survival time of these patients [306]. Further, the ability to integrate therapies is the primary focus of these studies, building on top of current treatment used in glioma by adding treatments used in other cancers instead of overhauling it. But why not change the course of therapy? In this dissertation, it is shown that IB halts invasion by a novel mechanism, and by doing so, enhances the efficacy of a traditionally potent chemotherapeutic. Though more validation and study is necessitated, this first step represents a paradigm shift in the current treatment regimen which involves obliterating the bulk of the tumor and following up with more fine-tuned treatment. Through this dissertation, I hope to display that use of a pre-treatment molecule before destruction of the primary tumor could yield a substantial benefit to the outcomes of treatment in glioblastoma. Though this is just one molecule and one step, it is important to highlight the implications of such a change.

6.2 Future Directions

This dissertation represents early progress in the identification and development of a novel compound Imipramine Blue. Further, it proves the overarching hypothesis that if this compound as an anti-invasive molecule is incorporated with chemotherapy, Doxorubicin, enhanced survival is achieved in glioblastoma. However, there is much more to do to fully prove this hypothesis and advance the state of this drug. For instance, is there an *in vivo* effect other than invasion that assists in the ability of Doxorubicin to cause remission? Will there be further effects with different anti-tumor treatments such as temozolomide and radiation, common anti-glioma treatments? Further, the class of compounds first screened in this study is interesting for the possibility of future anti-cancer research and deserve investigation as alternate molecules for halting invasion while inhibiting tumor growth. Last, to move forward with this compound there are many mechanistic, universality of cancer treatment, and drug delivery steps that would be useful for future cancer research and possibly other areas of research including inflammation biology.

The ability of IB to cause remission of tumors with Doxorubicin is extraordinary. The universality of this is still to be determined and it should be examined in other models. This includes tumors which are more readily treated with Doxil® including sarcoma and ovarian cancer to determine if there is benefit in models where it is already used. Further the universality of the treatment of brain cancer may also be explored in using other models such as continuation of the studies with the human glioblastoma cell line U87MGEGFRVIII which represents an inherent mutation found in almost 60% of brain cancers. Preliminary survival studies using convection-enhanced delivery are shown in Appendix 4 show a slight benefit to co-delivery of compounds, however, further study is necessary for conclusive evidence of IB enhancement of doxorubicin therapy in this less invasive model.

However, on the brain tumor side, it would be most interesting to continue studies incorporating IB with currently used treatments of glioblastoma. This includes temozolomide, radiotherapy, and anti-angiogenic therapy. The latter two are particularly interesting because of the application to multiple types of cancer and the strong correlation between these treatments and invasion induction [189]. Promising studies showing benefit with temozolomide and other anti-invasives indicate that there may be a strong effect. Further, initial data *in vitro* indicates that this combination yields a synergistic effect in U87MG (Appendix C). Further study into the reason for this synergy and if this is beneficial *in vivo* should be a high priority in development of this drug. Additionally, with the possible alteration in drug delivery characteristics after treatment with IB this synergy may be further amplified *in vivo* as was seen with Doxorubicin. Radiation therapy is used in over 50% of cancers in humans and thus if any benefit is seen to incorporation of IB with this therapy, there could be a huge impact on the cancer field at large. Radiation induced invasion and side effects are a major clinical problem along with the induction of cancer after treatment due to non-specific targeting of radiation. With more common use of highly specific techniques like stereotactic radiosurgery complementation of an anti-invasive drug could be highly helpful in tumor containment and subsequent removal. Further, the ability of IB to subdue many inflammatory pathways would likely reduce the induction of the invasion of the tumor cells resulting from microenvironmental effects. These have been shown to be highly important in the change in tumor phenotype though the mechanisms by which they act are not fully known. Lastly, anti-angiogenic therapy suffers the large problem of invasion induction. This is the best correlated of the treatments and the invasive response in multiple types of tumors. Use of IB before this last line treatment could lead to much better prognosis and is well worth investigating in preclinical models.

For all of these combinatorial approaches to be examined, it would be helpful to better understand the effects of IB on many aspects of cancer outside of the invasive

response and based on the proposed mechanism of action. Initial studies in angiogenic response are a start, however, this field is a well-developed area of cancer research with a variety of interesting techniques and measures. Therefore, use of a novel drug with possible anti-angiogenic action would both benefit the knowledge of the drug-tumor interactions as well as contribute to a better validation of these measures and understanding of the phenomenon in tumors in general. Further permeability studies *in vivo* and cell effects *in vitro* would be useful and more detailed studies involving tumor-associated blood vessels from human models in particular would assist a better understanding of the drug effects. Permeability studies could also lead into studies as to the effect of IB on things like interstitial tumor pressure. In Appendix 5, a manuscript is presented showing the effects of interstitial fluid flow on tumor cells and invasion. This flow is due to pressure differentials from tumors into the healthy brain. If this pressure build up can be altered by IB, this effect could be minimized. Further, decrease of pressure in the brain is the primary reason for observable symptoms and thus the reason for immediate surgical removal of tumors. Steroids are also used to decrease pressure and alleviate symptoms, particularly for inoperable tumors. If IB affects the interstitial tumor pressure, the degree of malignancy could be decreased and the ability to treat both operable and inoperable tumors could be enhanced. Examination of this pressure change would yield interesting information about both IB effects and the tumor environment in general.

On a more systemic basis, the ability of IB to halt ROS is substantial because of the role of ROS in many aspects of physiology including blood pressure and immune response. The correlation between inflammation and cancer progression is a growing field and thus the ability of IB to halt this response through inhibition of ROS and through alterations in chemokine secretion as shown in the microarray analysis deserve further exploration. A drug that can reduce the ability of a cancer to evade the immune system or induce the inflammatory response would be interesting with more novel

vaccine based or immune-cell based therapies which are showing promise in preclinical studies. Further, these responses could lead to secondary indications for the compound in immune disorders or inflammation. Use of novel ROS detection agents *in vivo* coupled with *in vitro* studies would yield positive changes in ROS secretion in the tumors and then the subsequent immune alterations could be more closely examined through immunohistochemistry and flow cytometric analysis. Since the literature well substantiates the involvement of the immune system in cancer progression, the results of such analysis would be highly impactful on a better understanding of both the drug and disease progression related to its mechanism.

To further substantiate the ability of IB to inhibit invasion in multiple types of cancer and to validate complimentary studies on the effects of IB *in vivo* on angiogenesis and inflammation, more in depth analysis of the mechanism is advisable. The understanding of the underlying mechanisms for the involved proteins is strong, though Nox4 is only recently becoming a well-studied molecule in cancer progression. Therefore, there is a strong base of techniques and background for the specific signaling analysis of the various components involved in halting cancer invasion of which we have only begun to examine. Preliminarily, further specificity studies of IB and Nox4 are desirable to determine if there is any interaction with other Nox family proteins and if so, what the comparable K_d s are for the various forms and isotypes. Comparison to diphenyliodide is advisable for examination of potency and specificity as this molecule is a pan-Nox inhibitor shown to elicit many of the same effects as IB. Further, the understanding of inherent mutations of Nox4 and if these affect the ability of IB to work in cancers would assist in incorporation of this treatment on a patient-by-patient basis. Lastly, using methods involving modeling and literature searches, drug interactions, signaling mechanisms, and specific binding structures could be determined to better assist in development of new compounds and integration of therapy. Along with this, revisit of other molecules in the drug screen and newer compounds developed since the drug

screen may provide more potent compounds for testing *in vivo* using the methodology put forth in this dissertation. Along with this, the switch from a purely anti-invasive compound at delivered doses to one that showed more cytotoxic activity likely through the same mechanism could yield a stronger anti-tumor effect alone without incorporation of other therapies. Last, combination of the classes of molecules may be examined for further benefit as these two classes are thought to inhibit NF κ B pathway through differing initial inhibition, there is evidence for a potent combinatorial effect beyond that seen with combinations with more traditional chemotherapeutics.

As with all drugs, testing in multiple models is beneficial both to prediction of clinical translation, and to understanding the limitations of the treatment. Though IB is shown to exert inhibitory activity on multiple models *in vitro*, further exploration of this drug *in vivo* is more useful for clinical translation. Syngeneic implantable rodent models, while offering many advantages used in this dissertation, lack many benefits necessary for validation of a drug. Using an inducible model of a brain cancer, possibly of medulloblastoma, a slower growing cancer that is highly invasive, may yield a better idea of the way IB could be used in a clinical setting. Further, use of human models such as primary glioblastomas either with IB alone or in combination of traditional therapies would indicate the ease of translatability to the clinical setting. Though there is initial work being done in these models at the moment, more thorough investigation and results are yet to be seen.

Further, use of IB outside of the nervous system is an interesting prospect. Using models that are highly metastatic would indicate if the halt of invasion can translate to inhibition of metastasis. There are few models that show this effect but examination in any of them with positive results would be highly significant to the cancer field at large. Development of such a therapy also offers possibilities for development in the drug delivery field. Intravenous delivery to solid tumors is always a possible mechanism due to the EPR effect, however, lymphatic delivery of an anti-invasive may yield a more

potent response due to lymphatic involvement in metastasis. It is well-known that nanocarriers delivered subcutaneously will traffic to the lymph, however, to what extent is this necessary for an anti-invasive and what are the optimal parameters and timepoints for halting metastasis has yet to be seen [307, 308]. Other models of cancer that are not solid tumors such as leukemia or lymphoma could represent an interesting area for delivery development and effects on invasive potential on these types of circulating tumors. This could be applied both to non-solid tumors as well as circulating tumor cells in the blood stream from solid tumors. This area is a rapidly growing sector of research where anti-invasive therapies could play a yet unforeseen role.

Lastly, taking advantage of the use of nanocarrier delivery systems, multi-modality treatment is an area for further expansion of the technology. In this dissertation, we have already seen that IB can be co-loaded with Doxorubicin and gadolinium to yield desired *in vivo* effects. However, can this multi-modality be furthered with other imaging agents and therapies for use in different models of cancer. The tuning of the combinatorial delivery of drugs and imaging agents for tracking metastasis, angiogenesis, and even inflammation while possibly modulating the ability of tumors to do these things is an area of research that could expand. There is already high interest in this type of therapeutic, termed theranostics and yielding NIH funding specifically for this type of research[308]. Incorporation of an anti-invasive with the other modalities of therapy and diagnostic is one step further in nanotechnology and another step closer to understanding and eradicating cancer.

Along with this, the drug delivery aspects of IB are yet to be fully explored. Using liposomes due to the FDA-approval, loading capabilities, and well-understood *in vivo* effects is just the first step. Local delivery of IB may yield impressive results post resection and allow better efficacy of subsequent therapies and even to subsequent surgeries if the tumors are seen to grown back as non-invasive entities. Further, in continuing use of liposomes, development of remote loading capabilities would optimize

manufacture thereby reducing cost of component lipids and waste of excess IB. Further these particles may then yield more potent delivery of the drug to the site while minimizing lipid side effects in patients.

This type of exploration would also lead into the development of the drug at a clinical level. With such promising results seen in animal models with little evidence of toxicity, movement into humans seems to be a high possibility. To begin, it would be beneficial to test toxicity on human cells derived from liver and spleen as the most common targets of liposome delivery, we would be able to identify potential toxicity. Outside of the laboratory, movement into clinical trials would be exciting. Most compounds being tested currently, as listed in the introduction, are targeting growth and apoptosis and are mostly being translated from other cancer models into glioblastoma. As aforementioned, glioblastoma is a somewhat unique disease and therefore, movement of a compound that has been developed for GBM and shown high efficacy in animal models represents a unique pathway to the clinic. Therefore, I believe that along with the other proposed routes of research, a parallel push to the clinic would represent the most impactful outcome of the work in this dissertation. Further, through a clinical result, the paradigm shift of pre-treatment of invasive glioblastoma to halt invasion before it worsens would yield, I believe, a significant standard of care change in treatment and thereby allow for a jump forward in the clinical outcome of this disease that has not been seen in decades.

In this vein, the investigations in this thesis represent the possibility to change the way we treat brain tumors and invasive tumors in general. The idea of pre-treatment of tumors before more aggressive therapies is hinted at with chemoprevention, however, few studies have thoroughly investigated this possibility. Further, development of agents with this specific purpose is not commonly pursued due to the lower impact of the studies that can be produced alone and the intensity involved in multi-compound delivery schedules. The current treatment paradigm is not working for glioblastoma as well as

other invasive models of cancer so there may need to be a total shift in the way we deal with cancer from the beginning to really eradicate the disease. Personalized therapies are interesting but expensive and chemotherapy is still widely used despite the multitude of side effects. Therefore, through development and use of agents that do not kill cancer cells but rather change them is an area for rapid expansion.

On the drug delivery side, this dissertation displays a trend that is beginning to occur. Generally, there are labs that develop compounds and labs that develop drug delivery methods. These tend to be exclusive and only after long clinical trials and exploration are compounds optimized in delivery vehicles. At this point, it's difficult to promote change in the methods due to FDA hurdles and necessary clinical trials. In this study, we show the introduction of a compound and development of the delivery system simultaneously. In this way, the compound can really be tested *in vivo* with more significant results and exploration. Further, studies for pharmacokinetics and biodistribution are well-understood due to the long-standing history of liposomal nanocarriers. This represents a shift in how we interface biomaterials with the cargo. By developing the two simultaneously, we avoid the circulation problems inherent to the compound and understand the tumor distribution of the complex. Further, we have the ability to better assess localization and circulation of these compounds through imaging agents. I think that this is a significant in the movement of the field to a more collaborative interface at the translational level.

Lastly, this thesis represents a highly collaborative work among chemists, engineers, biologists, and physicians to tackle one problem: glioma invasion. I think that the ability for us to move amongst groups of researchers as bioengineers is essential to the vitality and ingenuity of this field. The willingness to develop a variety of skill sets and interact can create a substantial alteration in the research ongoing in the field and better advance the clinical side as well as the experimental side to better tackle the difficult problems of disease.

APPENDIX A

MICROARRAY DATA FOR IB-AFFECTED GENES

Gene Symbol	Fold Change (Tumor v. Normal)	Fold Change (Treated v. Untreated)	Gene Title
Aamp	2.08	-2.14	angio-associated, migratory cell protein
Acta1	16.29	-2.34	actin, alpha 1, skeletal muscle
Anp32a	-1.01	-2.23	acidic (leucine-rich) nuclear phosphoprotein 32 family, member A
Arhgdia	-10.59	3.19	Rho GDP dissociation inhibitor (GDI) alpha
Cct6a	-6.19	2.75	Chaperonin containing Tcp1, subunit 6A (zeta 1)
Cebpd	-2.23	-2.63	CCAAT/enhancer binding protein (C/EBP), delta
Cxcl1	-39.89	-2.17	chemokine (C-X-C motif) ligand 1 (melanoma growth stimulating activity, alpha)
Cxcl13	-67.58	3.89	chemokine (C-X-C motif) ligand 13
Cxcl2	-36.24	-2.71	chemokine (C-X-C motif) ligand 2
Cxcl9	-9.60	2.14	chemokine (C-X-C motif) ligand 9
Cxcl9	-16.08	2.11	chemokine (C-X-C motif) ligand 9
Cybb	-46.87	2.51	Cytochrome b-245, beta polypeptide
Cybb	-21.68	2.09	cytochrome b-245, beta polypeptide
Fabp4	-3.42	-2.77	fatty acid binding protein 4, adipocyte
Gdf15	-2.47	-2.35	growth differentiation factor 15
Grxcr1	1.77	2.06	glutaredoxin, cysteine rich 1
Hapln2	9.09	-2.20	hyaluronan and proteoglycan link protein 2
Hbb	-9.62	-2.25	hemoglobin, beta
Il10	-7.47	-2.00	interleukin 10
Il1r2	-9.41	-2.14	interleukin 1 receptor, type II
Irf2	-2.93	1.99	interferon regulatory factor 2
Itga6	-3.12	2.16	Integrin, alpha 6
Jmjd3	-1.54	-2.27	jumonji domain containing 3
Ly86	-15.57	2.02	lymphocyte antigen 86
Map1b	7.48	2.02	microtubule-associated protein 1B
Mbp	38.89	-3.06	myelin basic protein
Mfhas1	-1.23	2.10	malignant fibrous histiocytoma amplified sequence 1

Gene Symbol	Fold Change (Tumor v. Normal)	Fold Change (Treated v. Untreated)	Gene Title
Mfrp	10.15	-1.99	membrane frizzled-related protein
Mobp	47.81	-2.25	myelin-associated oligodendrocyte basic protein
Mx1	-13.17	2.31	myxovirus (influenza virus) resistance 1
Nfrkb	-1.60	2.01	nuclear factor related to kappa B binding protein
Otx2	6.67	-2.04	orthodenticle homolog 2 (Drosophila)
P2ry14	-3.67	2.12	purinergic receptor P2Y, G-protein coupled, 14
Pf4	-8.96	-2.29	platelet factor 4
Pfn1	-2.42	-2.34	profilin 1
Ppp1r14a	17.65	-2.10	protein phosphatase 1, regulatory (inhibitor) subunit 14A
Ptgds	29.03	-2.09	prostaglandin D2 synthase (brain)
RT1-Db1	-12.17	2.06	RT1 class II, locus Db1
RT1-Db1	-12.17	2.06	RT1 class II, locus Db1
S100a8	-18.66	-2.10	S100 calcium binding protein A8
Scin	-16.73	2.80	Scinderin
Sepw1	3.62	-2.21	selenoprotein W, 1
Sf3b5	1.17	-2.59	splicing factor 3b, subunit 5
Slc6a6	-4.76	-2.07	solute carrier family 6 (neurotransmitter transporter, taurine), member 6
Sostdc1	26.63	-3.86	sclerostin domain containing 1
Tardbp	-2.26	-2.13	TAR DNA binding protein
Tgoln1	-1.31	2.14	trans-golgi network protein
Tram1	-3.55	2.32	Translocation associated membrane protein 1
Ttr	32.59	-7.53	transthyretin
Uba6	-3.84	2.22	Ubiquitin-like modifier activating enzyme 6
Vcan	-6.22	-2.17	versican

APPENDIX B

EFFECT OF IB ON ANGIOGENESIS

(Abridged work completed by undergraduate Eleanor De Hitta and used in her senior thesis)

B.1 Introduction

Gliomas develop their vascularized networks through the process of angiogenesis, the development of blood vessels. In tumor development, angiogenesis is marked by a few hallmark characteristics. Growth factors released from tumor cells activate receptors on nearby pre-existing blood vessels, causing the release of enzymes called matrix metalloproteinases (MMPs)[309]. Matrix metalloproteinases degrade the basement membrane or inner lining of the blood vessel to make room for the development of new blood vessels. In glioma, MMP-2 and MMP-9 are significantly overexpressed [310]. Simultaneously, the blood vessel's pre-existing endothelial cells release chemical messengers to induce endothelial cell recruitment towards the site of angiogenesis (known as endothelial cell chemotaxis). Blood vessels are mainly composed of endothelial cells. They are the building blocks of the blood vessel foundation. Endothelial cells will then adhere to the site of degraded basement membrane. Next, the newly recruited endothelial cells will form tube-like structures with neighboring endothelial cells. These networks will facilitate the development of blood vessel formation [311].

Throughout the process of angiogenesis, growth factors are overexpressed. An imbalance of these growth factors causes the newly formed vessels to be disorganized and underdeveloped[312]. The endothelial cells which make up the lining of the vessel have large gap junctions as a result of the imbalance in growth factors[313]. The creation of large gap junctions increases the permeability of the blood vessel, which causes fluid accumulation in tumors. Tumor permeability has been observed to increase up to 20 fold

compared to healthy patients.[314] The blood-brain barrier is the separation between blood and cerebrospinal fluid. It is highly selective of deciding what can reach brain tissue. Gliomas disrupt the structure of the blood-brain barrier, allowing for unwanted fluid to accumulate. Fluid accumulation (edema) can increase interstitial fluid pressure and neurological deficits. Furthermore, interstitial fluid pressure has been shown to decrease drug delivery. Although edema can be treated with steroid therapy, it is not favored due to the adverse side effects associated with steroids. Therefore, development of anti-angiogenic therapies is favored to reduce symptoms of edema and increase drug delivery.[314]

T1-based magnetic resonance (MR) contrast agents have enabled more applications of magnetic resonance imaging (MRI) in tumor detection, tumor characterization, and vascular imaging. Gadolinium (Gd) chelates are ideal for imaging because they decrease T1 relaxation times.[315] However, bolus injection timing is important due to gadolinium's small window of efficacy and three hour half-life.[316] For *in vivo* small animal studies, Gd-chelates cannot produce a clear image with an optimized 7T scanner. Ghaghada *et al.* synthesized gadolinium liposomes: core encapsulated, surface conjugated, and dual (core encapsulated and surface conjugated) formulations. Three days after tail vein injections of the different formulations, animals were imaged. Rats which were administered the dual gadolinium formulation exhibited significantly higher nanocarrier-based T1 relaxivity, signal to noise ratio, and contrast to noise ratio, compared to rats with contrast-enhanced and surface conjugated gadolinium liposomes.[315]

In this study, we examined the ability of a novel anti-invasive agent, Imipramine Blue, to alter the angiogenic state of the tumor. This is based on previous data showing enhanced efficacy of Doxorubicin nanocarriers to kill tumors when pretreated with Imipramine Blue and a host of literature describing the ability of anti-invasives to change angiogenesis.

B.2 Methods

B.2.1 Cell culture

U87MG human glioma cell line was purchased from American Type Culture Collection, (Manassas, VA) and grown in T-75 flasks in growth medium. U87MG growth medium consisted of Dulbecco's Modified Eagle's Medium (DMEM) supplemented with 10% Fetal Bovine Serum (FBS), 1% Penicillin/Streptomycin (P/S), 1% Non-Essential Amino Acids , and 1% L-glutamine (L-glut) (Gibco, Carlsbad, CA). RT2A and 3RT1-RT2A (eGFP-expressing RT2A) rat glioma cell lines were obtained from Helen Fillmore in the Department of Neurosurgery from the Virginia Commonwealth University. RT2A was grown in T-75 flasks in U87MG growth medium previously mentioned. 3RT1-RT2A growth medium included the same formulation for U87MG and RT2A growth medium with the addition of 1mg/ml G418 sulfate (Gemini Bio-Products, West Sacramento, CA). Basal media for U87MG, RT2A, and 3RT1-RT2A consisted of DMEM supplemented with 1% Penicillin/Streptomycin, 1% Non-Essential Amino Acids , and 1% L-glutamine.

Human Umbilical Vein Endothelial Cells (HUVEC) were a generous gift from Larry V. McIntyre and cultured in T-75 flasks treated with 0.2% gelatin (Sigma, St. Louis, MO) in Medium 199 (M199, Mediatech, Manassas, VA) supplemented with 16.28% Fetal Bovine Serum, 0.98% Penicillin/Streptomycin, 0.98% L-glutamine, 0.2% heparin (1000 USP units ml⁻¹, Baxter Healthcare, Deerfield, IL), and 0.16% endothelial mitogen (25 mg reconstituted in 2 ml M199, Biomedical Technologies, Stoughton, MA). Low serum media consisted of M199 supplemented with 0.05% Fetal Bovine Serum, 0.98% Penicillin/Streptomycin, 0.98% L-glutamine, 0.2% heparin, and 0.16% endothelial mitogen.

B.2.2 DQ Collagen Assay

A 96-well plate was coated with the dye-quenched collagen and BME solution (1 mg/ml each in DMEM). U87MG or RT2 were seeded in wells (50,000 cells/well in 50 μ l) and treated with varying concentrations of Imipramine Blue (0 to 100 μ M). Plates were then incubated for 16-24 hours and FITC imaged under 10x magnification. Average FITC intensity levels were determined using ImageJ Software, normalized to the control (0 μ M), and compared using a one-way ANOVA to detect significant differences. If the one-way ANOVA detected a significant difference, a Tukey comparison was used to determine which pairs were significantly different

B.2.3 Endothelial cell invasion assay

50,000 Human Vascular Endothelial Cells (HUVECs) per well were seeded in tissue culture inserts coated with the matrigel. Imipramine Blue was added to each well in increasing doses on the apical side. Wells were filled with basal media to the level of media in the tissue culture insert, preventing a pressure gradient. Plates were incubated for 24 hours then fixed with 4% paraformaldehyde, DAPI stained, and imaged to quantify invasion (as % of total). Invasion percentages were normalized to the control (0 μ M) and compared using a student's two sample t-test (2 tail, $\alpha=0.05$) to observe significant differences.

B.2.4 Liposome Synthesis

Imipramine Blue liposomes and saline liposomes were synthesized as previously described (Chapter 4) Dual gadolinium liposomes were synthesized as described ref. Briefly, DPPC, Gd-DTPA bis(stearylamide) (Gd-DTPA-BSA), cholesterol, and DSPE-PEG 2000 with a molar ratio of 30:25:40:5 were dissolved in a chloroform-methanol (1:1 v/v) solution. The lipid solution was then evaporated to dryness using a vacuum and hydrated with a solution of gadodiamide (OmniScan®) to a final lipid concentration of 40mM. The solution was stirred at 60°C for 90 minutes. The liposomes were then extruded five times through a 400 nm Nuclepore membrane, seven times through a 200

nm Nuclepore membrane, and ten times through a 100 nm Nuclepore membrane. The final liposome solution was then dialyzed against PBS to remove free gadolinium. Liposomes were measured by Dynamic Light Scattering to determine the diameter.

B.2.5 In vivo Vascular permeability quantification

The *in vivo* vascular permeability study followed the timeline outlined in **Table B.1**. Typically, rats inoculated with the untreated RT2 tumor model show signs of morbidity by day 12.

Table B.1: Timeline of treatment and imaging schedule

Day	Treatment
0	Inoculate tumor
4	Tail vein injections Group 1, nano-IB (n=3) Group 2, plain liposomes (n = 3)
7	Pre contrast images for random members of groups 1 and 2 Tail vein injections of dual gadolinium liposomes, both groups
10	MRI both groups
12	Perfusions

B.2.6 Animal studies

Tumors were inoculated as described with 200,000 RT2 cells in 10µl into the cortex of Fisher 344 male rats (six rats total). On day 4 after tumor inoculations, the rats were administered either saline liposomes or IB liposomes (5 mg/kg). Day 4 was chosen as the first day of injection because it is when angiogenesis is first seen in histological analysis. On day 7, both groups were administered 0.15 mmol Gd/ kg rat after pre-contrast MRI. Timeline is in Table ##.

B.2.7 Magnetic resonance imaging

On day 7 prior to tail vein injections, one animal from each group was MR imaged for precontrast reference. Animals were anesthetized by 1-2% Isoflurane, then placed in a 7T MRI (Bruker). A T1-weighted image was taken through the head using the following parameters: a range of 50ms - 2.0 s repetition time (TR), 48 ms echo time (TE), FOV = 40 mm x 40 mm with a 256 x 256 matrix, slice thickness = 5 mm, number of slices = 1, 4 averages per phase encode step requiring a total acquisition time of about 45 minutes per rat. Furthermore, a 3x3 cut out of a clear 96-well plate containing varying concentrations of dual-gadolinium liposomes were imaged for use as a standard for concentration determination.

B.2.8 Kinetic analysis for determination of permeability

Vascular Permeability was assessed by determining each tumor's endothelial transfer coefficient (K^{PS} [ml min⁻¹100 cc⁻¹ of tissue]) similarly to a method developed by Daldrup *et al.*[317] Concentration of gadolinium in the tumor (C_T) is a function of gadolinium accumulation in interstitial (C_I) and plasma spaces ($f_{pv}C_p$, where f_{pv} is the fractional plasma volume of the tumor tissue [mL cc⁻¹ of tissue] and C_p is the concentration of gadolinium in the plasma [mmol ml⁻¹]) as seen in Eq. 1.

$$C_T(t) = C_I(t) + f_{pv}C_p(t) \quad (1)$$

The rate of interstitial gadolinium accumulation (Eq. 2) is a function of the endothelial transfer coefficient (K^{PS}), the concentration of gadolinium in the plasma and the reflux from interstitial water back to the plasma, where k is the reflux rate constant.

$$\frac{dC_I(t)}{dt} = K^{PS}C_p(t) - kC_I(t) \quad (2)$$

The solution to Eq. 2 is shown below in Eq. 3.

$$C_I = K^{PS} \int_0^t C_p(\theta) e^{-k(t-\theta)} d\theta \quad (3)$$

Substituting C_I yields Eq. 4.

$$C_T(t) = K^{PS} \int_0^t C_p(\theta) e^{-k(t-\theta)} d\theta + f_{pv} C_p(t) \quad (4)$$

B.2.9 MRI data extraction

Pre-contrast images were not used for the kinetic analysis of MR images because it was determined that the difference in tumor sizes from day 7 and day 10 would affect the amount of gadolinium accumulated at the tumor. MR images were converted into MATLAB color maps by a program provided by Dr. Johannes Leisen. The color maps displayed T_1 relaxivity and inverse T_1 relaxivity ($1/T_1$) values. T_1 and $1/T_1$ color map scales were adjusted (T_1 : (0, 4000); $1/T_1$: (4E-4, 8E-4)). Areas on the 96-well plate T_1 color map corresponding to varying concentrations of gadolinium were traced, and average RGB (red, green, blue) values were recorded. The RGB values were then converted to T_1 values on the color map scale, and an exponential regression was created relating the amount of gadolinium (mmol) to T_1 values.

ImageJ was used for tumor analysis. Tumors on T_1 color maps were outlined. Tumor area and mean tumor RGB values were extracted. RGB values were converted to T_1 values using the color map scale. Finally, the T_1 values were converted to amounts of gadolinium (mmol) using the exponential regression. These values were divided by the product of the tumor area and MR image depth (volume of tumor section), converted to mmol/cc and recorded as $C_T(t=72 \text{ hours})$.

No pharmacokinetics studies have been published for the dual gadolinium liposome formulation developed by Ghaghada *et al.*, so gadolinium accumulation in the

plasma was modeled from a stealth liposome model.[315, 318] This model is analogous because of the similar lipid content. This model was applied to gadolinium accumulation. The vehicle of delivery (liposome) is what limits the amount of core encapsulated gadolinium which will be released into the plasma, so this is an applicable model for $C_p(t)$. It was assumed that dual-gadolinium liposomes would have the same release profile in the plasma concentrations of mg/ml were converted to mmol/ml.

Daldrup *et al.* used $k = 0$ for albumin-conjugated gadolinium.[317] Liposomes have a similar clearance rate as albumin, so k was also assumed to be 0 for the dual-gadolinium liposomes. Fractional plasma volume of 0.177 mL cc^{-1} was taken from control animals by a similar study by Gossman *et al.*[319] Rats were inoculated with U87 gliomas and MR imaged on day 16 to evaluate an anti-angiogenic therapy using the method described by Daldrup *et al.*[317] K^{PS} was then solved using Eq 4.

B.2.10 Perfusions and Brain Processing

On day 12 the animals were perfused intracardially with PBS. Prior to perfusion, the rats were anesthetized by an intraperitoneal injection of ketamine, xylazine, and acetylpromazine (respectively 50, 10, and 1.67 mg/kg). Extracted brains were fixed in 4% paraformaldehyde in PBS for 1 hour at 4°C then stored in 4% sucrose (wt-vol % in PBS) at 4°C until saturated, embedded in optimal cutting temperature compound (OCT), stored at -80°C and cryosectioned coronally into $16 \mu\text{m}$ slices.

B.3 Results

B.3.1 MMP Activity is not affected by IB until it reaches cytotoxic doses

Some significant differences were observed in U87 and RT2 MMP activity (**Figure B.1**). A significant difference was observed in U87 cells between $0.001 \mu\text{M}$ IB and $50 \mu\text{M}$ IB treatment groups ($p=0.000$). Similarly, significant differences were observed in RT2 cells between $1 \mu\text{M}$ IB and $50 \mu\text{M}$ IB ($p=0.016$). U87 MMP activity showed no definite increasing or decreasing trends as Imipramine Blue treatment

increased. As IB treatment increased, RT2 MMP activity increased from 0 μM IB to 0.1 μM IB and 1 μM IB, peaked, and then decreased from 1 μM IB to 100 μM IB.

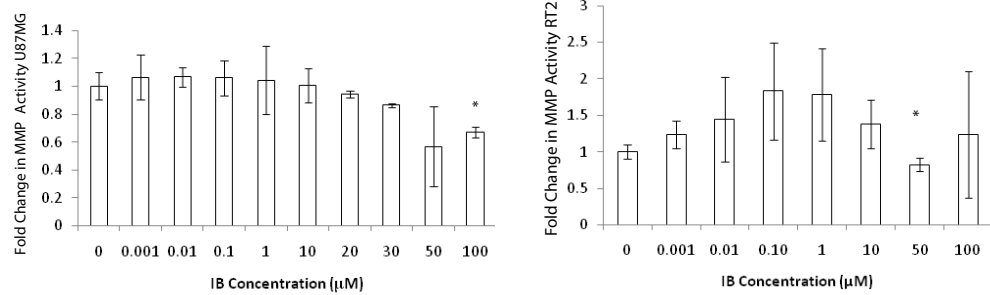


Figure B.1: MMP Activity in IB-Treated U87 (left) and RT2 (right) cells. Cells were seeded on a basement membrane extract which included a dye-quenched collagen IV. When the collagen IV is cleaved by MMP-2 and MMP-9, a green fluoroscein is emitted. Data graphed is the change in this intensity over the baseline 0 μM concentration. Only the high concentrations of IB showed significant decrease Collagen IV cleavage (* $p < 0.05$). At this concentration, IB is known to be cytotoxic to both cell lines.

B.3.2 Huvec invasion is not significantly affected by IB

HUVECs that were plated in matrigel and allowed to invade did not show a significant response to IB ($p = 0.08$, **Figure B.2**).

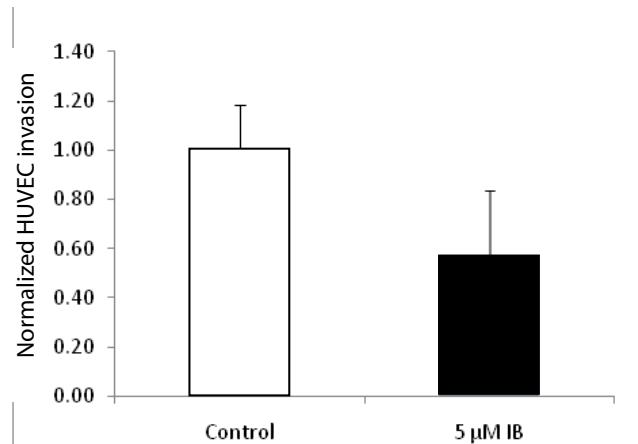


Figure B.2: Treated HUVEC invasion decreased but was not significant ($p=0.08$, in one experiment). HUVECs were seeded and treated either 0 μM IB or 5 μM IB ($n=3$ per treatment), incubated for 24 hours, 4% paraformaldehyde fixed, DAPI stained, and imaged. Invasion through the tissue culture insert was quantified and normalized to the control.

B.3.3 In vivo vascular permeability quantification

Though the IB-treated group seemed to have an increase in vascular permeability, no significant differences were observed between treatment groups in terms of endothelial transfer coefficients and cross-sectional tumor area ($p_1=0.3488$, $p_2=0.187$). MR images are seen in **Figure B.2**, displaying the inverse T_1 relaxivities which is indicative of the accumulated concentration of Dual-Gd liposomes.

Table B.2: Endothelial Transfer Coefficients (K^{PS}) and Cross-Sectional Tumor Areas

Saline Liposomes			Imipramine Blue Liposomes		
ID #	K^{PS}	Cross-sectional tumor area	ID #	K^{PS}	Cross-sectional tumor area
1	0.647	0.808	4	13.466	0.058
2	6.927	0.126	5	3.398	0.209
3	0.908	0.576	6	3.907	0.248
Mean \pm SD	2.83 ± 3.55	0.50 ± 0.35	Mean \pm SD	6.92 ± 5.67	6.92 ± 0.10

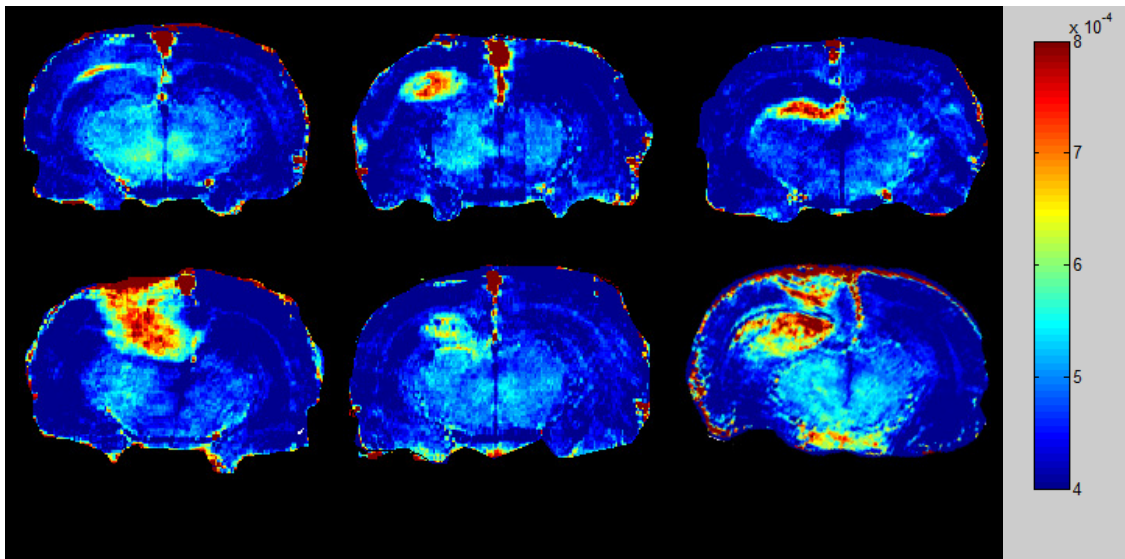


Figure B.3: $1/T_1$ MR Brain Image Color maps. Color maps generated from MR data representing the inverse relaxivities. The red denotes the areas where gadolinium accumulated. Top row shows tumors treated with saline liposomes. Bottom row shows tumors treated with imipramine blue liposomes.

B.3.4 In vivo staining of blood vessels reveals no observable differences

Performing staining of tumors after the study revealed no readily observable differences in blood vessel quantity or morphology. There appeared to be blood vessels heterogeneously distributed throughout the tumor and that this distribution was unaffected by the treatment. **Figure B.3** shows representative images from different regions throughout the tumors.

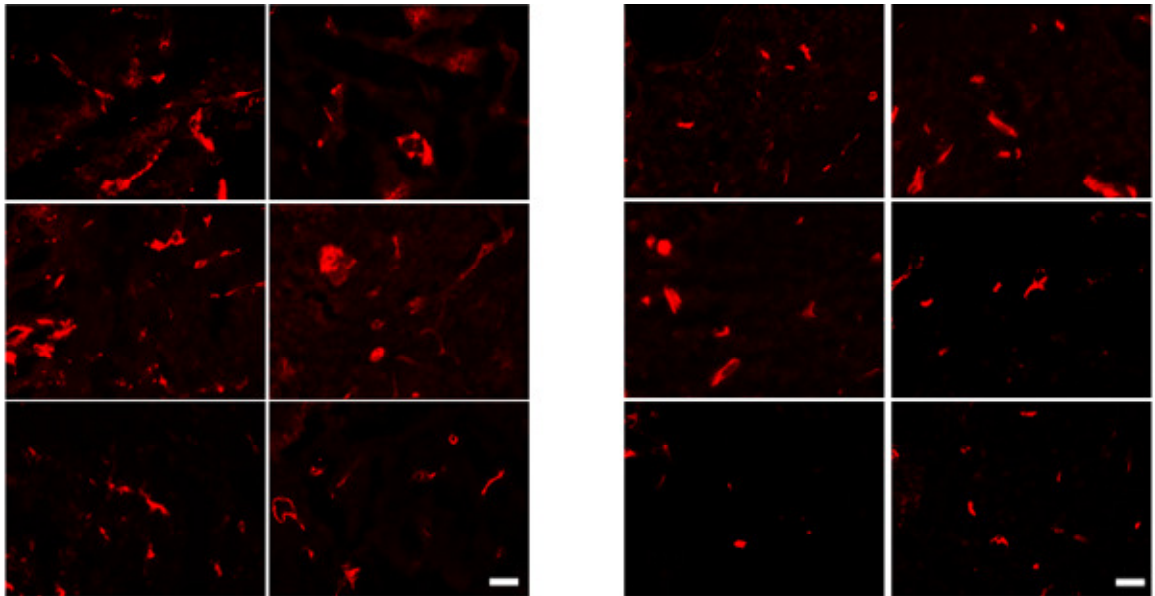


Figure B.4: Effects of Imipramine Blue on Blood Vessels of Rat Glioma (RT2). Rats were inoculated with glioma and treated with either nano-IB or saline. Brains were cryosectioned, stained for RECA-1, endothelial cell marker (red), and imaged throughout the tumor. Rats treated with saline (A) appeared to possibly have more blood vessels than those treated with IB (B). (Scale bar= 50 μ m)

B.4 Discussion

MMP-2 and MMP-9 activity appears to not be affected by varying concentrations of Imipramine Blue. Although U87 and RT2 cells treated with 50 μM IB were significantly different from other treatment groups, it is expected that the significant decrease observed is due to cell death. From previous *in vitro* cytotoxicity assays, 40 μM IB was determined to be the average lethal dose for U87 and RT2, *in vitro*. This supports the prediction that Imipramine Blue does not affect basement membrane degradation, the first stage of angiogenesis. For future studies, it is suggested that a positive control group be added, such as emodin, an MMP-2 and MMP-9 inhibitor observed in glioma cells.[320] The addition of a positive control group will confirm the appropriate sensitivity of the assay if no fluorescence is emitted. Zymography could also be performed for more quantitative results.

The HUVEC invasion assays suggest endothelial cell migration decreases when cells are treated with Imipramine Blue, but the results are not significant. Increasing the sample size for each treatment will provide more results, so a definite conclusion concerning IB-treated endothelial cells can be made. The assay performed only assesses the effect of IB on treated endothelial cells. Future experiments can simulate the effect of IB-treated glioma cells and their ability to recruit endothelial cells. This would involve glioma cells plated in a 24 well plate. Once adhered, cells would be treated with either 0 μM IB or 5 μM IB in basal media. Cells would be treated for 3 hours. *In vitro*, the effects of IB have been observed as early as 3 hours after treatment. After 3 hours of treatment, media will be replaced with low serum HUVEC media. Tissue culture inserts containing seeded with untreated HUVECs using the method mentioned previously, will then be placed in the glioma-coated 24-well plate and incubated for 24 hours. Invasion through the membrane will be quantified using the same method previously mentioned. The addition of the coated glioma cell lines will simulate the tumor environment with the secretion of its chemokines during incubation.

No conclusions were made on the effect of Imipramine Blue on tube formation. Future experiments should include tube formation assays involving HUVECs treated with: varying concentrations of IB and a positive control tube formation inhibitor such as Avastin.[321] This will assess Imipramine Blue's possible abilities to prevent endothelial cell tube formation.

No significant differences were observed between treatment groups in terms of endothelial transfer coefficients and cross-sectional tumor areas. A similar study was conducted comparing the effects of an anti-VEGF therapy on endothelial transfer coefficients in U87 inoculated tumors (400,000 cells in matrigel-media suspension per animal). Tumors were MR imaged on day 16. Given the cell amount inoculated and the additional amount of time to MR image, tumor sizes from the U87 study were larger. Furthermore, K^{PS} values were ten times greater in U87 PBS-treated tumors (control $28.6 \pm 8.6 \text{ mL min}^{-1}\text{cc}^{-1}$ of tissue, mean \pm SD) compared to the RT2 saline liposome-treated tumors (control $2.83 \pm 3.55 \text{ mL min}^{-1}\text{cc}^{-1}$ of tissue, mean \pm SD). Tumor size varied greatly within treatment groups. This could be due to improper tumor inoculation or natural tumor size variability depending on the individual animal. Increasing the sample size and using a new syringe needle will likely lower the variability within tumor groups.

Many assumptions were made for this study, limiting the results. Fractional plasma volume constants were taken from the control animals in the study by Daldrup et al. The study's treatment groups had significantly different fractional plasma volume constants. If the treated Imipramine Blue animals did have a difference in vascular permeability, then estimating the fractional plasma volume to be the same could have eliminated a possible significant difference in endothelial transfer coefficients between treatment groups. For future experiments, a better method for determining fractional plasma volume should be implemented. Additionally, a dual-gadolinium liposome pharmacokinetic study should be conducted to obtain a model for plasma gadolinium accumulation.

APPENDIX C

COMBINATORIAL TREATMENT WITH TEMOZOLOMIDE

(Project completed/in progress by Undergraduate Sydney Rowson)

C.1 Introduction

Imipramine Blue has shown efficacy at halting invasion of glioblastoma and benefit in combination with Doxorubicin *in vivo*. However, the most commonly used chemotherapeutic treatment in glioblastoma is oral temozolomide (TMZ), a DNA alkylating agent[20]. Integration of this chemotherapy with the traditional course of therapy including radiation and resection resulted in significant increases in remission and survival times. However, the outlook is still not promising for these patients. This is largely due to the invasion of tumors post-treatment which can be halted with Imipramine Blue (IB) a novel Nox4 inhibitor. However, there is another reason for failure of TMZ specifically which results from the resistance of tumors to the drug.

TMZ resistance occurs in a large percentage of glioblastoma patients and results from overactivity of the gene O⁶-Methylguanine-DNA Methyltransferase (MGMT)[33]. This enzyme removes methyl groups from the O⁶ position of guanine in DNA. Methylation is one mechanism by which genes are silenced and thus regulated within the genome within cells. It is also the mechanism by which many chemotherapeutics, such as TMZ and carmustine, act to damage the genome and induce apoptosis in cancer cells. High activity of MGMT leads to increased reversal of therapy-induced alkylation and thus resistance to chemotherapy[322].

Interestingly, MGMT itself is regulated through MGMT of the CpG island in the promoter region of many cancers[34]. When this area is hypermethylated, MGMT is less active, and cancer cells respond better to alkylating agent chemotherapy. Further, hypermethylation is correlated with increased survival time in patients[323]. Therefore, hypermethylation of the promoter region of MGMT is indicative of a more treatable

tumor that will respond to TMZ better. Further, induction of hypermethylation leads to beneficial treatment response to TMZ in previously resistance cell types. Since TMZ is the primary treatment in glioblastoma chemotherapy, it is valuable to have therapeutics which can cause this change and thereby increase response to TMZ in resistant tumors.

Imipramine Blue has already shown benefit with Doxorubicin, a topoisomerase II inhibitor used in a number of malignant cancers. Though no synergy was seen *in vitro*, there was a significant benefit to delivering these agents in sequence *in vivo*. This was attributed to the ability of IB to halt invasion of tumors *in vivo* thus allowing better response to the treatment. However, IB generates a host of downstream effects on cancer cells that could also benefit chemotherapy, both *in vivo* with Doxorubicin and possibly with TMZ.

In this study, we examined the ability of IB to increase the efficacy of TMZ in both glioblastoma cell lines and primary glioblastoma neurospheres. Further we examined the ability of IB to halt invasion of neurosphere primary glioblastoma cells.

C.2 Methods

C.2.1 Cell Culture

U87MG (ATCC) and RT2 (courtesy Helen Fillmore, Virginia Commonwealth University) glioma cells were maintained in DMEM containing 10% FBS and 1% Pen/Strep. Three primary neurosphere cultures were graciously given to us by Daniel Brat, Emory Department of Pathology. They were maintained in Neurobasal A (Invitrogen) media supplemented with N2 (Invitrogen, 1%), B27 (Invitrogen, 2%), FGF (Stemcell Technologies, 10ng/ml), EGF (StemCell Technologies, 20ng/ml), L-glutamine (VWR, 0.5%), pen/strep (VWR, 1%), and Heparin (StemCell Technologies, 0.4%) in non-tissue culture treated flasks. Neurospheres were grown in suspension and passaged upon reaching 200-500 μ m in size. Every 2-3 days, cultures were supplemented with media containing fresh FGF, EGF, and heparin (1 ml/day).

C.2.2 Cytotoxicity Assays

U87MG and RT2 cells were seeded at 100,000 cells/ml in 24-well plates overnight. They were then treated with IB (+IB) or ethanol (-IB) for 3 hours, then washed. Temozolomide in DMSO was added in increasing concentrations and cells were incubated with it for 96 hours. Readings were taken once a day using CCK8 cell counting assay by incubation and removal of media for assay. Fresh temozolomide was added every day after this assay. Neurosphere cytotoxicity assays were performed similarly, with differences in the culture techniques. Cells were seeded at 50,000 cells/ml and spheres were allowed to establish (approximately 1 week) in round-bottom 96 well plates. Cells were fed as normal during this time. For addition of drugs and readings, the plates were centrifuged at 1000 rpm and the media removed and cells washed. This was repeated for each reading.

C.3 Results

IB enhances the efficacy of temozolomide to induce its cytotoxic effect in the U87MG glioma cell line. There was a significant decrease in cell viability at 72 hours at the highest concentration 200 μ M and at 96 hours both 100 μ M and 200 μ M showed a significant increase in cell death with IB (**Figure C.1**). This indicates that IB yields enhanced cell death with temozolomide. Further, there was no cell death seen at the higher concentrations without IB indicating resistance of this cell line to the drug. None of the neurospheres showed death in the presence of TMZ or IB + TMZ after 96 hours.

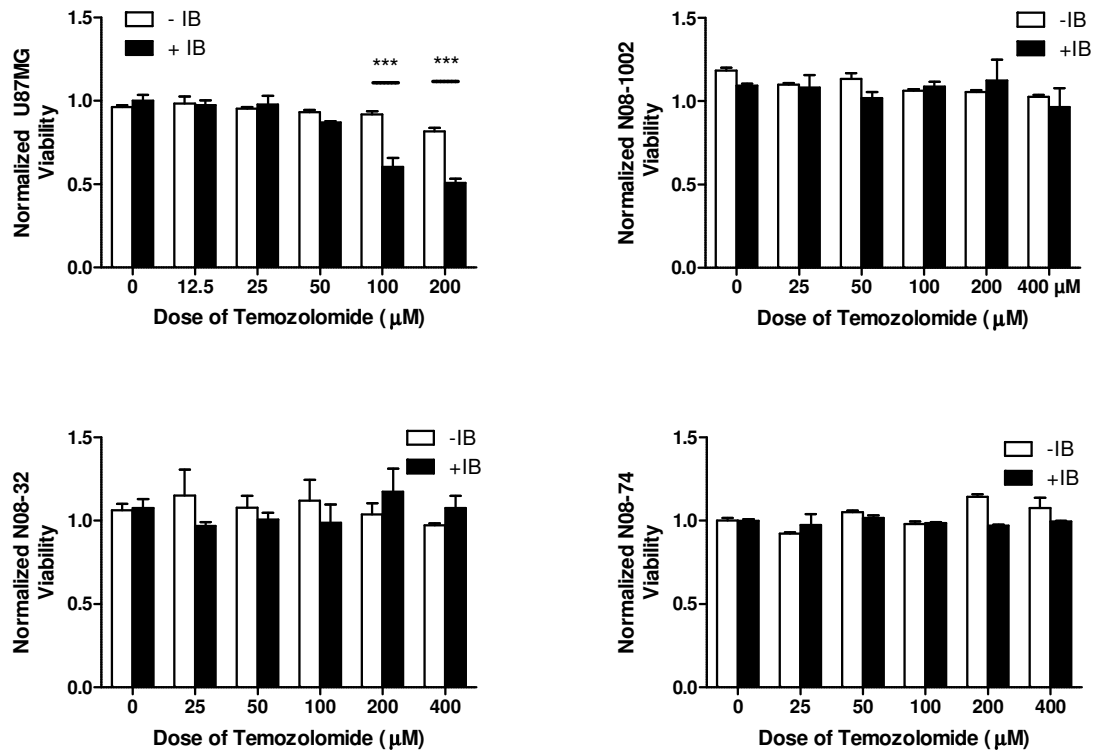


Figure C.1: Viability with Temozolomide and IB treatment

C.4 Discussion and Conclusion

It is apparent that there is a synergistic effect between IB and TMZ *in vitro* in U87MG glioblastoma. However, this effect does not seem to be universal and may indicate particular sensitivity of different models to the pathway that IB is affecting. Further, based on previous data, this sensitivity does not necessarily translate to the ability of IB to affect invasion. Though RT2 is the most responsive to the anti-invasive effects of IB, it does not have enhanced benefit from the delivery of IB with temozolomide. This may indicate another attribute of the inhibition of Nox4 that is not previously documented in the literature.

Future studies include further examination of the effect of IB on neurospheres including stem cell populations, establishment of neurospheres in the presence of treatment, and invasion assays in 3D. Preliminary work was done with these cultures,

however, further investigation of the universality of IB in these primary glioblastomas is highly useful information. Further, in cell lines and cultures where there is a benefit to giving IB with temozolomide, methylation site specific rtPCR is ongoing for determination of enhanced sensitivity due to the primary mechanism of resistance: MGMT activity.

APPENDIX D

IB-DXR NANOCARRIERS AGAINST U87MGEGFRVIII

(Abstract submitted to Society for Neuro-Oncology with Konstantinos Hadjipanayis, MD, PhD)

Glioblastoma invasion is a major reason for recurrence after treatment. Recently, we saw in a rat glioblastoma model (RT2) that combination of Doxorubicin and Imipramine Blue, a novel anti-invasive agent that acts via inhibition of Nox4, enhances survival as compared to Doxorubicin alone. This study used systemic delivery to examine the efficacy of this treatment. However, it is known that use of convection enhanced delivery (CED) can yield better distribution of therapeutics within tumors and thus show better efficacy. Further, use of a human glioblastoma line transformed to express the EGFR variant 3 receptor known to yield enhanced invasion and malignancy of tumor *in vivo* is more clinically relevant than the rat glioblastoma in previous study [324].

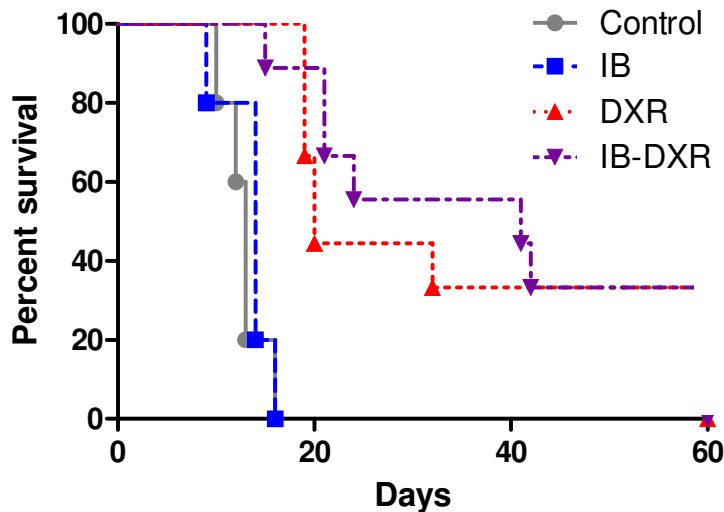


Figure D.1: Kaplan-Meier Survival Plots of mice implanted with U87MG EGFRVIII. Treatment occurred seven days after tumor inoculation via CED to the center of the tumor. Mice were monitored on a daily basis after treatment (n=6-8 per group).

In this study, we used liposomal nanocarriers containing Doxorubicin and Imipramine Blue for convection enhanced delivery to an aggressive human glioblastoma U87MG-EGFRV3. Mice were inoculated with tumors and treated seven days later via CED delivery with 5 μ l of nanocarriers containing: Saline (n=5), IB (16 μ g, n=5), DXR (20 μ g, n=8), or IB-DXR (16 μ g IB, 20 μ g DXR, n=8). Mice were monitored by MRI before and after treatment to determine tumor response and then allowed to live until they met the criteria for euthanasia. Postmortem, brains were sectioned and stained for hematoxylin and eosin. Further, the combinatorial treatment was tested *in vitro* on the cell line to determine any synergistic effects on cell viability.

Both the DXR and IB-DXR groups showed enhanced efficacy (**Figure D.1**) by increasing survival times above control groups (p<0.001 for each as compared to control using Mantel-Wilcox test). There was no benefit for co-delivery of the IB with DXR. However, in the previous studies the drugs were delivered sequentially and thus there may be a benefit if this strategy is employed in the model. However, there was complete survival and remission in 3 animals per group that received the DXR-loaded nanocarriers indicated a benefit to this therapeutic in CED against EGFRV3 positive glioblastomas. Histology and *in vitro* studies are ongoing to determine differences between tumor and cell viability in response to combinatorial treatment. However, this data is striking in the ability of the nanocarriers delivered via CED to yield complete survival in this highly aggressive model of glioblastoma.

APPENDIX E

EFFECTS OF INTERSTITIAL FLOW ON GLIOMA INVASION

(Manuscript in preparation from year abroad on Fulbright Fellowship)

From: Interstitial flow increases glioma invasion via CXCR4-dependent autologous chemotaxis in a 3D microenvironment

Jennifer M Munson² Ulrike Haessler¹ , Ravi V Bellamkonda^B , Melody A Swartz¹

¹Laboratory of Lymphatic and Cancer Bioengineering, Institute of Bioengineering and Swiss Institute for Experimental Cancer Research, École Polytechnique Fédérale de Lausanne (EPFL), Switzerland

² Department of Biomedical Engineering, Georgia Institute of Technology, Atlanta, GA, USA

E.1 Abstract

Brain tumor invasion is a significant clinical problem leading to recurrence and resistance to treatment. Glioma cells invade in distinctive patterns that correlate with chemokine gradients, flow patterns, and structural heterogeneity in the brain. In other tumors, interstitial flow caused by lymphatic drainage actively enhances invasion and metastasis towards lymphatics. We hypothesized that fluid drainage from brain tumors into the cerebrospinal fluid could play an active role in glioma invasion. Using *in vitro* 3D glioma model systems, we show that slow interstitial flow can enhance cell invasion in multiple glioblastoma models. These flow effects were CXCR4-dependent, as they could be abrogated upon blocking CXCR4 or adding exogenous CXCL12 to the matrix. Using immunocytochemistry and western blotting, we show that CXCR4 is actually activated under flow conditions for the most flow-responsive cell possibly contributing to the enhanced chemokinesis observed through live imaging. Lastly, we identify a group of cells that has enhanced chemotactic potential in the direction of flow by using live

imaging and analysis, that can be blocked by inhibiting CXCR4 or through saturation of CXCL12 in the matrix. We propose that this migration in the flow direction is caused by autologous chemotaxis and using modeling we show that a local pericellular gradient can be formed under slow flow conditions. This study has implications for the study of brain tumors in that interstitial flow is an active regulator of the invasive potential of cancer cells and not just a passive carrier.

E.2 Introduction

Glioblastoma (GBM) is a highly infiltrative and deadly form of brain cancer. It is characterized by diffuse growth and invasion of tumor cells into the surrounding brain tissue [11]. The migration of glioma cells into the brain has a very distinctive pattern including invasion along white matter tracts, blood vessel basement membranes, and movement around the outside of the brain parenchyma [12]. These patterns have been examined to determine the reason for this selective invasion though no definitive answer has been found [325-327]. It is unclear why GBM invasion follows such patterns, but hypotheses include following the path of least resistance, fluid flow, structural cues, and protein interactions to the white matter tracts [13, 14, 328].

As for chemokines that guide invasion, CXCL12 and its receptor CXCR4 have been the most strongly correlated in brain cancer as well as in brain development [329, 330]. CXCR4 upregulation is found in almost every cancer type and is implicated in cell homing to metastatic sites. More invasive tumors express higher levels of both CXCR4 and CXCL12 [331, 332]. Further, activation of CXCR4 by phosphorylation is found in abundance in higher grade brain tumors [333]. Thus, CXCL12 likely guides brain tumor invasion, yet its relationship to the invasive patterns seen along white matter tracts has not been clarified.

Fluid flow in the brain, on the other hand, has been studied and correlated with white matter tracts [13]. Such interstitial fluid flow can theoretically redistribute

chemokine gradients that can, in turn, guide cell migration[334]. For example, melanoma and breast carcinoma invasion is correlated with expression of the chemokine receptor CCR7, and we showed in vitro that slow interstitial flow could enhance the invasion of CCR7-expressing human cancer cells that also expressed CCR7 ligands [335]. Since CCR7-directed migration is required for immune cell migration to the lymphatics, and since fluid flow is always directed from the periphery towards locally draining lymphatic vessels, this “autologous chemotaxis” could be an important mechanism of leukocyte homing to the lymph nodes, a mechanism which tumor cells mimic[336]. Further, we showed that stromal fibroblasts can enhance cell invasion due to a TGF- β -dependent mechanism that is activated by flow. Both of these mechanisms may promote invasion towards draining lymphatic vessels in the periphery[337].

Though lymphatic vessels are not present in the brain, fluid flow in the brain is tightly regulated and drains to lymphatic pathways in the neck[338]. Ependymal cells in the choroid plexus secrete CSF, which flows in response to ciliary beating along the ventricle lining. Disregulation of these ciliary cells leads to improper neuronal patterning and developmental problems [339]. Flow normally is generated at the choiroid plexus in the fourth ventricle, moves through the interstitium of the brain and drains around the outside of the brain to be reabsorbed in the ventricles[340]. However, when a brain tumor develops there is a change in the flow pattern resulting from pressure differentials caused by tumor fluid influx, cyst development, and edema resulting in drainage from the tumor into the CSF and yielding hydrocephalus [341]. Glioblastoma commonly develops in the frontal lobes of the cortex coming in close contact with white matter tracts, paths of least resistance along which fluid can drain through the brain. It has been found that tumors originating further from these tracts have a better prognosis after treatment and less recurrence implicating these pathways in tumor spread [342].

These flow pathways not only correlate with the structural features of white matter tracts but also have been correlated with chemokine gradients (such as CXCL12)

and growth factor gradients (such as VEGF) leading to angiogenesis and migration at the leading edges of these tumors [10]. Further, other tracts such as blood vessels and meningeal linings are hotspots for tumor cell migration and correlate with least resistance flow pathways and chemokine secretion in the brain [258, 343]. Therefore, it stands to reason that these three features are interrelated.

Here we propose a new mechanism for tumor cell invasion in the brain: namely, that fluid flow directs CXCL12 gradients and increases CXCR4 activity in glioma cells, leading to directed cell migration. *In vivo*, we observed a strong correlation between CXCL12, flow patterns, and glioma invasion patterns in the rat brain. Using three-dimensional *in vitro* culture systems, we show that glioma cells, when exposed to interstitial flow, become more invasive, both randomly and in the flow direction. This increase in invasion was dependent on CXCR4 signaling, and involved at least two mechanisms: autologous chemotaxis (i.e., gradient amplification of cell-secreted CXCL12 in the flow direction, causing chemotaxis) and flow-increased CXCR4 phosphorylation. Therefore, we introduce fluid flow as an important modulator of glioma invasion.

E.3 Methods

In vivo glioma analysis

Fisher 344 male rats were inoculated with 3RT1-RT2 (eGFP expressing RT2) glioma via stereotactic injection. A 2mm incision was made and a burr hole drilled 3mm lateral and 1mm anterior to bregma. A Hamilton syringe was used to inject 250,000 cells in 10 μ l L15 media 3.3 mm below the dura. On day 10 after injection, Evans blue (50 mg/kg in saline) was injected into the tail vein 12 hours prior to intracardial perfusion with 4% paraformaldehyde. Brains were collected, incubated in sucrose, cryoembedded, and sectioned at 16 μ m before staining for CXCL12 and GFP. Images were acquired

using confocal microscopy (Zeiss LSM510 Meta) and analyzed for co-localization of pixels with ImageJ software (NIH, Bethesda MD).

Cell lines and culture

RT2 cells were a kind gift from Helen Fillmore; U87MG and C6 cells were from ATCC (city, state) and 9L cells were kindly provided by the Neurosurgery Tissue Bank at University of California San Francisco. All cells were cultured in DMEM (Gibco) with 10% Fetal Bovine Serum and 1% penicillin/streptomycin, passaged with 0.05% trypsin.

3D cell assays

Experiments were performed with 12mm diameter, 8 μ m pore cell culture inserts (Millipore, Billerica, MA) in a modified Boyden chamber assay. 10⁵ tumor cells were seeded in 100 μ l in 0.1% hyaluronan (Glycosan Biosystems) and 0.12% rat tail collagen I (BD Biosciences). For chemotactic studies, CXCL12 (100nM) was added to the bottom, top, or both (with addition to the gel). After 16 hr in a 37°C/5% CO₂ incubator, gel containing nonmigrated cells was removed and the inserts were fixed in chilled 4% paraformaldehyde. Cells were stained using DAPI and counted using an inverted microscope. For experiments with blocking by AMD3100 (10 μ M) or CXCL12 presence (100nM) the chemical was incorporated into the gel and present in all media.

Migration under Flow

The above setup was modified to examine the effects of physiological flow on tumor cell migration. After the gel was cast and allowed to set, a pressure head of 1cm media was established that led to an average velocity of 0.7 μ m/s through the cell/gel compartment (flow rate determined in separate experiments using measured permeability; data not shown). For static conditions, media was placed on top to prevent drying out and brought to the media line on the outside to ensure no pressure differential. Migration in the presence of basal media, media with CXCL12 (100nM), or AMD3100 (10 μ M) was assessed.

Western Blot Analysis

CXCR4 and p-CXCR4 expression was analyzed by Western blot using 0.5 mg/ml chicken anti-CXCR4 (Sigma), rabbit anti-p-CXCR4 (S339) (AbCam), HRP-conjugated goat anti-chicken IgG and anti-rabbit IgG (BioRad), and a Western Pico ECL substrate kit (Pierce, Rockford, IL).

Antibodies, Flow Cytometry, and Immunofluorescence

The following antibodies were used for immunostaining mouse brain tissue: anti-mouse CXCL12 (AbCam), FITC-labeled anti-rat GFP, anti-mouse fluoromyelin, and DAPI (all from Invitrogen). For cultured cells, anti-rat CXCR4 (Sigma), phospho-CXCR4 (AbCam), and PhAkt (AbCam) were used. Alexafluor-labeled secondary antibodies were obtained from Invitrogen, and AF594 phalloidin (Invitrogen) was used for F-actin. For flow cytometric analysis, permeabilized and non-permeabilized cells were compared for CXCR4 expression.

ELISA for CXCL12

CXCL12 protein secretion was quantified using an ELISA kit (R&D) from cells seeded in 2D or 3D culture conditions in basal medium after 16h static or flow conditions. To account for matrix-bound ligands, three compartments were analyzed: free protein in the medium, matrix-associated protein (by digestion with collagenase D (BD Biosciences), and cells (by lysis using standard RIPA buffer protocols Sigma). Protein amounts were normalized to cell number harvested in each experiment and data combined over experiments.

Live imaging and analysis of cells under flow

RT2 cells were seeded at 5×10^5 cells/ml in a 3D flow chamber (Shields et al, 2007) in 3D gels as described for static-flow assays but with L-15 medium in place of DMEM and at a density of. Images were taken every 15 minutes for 16-24 hours at four locations for each chamber (4 chambers total: 2 static, 2 flow). Cells in videos were tracked using ImageJ and analyzed using MATLAB for migration parameters. A reference point was selected in each frame to account for focus drift due to experimental

set-up and used in analysis. After live imaging, FITC-dextran was flowed through the system to determine flow rates by FRAP analysis and assess any fluid channeling.

Polarization assays and CXCR4 image analysis

RT2 glioma cells, at 5×10^5 cells/ml in the hyaluronan/collagen matrix, were seeded into radial flow chambers [140, 337] and exposed to pressure-driven flow for 16 hours. Chambers were fixed in 4% paraformaldehyde, permeabilized with 0.05% triton, and immunostained using the appropriate antibodies. High resolution images were taken using confocal microscopy and wide-field microscopy was used for assessment of polarized cells in all regions of the chamber. For image analysis studies, imaging parameters were held constant for all pictures and intensities were measured in ImageJ and normalized to static conditions.

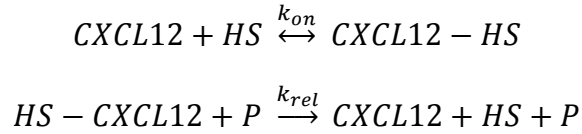
Computation of Extracellular CXCL12 Distribution

Extracellular CXCL12 gradients were computed using a 3D model according to:

$$\frac{dC_i}{dt} + v \cdot \nabla C_i = D_i \nabla^2 C_i + R_i$$

where C_i is concentration of species i , t is time, v is velocity, D_i is the diffusion coefficient, and R_i is the rate of reaction (matrix binding and cleaving of chemokine). The cell was modeled as a 20 μm diameter sphere embedded 150 μm from the bottom surface of a 500 μm thick porous ECM (Hyaluronan) with 3 μm of medium atop the matrix. The Brinkman equation was used to determine the velocity profile through the ECM around the cell using a value for permeability of $K = 10^{-12} \text{ cm}^2$ (determined from the literature) and range of $v = 0, 0.02, 0.2, \text{ and } 2 \mu\text{m/s}$ [344]. Three species i were modeled: P, the cell-released protease; CXCL12, the cell-released CXCL12; and HS-CXCL12, the matrix-bound CXCL12. Constant flux boundary conditions were assumed for both P and CXCL12 at cell surfaces, with CXCL12 fluxes measured experimentally (Supplemental data), along with zero flux inlet boundary conditions. The diffusion coefficients were

assumed to be 140 $\mu\text{m}^2/\text{s}$ for CXCL12 and 80 $\mu\text{m}^2/\text{s}$ for P [334]. The following binding/release kinetics were used to model the species:



where HS = heparin sulfate binding sites; HS-CXCL12 = matrix-bound CXCL12; and k_{on} , k_{off} , and k_{rel} are rate constants for the reactions shown. k_{on} and k_{off} were assumed to be $9.3 \times 10^4 \text{ M}^{-1} \text{ s}^{-1}$ and $0.116 \times 10^{-4} \text{ M}^{-1} \text{ s}^{-1}$, respectively, based on our own measurements ($K_d=12.4 \text{ nM}$, Supplemental data), and k_{rel} was assumed to be $1 \times 10^5 \text{ M}^{-1} \text{ s}^{-1}$. HS was calculated to be 2.6 mM with 1% HA content in the gel.

The rate equations were as follows:

$$R_{\text{CXCL12}} = -k_{on}C_{\text{CXCL12}}C_{\text{HS}} + k_{off}C_{\text{HS}-\text{CXCL12}} + k_{rel}C_{\text{HS}-\text{CXCL12}}C_P$$

$$R_{\text{HS}-\text{CXCL12}} = k_{on}C_{\text{CXCL12}}C_{\text{HS}} - k_{off}C_{\text{HS}-\text{CXCL12}} - k_{rel}C_{\text{HS}-\text{CXCL12}}C_P = -R_{\text{CXCL12}}$$

where R refers to the overall rate of production and C refers to the concentration of each of the components. C_{HS} was assumed to be much greater than C_{CXCL12} based on the calculated number of binding sites to total CXCL12 ligand concentration ratio and so was treated as a constant. Mass balances for free ligand, bound ligand, and protease were solved simultaneously using transient analysis to estimate the combined CXCL12 gradient established after 50,000 s (approximately equal to the experimental time frame). The calculations were performed using COMSOL Multiphysics modeling software (Bern, Switzerland) on a personal computer.

Statistical Analysis

Data was analyzed using one-way ANOVA with Tukey's post-test for pairs of data and Bennett's test for unequal variance was used to adjust significance. Results are reported as test statistic (degrees of freedom) = value, with $p<\#$ and $*p<0.05$, $**p<0.01$, and $***p<0.001$. Data are shown as mean \pm standard error of the mean unless noted otherwise.

E.4 Results

In vivo, RT2 glioma invasion correlates with fluid flow and CXCL12 expression

To determine whether invasion pathways correlate with fluid flow patterns and CXCL12 expression, we inoculated male Fisher 344 rats with eGFP-expressing RT2 GBM [84], a highly invasive model of GBM that shows many attributes of human GBM invasion. Nine days later, flow pathways were visualized by Evans blue injected into the tail vein, which binds albumin and leaks out of tumor vasculature[345]. Serial sections were compared for localization of white matter tracts and nuclei (**Figure E.1A**), cancer cells (**Figure E.1B, F**), flow patterns (**Figure E.1C,G**) and CXCL12 (**Figure E.1D,H**). Coronal images were overlaid (**Figure E.1I,J**), the tumor bulk subtracted out, and overlap R calculated yielding an overlap in pixels for all three of the components . Results confirm previous implications that these features indeed overlap in the brain from the tumor bulk into the healthy tissue.

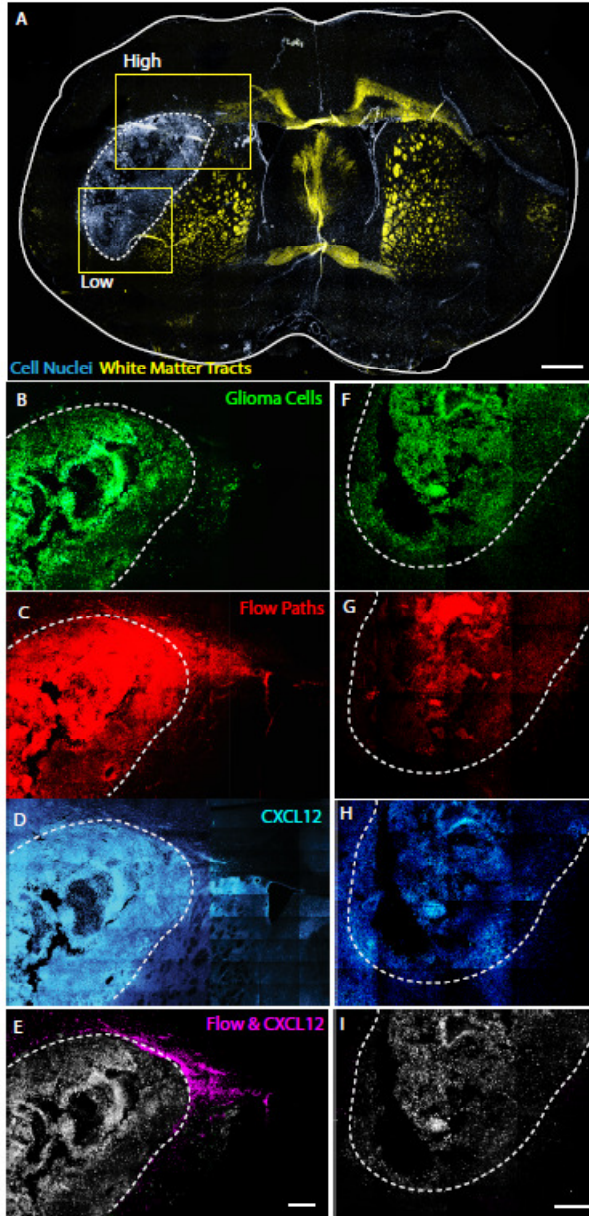


Figure E.1: Flow pathways, CXCL12 gradients, and tumor invasion overlap in the brain. (A) Structural staining of coronal brain slice (scale bar=1mm) with tumor outlined (white dotted line), showing white matter tracts (yellow, Fluoromyelin stain) and cell nuclei (gray-blue, DAPI). (B) Two regions on the tumor were selected for examination: high flow and low flow as determined by Evans blue dye flow from tumor vessels into interstitial space. In high flow regions, tumor cells (green, GFP) show invasion with flow patterns (red, Evans Blue) in the same direction as CXCL12 gradients (cyan, CXCL12) outside of the tumor bulk (white dotted line). In low flow regions, there is less staining outside of tumor bulk (white dotted line). (C) Colocalized CXCL12 and flow (lavender) relative to the tumor margin (white) (Scale bars=300µm). The overlap correlation between flow, CXCL12, and tumor cells outside the tumor margin was $R^2 = 0.957$.

Glioma invasion is enhanced in response to interstitial flow or CXCL12 gradients

We compared four glioblastoma cell lines *in vitro* for response to interstitial flow: RT2 (invasive, rat-derived GBM), U87MG (*in vitro* invasive, human-derived GBM), C6 (invasive, rat-derived GBM), and 9L (non-invasive, rat-derived astrocytoma). Using 3D cultures in porous inserts (8 μm pore size) with interstitial flow rates of 0 or 0.72 ± 0.02 $\mu\text{m}/\text{s}$, we found that the three invasive cell lines invaded more under flow conditions, with roughly twice the number of cells invading through the gel and across the membrane in the flow direction compared to that in static conditions. Interestingly, the noninvasive astrocytoma 9L did not increase invasion in response to flow (**Figure E.2**). This was consistent with flow-enhanced invasion shown previously for carcinoma cell lines [335].

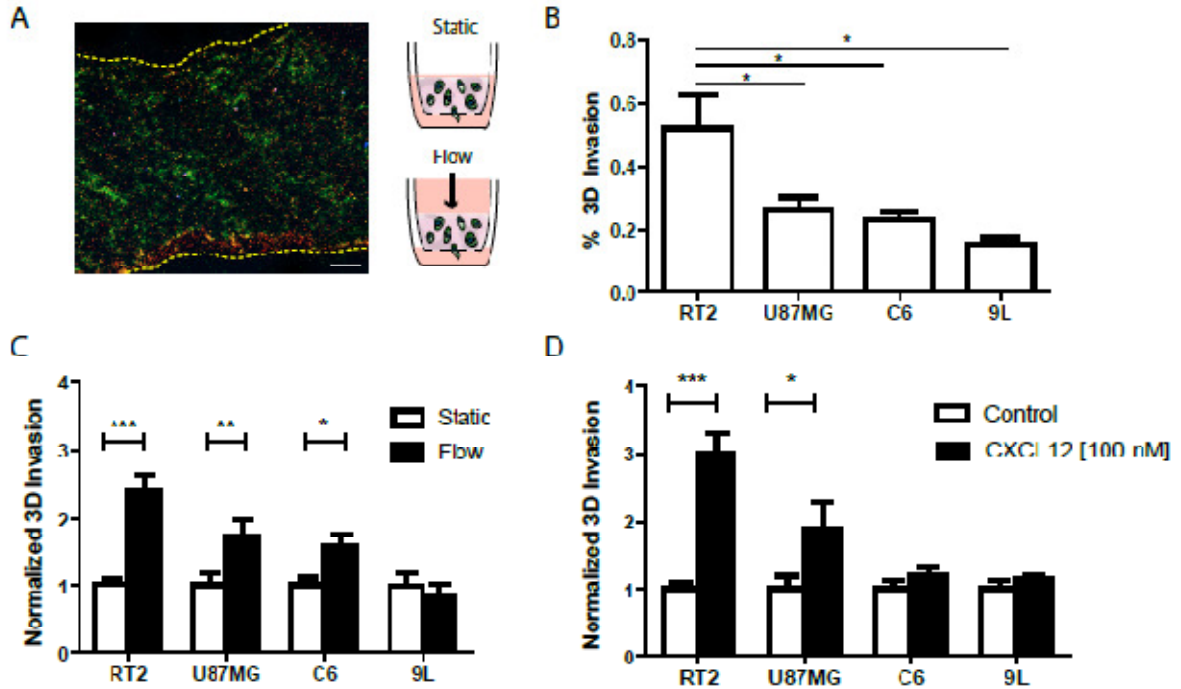


Figure E.2 Glioma invasion is increased by interstitial flow in a 3D culture model. (A) Cross-section of 3D culture from insert after flow application stained for hyaluronan (red) and type I collagen (green); cell nuclei are blue (Scale bar = 50 μ m). (B) Baseline invasiveness of four glioma cell lines under static conditions after 16h. (C) Effects of slow (0.2 μ m/min) interstitial flow on invasion. (D) Chemoinvasion of cells up a gradient of CXCL12 under static conditions. Data shown are means and standard deviations from 4-10 independent experiments; * p <0.05, ** p <0.01, *** p <0.001.

We next compared the invasiveness and chemotactic response to CXCL12 gradients of the four cell lines, since response to CXCL12 has previously been correlated with degree of malignancy [346, 347]. Cells were cultured in a 3D matrix in porous inserts and allowed to chemoinvade towards CXCL12 in the lower chamber under static conditions. Invasion increases towards CXCL12 gradients were similar to those seen in response to flow. Hence, our data suggest that the more malignant tumor cell lines respond more strongly to both flow and gradients of CXCL12 and that their response to

flow and CXCL12 gradients are similar, with the RT2 cell line showing the strongest flow response. In fact, this data shows strong correlation (**Figure E.3**)

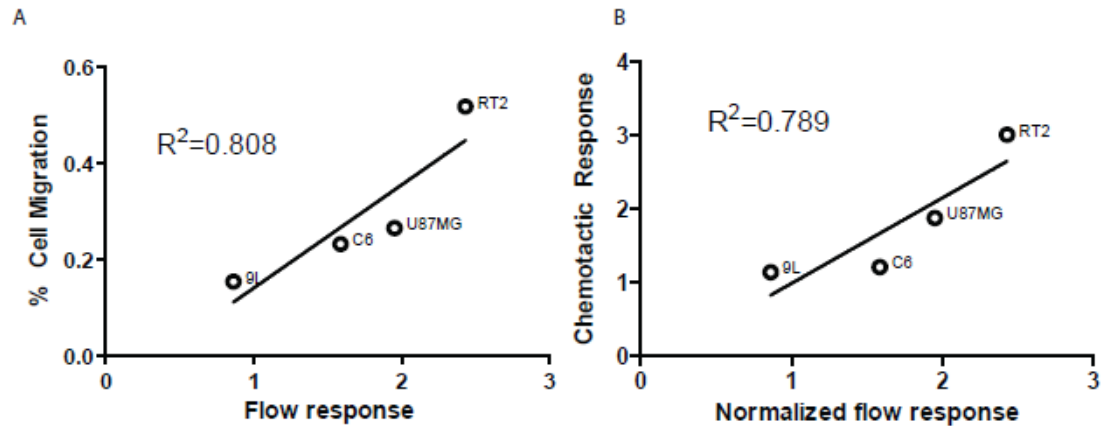


Figure E.3 Flow response correlates with chemotaxis and invasion in cell lines. (A) For all cell lines tested, correlation of normalized flow-enhanced invasion vs. % migration in 3D. (B) Correlation of normalized flow-enhanced invasion vs. chemotactic migration up an exogenous gradient of CXCL12.

Flow-enhanced invasion is CXCR4-dependent

To determine whether the increased invasion of glioma cells was correlated to CXCL12 signaling, we examined invasion under flow with either AMD 3100, a CXCR4 antagonist, or 100 nM exogenous CXCL12 (uniformly distributed) to overpower any possible endogenous CXCL12 gradients that may exist [348]. Under these conditions, the flow response did not occur in RT2 (**Figure E.4A**) nor for C6 and U87MG (**Figure E.5**), though CXCL12 did enhance cell invasion in general as expected from previous chemotaxis assays ($F(5,64)=12.67$, $p<0.001$). Interestingly, the secretion and expression of CXCL12 did not increase in any cell line between static and flow conditions. Similarly the % of cells expressing CXCR4 and the overall mean value of CXCR4 did not

significantly increase (Figure E.6). This indicates that there is not simply a change in cellular expression in response to flow that accounting for the CXCR4 dependence.

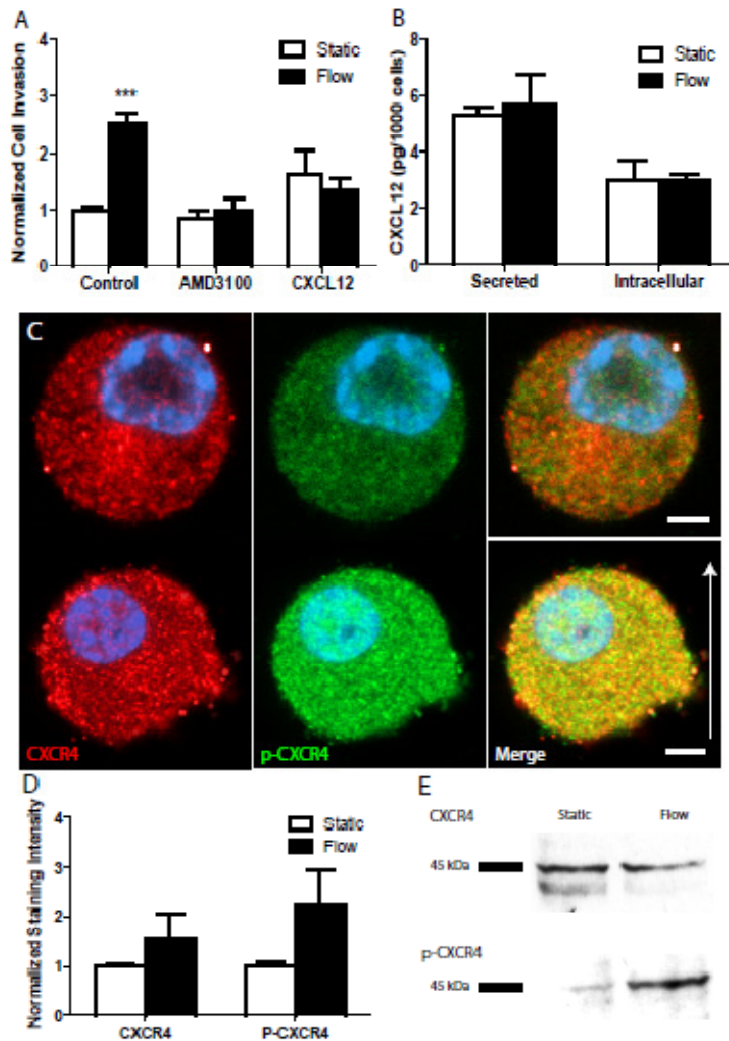


Figure E.4: Flow-enhanced invasion is CXCR4 dependent. (A) The enhanced invasiveness of RT2 glioma in flow vs. static conditions is lost when CXCR4 is blocked with AMD3100 or when 100 nM exogenous CXCL12 is added uniformly, without a gradient. (B) CXCL12 protein levels as measured by ELISA. (C) Representative images of RT2 cells (nuclei, blue), stained for CXCR4 (red) and phosphorylated CXCR4 (green) after 16h of flow or static conditions; scale bar=5 μ m and arrow indicates direction of flow. (D) Quantification of signal intensity (normalized) from immunostained cells; n=62 cells from 2 separate experiments. (E) Representative Western blots of total and phosphorylated CXCR4 after 16h of static or flow conditions.

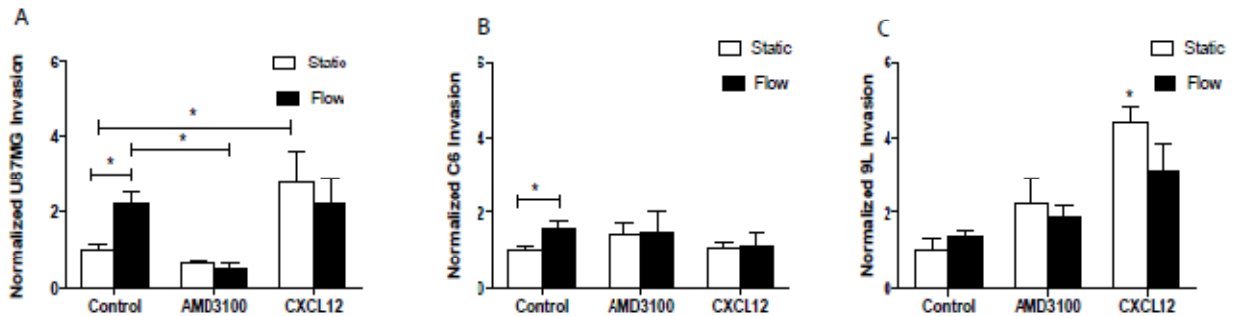


Figure E.5 Blocking or activating CXCR4 inhibits flow-enhanced invasion increase in glioma models (A) Blocking and activation in U87MG showing decreased flow response. (B) Blocking and activation in C6 glioma showing decreased flow response. (C) Blocking and activation in 9L showing no change in flow response though activation with CXCL12 enhances invasion.

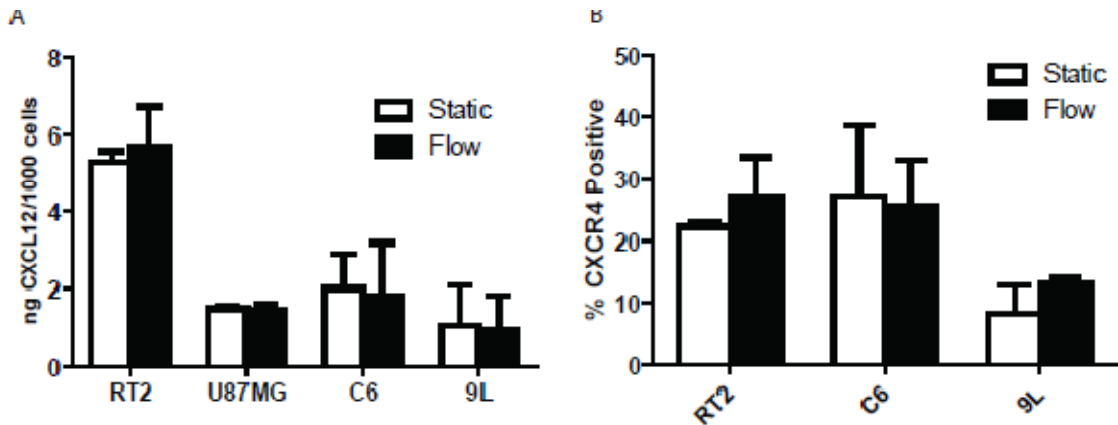


Figure E.6 CXCL12 and CXCR4 expression levels do not change under flow conditions. (A) CXCL12 expression (secreted + cellular) levels for cell lines under static and flow conditions. (B) CXCR4 expression levels as determine by flow cytometry for cell lines expressed as a % of the viable cell population.

CXCR4-dependence could be due to activation under flow conditions

Using again the radial flow chamber, cells were exposed to flow and stained for CXCR4 and phosphorylated CXCR4 (p-CXCR4). Phosphorylation of CXCR4 is known to indicate activation of this receptor and increased activity at tumor borders is correlated with increasing progression of disease in humans [333, 349, 350]. It was noticed that there was an increase in staining for CXCR4 of cells though overall this was slight when averaged over the entire chamber and experiments. p-CXCR4 appeared to increase significantly between static and control conditions (Figure 4A). Upon analysis based on intensity of pixels, there was a greater increase in p-CXCR4 staining under flow conditions though neither change was significant (**Figure E.4C, D**) (CXCR4: $t(18)=0.7624$, n.s. p-CXCR4: $t(18)=1.268$, n.s.). To further confirm this increase, cells from tissue culture inserts were collected for Western blotting and there was an increase in p-CXCR4 between static and flow conditions for RT2 (**Figure E.4E**) though not for CXCR4 (Figure 4C). This change was not seen for the other cell lines though indicating that this is not necessarily the primary mechanism for enhanced cell invasion under flow conditions.

Cells polarize in flow direction in a CXCR4-dependent manner

Cells were seeded in radial flow chambers (described in [351]) for further observation since imaging in tissue culture inserts is limited to those crossing the membrane (**Figure 4B**). Flow was applied from the center point radially through the matrix. After overnight flow, cells were fixed and stained for PhAkt (green) which is known to localize to the leading edge of migrating cells (Figure 3E). There was an increase in polarized cells from static to flow conditions ($t(26)=3.22$, $p<0.01$) and this polarization was blocked with AMD3100 ($t(34)=3.873$, $p<0.01$) (Figure 3D). Further, cells exposed to CXCL12 were polarized to a similar extent as those exposed to flow but not significantly different from CXCL12-exposed static cells (data not shown). This data

confirms visually the CXCR4-dependent mechanism of flow-enhanced invasion in RT2 glioma that was seen for all cell lines in tissue culture inserts.

Live imaging reveals both increases in chemokinesis and chemotaxis of glioma under flow

Cells were seeded in pillar chambers in the same 3D matrix as described previously (Haessler, et al. 2011). Flow was applied passing first through an empty gel before flowing through cells in 3D and after experiments while imaging under brightfield. Flow rates were determined and ranged over experiments between $2\mu\text{m/s}$ - $20\mu\text{m/s}$. Cell tracking and analysis over multiple locations (**Figure E.7A** and **Figure E.8**) and replicates revealed a significant increase in the number of RT2 cells migrating under flow from static conditions (**Figure E.7B**, $t(12)=5.35$, $p<0.01$). We also analyzed persistence to determine if cells were changing directness with which they migrate revealing no change under flow. Similarly, cell speed and frequency of cell speeds (**Figure E.7D**) did not change significantly under flow conditions. We did, however, observe a shift in cell velocities (V_F) towards the direction of flow (**Figure E.7C**), however, this change was non-significant due to the small number of cells with this velocity shift (**Figure E.7E**). Averaging V_F over the per cell velocity reveals a shift again in the direction of flow accounting for variability within the sample (**Figure E.7F** and **G**). The results of this analysis reveal that there is a significant increase in chemokinesis under flow conditions which could account for the increased invasion seen in previous assays. However, there is a subpopulation of cells that actually begins to migrate in the direction of flow which may be due to a chemotactic mechanism.

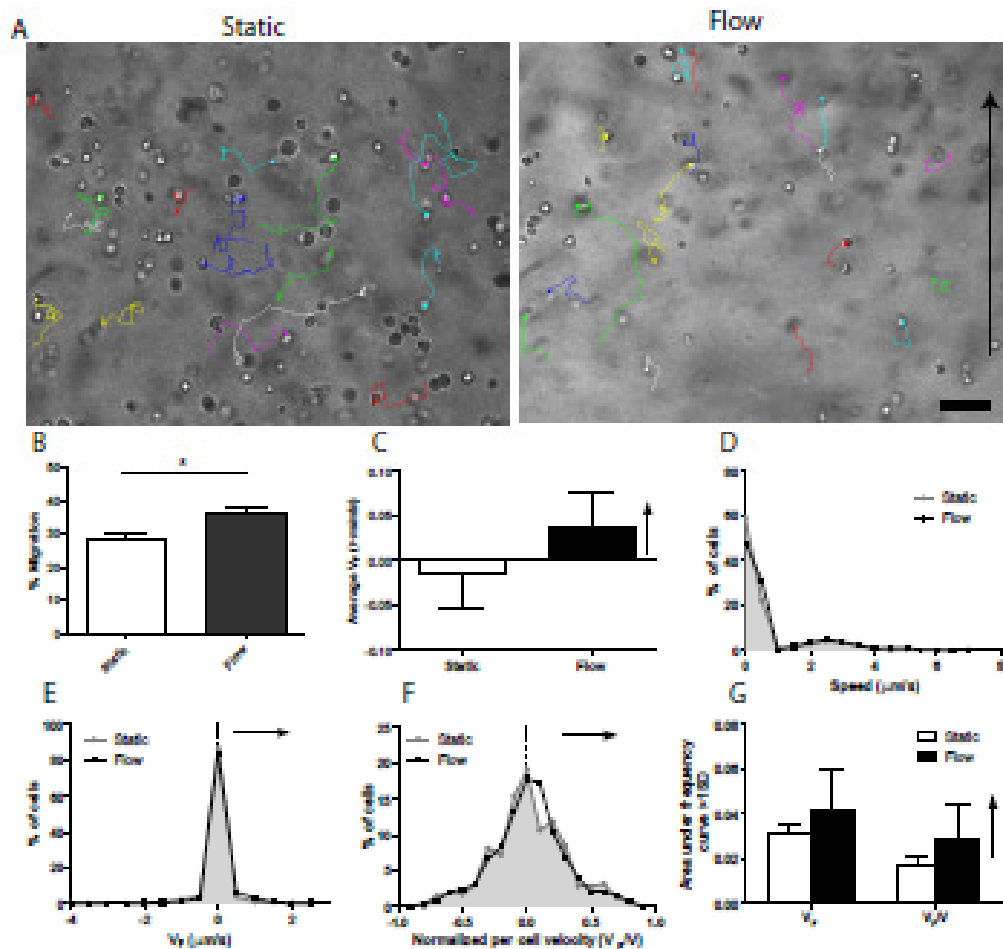


Figure E.7: Cell migration favors the flow direction. (A) Representative images with tracks shown from videos of RT2 cells migrating under static and flow conditions for 16 h; scale bar=50 μm . Tracks end at the dot with preceding path shown. (B) Quantification of the fraction of cells that migrate more than 2 cell diameters in 16 h; * $p < 0.05$. (C) Average cell velocity in the flow direction. (D) Histogram of the distribution of average cell speed. (E) Histogram of velocity in the flow direction, normalized to the average speed for each cell (V_F/V). Shaded areas are those outside of the standard deviation. (F) Area-under-the-curve analysis showing one standard deviation showing change in flow direction of this frequency indicating more cells moving in the flow direction.

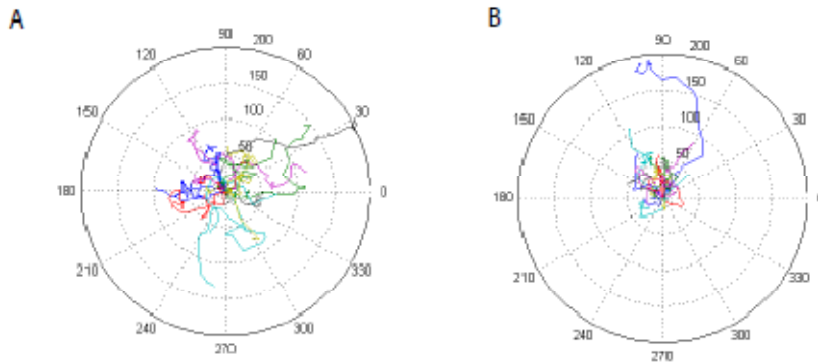


Figure E.8: Cells tend to migrate in the direction of flow when analyzed. A) Polar plot of video of cells in static conditions in 3D matrix and B) polar plot of Video of cells exposed to flow. Plots indicate a slight tendency of cells to migrate in the flow direction. These plots represent 2 examples for one set of experiments used in Figure 5.

Cells polarize in the direction of flow

Using the radial flow chamber setup again, we analyzed the degree to which cells were polarized in the direction of flow. For each image, the position in reference to the central flow inlet was noted and cells polarized cells were given a direction based on a $-30^{\circ}/30^{\circ}$ zone around the direction of flow and the directions 90° from this point. Under static conditions, cells were approximately equally polarized in all directions (307 cells total, 12.4% polarized) (**Figure E.9A**). When flow was applied, there was a significant increase in the percentage of cells polarized in the flow direction (435 cells total, 25.5% polarized; $F(3, 100) = 19.88, p < 0.001$) indicating a preference for migration or priming in the direction of flow. Further, when the CXCR4 receptor was blocked with AMD3100 and flow applied, this shift went away and the cells returned to near static polarization (158 cells total, 16.5% polarized). Therefore, flow acts to polarize cells in the direction of flow in a CXCR4-dependent manner ($F(3,49) = 6.678, p < 0.001$).

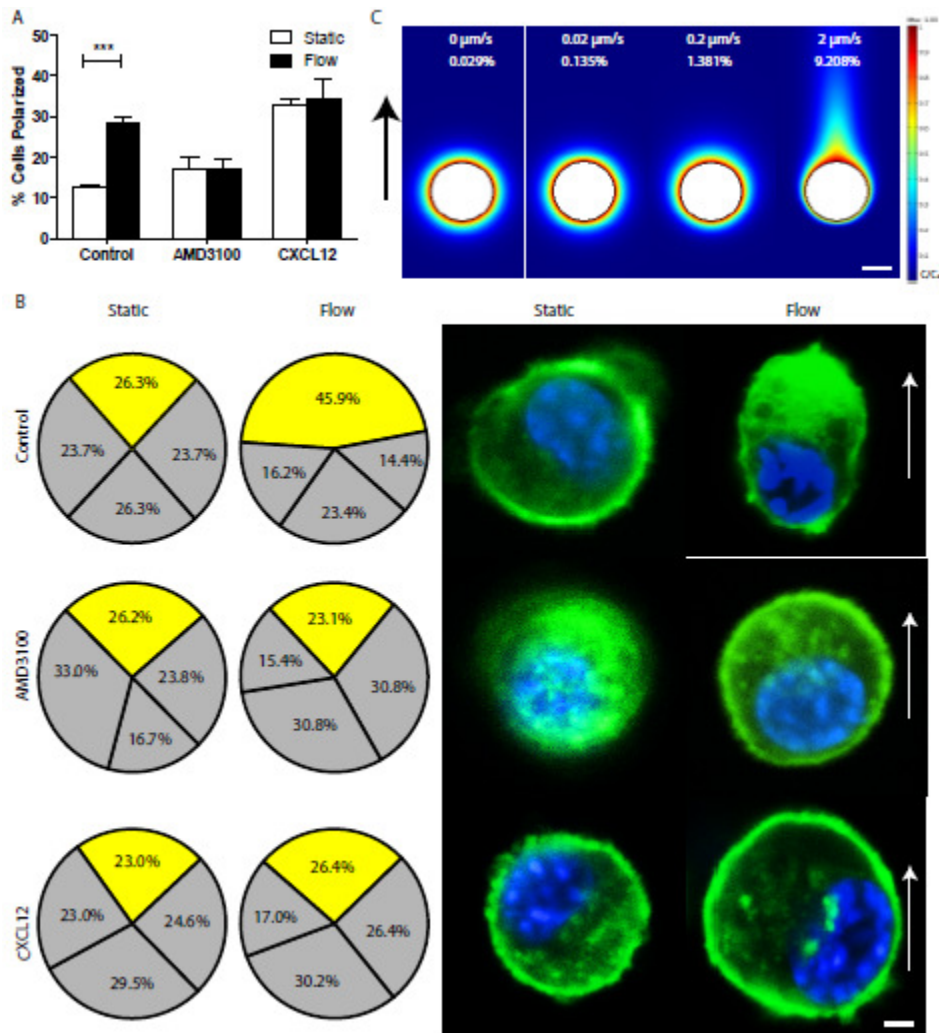


Figure E.9: Flow-directed cell migration is consistent with CXCR4-mediated autologous chemotaxis. (A) Polarization of cells in response to flow in presence/absence of AMD3100 or CXCL12 (** $p < 0.001$). (B) Radial flow chamber analysis for cell polarization in each direction (0° , 90° , 180° , and 270° to flow direction) shows increase in polarization in flow direction (0°) and blocking with AMD3100 and CXCL12. (C) Representative images for each condition with PhAKT staining (green) and nuclei (blue) under flow (right column) and static (left column) (scale bar= $5 \mu\text{m}$). White arrows indicate flow direction. Scale bars= $10 \mu\text{m}$. * $p < 0.05$. (D) Model of CXCL12 secretion by RT2, binding to HA-Collagen matrix, under increasing flow rates shows increasing %gradient of CXCL12 across the cell body (scale bar= $10\mu\text{m}$).

CXCL12-dependent autologous chemotaxis explains directional cell polarization and migration

Autologous chemotaxis has been proposed as a mechanism for enhancement of tumor cell invasion and dendritic cell migration under flow conditions [335, 336]. Cancer cells that express both the chemokine, CXCL12, and its receptor, CXCR4 are candidates for this type of chemotaxis. Under static conditions the cell secretes CXCL12 (for RT2 0.16 pg CXCL12 secreted/h/1000 cells), this chemokine binds the matrix radially outward from the cell surface where it can be later cleaved through cell secretion of matrix degrading enzymes (MMPs). Therefore, the cell feels no gradient around itself and stays in place. However, when there is interstitial flow, now when the cell secretes CXCL12 the chemokine is carried downstream of the cell and binds the matrix. This results in an uneven distribution of CXCL12 around the cell body.

Using experimentally-determined parameters for matrix K_d (12.6 nM, **Figure E.10**), and CXCL12 secretion rates, along with literature-reported values for matrix degradation, and diffusion, we modeled the gradient formation at increasing flow rates (Figure 6C). Gradients across the cell formed with as little as 0.02 $\mu\text{m/s}$ and increased significantly at 2 $\mu\text{m/s}$ a physiologically relevant flow rate in brain tumor or edema conditions [13, 340, 341]. Gradients observed under these flow rates (**Figure E.9C**) have been shown to be high enough to elicit migration in other cell types such as neutrophils and fibroblasts [352, 353].

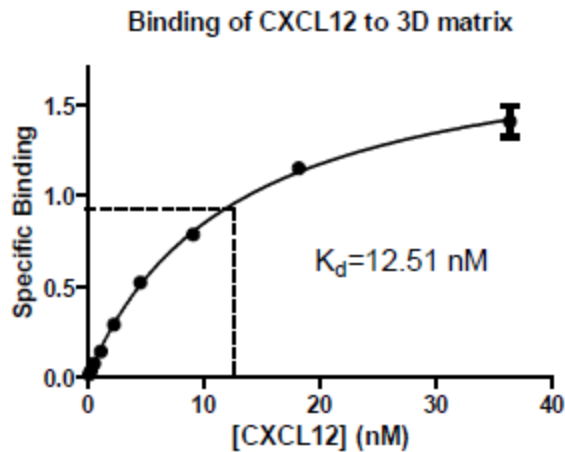


Figure E.10 CXCL12 binds to the hyaluronan/collagen matrix. Binding used to determine the K_d for CXCL12 and the matrix. This value was used as a modeling parameter for development of the gradient in Figure 6D.

Lastly, to further explore the role of CXCL12 in glioma and how it might be involved in autologous chemotaxis, polarization in the direction of flow was determined in the presence of CXCL12 (**Figure E.9B**). Though there were more cells polarized than under static conditions and CXCR4-blocking (171 cells total, 30.9% polarized), the tendency towards polarization in the direction of flow was lost. This indicates that there is a chemotactic mechanism occurring under flow conditions separate from the chemokinetic mechanism which can be blocked through antagonism of CXCR4. Additionally, the change from general polarization to polarization in the direction of flow accounted for 12.8% of the cell population and through immunocytochemistry, the total amount of cells presenting both CXCL12 and CXCR4 was around 18.9% indicating that there may be a subpopulation of cells that are inclined to autologous chemotaxis, though far more cells express CXCR4 which can lead to chemokinesis to account for the remainder of the flow response seen in our assays.

Thus, using multiple *in vitro* modeling systems, our experimental results demonstrate that significantly, 1) interstitial flow increases invasion of multiple glioma cell lines *in vitro*, and 2) this increase is CXCR4-dependent resulting in both increased chemokinesis and chemotaxis in the direction of flow as shown through live cell imaging and immunocytochemistry. Lastly, we propose that the chemotaxis seen under flow is due to autologous chemotaxis resulting in CXCL12-mediated polarization.

E.5 Discussion

In this study, we propose a new mechanism to explain patterns of glioma invasion in the brain. It has previously been proposed that cancer cells respond to heterogeneity of extracellular matrix as evidenced by migration along leptomeningeal pathways, the basement membranes of vasculature, and the spread of cells along subpial lining [10, 15]. It has also been proposed that cancer cells respond to the structural cues and reduced resistance for invasion along white matter tracts and neuronal structures to account for farther distant metastases [14, 325, 328]. The idea of fluid flow enhancing metastases to far-distant locations in the central nervous system has been attributed to passive movement of cancer cells in cerebrospinal fluid as evidenced by presence of cancer cells in CSF samples and the coincidence of flow pathways with migration pathways [13, 37, 327]. Lastly, the ever-growing literature for chemokine involvement in paracrine loops in the brain shows the ability of adult neurons and glia in the brain to secrete growth factors and chemokines leading to migration and chemoattraction, expanding upon the already strong base of systemic metastases for other cancer types [69, 258, 331, 354].

These theories treat these phenomena as separate entities, determining that each must be responsible for the spread of cancer cells in its own way and that the colocalization of the structure, chemokines, flow pathways, and invasion is somewhat of a coincidence. Studies have aimed to integrate structural cues with chemokinetic cues, matrix alterations with chemokines, and cell-cell interactions with chemokines to explore

the interactions of these enhancers of invasion leading to varied results [71, 105]. However, this study presents the first exploration of the ability of interstitial flow to not just act as a passive carrier of glioma cells in the central nervous system, but as an active modulator of glioma malignancy and invasion. This is important in the way we approach the study of brain tumors and the design of therapeutics.

To begin to observe this coincidence we provided an observational *in vivo* examination of CXCL12 gradients, tumor cell invasion in a model of astrocytoma that shows many of the hallmarks of glioblastoma invasion inherent to the human disease, and the fluid flow pathways as assessed as drainage from the tumor. This result shows that there is a co-localization of these elements in the brain and this also correlates with the direction in which the major white matter tracts (corpus callosum) spread through the brain. Building upon these observations, which have been previously implicated in the literature, though not explored simultaneously, we hypothesized that they are not only interrelated in location but in mechanism [10, 12, 13, 121, 325]. To do this, examination *in vitro* was necessary to dissect the reasons behind invasion and elucidate a mechanism in a controlled manner.

Many cell culture model systems have been developed for the study of glioma migration including the brain slice model, Boyden chamber, and neurosphere culture [128, 355]. In an effort to determine the effects of interstitial flow, we optimized a 3D cell culture system using hyaluronan and collagen to mimic the brain microenvironment while allowing passage of flow. Using a simple tissue culture insert that allowed for higher throughput examination and more complex systems that could yield defined flow rates and allow for cell visualization we repeatedly observed the same phenomenon: increase of invasion of cells under flow conditions as compared to the normal static counterpart.

Flow implication in function of cells is a common occurrence. In the immune system, interstitial flow increases in response to injury allowing chemokine gradients to form

towards the lymphatics and initiate dendritic cell homing and has also been advantageously used for development of vaccines [356]. Further, the transmural flow at the walls of lymphatics activates the endothelial cells altering transport functions of the lining and has been implicated in increasing chemokine signaling shown to increase tumor cell invasion further[134, 335]. Interstitial flow is also implicated in altering the tumor stroma, increasing fibroblasts invasion, changing the extracellular matrix alignment, and establishing signaling for blood vessels [133, 337, 357]. In the nervous system, the exploration of flow has largely been confined to neurodevelopment and disease states such as hydrocephalus. We argue that tumor drainage is an important phenomenon in the invasion and dispersal of tumors from the primary site.

To elucidate the way in which tumor cells are impacted by interstitial flow we examined the involvement of the chemokine/receptor pair, CXCL12/CXCR4. Highly implicated in cancer progression and in particular in all aspects of brain tumor progression including proliferation, survival, angiogenesis and invasion, and showing correlation with patterns of invasion in the brain, we targeted this chemokine/receptor pair [331, 346, 354, 358]. The ability of AMD3100 to block the flow-induced increase of invasion was striking and indicated that there was an involvement of the CXCR4 receptor in the enhancement of migration. Further, when cells were faced with global CXCL12 concentrations higher than those necessary to elicit chemotactic responses, they no longer enhanced invasion in response to flow though general cell movement was increased.

Increases in the amount of CXCL12 secreted or CXCR4 expressed would be one explanation for the flow response, though for all cell lines, this was not the case. The activation of CXCR4 is another explanation for the loss of flow effect in the presence of CXCL12 since CXCL12 is known to activate the receptor and activation is correlated with a higher grade tumor with more invasive phenotype[333]. However, the strong increase in phosphorylation was only seen for the strongest flow-responsive cell line (RT2). Hence, the increase in receptor activation can only account for some of the

increased invasion seen under flow conditions. We show that the migration of cells in response to flow may have two components: first the increase in chemokinesis stemming from increased activation of the cell (both by CXCR4 or other mechanisms) and increased chemotaxis (via autologous chemotaxis).

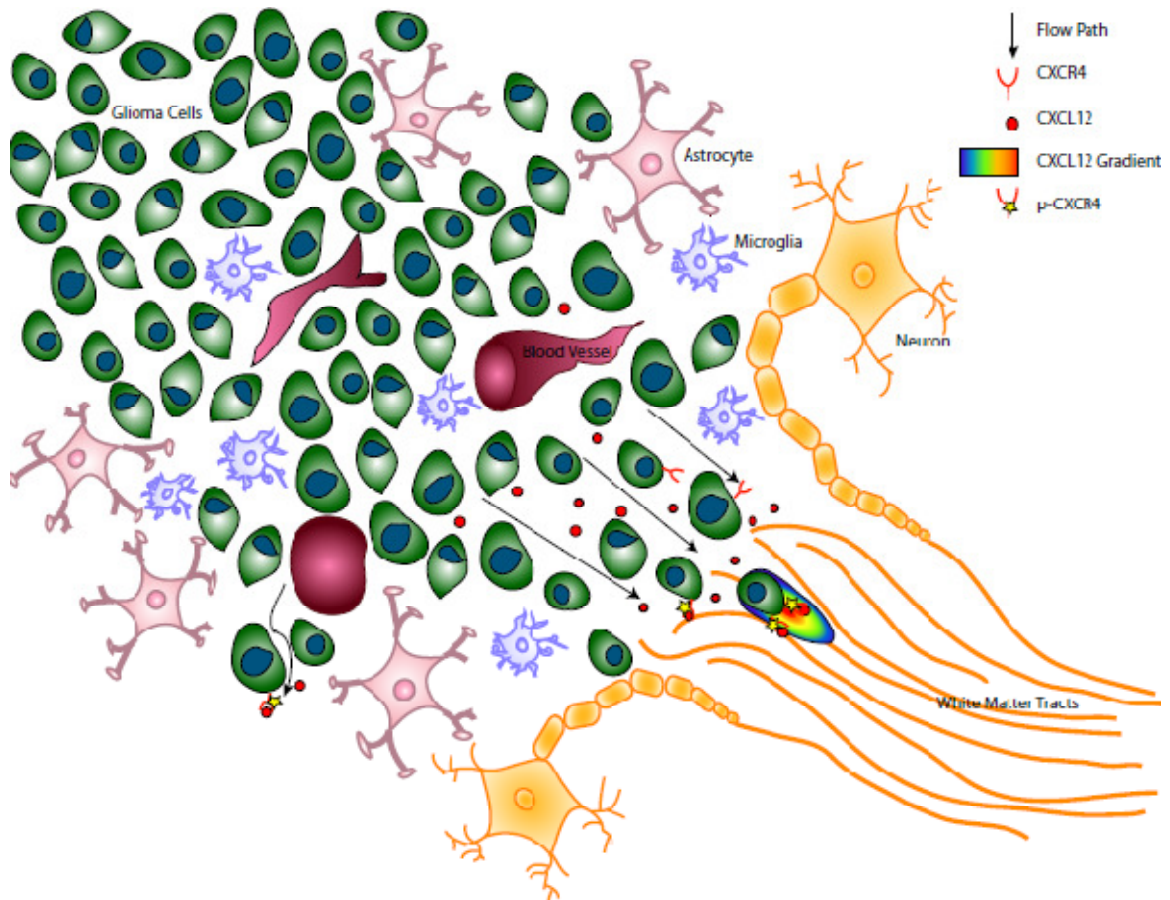


Figure E.11: Hypothesized mechanism of how fluid flow affects glioma invasion patterns. The biophysical tumor microenvironment, both in terms of the extracellular matrix cues and fluid flow cues, guide preferential invasion patterns. Fluid flow is faster along paths of least resistance, namely white matter tracts. A fraction of glioma cells both secrete CXCL12 and express CXCR4, enabling them to chemotact in the flow direction towards gradients of self-secreted CXCL12 that is skewed by flow. Additionally, flow increases CXCR4 expression and activation, which can further enhance invasiveness

Using modeling and implicit experiments, we show that the directional polarization of cells disappears when confronted with a uniform CXCL12 gradient in the RT2 model of invasive glioma and that gradients can form around cells with as little as $0.02\mu\text{m/s}$, below the experimentally observed flow rates of $0.2\text{-}0.9\mu\text{m/s}$ in the rat brain. Gradients as low as 1% across a cell body have been shown to elicit directional migration [352, 353]. In the hydrocephalic brain that arises during tumor growth and progression, flow rates can increase by 1-fold as drainage occurs which would yield an even increased gradient around cells in the interstitium and implicitly increased cell invasion to across distances[341, 359].

The evidence presented here implicates interstitial flow as an active player in the invasion of brain tumors into healthy tissue. Through *in vitro* analysis based on *in vivo* and literature-based observations, slow flow rates in the interstitium are substantial enough to increase tumor invasion and hence decrease the survival time in patients. The coincidence of flow patterns with white matter tracts could indicate an alternate theory though it is more likely that these two phenomena work in concert to enhance cell invasion in the brain. Through fluid flow towards the white matter tracts and the structural cues of the tracts themselves, tumor invasion can be enhanced further. Similarly, many cell types in the brain secrete CXCL12 yielding reservoirs of the chemokine throughout the cortex. One particular region, the meningeal lining, secretes CXCL12 and could be an added factor in enhanced invasion in the brain [343]. Further, microglia and astrocytes have been implicated in enhancing progression of glioma, but in our studies, there was not an observable interaction with interstitial flow as has been seen with other cancers [69, 71, 337]. However, such microenvironmental factors are important in the study of glioma invasion as they have been studied in other cancers.

In this study we aimed to examine one aspect of the brain microenvironment in the context of glioma invasion: interstitial flow (**Figure E.11**). Previously ignored as a passive component of glioma spreading and brain function, we have shown data that flow

in the brain is an active modulator and the way in which it enhances glioma function involves interactions of chemokine/receptors common to glioma. Further, we have provided evidence to hypothesize the existence of autologous chemotaxis in another cancer model existing away from lymphatic function. This study has implications in current therapies involving enhancing convection through the tumor (convection-enhanced delivery) in order to deliver drugs, microenvironmental 3D modeling, and how we translate observations and testing of glioma invasion *in vitro* to an *in vivo* setting.

REFERENCES

1. *National Cancer Institute Brain Tumor Study in Adults: Fact Sheet*, U.S.D.o.H.a.H. Services, Editor. 2000, National Cancer Institute: Bethesda, MD.
2. *Stats and facts. Breast cancer: progress and challenges*. Manag Care Interface, 1999. **12**(7): p. 36-7.
3. Abrams, P., *Facts and future lines of research in prostate cancer: concluding remarks*. BJU Int, 2000. **85 Suppl 2**: p. 49-51.
4. Dorsey, E.R., et al., *Funding of US biomedical research, 2003-2008*. JAMA, 2010. **303**(2): p. 137-43.
5. Legler, J.M., et al., *Cancer surveillance series [corrected]: brain and other central nervous system cancers: recent trends in incidence and mortality*. J Natl Cancer Inst, 1999. **91**(16): p. 1382-90.
6. Mikkelsen, T., *Brain tumor invasion : biological, clinical, and therapeutic considerations*. 1998, New York: Wiley-Liss. xv, 464 p.
7. Kleihues, P., P.C. Burger, and B.W. Scheithauer, *The new WHO classification of brain tumours*. Brain Pathol, 1993. **3**(3): p. 255-68.
8. Louis, D.N., et al., *The 2007 WHO classification of tumours of the central nervous system*. Acta Neuropathol, 2007. **114**(2): p. 97-109.
9. Scherer, H.J., *Structural Development in Gliomas*. American Journal of Cancer, 1938. **34**(3): p. 333-351.
10. Zagzag, D., et al., *Hypoxia- and vascular endothelial growth factor-induced stromal cell-derived factor-1alpha/CXCR4 expression in glioblastomas: one plausible explanation of Scherer's structures*. Am J Pathol, 2008. **173**(2): p. 545-60.
11. Claes, A., A.J. Idema, and P. Wesseling, *Diffuse glioma growth: a guerilla war*. Acta Neuropathol, 2007. **114**(5): p. 443-58.
12. Giese, A. and M. Westphal, *Glioma invasion in the central nervous system*. Neurosurgery, 1996. **39**(2): p. 235-50; discussion 250-2.

13. Geer, C.P. and S.A. Grossman, *Interstitial fluid flow along white matter tracts: a potentially important mechanism for the dissemination of primary brain tumors*. J Neurooncol, 1997. **32**(3): p. 193-201.
14. Johnson, J., et al., *Quantitative analysis of complex glioma cell migration on electrospun polycaprolactone using time-lapse microscopy*. Tissue Eng Part C Methods, 2009. **15**(4): p. 531-40.
15. Bellail, A.C., et al., *Microregional extracellular matrix heterogeneity in brain modulates glioma cell invasion*. Int J Biochem Cell Biol, 2004. **36**(6): p. 1046-69.
16. Rong, Y., et al., *'Pseudopalisading' necrosis in glioblastoma: a familiar morphologic feature that links vascular pathology, hypoxia, and angiogenesis*. J Neuropathol Exp Neurol, 2006. **65**(6): p. 529-39.
17. Mendez, O., et al., *Knock down of HIF-1alpha in glioma cells reduces migration in vitro and invasion in vivo and impairs their ability to form tumor spheres*. Mol Cancer, 2010. **9**: p. 133.
18. Nishikawa, R., *Standard therapy for glioblastoma--a review of where we are*. Neurol Med Chir (Tokyo), 2010. **50**(9): p. 713-9.
19. Chaichana, K.L., et al., *Recurrence and malignant degeneration after resection of adult hemispheric low-grade gliomas*. J Neurosurg, 2010. **112**(1): p. 10-7.
20. Dinnes, J., et al., *A rapid and systematic review of the effectiveness of temozolomide for the treatment of recurrent malignant glioma*. Br J Cancer, 2002. **86**(4): p. 501-5.
21. Nabors, L.B. and J. Fiveash, *Treatment of adults with recurrent malignant glioma*. Expert Rev Neurother, 2005. **5**(4): p. 509-14.
22. Park, J.K., et al., *Scale to predict survival after surgery for recurrent glioblastoma multiforme*. J Clin Oncol, 2010. **28**(24): p. 3838-43.
23. Sanai, N., M.Y. Polley, and M.S. Berger, *Insular glioma resection: assessment of patient morbidity, survival, and tumor progression*. J Neurosurg, 2010. **112**(1): p. 1-9.
24. Stummer, W., et al., *Extent of resection and survival in glioblastoma multiforme: identification of and adjustment for bias*. Neurosurgery, 2008. **62**(3): p. 564-76; discussion 564-76.
25. Raore, B., et al., *Metastasis Infiltration: An Investigation of the Postoperative Brain-Tumor Interface*. Int J Radiat Oncol Biol Phys, 2010.

26. Attenello, F.J., et al., *Use of Gliadel (BCNU) wafer in the surgical treatment of malignant glioma: a 10-year institutional experience*. *Ann Surg Oncol*, 2008. **15**(10): p. 2887-93.
27. Kleinberg, L.R., et al., *Clinical course and pathologic findings after Gliadel and radiotherapy for newly diagnosed malignant glioma: implications for patient management*. *Cancer Invest*, 2004. **22**(1): p. 1-9.
28. Westphal, M., et al., *Gliadel wafer in initial surgery for malignant glioma: long-term follow-up of a multicenter controlled trial*. *Acta Neurochir (Wien)*, 2006. **148**(3): p. 269-75; discussion 275.
29. Westphal, M., K. Lamszus, and D. Hilt, *Intracavitary chemotherapy for glioblastoma: present status and future directions*. *Acta Neurochir Suppl*, 2003. **88**: p. 61-7.
30. Nataf, F., et al., *Radiosurgery with or without A 2-mm margin for 93 single brain metastases*. *Int J Radiat Oncol Biol Phys*, 2008. **70**(3): p. 766-72.
31. Stupp, R., et al., *Radiotherapy plus concomitant and adjuvant temozolomide for glioblastoma*. *N Engl J Med*, 2005. **352**(10): p. 987-96.
32. Fabel, K., et al., *Long-term stabilization in patients with malignant glioma after treatment with liposomal doxorubicin*. *Cancer*, 2001. **92**(7): p. 1936-42.
33. Hegi, M.E., et al., *MGMT gene silencing and benefit from temozolomide in glioblastoma*. *N Engl J Med*, 2005. **352**(10): p. 997-1003.
34. Metellus, P., et al., *Prognostic impact of O6-methylguanine-DNA methyltransferase silencing in patients with recurrent glioblastoma multiforme who undergo surgery and carmustine wafer implantation: a prospective patient cohort*. *Cancer*, 2009. **115**(20): p. 4783-94.
35. Lata, S. and A. Molczyk, *[Side effects of temozolomide treatment in patient with glioblastoma multiforme--case study]*. *Przegl Lek*, 2010. **67**(5): p. 445-6.
36. Brandes, A.A., et al., *Recurrence pattern after temozolomide concomitant with and adjuvant to radiotherapy in newly diagnosed patients with glioblastoma: correlation With MGMT promoter methylation status*. *J Clin Oncol*, 2009. **27**(8): p. 1275-9.
37. Seiz, M., et al., *Far-distant metastases along the CSF pathway of glioblastoma multiforme during continuous low-dose chemotherapy with temozolomide and celecoxib*. *Neurosurg Rev*, 2010. **33**(3): p. 375-81; discussion 381.

38. Okawa, T., [*History of radiotherapy for cancer*]. Gan To Kagaku Ryoho, 1999. **26 Suppl 1**: p. 15-22.
39. Bucci, B., et al., *Fractionated ionizing radiation exposure induces apoptosis through caspase-3 activation and reactive oxygen species generation*. Anticancer Res, 2006. **26(6B)**: p. 4549-57.
40. Lehnert, B.E. and R. Iyer, *Exposure to low-level chemicals and ionizing radiation: reactive oxygen species and cellular pathways*. Hum Exp Toxicol, 2002. **21(2)**: p. 65-9.
41. Epstein, J.B., et al., *Quality of life and oral function in patients treated with radiation therapy for head and neck cancer*. Head Neck, 2001. **23(5)**: p. 389-98.
42. Ohuchida, K., et al., *Radiation to stromal fibroblasts increases invasiveness of pancreatic cancer cells through tumor-stromal interactions*. Cancer Res, 2004. **64(9)**: p. 3215-22.
43. Wild-Bode, C., et al., *Sublethal irradiation promotes migration and invasiveness of glioma cells: implications for radiotherapy of human glioblastoma*. Cancer Res, 2001. **61(6)**: p. 2744-50.
44. Bauman, G.S., et al., *Effects of radiation on a three-dimensional model of malignant glioma invasion*. Int J Dev Neurosci, 1999. **17(5-6)**: p. 643-51.
45. Ogawa, Y., et al., *Reactive oxygen species-producing site in radiation and hydrogen peroxide-induced apoptosis of human peripheral T cells: Involvement of lysosomal membrane destabilization*. Int J Mol Med, 2004. **13(5)**: p. 655-60.
46. Argyriou, A.A., E. Giannopoulou, and H.P. Kalofonos, *Angiogenesis and anti-angiogenic molecularly targeted therapies in malignant gliomas*. Oncology, 2009. **77(1)**: p. 1-11.
47. Ferrara, N., et al., *Discovery and development of bevacizumab, an anti-VEGF antibody for treating cancer*. Nat Rev Drug Discov, 2004. **3(5)**: p. 391-400.
48. Ferrara, N., K.J. Hillan, and W. Novotny, *Bevacizumab (Avastin), a humanized anti-VEGF monoclonal antibody for cancer therapy*. Biochem Biophys Res Commun, 2005. **333(2)**: p. 328-35.
49. Kamba, T. and D.M. McDonald, *Mechanisms of adverse effects of anti-VEGF therapy for cancer*. Br J Cancer, 2007. **96(12)**: p. 1788-95.
50. Jain, R.K., *Normalization of tumor vasculature: an emerging concept in antiangiogenic therapy*. Science, 2005. **307(5706)**: p. 58-62.

51. Terzis, A.J., et al., *Proliferation, migration and invasion of human glioma cells exposed to paclitaxel (Taxol) in vitro*. Br J Cancer, 1997. **75**(12): p. 1744-52.
52. Zhao, M., et al., *Magnetic paclitaxel nanoparticles inhibit glioma growth and improve the survival of rats bearing glioma xenografts*. Anticancer Res, 2010. **30**(6): p. 2217-23.
53. Baker, M.J., et al., *Complete response of a recurrent, multicentric malignant glioma in a patient treated with phenylbutyrate*. J Neurooncol, 2002. **59**(3): p. 239-42.
54. Huysentruyt, L.C., L.M. Shelton, and T.N. Seyfried, *Influence of methotrexate and cisplatin on tumor progression and survival in the VM mouse model of systemic metastatic cancer*. Int J Cancer, 2010. **126**(1): p. 65-72.
55. Tonn, J.C., et al., *Effect of synthetic matrix-metalloproteinase inhibitors on invasive capacity and proliferation of human malignant gliomas in vitro*. Int J Cancer, 1999. **80**(5): p. 764-72.
56. Ahluwalia, M.S., et al., *Targeting SRC in glioblastoma tumors and brain metastases: rationale and preclinical studies*. Cancer Lett, 2010. **298**(2): p. 139-49.
57. De Witt Hamer, P.C., *Small molecule kinase inhibitors in glioblastoma: a systematic review of clinical studies*. Neuro Oncol, 2010. **12**(3): p. 304-16.
58. Levin, V.A., *Are gliomas preventable?* Recent Results Cancer Res, 2007. **174**: p. 205-15.
59. Griffin, A.C., *Cancer chemoprevention*. J Cancer Res Clin Oncol, 1980. **98**(1): p. 1-7.
60. Hanahan, D. and R.A. Weinberg, *The hallmarks of cancer*. Cell, 2000. **100**(1): p. 57-70.
61. Hanahan, D. and R.A. Weinberg, *Hallmarks of cancer: the next generation*. Cell, 2011. **144**(5): p. 646-74.
62. Pietras, K. and A. Ostman, *Hallmarks of cancer: interactions with the tumor stroma*. Exp Cell Res, 2010. **316**(8): p. 1324-31.
63. Igney, F.H. and P.H. Krammer, *Death and anti-death: tumour resistance to apoptosis*. Nat Rev Cancer, 2002. **2**(4): p. 277-88.

64. Clarke, J., N. Butowski, and S. Chang, *Recent advances in therapy for glioblastoma*. Arch Neurol, 2010. **67**(3): p. 279-83.
65. Huang, T.T., et al., *Targeted therapy for malignant glioma patients: lessons learned and the road ahead*. Neurotherapeutics, 2009. **6**(3): p. 500-12.
66. Mantovani, A., *Cancer: Inflaming metastasis*. Nature, 2009. **457**(7225): p. 36-7.
67. Seo, N., S. Hayakawa, and Y. Tokura, *Mechanisms of immune privilege for tumor cells by regulatory cytokines produced by innate and acquired immune cells*. Semin Cancer Biol, 2002. **12**(4): p. 291-300.
68. Shields, J.D., et al., *Induction of lymphoidlike stroma and immune escape by tumors that express the chemokine CCL21*. Science, 2010. **328**(5979): p. 749-52.
69. Le, D.M., et al., *Exploitation of astrocytes by glioma cells to facilitate invasiveness: a mechanism involving matrix metalloproteinase-2 and the urokinase-type plasminogen activator-plasmin cascade*. J Neurosci, 2003. **23**(10): p. 4034-43.
70. Leaver, H.A., M.T. Rizzo, and I.R. Whittle, *Glioma cell death: cell-cell interactions and signalling networks*. Mol Neurobiol, 2010. **42**(1): p. 89-96.
71. Zhai, H., F.L. Heppner, and S.E. Tsirka, *Microglia/macrophages promote glioma progression*. Glia, 2011. **59**(3): p. 472-85.
72. Jain, R.K., et al., *Angiogenesis in brain tumours*. Nat Rev Neurosci, 2007. **8**(8): p. 610-22.
73. de Waal, R.M. and W.P. Leenders, *Sprouting angiogenesis versus co-option in tumor angiogenesis*. EXS, 2005(94): p. 65-76.
74. Machein, M.R. and K.H. Plate, *Role of VEGF in developmental angiogenesis and in tumor angiogenesis in the brain*. Cancer Treat Res, 2004. **117**: p. 191-218.
75. Hagedorn, M. and A. Bikfalvi, *Target molecules for anti-angiogenic therapy: from basic research to clinical trials*. Crit Rev Oncol Hematol, 2000. **34**(2): p. 89-110.
76. Narayana, A., et al., *Antiangiogenic therapy using bevacizumab in recurrent high-grade glioma: impact on local control and patient survival*. J Neurosurg, 2009. **110**(1): p. 173-80.
77. Lamszus, K., P. Kunkel, and M. Westphal, *Invasion as limitation to anti-angiogenic glioma therapy*. Acta Neurochir Suppl, 2003. **88**: p. 169-77.

78. Barth, R.F. and B. Kaur, *Rat brain tumor models in experimental neuro-oncology: the C6, 9L, T9, RG2, F98, BT4C, RT-2 and CNS-1 gliomas*. J Neurooncol, 2009. **94**(3): p. 299-312.
79. Dai, C. and E.C. Holland, *Glioma models*. Biochim Biophys Acta, 2001. **1551**(1): p. M19-27.
80. de Vries, N.A., J.H. Beijnen, and O. van Tellingen, *High-grade glioma mouse models and their applicability for preclinical testing*. Cancer Treat Rev, 2009. **35**(8): p. 714-23.
81. de Vries, N.A., et al., *Rapid and robust transgenic high-grade glioma mouse models for therapy intervention studies*. Clin Cancer Res, 2010. **16**(13): p. 3431-41.
82. Sonabend, A.M., I.V. Ulasov, and M.S. Lesniak, *Emerging role of new transgenic mouse models in glioma research*. Expert Rev Anticancer Ther, 2007. **7**(12 Suppl): p. S7-13.
83. Beckman, G., et al., *G-6-PD and PGM phenotypes of 16 continuous human tumor cell lines. Evidence against cross-contamination and contamination by HeLa cells*. Hum Hered, 1971. **21**(3): p. 238-41.
84. Fillmore, H.L., et al., *An in vivo rat model for visualizing glioma tumor cell invasion using stable persistent expression of the green fluorescent protein*. Cancer Lett, 1999. **141**(1-2): p. 9-19.
85. Grobbs, B., P.P. De Deyn, and H. Slegers, *Rat C6 glioma as experimental model system for the study of glioblastoma growth and invasion*. Cell Tissue Res, 2002. **310**(3): p. 257-70.
86. Wessels, J.T., et al., *In vivo imaging in experimental preclinical tumor research--a review*. Cytometry A, 2007. **71**(8): p. 542-9.
87. Johnson, M., et al., *Differential biodistribution of adenoviral vector in vivo as monitored by bioluminescence imaging and quantitative polymerase chain reaction*. Hum Gene Ther, 2006. **17**(12): p. 1262-9.
88. Vilalta, M., et al., *Biodistribution, long-term survival, and safety of human adipose tissue-derived mesenchymal stem cells transplanted in nude mice by high sensitivity non-invasive bioluminescence imaging*. Stem Cells Dev, 2008. **17**(5): p. 993-1003.
89. de Bouard, S., et al., *Antiangiogenic and anti-invasive effects of sunitinib on experimental human glioblastoma*. Neuro Oncol, 2007. **9**(4): p. 412-23.

90. Rehemtulla, A., et al., *Rapid and quantitative assessment of cancer treatment response using in vivo bioluminescence imaging*. Neoplasia, 2000. **2**(6): p. 491-5.
91. Alexiou, G.A., et al., *Assessment of glioma proliferation using imaging modalities*. J Clin Neurosci, 2010. **17**(10): p. 1233-8.
92. Gerstner, E.R., et al., *Advances in neuroimaging techniques for the evaluation of tumor growth, vascular permeability, and angiogenesis in gliomas*. Curr Opin Neurol, 2008. **21**(6): p. 728-35.
93. Harney, A.S. and T.J. Meade, *Molecular imaging of in vivo gene expression*. Future Med Chem, 2010. **2**(3): p. 503-19.
94. Cenic, A., et al., *Dynamic CT measurement of cerebral blood flow: a validation study*. AJNR Am J Neuroradiol, 1999. **20**(1): p. 63-73.
95. Taylor, C.R. and R.M. Levenson, *Quantification of immunohistochemistry--issues concerning methods, utility and semiquantitative assessment II*. Histopathology, 2006. **49**(4): p. 411-24.
96. Price, S.J., et al., *Detecting glioma invasion of the corpus callosum using diffusion tensor imaging*. Br J Neurosurg, 2004. **18**(4): p. 391-5.
97. Price, S.J., et al., *Improved delineation of glioma margins and regions of infiltration with the use of diffusion tensor imaging: an image-guided biopsy study*. AJNR Am J Neuroradiol, 2006. **27**(9): p. 1969-74.
98. Wallner, K.E., et al., *Patterns of failure following treatment for glioblastoma multiforme and anaplastic astrocytoma*. Int J Radiat Oncol Biol Phys, 1989. **16**(6): p. 1405-9.
99. Trehin, R., et al., *Fluorescent nanoparticle uptake for brain tumor visualization*. Neoplasia, 2006. **8**(4): p. 302-11.
100. Jain, R.K., *Transport of molecules, particles, and cells in solid tumors*. Annu Rev Biomed Eng, 1999. **1**: p. 241-63.
101. Jain, R.K., *Delivery of molecular and cellular medicine to solid tumors*. Adv Drug Deliv Rev, 2001. **46**(1-3): p. 149-68.
102. Kim, J.J. and I.F. Tannock, *Repopulation of cancer cells during therapy: an important cause of treatment failure*. Nat Rev Cancer, 2005. **5**(7): p. 516-25.
103. Madani, I., W. De Neve, and M. Mareel, *Does ionizing radiation stimulate cancer invasion and metastasis?* Bull Cancer, 2008. **95**(3): p. 292-300.

104. Barcellos-Hoff, M.H. and S.A. Ravani, *Irradiated mammary gland stroma promotes the expression of tumorigenic potential by unirradiated epithelial cells*. Cancer Res, 2000. **60**(5): p. 1254-60.
105. Nakamura, J.L., D.A. Haas-Kogan, and R.O. Pieper, *Glioma invasiveness responds variably to irradiation in a co-culture model*. Int J Radiat Oncol Biol Phys, 2007. **69**(3): p. 880-6.
106. Park, C.M., et al., *Ionizing radiation enhances matrix metalloproteinase-2 secretion and invasion of glioma cells through Src/epidermal growth factor receptor-mediated p38/Akt and phosphatidylinositol 3-kinase/Akt signaling pathways*. Cancer Res, 2006. **66**(17): p. 8511-9.
107. Gliemroth, J., et al., *Proliferation, migration, and invasion of human glioma cells exposed to fractionated radiotherapy in vitro*. Neurosurg Rev, 2003. **26**(3): p. 198-205.
108. Tugues, S., et al., *Vascular endothelial growth factors and receptors: Anti-angiogenic therapy in the treatment of cancer*. Mol Aspects Med, 2011.
109. Murphy, E.A., et al., *Nanoparticle-mediated drug delivery to tumor vasculature suppresses metastasis*. Proc Natl Acad Sci U S A, 2008. **105**(27): p. 9343-8.
110. Miller, K.D., et al., *Randomized phase II trial of the anti-angiogenic potential of doxorubicin and docetaxel; primary chemotherapy as Biomarker Discovery Laboratory*. Breast Cancer Res Treat, 2005. **89**(2): p. 187-97.
111. Gomori, E., et al., *Microsatellite analysis of primary and recurrent glial tumors suggests different modalities of clonal evolution of tumor cells*. J Neuropathol Exp Neurol, 2002. **61**(5): p. 396-402.
112. Di Nicolantonio, F., et al., *Cancer cell adaptation to chemotherapy*. BMC Cancer, 2005. **5**: p. 78.
113. Eramo, A., et al., *Chemotherapy resistance of glioblastoma stem cells*. Cell Death Differ, 2006. **13**(7): p. 1238-41.
114. Quintana, E., et al., *Efficient tumour formation by single human melanoma cells*. Nature, 2008. **456**(7222): p. 593-8.
115. Borovski, T., et al., *Cancer stem cell niche: the place to be*. Cancer Res, 2011. **71**(3): p. 634-9.

116. Yamahara, T., et al., *Morphological and flow cytometric analysis of cell infiltration in glioblastoma: a comparison of autopsy brain and neuroimaging*. Brain Tumor Pathol, 2010. **27**(2): p. 81-7.
117. Grampa, G. and G. Baroldi, [*Glioma with extracranial metastases*]. Oncologia, 1958. **11**(1): p. 1-15.
118. Zeitlhofer, J. and H. Kranus, [*Extracranial metastases of glioma*]. Zentralbl Neurochir, 1952. **12**(6): p. 347-56.
119. Mondin, V., et al., *A survey of metastatic central nervous system tumors to cervical lymph nodes*. Eur Arch Otorhinolaryngol. **267**(11): p. 1657-66.
120. Ellingson, B.M., et al., *Spatially quantifying microscopic tumor invasion and proliferation using a voxel-wise solution to a glioma growth model and serial diffusion MRI*. Magn Reson Med, 2011. **65**(4): p. 1131-43.
121. Zhang, X., et al., *Experiment and observation on invasion of brain glioma in vivo*. J Clin Neurosci, 2002. **9**(6): p. 668-71.
122. Winkler, F., et al., *Imaging glioma cell invasion in vivo reveals mechanisms of dissemination and peritumoral angiogenesis*. Glia, 2009. **57**(12): p. 1306-15.
123. Zhang, F., et al., *In Vivo MRI Tracking of Cell Invasion and Migration in a Rat Glioma Model*. Mol Imaging Biol, 2010.
124. Bernas, L.M., P.J. Foster, and B.K. Rutt, *Magnetic resonance imaging of in vitro glioma cell invasion*. J Neurosurg, 2007. **106**(2): p. 306-13.
125. Szentirmai, O., et al., *Noninvasive bioluminescence imaging of luciferase expressing intracranial U87 xenografts: correlation with magnetic resonance imaging determined tumor volume and longitudinal use in assessing tumor growth and antiangiogenic treatment effect*. Neurosurgery, 2006. **58**(2): p. 365-72; discussion 365-72.
126. Zhu, L., et al., *Real-Time Video Imaging of Protease Expression In Vivo*. Theranostics, 2011. **1**: p. 18-27.
127. Lee, S., J. Xie, and X. Chen, *Activatable molecular probes for cancer imaging*. Curr Top Med Chem. **10**(11): p. 1135-44.
128. Pilkington, G.J., et al., *In vitro and in vivo models for the study of brain tumour invasion*. Anticancer Res, 1997. **17**(6B): p. 4107-9.

129. Vinader, V., et al., *An agarose spot chemotaxis assay for chemokine receptor antagonists*. J Pharmacol Toxicol Methods, 2011.
130. Sun, P., et al., *DNER, an epigenetically modulated gene, regulates glioblastoma-derived neurosphere cell differentiation and tumor propagation*. Stem Cells, 2009. **27**(7): p. 1473-86.
131. Albini, A. and D.M. Noonan, *The 'chemoinvasion' assay, 25 years and still going strong: the use of reconstituted basement membranes to study cell invasion and angiogenesis*. Curr Opin Cell Biol, 2010. **22**(5): p. 677-89.
132. Albini, A., et al., *The "chemoinvasion assay": a tool to study tumor and endothelial cell invasion of basement membranes*. Int J Dev Biol, 2004. **48**(5-6): p. 563-71.
133. Tomei, A.A., et al., *Fluid flow regulates stromal cell organization and CCL21 expression in a tissue-engineered lymph node microenvironment*. J Immunol, 2009. **183**(7): p. 4273-83.
134. Miteva, D.O., et al., *Transmural flow modulates cell and fluid transport functions of lymphatic endothelium*. Circ Res, 2010. **106**(5): p. 920-31.
135. Ohnishi, T., et al., *A novel model of glioma cell invasion using organotypic brain slice culture*. Cancer Res, 1998. **58**(14): p. 2935-40.
136. Yoshida, D., et al., *Tracking cell invasion of human glioma cells and suppression by anti-matrix metalloproteinase agent in rodent brain-slice model*. Brain Tumor Pathol, 2002. **19**(2): p. 69-76.
137. Nygaard, S.J., et al., *Dynamic determination of human glioma invasion in vitro*. J Neurosurg, 1998. **89**(3): p. 441-7.
138. Giese, A., et al., *Glioma cell adhesion and migration on human brain sections*. Anticancer Res, 1998. **18**(4A): p. 2435-47.
139. Pedersen, J.A., S. Lichter, and M.A. Swartz, *Cells in 3D matrices under interstitial flow: effects of extracellular matrix alignment on cell shear stress and drag forces*. J Biomech, 2010. **43**(5): p. 900-5.
140. Ng, C.P. and M.A. Swartz, *Fibroblast alignment under interstitial fluid flow using a novel 3-D tissue culture model*. Am J Physiol Heart Circ Physiol, 2003. **284**(5): p. H1771-7.
141. Haessler, U., et al., *An agarose-based microfluidic platform with a gradient buffer for 3D chemotaxis studies*. Biomed Microdevices, 2009. **11**(4): p. 827-35.

142. Griffith, L.G. and M.A. Swartz, *Capturing complex 3D tissue physiology in vitro*. Nat Rev Mol Cell Biol, 2006. **7**(3): p. 211-24.
143. Bajetto, A., et al., *Expression of CXC chemokine receptors 1-5 and their ligands in human glioma tissues: role of CXCR4 and SDF1 in glioma cell proliferation and migration*. Neurochem Int, 2006. **49**(5): p. 423-32.
144. Kaczarek, E., et al., *Dissecting glioma invasion: interrelation of adhesion, migration and intercellular contacts determine the invasive phenotype*. Int J Dev Neurosci, 1999. **17**(5-6): p. 625-41.
145. Goldbrunner, R.H., J.J. Bernstein, and J.C. Tonn, *ECM-mediated glioma cell invasion*. Microsc Res Tech, 1998. **43**(3): p. 250-7.
146. Gimona, M., *The microfilament system in the formation of invasive adhesions*. Semin Cancer Biol, 2008. **18**(1): p. 23-34.
147. Hao, H., et al., *Focal adhesion kinase as potential target for cancer therapy (Review)*. Oncol Rep, 2009. **22**(5): p. 973-9.
148. Courtneidge, S.A., et al., *The SRC substrate Tks5, podosomes (invadopodia), and cancer cell invasion*. Cold Spring Harb Symp Quant Biol, 2005. **70**: p. 167-71.
149. Friedl, P. and K. Wolf, *Proteolytic interstitial cell migration: a five-step process*. Cancer Metastasis Rev, 2009. **28**(1-2): p. 129-35.
150. Nakano, A., et al., *Matrix metalloproteinases and tissue inhibitors of metalloproteinases in human gliomas*. J Neurosurg, 1995. **83**(2): p. 298-307.
151. Chintala, S.K. and J.K. Rao, *Invasion of human glioma: role of extracellular matrix proteins*. Front Biosci, 1996. **1**: p. d324-39.
152. Rubenstein, B.M. and L.J. Kaufman, *The role of extracellular matrix in glioma invasion: a cellular Potts model approach*. Biophys J, 2008. **95**(12): p. 5661-80.
153. Uhm, J.H., et al., *Mechanisms of glioma invasion: role of matrix-metalloproteinases*. Can J Neurol Sci, 1997. **24**(1): p. 3-15.
154. Jin, S.G., et al., *The effect of hyaluronic Acid on the invasiveness of malignant glioma cells : comparison of invasion potential at hyaluronic Acid hydrogel and matrigel*. J Korean Neurosurg Soc, 2009. **46**(5): p. 472-8.
155. Demchik, L.L., et al., *Cathepsin B and glioma invasion*. Int J Dev Neurosci, 1999. **17**(5-6): p. 483-94.

156. Goldbrunner, R.H., J.J. Bernstein, and J.C. Tonn, *Cell-extracellular matrix interaction in glioma invasion*. Acta Neurochir (Wien), 1999. **141**(3): p. 295-305; discussion 304-5.
157. Tysnes, B.B. and R. Mahesparan, *Biological mechanisms of glioma invasion and potential therapeutic targets*. J Neurooncol, 2001. **53**(2): p. 129-47.
158. Nobes, C.D. and A. Hall, *Rho, rac, and cdc42 GTPases regulate the assembly of multimolecular focal complexes associated with actin stress fibers, lamellipodia, and filopodia*. Cell, 1995. **81**(1): p. 53-62.
159. Gimona, M., et al., *Assembly and biological role of podosomes and invadopodia*. Curr Opin Cell Biol, 2008. **20**(2): p. 235-41.
160. Yamaguchi, H. and J. Condeelis, *Regulation of the actin cytoskeleton in cancer cell migration and invasion*. Biochim Biophys Acta, 2007. **1773**(5): p. 642-52.
161. dos Remedios, C.G., et al., *Actin binding proteins: regulation of cytoskeletal microfilaments*. Physiol Rev, 2003. **83**(2): p. 433-73.
162. Yamazaki, D., S. Kurisu, and T. Takenawa, *Regulation of cancer cell motility through actin reorganization*. Cancer Sci, 2005. **96**(7): p. 379-86.
163. Bubb, M.R., et al., *Depolymerization of actin filaments by profilin. Effects of profilin on capping protein function*. J Biol Chem, 2003. **278**(27): p. 24629-35.
164. Kwiatkowski, D.J., *Functions of gelsolin: motility, signaling, apoptosis, cancer*. Curr Opin Cell Biol, 1999. **11**(1): p. 103-8.
165. Bershadsky, A.D., et al., *The state of actin assembly regulates actin and vinculin expression by a feedback loop*. J Cell Sci, 1995. **108** (Pt 3): p. 1183-93.
166. Schmitt-Ney, M. and J.F. Habener, *Cell-density-dependent regulation of actin gene expression due to changes in actin treadmilling*. Exp Cell Res, 2004. **295**(1): p. 236-44.
167. Lyubimova, A., A.D. Bershadsky, and A. Ben-Ze'ev, *Autoregulation of actin synthesis requires the 3'-UTR of actin mRNA and protects cells from actin overproduction*. J Cell Biochem, 1999. **76**(1): p. 1-12.
168. Pendyala, S. and V. Natarajan, *Redox regulation of Nox proteins*. Respir Physiol Neurobiol, 2010. **174**(3): p. 265-71.
169. Brown, D.I. and K.K. Griendling, *Nox proteins in signal transduction*. Free Radic Biol Med, 2009. **47**(9): p. 1239-53.

170. Chen, K., S.E. Craige, and J.F. Keane, Jr., *Downstream targets and intracellular compartmentalization in Nox signaling*. Antioxid Redox Signal, 2009. **11**(10): p. 2467-80.
171. Li, B., et al., *NOX4 expression in human microglia leads to constitutive generation of reactive oxygen species and to constitutive IL-6 expression*. J Innate Immun, 2009. **1**(6): p. 570-81.
172. Sorescu, D., et al., *Superoxide production and expression of nox family proteins in human atherosclerosis*. Circulation, 2002. **105**(12): p. 1429-35.
173. Griffith, B., et al., *NOX enzymes and pulmonary disease*. Antioxid Redox Signal, 2009. **11**(10): p. 2505-16.
174. Sorce, S. and K.H. Krause, *NOX enzymes in the central nervous system: from signaling to disease*. Antioxid Redox Signal, 2009. **11**(10): p. 2481-504.
175. Goyal, P., et al., *Identification of novel Nox4 splice variants with impact on ROS levels in E49 cells*. Biochem Biophys Res Commun, 2005. **329**(1): p. 32-9.
176. Wu, W.S., *The signaling mechanism of ROS in tumor progression*. Cancer Metastasis Rev, 2006. **25**(4): p. 695-705.
177. Takada, Y. and B.B. Aggarwal, *Flavopiridol inhibits NF-kappaB activation induced by various carcinogens and inflammatory agents through inhibition of IkappaBalpha kinase and p65 phosphorylation: abrogation of cyclin D1, cyclooxygenase-2, and matrix metalloprotease-9*. J Biol Chem, 2004. **279**(6): p. 4750-9.
178. Shono, T., et al., *Enhanced expression of NADPH oxidase Nox4 in human gliomas and its roles in cell proliferation and survival*. Int J Cancer, 2008. **123**(4): p. 787-92.
179. Diaz, B., et al., *Tks5-dependent, nox-mediated generation of reactive oxygen species is necessary for invadopodia formation*. Sci Signal, 2009. **2**(88): p. rE3.
180. Chen, T.C., et al., *Green tea epigallocatechin gallate enhances therapeutic efficacy of temozolomide in orthotopic mouse glioblastoma models*. Cancer Lett, 2011. **302**(2): p. 100-8.
181. Groves, M.D., et al., *Phase II trial of temozolomide plus marimastat for recurrent anaplastic gliomas: a relationship among efficacy, joint toxicity and anticonvulsant status*. J Neurooncol, 2006. **80**(1): p. 83-90.

182. Groves, M.D., et al., *Phase II trial of temozolomide plus the matrix metalloproteinase inhibitor, marimastat, in recurrent and progressive glioblastoma multiforme*. J Clin Oncol, 2002. **20**(5): p. 1383-8.
183. Lettau, I., et al., *Matrix metalloproteinase-19 is highly expressed in astroglial tumors and promotes invasion of glioma cells*. J Neuropathol Exp Neurol, 2010. **69**(3): p. 215-23.
184. Pullen, N.A. and H.L. Fillmore, *Induction of matrix metalloproteinase-1 and glioma cell motility by nitric oxide*. J Neurooncol, 2010. **96**(2): p. 201-9.
185. Weinstein, I.B. and A. Joe, *Oncogene addiction*. Cancer Res, 2008. **68**(9): p. 3077-80; discussion 3080.
186. Weinstein, I.B. and A.K. Joe, *Mechanisms of disease: Oncogene addiction--a rationale for molecular targeting in cancer therapy*. Nat Clin Pract Oncol, 2006. **3**(8): p. 448-57.
187. Di, C., et al., *Emerging therapeutic targets and agents for glioblastoma migrating cells*. Anticancer Agents Med Chem, 2010. **10**(7): p. 543-55.
188. Glover, K.Y., R. Perez-Soler, and V.A. Papadimitradopoulou, *A review of small-molecule epidermal growth factor receptor-specific tyrosine kinase inhibitors in development for non-small cell lung cancer*. Semin Oncol, 2004. **31**(1 Suppl 1): p. 83-92.
189. de Groot, J.F., et al., *Tumor invasion after treatment of glioblastoma with bevacizumab: radiographic and pathologic correlation in humans and mice*. Neuro Oncol, 2010. **12**(3): p. 233-42.
190. Huang, P.H., et al., *Quantitative analysis of EGFRvIII cellular signaling networks reveals a combinatorial therapeutic strategy for glioblastoma*. Proc Natl Acad Sci U S A, 2007. **104**(31): p. 12867-72.
191. Takahashi, S., et al., *Downregulation of uPARAP mediates cytoskeletal rearrangements and decreases invasion and migration properties in glioma cells*. J Neurooncol, 2010.
192. Zhang, B., et al., *Reduction of Akt2 inhibits migration and invasion of glioma cells*. Int J Cancer, 2009. **125**(3): p. 585-95.
193. Mayer, L.D., et al., *Influence of vesicle size, lipid composition, and drug-to-lipid ratio on the biological activity of liposomal doxorubicin in mice*. Cancer Res, 1989. **49**(21): p. 5922-30.

194. Gabizon, A., et al., *Pharmacokinetic and imaging studies in patients receiving a formulation of liposome-associated adriamycin*. Br J Cancer, 1991. **64**(6): p. 1125-32.
195. Papahadjopoulos, D., et al., *Sterically stabilized liposomes: improvements in pharmacokinetics and antitumor therapeutic efficacy*. Proc Natl Acad Sci U S A, 1991. **88**(24): p. 11460-4.
196. Gabizon, A., et al., *Clinical studies of liposome-encapsulated doxorubicin*. Acta Oncol, 1994. **33**(7): p. 779-86.
197. Ruoslahti, E., S.N. Bhatia, and M.J. Sailor, *Targeting of drugs and nanoparticles to tumors*. J Cell Biol, 2010. **188**(6): p. 759-68.
198. Cho, K., et al., *Therapeutic nanoparticles for drug delivery in cancer*. Clin Cancer Res, 2008. **14**(5): p. 1310-6.
199. Pauwels, E.K. and P. Erba, *Towards the use of nanoparticles in cancer therapy and imaging*. Drug News Perspect, 2007. **20**(4): p. 213-20.
200. Hashizume, H., et al., *Openings between defective endothelial cells explain tumor vessel leakiness*. Am J Pathol, 2000. **156**(4): p. 1363-80.
201. Gulati, M., et al., *Study of azathioprine encapsulation into liposomes*. J Microencapsul, 1998. **15**(4): p. 485-94.
202. Moghimi, S.M., A.C. Hunter, and J.C. Murray, *Long-circulating and target-specific nanoparticles: theory to practice*. Pharmacol Rev, 2001. **53**(2): p. 283-318.
203. Zagzag, D., et al., *Molecular events implicated in brain tumor angiogenesis and invasion*. Pediatr Neurosurg, 2000. **33**(1): p. 49-55.
204. Maeda, H., *The enhanced permeability and retention (EPR) effect in tumor vasculature: the key role of tumor-selective macromolecular drug targeting*. Adv Enzyme Regul, 2001. **41**: p. 189-207.
205. Semple, S.C., A. Chonn, and P.R. Cullis, *Interactions of liposomes and lipid-based carrier systems with blood proteins: Relation to clearance behaviour in vivo*. Advanced Drug Delivery Reviews, 1998. **32**(1-2): p. 3-17.
206. Zalutsky, M.R., *Current status of therapy of solid tumors: brain tumor therapy*. J Nucl Med, 2005. **46 Suppl 1**: p. 151S-6S.

207. Bai, X., et al., *Honokiol, a small molecular weight natural product, inhibits angiogenesis in vitro and tumor growth in vivo*. J Biol Chem, 2003. **278**(37): p. 35501-7.
208. Wolf, I., et al., *Honokiol, a natural biphenyl, inhibits in vitro and in vivo growth of breast cancer through induction of apoptosis and cell cycle arrest*. Int J Oncol, 2007. **30**(6): p. 1529-37.
209. Shigemura, K., et al., *Honokiol, a natural plant product, inhibits the bone metastatic growth of human prostate cancer cells*. Cancer, 2007. **109**(7): p. 1279-89.
210. Fried, L.E. and J.L. Arbiser, *Honokiol, a multifunctional antiangiogenic and antitumor agent*. Antioxid Redox Signal, 2009. **11**(5): p. 1139-48.
211. Ahn, K.S., et al., *Honokiol potentiates apoptosis, suppresses osteoclastogenesis, and inhibits invasion through modulation of nuclear factor-kappaB activation pathway*. Mol Cancer Res, 2006. **4**(9): p. 621-33.
212. Rayet, B. and C. Gelin, *Aberrant rel/nfkb genes and activity in human cancer*. Oncogene, 1999. **18**(49): p. 6938-47.
213. Pikarsky, E., et al., *NF-kappaB functions as a tumour promoter in inflammation-associated cancer*. Nature, 2004. **431**(7007): p. 461-6.
214. Tertilt, M., A. Jozkowicz, and J. Dulak, *Oxidative stress in tumor angiogenesis-therapeutic targets*. Curr Pharm Des, 2010. **16**(35): p. 3877-94.
215. Cooney, R.V., et al., *Inhibition of cellular transformation by triphenylmethane: a novel chemopreventive agent*. Carcinogenesis, 1992. **13**(7): p. 1107-12.
216. Salhia, B., et al., *Molecular pathways triggering glioma cell invasion*. Expert Rev Mol Diagn, 2006. **6**(4): p. 613-26.
217. Karumbaiah, L., et al., *Targeted downregulation of N-acetylgalactosamine 4-sulfate 6-O-sulfotransferase significantly mitigates chondroitin sulfate proteoglycan-mediated inhibition*. Glia, 2011. **59**(6): p. 981-96.
218. Horowitz, A.T., Y. Barenholz, and A.A. Gabizon, *In vitro cytotoxicity of liposome-encapsulated doxorubicin: dependence on liposome composition and drug release*. Biochim Biophys Acta, 1992. **1109**(2): p. 203-9.
219. Broaddus, W.C., et al., *Enhanced radiosensitivity of malignant glioma cells after adenoviral p53 transduction*. J Neurosurg, 1999. **91**(6): p. 997-1004.

220. Zhang, W., et al., *Inhibition of human malignant glioma cell motility and invasion in vitro by hypericin, a potent protein kinase C inhibitor*. *Cancer Lett*, 1997. **120**(1): p. 31-8.
221. Bello, L., et al., *Simultaneous inhibition of glioma angiogenesis, cell proliferation, and invasion by a naturally occurring fragment of human metalloproteinase-2*. *Cancer Res*, 2001. **61**(24): p. 8730-6.
222. Zagzag, D., et al., *Geldanamycin inhibits migration of glioma cells in vitro: a potential role for hypoxia-inducible factor (HIF-1alpha) in glioma cell invasion*. *J Cell Physiol*, 2003. **196**(2): p. 394-402.
223. *Central Brain Tumor Registry of the United States Statistical Report: Primary Brain and Central Nervouse System Tumors Diagnosed in the United States in 2004-2006*. 2010, Central Brain Tumor Registry of the United States: Hinsdale, IL.
224. Stupp, R., *Malignant glioma: ESMO clinical recommendations for diagnosis, treatment and follow-up*. *Ann Oncol*, 2007. **18 Suppl 2**: p. ii69-70.
225. Couldwell, W.T. and V.W. Yong, *Glioma invasion*. *J Neurosurg*, 2001. **95**(3): p. 379-80.
226. Noha, M., et al., *Suppression of cell invasion on human malignant glioma cell lines by a novel matrix-metalloproteinase inhibitor SI-27: in vitro study*. *J Neurooncol*, 2000. **48**(3): p. 217-23.
227. Jung, Y.D. and L.M. Ellis, *Inhibition of tumour invasion and angiogenesis by epigallocatechin gallate (EGCG), a major component of green tea*. *Int J Exp Pathol*, 2001. **82**(6): p. 309-16.
228. Larson, D.A., et al., *Phase II study of high central dose Gamma Knife radiosurgery and marimastat in patients with recurrent malignant glioma*. *Int J Radiat Oncol Biol Phys*, 2002. **54**(5): p. 1397-404.
229. Wick, W., et al., *Prevention of irradiation-induced glioma cell invasion by temozolomide involves caspase 3 activity and cleavage of focal adhesion kinase*. *Cancer Res*, 2002. **62**(6): p. 1915-9.
230. Immordino, M.L., F. Dosio, and L. Cattel, *Stealth liposomes: review of the basic science, rationale, and clinical applications, existing and potential*. *Int J Nanomedicine*, 2006. **1**(3): p. 297-315.

231. Yuan, F., et al., *Microvascular permeability and interstitial penetration of sterically stabilized (stealth) liposomes in a human tumor xenograft*. *Cancer Res*, 1994. **54**(13): p. 3352-6.
232. Yuan, F., et al., *Vascular permeability in a human tumor xenograft: molecular size dependence and cutoff size*. *Cancer Res*, 1995. **55**(17): p. 3752-6.
233. Allen, T.M., *Long-circulating (sterically stabilized) liposomes for targeted drug delivery*. *Trends Pharmacol Sci*, 1994. **15**(7): p. 215-20.
234. Gabizon, A. and D. Papahadjopoulos, *The role of surface charge and hydrophilic groups on liposome clearance in vivo*. *Biochim Biophys Acta*, 1992. **1103**(1): p. 94-100.
235. Gabizon, A., et al., *Effect of liposome composition and other factors on the targeting of liposomes to experimental tumors: biodistribution and imaging studies*. *Cancer Res*, 1990. **50**(19): p. 6371-8.
236. Fierz-David, H.E. and L. Blangey, *Fundamental Process of Dye Chemistry*. 1979, New York: Interscience Publishers.
237. McNeeley, K.M., et al., *Masking and triggered unmasking of targeting ligands on nanocarriers to improve drug delivery to brain tumors*. *Biomaterials*, 2009. **30**(23-24): p. 3986-95.
238. Singla, A.K., A. Garg, and D. Aggarwal, *Paclitaxel and its formulations*. *Int J Pharm*, 2002. **235**(1-2): p. 179-92.
239. Candolfi, M., et al., *Intracranial glioblastoma models in preclinical neuro-oncology: neuropathological characterization and tumor progression*. *J Neurooncol*, 2007. **85**(2): p. 133-48.
240. Ji, Y., et al., *Characterization of the tumor invasion area in the rat intracerebral glioma*. *J Neurooncol*, 1996. **30**(3): p. 189-97.
241. Greish, K., *Enhanced permeability and retention (EPR) effect for anticancer nanomedicine drug targeting*. *Methods Mol Biol*, 2010. **624**: p. 25-37.
242. Dams, E.T., et al., *Accelerated blood clearance and altered biodistribution of repeated injections of sterically stabilized liposomes*. *J Pharmacol Exp Ther*, 2000. **292**(3): p. 1071-9.
243. Kim, M.S., et al., *Emodin suppresses hyaluronic acid-induced MMP-9 secretion and invasion of glioma cells*. *Int J Oncol*, 2005. **27**(3): p. 839-46.

244. Nowicki, M.O., et al., *Lithium inhibits invasion of glioma cells; possible involvement of glycogen synthase kinase-3*. Neuro Oncol, 2008. **10**(5): p. 690-9.
245. Seufert, S., et al., *PPAR Gamma Activators: Off-Target Against Glioma Cell Migration and Brain Invasion*. PPAR Res, 2008. **2008**: p. 513943.
246. Grommes, C., et al., *Inhibition of in vivo glioma growth and invasion by peroxisome proliferator-activated receptor gamma agonist treatment*. Mol Pharmacol, 2006. **70**(5): p. 1524-33.
247. Shen, J., et al., *Marchantin C: a potential anti-invasion agent in glioma cells*. Cancer Biol Ther, 2010. **9**(1): p. 33-9.
248. Olson, M.F. and E. Sahai, *The actin cytoskeleton in cancer cell motility*. Clin Exp Metastasis, 2009. **26**(4): p. 273-87.
249. Disanza, A., et al., *Actin polymerization machinery: the finish line of signaling networks, the starting point of cellular movement*. Cell Mol Life Sci, 2005. **62**(9): p. 955-70.
250. Hall, A. and C.D. Nobes, *Rho GTPases: molecular switches that control the organization and dynamics of the actin cytoskeleton*. Philos Trans R Soc Lond B Biol Sci, 2000. **355**(1399): p. 965-70.
251. Forget, M.A., et al., *The expression of rho proteins decreases with human brain tumor progression: potential tumor markers*. Clin Exp Metastasis, 2002. **19**(1): p. 9-15.
252. Gebhardt, C., et al., *SI00A8 and SI00A9 in inflammation and cancer*. Biochem Pharmacol, 2006. **72**(11): p. 1622-31.
253. Hermani, A., et al., *SI00A8 and SI00A9 activate MAP kinase and NF-kappaB signaling pathways and trigger translocation of RAGE in human prostate cancer cells*. Exp Cell Res, 2006. **312**(2): p. 184-97.
254. Yong, H.Y. and A. Moon, *Roles of calcium-binding proteins, SI00A8 and SI00A9, in invasive phenotype of human gastric cancer cells*. Arch Pharm Res, 2007. **30**(1): p. 75-81.
255. Kuzumaki, N., et al., *[Tumor suppressive function of gelsolin]*. Gan To Kagaku Ryoho, 1997. **24**(11): p. 1436-41.
256. Demuth, T. and M.E. Berens, *Molecular mechanisms of glioma cell migration and invasion*. J Neurooncol, 2004. **70**(2): p. 217-28.

257. Mueller, M.M., T. Werbowetski, and R.F. Del Maestro, *Soluble factors involved in glioma invasion*. Acta Neurochir (Wien), 2003. **145**(11): p. 999-1008.
258. Hoelzinger, D.B., T. Demuth, and M.E. Berens, *Autocrine factors that sustain glioma invasion and paracrine biology in the brain microenvironment*. J Natl Cancer Inst, 2007. **99**(21): p. 1583-93.
259. Idani, H., et al., *Intra-tumoral injection of doxorubicin (adriamycin) encapsulated in liposome inhibits tumor growth, prolongs survival time and is not associated with local or systemic side effects*. Int J Cancer, 2000. **88**(4): p. 645-51.
260. Sugahara, T., et al., *Posttherapeutic intraaxial brain tumor: the value of perfusion-sensitive contrast-enhanced MR imaging for differentiating tumor recurrence from nonneoplastic contrast-enhancing tissue*. AJNR Am J Neuroradiol, 2000. **21**(5): p. 901-9.
261. Apetoh, L., et al., *Toll-like receptor 4-dependent contribution of the immune system to anticancer chemotherapy and radiotherapy*. Nat Med, 2007. **13**(9): p. 1050-9.
262. Zhang, H., G. Wang, and H. Yang, *Drug delivery systems for differential release in combination therapy*. Expert Opin Drug Deliv, 2011. **8**(2): p. 171-90.
263. Abe, T., et al., *Expression of multidrug resistance protein gene in patients with glioma after chemotherapy*. J Neurooncol, 1998. **40**(1): p. 11-8.
264. Ogawara, K., et al., *In vivo anti-tumor effect of PEG liposomal doxorubicin (DOX) in DOX-resistant tumor-bearing mice: Involvement of cytotoxic effect on vascular endothelial cells*. J Control Release, 2009. **133**(1): p. 4-10.
265. Siegal, T., A. Horowitz, and A. Gabizon, *Doxorubicin encapsulated in sterically stabilized liposomes for the treatment of a brain tumor model: biodistribution and therapeutic efficacy*. J Neurosurg, 1995. **83**(6): p. 1029-37.
266. Sakakibara, T., et al., *Doxorubicin encapsulated in sterically stabilized liposomes is superior to free drug or drug-containing conventional liposomes at suppressing growth and metastases of human lung tumor xenografts*. Cancer Res, 1996. **56**(16): p. 3743-6.
267. Tardi, P.G., N.L. Boman, and P.R. Cullis, *Liposomal doxorubicin*. J Drug Target, 1996. **4**(3): p. 129-40.
268. Vaage, J., et al., *Therapy of mouse mammary carcinomas with vincristine and doxorubicin encapsulated in sterically stabilized liposomes*. Int J Cancer, 1993. **54**(6): p. 959-64.

269. Wu, J., et al., *Reversal of multidrug resistance by transferrin-conjugated liposomes co-encapsulating doxorubicin and verapamil*. J Pharm Pharm Sci, 2007. **10**(3): p. 350-7.
270. Gaber, M.H., et al., *Thermosensitive sterically stabilized liposomes: formulation and in vitro studies on mechanism of doxorubicin release by bovine serum and human plasma*. Pharm Res, 1995. **12**(10): p. 1407-16.
271. Lasic, D.D., *Doxorubicin in sterically stabilized liposomes*. Nature, 1996. **380**(6574): p. 561-2.
272. Onishi, M., et al., *Angiogenesis and invasion in glioma*. Brain Tumor Pathol, 2011. **28**(1): p. 13-24.
273. Cheng, C.K., Q.W. Fan, and W.A. Weiss, *PI3K signaling in glioma--animal models and therapeutic challenges*. Brain Pathol, 2009. **19**(1): p. 112-20.
274. Engelman, J.A., *Targeting PI3K signalling in cancer: opportunities, challenges and limitations*. Nat Rev Cancer, 2009. **9**(8): p. 550-62.
275. Dhillon, A.S., et al., *MAP kinase signalling pathways in cancer*. Oncogene, 2007. **26**(22): p. 3279-90.
276. Li, N. and M. Karin, *Is NF-kappaB the sensor of oxidative stress?* FASEB J, 1999. **13**(10): p. 1137-43.
277. Tobar, N., et al., *NOX4-dependent ROS production by stromal mammary cells modulates epithelial MCF-7 cell migration*. Br J Cancer, 2010. **103**(7): p. 1040-7.
278. Takada, Y., et al., *Flavopiridol suppresses tumor necrosis factor-induced activation of activator protein-1, c-Jun N-terminal kinase, p38 mitogen-activated protein kinase (MAPK), p44/p42 MAPK, and Akt, inhibits expression of antiapoptotic gene products, and enhances apoptosis through cytochrome c release and caspase activation in human myeloid cells*. Mol Pharmacol, 2008. **73**(5): p. 1549-57.
279. Martyn, K.D., et al., *Functional analysis of Nox4 reveals unique characteristics compared to other NADPH oxidases*. Cell Signal, 2006. **18**(1): p. 69-82.
280. von Lohneysen, K., et al., *Mutational analysis reveals distinct features of the Nox4-p22 phox complex*. J Biol Chem, 2008. **283**(50): p. 35273-82.
281. von Lohneysen, K., et al., *Structural insights into Nox4 and Nox2: motifs involved in function and cellular localization*. Mol Cell Biol, 2010. **30**(4): p. 961-75.

282. Blouw, B., et al., *A role for the podosome/invadopodia scaffold protein Tks5 in tumor growth in vivo*. Eur J Cell Biol, 2008. **87**(8-9): p. 555-67.
283. Prados, M.D. and V. Levin, *Biology and treatment of malignant glioma*. Semin Oncol, 2000. **27**(3 Suppl 6): p. 1-10.
284. Kim, J.Y., et al., *Src-mediated regulation of inflammatory responses by actin polymerization*. Biochem Pharmacol, 2010. **79**(3): p. 431-43.
285. Manea, A., et al., *Transcriptional regulation of NADPH oxidase isoforms, Nox1 and Nox4, by nuclear factor-kappaB in human aortic smooth muscle cells*. Biochem Biophys Res Commun, 2010. **396**(4): p. 901-7.
286. Manea, A., et al., *Jak/STAT signaling pathway regulates nox1 and nox4-based NADPH oxidase in human aortic smooth muscle cells*. Arterioscler Thromb Vasc Biol, 2010. **30**(1): p. 105-12.
287. Maurer, H.H., *Screening procedures for simultaneous detection of several drug classes used for high throughput toxicological analyses and doping control. A review*. Comb Chem High Throughput Screen, 2000. **3**(6): p. 467-80.
288. Terstappen, G.C. and A. Reggiani, *In silico research in drug discovery*. Trends Pharmacol Sci, 2001. **22**(1): p. 23-6.
289. Van Dyke, T. and T. Jacks, *Cancer modeling in the modern era: progress and challenges*. Cell, 2002. **108**(2): p. 135-44.
290. Friedl, P. and K. Wolf, *Tumour-cell invasion and migration: diversity and escape mechanisms*. Nat Rev Cancer, 2003. **3**(5): p. 362-74.
291. Wolf, K., et al., *Compensation mechanism in tumor cell migration: mesenchymal-amoeboid transition after blocking of pericellular proteolysis*. J Cell Biol, 2003. **160**(2): p. 267-77.
292. Liotta, L.A. and E. Kohn, *Anoikis: cancer and the homeless cell*. Nature, 2004. **430**(7003): p. 973-4.
293. Mischel, P.S. and T.F. Cloughesy, *Targeted molecular therapy of GBM*. Brain Pathol, 2003. **13**(1): p. 52-61.
294. von Mehren, M., G.P. Adams, and L.M. Weiner, *Monoclonal antibody therapy for cancer*. Annu Rev Med, 2003. **54**: p. 343-69.

295. Kinsella, P., M. Clynes, and V. Amberger-Murphy, *Imatinib and docetaxel in combination can effectively inhibit glioma invasion in an in vitro 3D invasion assay*. J Neurooncol, 2011. **101**(2): p. 189-98.
296. Raman, K. and B. Kuberan, *Click-xylosides mitigate glioma cell invasion in vitro*. Mol Biosyst, 2010. **6**(10): p. 1800-2.
297. Gessler, F., et al., *Inhibition of tissue factor/protease-activated receptor-2 signaling limits proliferation, migration and invasion of malignant glioma cells*. Neuroscience, 2010. **165**(4): p. 1312-22.
298. Lim, Y.C., et al., *(-)-Epigallocatechin-3-gallate (EGCG) inhibits HGF-induced invasion and metastasis in hypopharyngeal carcinoma cells*. Cancer Lett, 2008. **271**(1): p. 140-52.
299. Charrois, G.J. and T.M. Allen, *Multiple injections of pegylated liposomal Doxorubicin: pharmacokinetics and therapeutic activity*. J Pharmacol Exp Ther, 2003. **306**(3): p. 1058-67.
300. Hsu, M.J. and R.L. Juliano, *Interactions of liposomes with the reticuloendothelial system. II: Nonspecific and receptor-mediated uptake of liposomes by mouse peritoneal macrophages*. Biochim Biophys Acta, 1982. **720**(4): p. 411-9.
301. Ellens, H., E. Mayhew, and Y.M. Rustum, *Reversible depression of the reticuloendothelial system by liposomes*. Biochim Biophys Acta, 1982. **714**(3): p. 479-85.
302. Hu, B., et al., *Angiopoietin-2 induces human glioma invasion through the activation of matrix metalloprotease-2*. Proc Natl Acad Sci U S A, 2003. **100**(15): p. 8904-9.
303. Netti, P.A., et al., *Enhancement of fluid filtration across tumor vessels: implication for delivery of macromolecules*. Proc Natl Acad Sci U S A, 1999. **96**(6): p. 3137-42.
304. Zitvogel, L., et al., *Immunological aspects of cancer chemotherapy*. Nat Rev Immunol, 2008. **8**(1): p. 59-73.
305. Baumgartner, G., et al., *The impact of extracellular matrix on the chemoresistance of solid tumors--experimental and clinical results of hyaluronidase as additive to cytostatic chemotherapy*. Cancer Lett, 1998. **131**(1): p. 85-99.
306. *Abstracts from the 15th Annual Meeting of the Society for Neuro-Oncology*. in *Society for Neuro-oncology*. 2010. Montreal, Quebec, Canada: Neuro-oncology.

307. Parker, R.J., S.M. Sieber, and J.N. Weinstein, *Effect of liposome encapsulation of a fluorescent dye on its uptake by the lymphatics of the rat*. *Pharmacology*, 1981. **23**(3): p. 128-36.
308. Sumer, B. and J. Gao, *Theranostic nanomedicine for cancer*. *Nanomedicine (Lond)*, 2008. **3**(2): p. 137-40.
309. Vajkoczy, P., et al., *Microtumor growth initiates angiogenic sprouting with simultaneous expression of VEGF, VEGF receptor-2, and angiopoietin-2*. *J Clin Invest*, 2002. **109**(6): p. 777-85.
310. Forsyth, P.A., et al., *Gelatinase-A (MMP-2), gelatinase-B (MMP-9) and membrane type matrix metalloproteinase-1 (MT1-MMP) are involved in different aspects of the pathophysiology of malignant gliomas*. *British Journal Of Cancer*, 1999. **79**(11-12): p. 1828-1835.
311. Vajkoczy, P., et al., *Microtumor growth initiates angiogenic sprouting with simultaneous expression of VEGF, VEGF receptor-2, and angiopoietin-2*. *The Journal Of Clinical Investigation*, 2002. **109**(6): p. 777-785.
312. Cho, K., et al., *Therapeutic Nanoparticles for Drug Delivery in Cancer*. *Clinical Cancer Research*, 2008. **14**(5): p. 1310-1316.
313. Kim, K.Y., *Nanotechnology platforms and physiological challenges for cancer therapeutics*. *Nanomedicine: Nanotechnology, Biology and Medicine*, 2007. **3**(2): p. 103-110.
314. Jain, R.K., et al., *Angiogenesis in brain tumours*. *Nat Rev Neurosci*, 2007. **8**(8): p. 610-622.
315. Ghaghada, K.B., et al., *New Dual Mode Gadolinium Nanoparticle Contrast Agent for Magnetic Resonance Imaging*. *PLoS ONE*, 2009. **4**(10): p. e7628.
316. OGAN, M.D., et al., *Albumin Labeled with Gd-DTPA: An Intravascular Contrast-Enhancing Agent for Magnetic Resonance Blood Pool Imaging: Preparation and Characterization*. *Investigative Radiology*, 1987. **22**(8): p. 665-671.
317. Daldrup, H., et al., *Correlation of dynamic contrast-enhanced magnetic resonance imaging with histologic tumor grade: comparison of macromolecular and small-molecular contrast media*. *Pediatric Radiology*, 1998. **28**(2): p. 67-78.
318. Woodle, M.C., M.S. Newman, and P.K. Working, *Biological Properties of Sterically Stabilized Liposomes*, in *Stealth Liposomes*, D.D. Lasic and F. Martin, Editors. 1995, Taylor & Francis Inc: Boca Raton.

319. Gossmann, A., et al., *Dynamic contrast-enhanced magnetic resonance imaging as a surrogate marker of tumor response to anti-angiogenic therapy in a xenograft model of glioblastoma multiforme*. Journal of Magnetic Resonance Imaging, 2002. **15**(3): p. 233-240.
320. Kim, M.S., et al., *Emodin suppresses hyaluronic acid-induced MMP-9 secretion and invasion of glioma cells*. International Journal of Oncology, 2005. **27**(3): p. 839-846.
321. Norden, A.D., et al., *Bevacizumab for recurrent malignant gliomas: efficacy, toxicity, and patterns of recurrence*. Neurology, 2008. **70**(10): p. 779-787.
322. Dunn, J., et al., *Extent of MGMT promoter methylation correlates with outcome in glioblastomas given temozolomide and radiotherapy*. Br J Cancer, 2009. **101**(1): p. 124-31.
323. Sadones, J., et al., *MGMT promoter hypermethylation correlates with a survival benefit from temozolomide in patients with recurrent anaplastic astrocytoma but not glioblastoma*. Eur J Cancer, 2009. **45**(1): p. 146-53.
324. Kim, K., et al., *Epidermal growth factor receptor vIII expression in U87 glioblastoma cells alters their proteasome composition, function, and response to irradiation*. Mol Cancer Res, 2008. **6**(3): p. 426-34.
325. Giese, A., *Glioma invasion--pattern of dissemination by mechanisms of invasion and surgical intervention, pattern of gene expression and its regulatory control by tumorsuppressor p53 and proto-oncogene ETS-1*. Acta Neurochir Suppl, 2003. **88**: p. 153-62.
326. Tonn, J.C. and R. Goldbrunner, *Mechanisms of glioma cell invasion*. Acta Neurochir Suppl, 2003. **88**: p. 163-7.
327. Tuettenberg, J., et al., *Recurrence pattern in glioblastoma multiforme patients treated with anti-angiogenic chemotherapy*. J Cancer Res Clin Oncol, 2009. **135**(9): p. 1239-44.
328. Giese, A., et al., *Migration of human glioma cells on myelin*. Neurosurgery, 1996. **38**(4): p. 755-64.
329. Lazarini, F., et al., *Role of the alpha-chemokine stromal cell-derived factor (SDF-1) in the developing and mature central nervous system*. Glia, 2003. **42**(2): p. 139-48.
330. Teicher, B.A. and S.P. Fricker, *CXCL12 (SDF-1)/CXCR4 pathway in cancer*. Clin Cancer Res, 2010. **16**(11): p. 2927-31.

331. Ehtesham, M., et al., *CXCR4 expression mediates glioma cell invasiveness*. *Oncogene*, 2006. **25**(19): p. 2801-6.
332. Salmaggi, A., et al., *CXCL12 expression is predictive of a shorter time to tumor progression in low-grade glioma: a single-institution study in 50 patients*. *J Neurooncol*, 2005. **74**(3): p. 287-93.
333. Woerner, B.M., et al., *Widespread CXCR4 activation in astrocytomas revealed by phospho-CXCR4-specific antibodies*. *Cancer Res*, 2005. **65**(24): p. 11392-9.
334. Fleury, M.E., K.C. Boardman, and M.A. Swartz, *Autologous morphogen gradients by subtle interstitial flow and matrix interactions*. *Biophys J*, 2006. **91**(1): p. 113-21.
335. Shields, J.D., et al., *Autologous chemotaxis as a mechanism of tumor cell homing to lymphatics via interstitial flow and autocrine CCR7 signaling*. *Cancer Cell*, 2007. **11**(6): p. 526-38.
336. Randolph, G.J., V. Angeli, and M.A. Swartz, *Dendritic-cell trafficking to lymph nodes through lymphatic vessels*. *Nat Rev Immunol*, 2005. **5**(8): p. 617-28.
337. Shieh, A.C., et al., *Tumor cell invasion is promoted by interstitial flow-induced matrix priming by stromal fibroblasts*. *Cancer Res*, 2011. **71**(3): p. 790-800.
338. Abbott, N.J., *Evidence for bulk flow of brain interstitial fluid: significance for physiology and pathology*. *Neurochem Int*, 2004. **45**(4): p. 545-52.
339. Sawamoto, K., et al., *New neurons follow the flow of cerebrospinal fluid in the adult brain*. *Science*, 2006. **311**(5761): p. 629-32.
340. Rosenberg, G.A., W.T. Kyner, and E. Estrada, *Bulk flow of brain interstitial fluid under normal and hyperosmolar conditions*. *Am J Physiol*, 1980. **238**(1): p. F42-9.
341. Reulen, H.J., et al., *Clearance of edema fluid into cerebrospinal fluid. A mechanism for resolution of vasogenic brain edema*. *J Neurosurg*, 1978. **48**(5): p. 754-64.
342. Ramnarayan, R., et al., *Overall survival in patients with malignant glioma may be significantly longer with tumors located in deep grey matter*. *J Neurol Sci*, 2007. **260**(1-2): p. 49-56.
343. Reiss, K., et al., *Stromal cell-derived factor 1 is secreted by meningeal cells and acts as chemotactic factor on neuronal stem cells of the cerebellar external granular layer*. *Neuroscience*, 2002. **115**(1): p. 295-305.

344. Wang, T.W. and M. Spector, *Development of hyaluronic acid-based scaffolds for brain tissue engineering*. Acta Biomater, 2009. **5**(7): p. 2371-84.
345. Saria, A. and J.M. Lundberg, *Evans blue fluorescence: quantitative and morphological evaluation of vascular permeability in animal tissues*. J Neurosci Methods, 1983. **8**(1): p. 41-9.
346. do Carmo, A., et al., *CXCL12/CXCR4 promotes motility and proliferation of glioma cells*. Cancer Biol Ther, 2010. **9**(1): p. 56-65.
347. Zhang, J., S. Sarkar, and V.W. Yong, *The chemokine stromal cell derived factor-1 (CXCL12) promotes glioma invasiveness through MT2-matrix metalloproteinase*. Carcinogenesis, 2005. **26**(12): p. 2069-77.
348. Rubin, J.B., et al., *A small-molecule antagonist of CXCR4 inhibits intracranial growth of primary brain tumors*. Proc Natl Acad Sci U S A, 2003. **100**(23): p. 13513-8.
349. Ping, Y.F., et al., *[Activation of CXCR4 in human glioma stem cells promotes tumor angiogenesis]*. Zhonghua Bing Li Xue Za Zhi, 2007. **36**(3): p. 179-83.
350. Yang, S.X., et al., *Activation of chemokine receptor CXCR4 in malignant glioma cells promotes the production of vascular endothelial growth factor*. Biochem Biophys Res Commun, 2005. **335**(2): p. 523-8.
351. Ng, C.P. and M.A. Swartz, *Mechanisms of interstitial flow-induced remodeling of fibroblast-collagen cultures*. Ann Biomed Eng, 2006. **34**(3): p. 446-54.
352. Schneider, I.C. and J.M. Haugh, *Quantitative elucidation of a distinct spatial gradient-sensing mechanism in fibroblasts*. J Cell Biol, 2005. **171**(5): p. 883-92.
353. Li Jeon, N., et al., *Neutrophil chemotaxis in linear and complex gradients of interleukin-8 formed in a microfabricated device*. Nat Biotechnol, 2002. **20**(8): p. 826-30.
354. Hong, X., et al., *SDF-1 and CXCR4 are up-regulated by VEGF and contribute to glioma cell invasion*. Cancer Lett, 2006. **236**(1): p. 39-45.
355. Souza, G.R., et al., *Three-dimensional tissue culture based on magnetic cell levitation*. Nat Nanotechnol, 2010. **5**(4): p. 291-6.
356. Swartz, M.A., J.A. Hubbell, and S.T. Reddy, *Lymphatic drainage function and its immunological implications: from dendritic cell homing to vaccine design*. Semin Immunol, 2008. **20**(2): p. 147-56.

357. Boardman, K.C. and M.A. Swartz, *Interstitial flow as a guide for lymphangiogenesis*. *Circ Res*, 2003. **92**(7): p. 801-8.
358. Zhou, Y., et al., *CXCR4 is a major chemokine receptor on glioma cells and mediates their survival*. *J Biol Chem*, 2002. **277**(51): p. 49481-7.
359. Luetmer, P.H., et al., *Measurement of cerebrospinal fluid flow at the cerebral aqueduct by use of phase-contrast magnetic resonance imaging: technique validation and utility in diagnosing idiopathic normal pressure hydrocephalus*. *Neurosurgery*, 2002. **50**(3): p. 534-43; discussion 543-4.

VITA

Jennifer Megan Munson was born in Marietta, GA on November 17, 1983 to Chris and Joan Munson. After completing an International Baccalaureate degree at Campbell High School in Smyrna, GA, she attended Tulane University in New Orleans, LA. She graduated with a bachelor's of science in Chemical Engineering and Neuroscience in 2006. She then worked at both Genentech in South San Francisco, CA in cell culture process development until Fall 2007 when she began attending graduate school at Georgia Tech. During her time at Georgia Tech, she spent ten months abroad in Lausanne, Switzerland on a Fulbright Fellowship studying the effects of interstitial flow on glioma invasion. She currently lives in Atlanta, GA with her two cats, Pie and Bean, and her fiancé, Charles. She enjoys swimming, reading children's novels, and traveling in her free time.